Flows of Incompressible Newtonian and Generalized Newtonian Fluids over a Circular Cylinder

By

Kayla M. Klein

Submitted to the graduate degree program in Mechanical Engineering

and the Graduate Faculty of the University of Kansas

in partial fulfillment of requirements for the degree of

Master of Science.

_____

Dr. Karan S. Surana, Thesis Advisor and Chairperson

_____

Dr. Albert Romkes, Co-Advisor

_____

Dr. Peter W. Tenpas

Date Defended: _____

The Thesis Committee for Kayla M. Klein certifies

that this is the approved Version of the following thesis:

Flows of Incompressible Newtonian and Generalized Newtonian Fluids over a Circular Cylinder

Committee:

Dr. Karan S. Surana, Thesis Advisor and Chairperson

Dr. Albert Romkes, Co-Advisor

Dr. Peter W. Tenpas

Date Approved:

Abstract

This thesis presents numerical solutions of the boundary value problems describing the isothermal and non-isothermal steady flows of incompressible Newtonian, power-law and Carreau fluids over a circular cylinder using the hpk finite element process based on the residual functional (least squares process). This computational framework yields unconditionally stable algebraic systems for non-linear partial differential equations that result from the mathematical models, regardless of the choices of h, p and k and the dimensionless parameters in the mathematical models. It is shown that for such fluids, the energy equation and heat flux equations are decoupled (or weakly coupled) from the rest of the mathematical model resulting from the conservation of mass, balance of momenta and the constitutive theory for the deviatoric Cauchy stress tensor. Thus, one could solve for velocities, pressure and deviatoric Cauchy stress independent of the energy equation and heat flux equations. However, the weak coupling between the energy equation and the heat flux equations and the remaining mathematical model permits numerical solutions of the combined mathematical model in the present computational framework. Numerical studies are presented for progressively increasing flow rates corresponding to Re = 20, 40, 60, 100 and 200 for Newtonian and Carreau fluids and Re_n = 15.6, 37.2, 64.2, 118.8 and 285.0 for power-law fluids. The inlet length and the height of the domain are established so that boundaries of the domain do not influence the flow feature around and in the neighborhood of the cylinder for all Reynolds numbers considered. The choice of discretization and p-levels are determined such that the integrated sum of the squares of the residuals for the whole domain are always of the order of $O\left(10^{-6}\right)$ or lower for converged solutions. The choice of $\|g_i\|_{max} \leq O\left(10^{-6}\right)$ always ensures that Newton's linear method with line search

yields an accurate solution of the system of non-linear algebraic equations resulting from the least squares process. The residual functional values of the order of $O\left(10^{-6}\right)$ or lower ensure that GDEs are satisfied accurately over the entire domain and, thus the numerical solutions presented in this thesis can be viewed as benchmark quality solutions.

In cases of generalized Newtonian fluids (power-law and Carreau models) only shear thinning fluids are considered. Numerical studies demonstrate decoupled behavior of the temperature field from the rest of the deformation field. Shear thinning behavior and viscous dissipation for progressively increasing Reynolds numbers are simulated accurately without any difficulty.

Acknowledgements

I would like thank my advisors, Dr. Karan Surana and Dr. Albert Romkes, for their support and academic guidance throughout the past two years. Without their advice and instruction, the work presented in this thesis would not be possible. I would also like to thank my committee member Dr. Peter Tenpas for serving on my committee. Thank you to the Department of Mechanical Engineering at The University of Kansas for their financial support through various graduate teaching appointments.

Finally, I would like to thank my family and friends for their support during my graduate studies. This includes my fellow computational mechanics laboratory graduate students from whom I have gained an abundance of knowledge.

Contents

List of Tables

List of Figures

Nomenclature

ρ	Density
η	Viscosity
η^0	Zero Shear Rate Viscosity
η^∞	Carreau Model Infinite Shear Rate Viscosity
n	Power-Law Index
m	Carreau Model Index
λ	Carreau Model Fluid Constant
D	Diameter of the Cylinder
R	Radius of the Cylinder
L	Length
c_p	Specific Heat
k	Thermal Conductivity
Re	Reynolds Number
Re_n	Power-Law Reynolds Number
Br	Brinkman Number
Ec	Eckret Number

u	Velocity in the x-Direction
v	Velocity in the y-Direction
p	Pressure
τ_{xx}	Normal Stress in x-Direction
τ_{yy}	Normal Stress in y-Direction
τ_{xy}	Shear Stress in xy-Plane
T	Temperature
q_x	Heat Conduction in x-direction
q_y	Heat Conduction in y-direction
t	Time
GDEs	Governing Differential Equations
PDEs	Partial Differential Equations
LSP	Least Squares Process
dofs	Degrees of Freedom
$[\tau]$	Deviatonic Cauchy Stress Tensor
$[D]$	Strain Rate Tensor
I_2	Second Invariant of Strain Rate Tensor
Ω	Domain of Definition
Ω_T	Discretized Domain
Ω_e	Finite Element Domain
Γ	Closed Boundary of Domain
${}^i\phi$	Dependent Variables
${}^i\phi^e$	Local Approximations

$[N]$	Local Approximation Functions
E_i^e	Error (Residual) Equation for an Element 'e'
$\{\delta\}$	Dofs
I	Error Functional for Least Squares Finite Element Formulation
g	Measure of how well GDE is Satisfied in Point-Wise Sense
p-level	Degree of Local Approximation
$\{\delta\}_0$	Assumed Solution for Newton's Linear Method

Chapter 1

Introduction, Literature Review and Scope of Work

1.1 Introduction

The flow of incompressible fluids over a circular cylinder is a commonly studied problem in fluid mechanics due to many industrial applications. The complex flow physics around the cylinder requires prudent computational methods, mesh refining strategies and p-level choices to simulate such flows numerically. For this reason, this problem is often used as a benchmark problem to test accuracy of numerical methods. At very low Reynolds numbers the flow is laminar, but as the Reynolds number is increased, recirculation and a wake begin to form behind the cylinder and the flow eventually becomes turbulent.

In order to simulate true physics of flow around a cylinder of incompressible fluids, we must consider three dimensional flow and time evolutions using full Navier Stokes equations. In this approach, it is possible to simulate laminar flows at very low Reynolds

numbers, detect onset of turbulence with progressively increasing Reynolds numbers, as well as simulate turbulent flows for high Reynolds numbers. This has been an ongoing effort and there are many published works on the subject. It is generally concluded that the computational resources required to do this are enormous due to excessively refined meshes and high p-level requirements. On the other hand, in the simulations of the solution of BVPs associated with these flows, these requirements are not as severe. Hence, such studies are often conducted to gain insight into the flow physics, keeping well in mind that simulation of the turbulence in these approaches is not possible. Although there are many published works on these numerical studies, benchmark quality numerical studies are rarely available. This is the subject of study in the present work. In the following, we present literature review associated with flows of: (i) Newtonian fluids, (ii) power-law fluids and (iii) those described by Carreau model over a cylinder for both isothermal and non-isothermal cases.

1.2 Literature Review

Newtonian Fluids

There are many published works on progressively increasing Reynolds number flows over a cylinder and their numerical simulations for BVPs. Williamson [1] and Zdravkovich [2, 3] showed that steady flow without separation occurs up to $Re \leq$ 5-6. Steady flow with symmetric vortices behind the cylinder occur up to $Re <$ 49, at which laminar vortex shedding begins to occur. Eventually, around $Re \approx$ 190-260, the flow properties at the wake become three-dimensional. Another study suggested that the onset of three-dimensional

instability occurs at $Re = 180$, but two-dimensional computational results agree reasonably up to Re = 200 [4]. Using a spectral element method, Posdziech and Grundmann were able to determine that the onset of steady and unsteady flow transitions occur at $Re = 46.7$ [5]. Authors point out that many deviations in the current literature are likely due to dependency on the discretizations used. Other literature focuses on specific parts of the flow such as vortex rings [6], experimental data around the wake [7] and fluctuation lift for very high Reynolds numbers [8].

Grove et al. [9] presented studies to determine how various parameters change with Reynolds number up to 177. They determined that the equation of pressure drag coefficient for the cylinder as a function of Re is given by $C_{D,P} = 0.62 + 12.6/Re$ for $10 \leq Re \leq 177$. It was also shown that the rear pressure coefficient reaches a value of -0.45 and stays unchanged between $25 \leq Re \leq 177$. Fornberg ran two separate studies for two-dimensional flows that investigated how the wake forms in steady viscous flows for increasing Reynolds numbers [10, 11]. They showed that vorticity starts to recirculate back from the end of the wake region when approaching $Re = 300$ [10]. The second study extended the previous study up to $Re = 600$ where the wake bubble begins to grow in width and length [11].

Generalized Newtonian Fluids: Power-Law and Carreau Models (Isothermal Flows)

Many published works for Power-law fluids consider $Re \leq 40$ [12–17] in the numerical simulations. For shear-thinning fluids ($n < 1$) and shear-thickening fluids ($n > 1$), this critical Re is likely to be different than that of a Newtonian fluid ($n = 1$), however this aspect is not addressed in these studies. D'Alessio and Pascal [16] compute the drag coefficient,

separation angle and wake length for shear-thinning and shear-thickening fluids at $Re =$ 5, 20 and 40 using a finite difference technique. It was shown that as Reynolds number increases, convergence issues are encountered as the fluid behavior deviates from Newtonian behavior, $n <$ 0.95 or $n >$ 1.1. Similarly, the closed form solution for steady flow across an array of circular cylinders is only valid for $n \geq 0.8$ [17]. Studies were reported by Chhabra et al. [15] and Bharti et al. [14] using second-order finite difference method and semi-implicit finite volume method, respectively. In both works, the range of fluids is extended to include $0.2 \leq n \leq 2$. The data for these studies are presented in characteristic values, such as drag and pressure coefficients rather than providing results of the velocity, pressure and stress distributions. Streamline plots are given for various power-law indices and Reynolds numbers, but quantifiable data are not given. Sivakumar et al. investigated the influence of power-law index on the formation of the wake and onset of wake instability [18]. It was shown that the wake formation is delayed with decreasing power-law index, so a shear-thinning fluid will form similar size wakes as a Newtonian fluid, but at a higher Reynolds number. However, it was noted that if the power-law index decreases below 0.6, the critical Re begins to decrease.

There have been only a few time-accurate flow studies that compare steady and unsteady flow regimes for Newtonian and non-Newtonian Power-law fluids. As previously discussed, Patnana et al. modeled the unsteady flow of power-law fluids over an unconfined cylinder using the finite volume method for $40 \leq Re \leq 140$ and $0.4 \leq n \leq 1.8$ [19]. They clearly showed that a lower power-law index allows for a higher critical Reynolds number. Also, the effects of power-law index on the drag coefficient becomes less apparent at high Reynolds number of around 140. Coelho and Pinho focused on vortex shedding and formation length for Newtonian, shear thinning and elastic fluids [20–22]. They reported that

the critical formation length, l_{cf}/D, for Newtonian fluids is 3.4. In the laminar shedding regime, shear-thinning reduced the boundary-layer thickness and the diffusion [21]. Even though power-law model exhibits serious problems of excessively high viscosity in low shear regions [23], its use remains a common practice. The Carreau model eliminates this issue by making viscosity approach zero and infinite shear rate viscosity values asymptotically. Surana et al. [23] showed this by computing solutions for incompressible flow between parallel plates using k-version finite element method [24, 25].

Non-isothermal Flows

Khan et al. [26] solved the momentum integral equation using the Von Karman-Pohlhausen method. The results showed that the drag coefficients and heat transfer coefficients increase as the power-law index decreases. Other studies focus on changes in flow characteristics due to Reynolds number, Prandtl number (Pr) or Nusselt number [27, 28]. These studies show that heat transfer is directly related to both Reynolds number and Prandtl number. Also, when comparing two boundary conditions at the cylinder surface: uniform heat flux (UNF) and constant wall temperature (CWT), it was shown that UNF boundary conditions exhibit a higher heat transfer coefficient than those of CWT [27]. Soares and Ferreira extend this work to include power-law fluid, they showed that the affects of the power-law index on pressure drag, frictional drag and surface-averaged Nusselt number are affected more by kinematic conditions on the cylinder rather than thermal conditions [28]. For any given Reynolds number, decreasing power-law index will decrease the heat transfer from a hot cylinder to the purely viscous power-law fluid [29]. The polymeric fluids have both elastic and shear-thinning behavior, that could affect the non-isothermal flow physics. This

was analyzed using a differential-type White-Metzner model for the non-Newtonian behavior but the effect of Prandtl number on the overall Nusselt number was not reported [30].

1.3 Scope of Work

Originally this work started with computations of evolutions for flows around a circular cylinder. Soon, it became obvious that without massive parallel computing, this was a formidable task. In view of this, we limit the scope of present investigations to the numerical simulations of BVPs associated with the flows of incompressible Newtonian, power-law and Carreau fluids over a circular cylinder in $\mathbb{R}^2$. Both isothermal and non-isothermal cases are considered. The purpose of these studies is to provide benchmark quality numerical results for flow rates associated with Reynolds numbers of 20, 40 , 60, 100, and 200 for Newtonian fluids.

Details of the mathematical model in Eulerian description and its dimensionless term are given in Chapter 2. The system of non-linear partial differential equations (PDEs) resulting from the mathematical model are solved numerically using the hpk finite element method in which the integral form is constructed using the residual functionals resulting from the PDEs, i.e. least squares finite element method [31–34]. The discretizations and the choice of p-levels are determined to ensure that the residual functional is low enough (close to zero) to ensue the benchmark quality numerical results.

Chapter 2 gives details of the mathematical models including their dimensionless forms. Chapter 3 contains a brief description of the hpk least squares finite element processes in which the system of nonlinear algebraic equations are solved using Newton's linear method with line search. This approach yields variationally consistent [25, 31–35] integral

forms in which the resulting computational processes are unconditionally stable, i.e. the coefficient matrices in the algebraic systems are always positive definite. Chapter 3 also contains details of residual equations, local approximations and approximation spaces for both isothermal and non-isothermal cases. Numerical studies are presented in Chapter 4. Chapter 5 contains summary and conclusions. Additional numerical results are given in Appendices A and B.

Chapter 2

Mathematical Models

2.1 Introduction

In the development of the mathematical models in Eulerian description we consider the fluid to be isotropic, homogeneous and incompressible. The conservation of mass, balance of momenta and the first law of thermodynamics yield the familiar continuity equation, momentum equations and energy equation. The entropy inequality with decomposition of Cauchy stress tensor into equilibrium stress and deviatoric Cauchy stress tensor provides mechanisms for establishing equilibrium stress as mechanical pressure (by using incompressibility constraint). The constitutive theory for the deviatoric Cauchy stress tensor for Newtonian and generalized Newtonian fluids is based on rate constitutive theories derived using the theory of generators and invariants [36, 37]. The Fourier heat conduction law is assumed to hold for the heat vector. This can be derived using the entropy inequality, as well as, the theory of generators and invariants [36, 37]. The resulting mathematical model is non-dimensionalized using reference quantities and dimensionless variables. Details are

presented in the following sections.

2.2 Mathematical Model

We use Einstein notation to present details of the mathematical model. Let x_i; i = 1,2,3 be the x, y, z axes of the fixed orthogonal Cartesian frame and v_i; i = 1,2,3 be the u, v, w velocities at a material point located at x_i; i = 1,2,3 in the current configuration at time t. The reference configuration is assumed to be at time $t_0 = 0$. We generally use over bar (-) on all quantities to emphasize the Eulerian description. However, since in this work we only consider Eulerian description, over bar is omitted. It is understood that all dependent variables are functions of position coordinates x_i; i = 1,2,3 of a material point in the current configuration and time t.

The conservation of mass, balance of momenta and the first law of thermodynamics yield the continuity equation, momentum equations and energy equation [36, 37].

Continuity equation:

$$\rho \frac{\partial v_i}{\partial x_i} = 0 \tag{2.1}$$

Momentum equations (in the absence of body forces):

$$\rho \frac{\partial v_i}{\partial t} + v_j \frac{\partial v_i}{\partial x_j} + \frac{\partial p}{\partial x_i} - \frac{\partial \tau_{ij}}{\partial x_j} = 0 \tag{2.2}$$

Energy equation:

Assuming that the specific internal energy is given by $c_p T$, in which the specific heat c_p is constant, we can derive the following using first law of thermodynamics.

$$\rho c_p \left(\frac{\partial T}{\partial t} + v_i \frac{\partial T}{\partial x_i} \right) + \frac{\partial q_i}{\partial x_i} - \tau_{ij} \frac{\partial v_i}{\partial x_j} = 0 \tag{2.3}$$

In which v_i are the velocities in the x_i directions, ρ is density, $p = p(\theta)$ is mechanical pressure, τ_{ij} are deviatoric Cauchy stress tensor components in x-frame, q_i are heat fluxes and T is absolute temperature.

Equations (2.1) - (2.3) assume existence of τ_{ij} and q_i and hence are independent of the constitution of the matter. Dependence of τ_{ij} and q_i on the deformation field is established using the second law of thermodynamics, i.e. entropy inequality [36, 37].

2.2.1 Constitutive equations

Following references [36, 37], we can present the following constitutive equations for the deviatoric Cauchy stress tensor $[\tau]$ and the heat vector $\{q\}$.

Deviatoric Cauchy stress tensor $[\tau]$*:*

For a homogeneous, isotropic, and incompressible fluid, the first order rate theory [36, 37] gives the following.

$$\tau_{ij} = 2\eta D_{ij} \tag{2.4}$$

$$\text{in which} \qquad D_{ij} = \frac{1}{2}\left(\frac{\partial v_i}{\partial x_j} + \frac{\partial v_j}{\partial x_i}\right) \tag{2.5}$$

where D_{ij} is the symmetric part of the velocity gradient tensor (strain rate tensor) and η is the viscosity of the medium. The constitutive theory allows η to be a function of temperature T and the invariants of the strain rate tensor $[D]$. Due to incompressibility assumption, η is only dependent on the second invariant I_2 of $[D]$. Dependence of η on I_2 permits power-law model and Carreau model for η. In the case of Newtonian fluids, η is not a function of I_2 but can still be dependent on temperature T. We consider constant η in the present work.

Power-Law:

In the power-law model of viscosity [38] we consider

$$\eta = \eta^0 \left(I_2\right)^{\frac{n-1}{2}} \tag{2.6}$$

in which η^0 is zero shear rate viscosity, n is power-law index and I_2 is the second invariant of the strain rate tensor defined by

$$I_2 = \frac{1}{2}\left(\left(tr\left[D\right]\right)^2 - tr\left(\left[D\right]^2\right)\right) \tag{2.7}$$

where parameters η^0 and n are experimentally determined for a given fluid. For $n < 1$ and $n > 1$, the fluid is considered shear thinning and shear thickening, respectively. For $n = 1$ we recover Newtonian fluid.

Carreau Model:

In Carreau model of viscosity [38], we consider

$$\eta = \eta^0 + \left(\eta^0 - \eta^\infty\right)\left(1 + \lambda^2 I_2\right)^{\frac{m-1}{2}} \tag{2.8}$$

where η^∞ is the infinite shear rate viscosity, λ is a fluid constant and m is the fluid index. In power-law, as obvious from equation (2.6), for very low values of I_2, η increases drastically. In the limit of $I_2 \to 0$, $\eta \to \infty$. This is non-physical and presents serious problems in numerical simulations using power-law model for viscosity η [23]. In Carreau model, viscosity η approaches $\eta^0$and η^∞ asymptotically for zero and infinite shear rates, hence the problems associated with power-law model are avoided.

Heat Vector $\{q\}$:

We consider Fourier heat conduction law [36, 37] for the constitutive theory for $\{q\}$.

$$q_i = -k\frac{\partial T}{\partial x_i} \tag{2.9}$$

in which $k = k(T)$ is thermal conductivity of the medium. In the present work we consider constant thermal conductivity.

2.3 Mathematical Model in $\mathbb{R}^2$, Explicit Form: BVP

In the following we give explicit details of the mathematical model in $\mathbb{R}^2$ using u, v as velocities, x, y as coordinate directions and τ_{xx}, τ_{xy} and τ_{yy} as deviatoric Cauchy stress tensor components. Consider stationary state of the evolutions described by equations (2.1) - (2.3), i.e. BVP.

Continuity:

$$\rho\left(\frac{\partial u}{\partial x}+\frac{\partial v}{\partial y}\right)=0 \tag{2.10}$$

Momentum Equations:

$$\begin{aligned}\rho\left(u\frac{\partial u}{\partial x}+v\frac{\partial u}{\partial y}\right)+\frac{\partial p}{\partial x}-\frac{\partial \tau_{xx}}{\partial x}-\frac{\partial \tau_{xy}}{\partial y}=0\\ \rho\left(u\frac{\partial v}{\partial x}+v\frac{\partial v}{\partial y}\right)+\frac{\partial p}{\partial y}-\frac{\partial \tau_{xy}}{\partial x}-\frac{\partial \tau_{yy}}{\partial y}=0\end{aligned} \tag{2.11}$$

Energy Equation:

$$\begin{aligned}c_p\rho\left(u\frac{\partial T}{\partial x}+v\frac{\partial T}{\partial y}\right)+\frac{\partial q_x}{\partial x}+\frac{\partial q_y}{\partial y}-\\ \tau_{xx}\left(\frac{\partial u}{\partial x}\right)-\tau_{yy}\left(\frac{\partial v}{\partial y}\right)-\tau_{xy}\left(\frac{\partial u}{\partial y}+\frac{\partial v}{\partial x}\right)=0\end{aligned} \tag{2.12}$$

Constitutive Equations:

$$\tau_{xx}=2\eta\frac{\partial u}{\partial x},\quad \tau_{xy}=\eta\left(\frac{\partial u}{\partial y}+\frac{\partial v}{\partial x}\right),\quad \tau_{yy}=2\eta\frac{\partial v}{\partial y} \tag{2.13}$$

$$q_x=-k\frac{\partial T}{\partial x},\quad q_y=-k\frac{\partial T}{\partial y} \tag{2.14}$$

Equations (2.6) and (2.8) hold for power-law and Carreau model with I_2 given by

$$I_2=\left(\frac{\partial u}{\partial x}\right)\left(\frac{\partial v}{\partial y}\right)-\frac{1}{4}\left(\frac{\partial u}{\partial y}+\frac{\partial v}{\partial x}\right)^2 \tag{2.15}$$

2.4 Dimensionless Form of the Mathematical Model in $\mathbb{R}^2$

It is well known that in calculating the numerical solutions of the BVPs using finite element method, the GDEs in the mathematical model must be non-dimensionalized to ensure that the resulting algebraic system remains well conditioned [33]. We consider equations (2.10) - (2.15) and rewrite these using hat (ˆ) on all quantities indicating that all quantities have their usual units (i.e. dimensions). We introduce the following reference quantities and dimensionless variables.

$$
\begin{aligned}
&x = \hat{x}/L_0, \quad y = \hat{y}/L_0, \quad u = \hat{u}/u_0, \quad v = \hat{v}/u_0, \quad \eta = \hat{\eta}/\eta_0,\\
&p = \hat{p}/p_0, \quad \tau_{xx} = \hat{\tau}_{xx}/\tau_0, \quad \tau_{xy} = \hat{\tau}_{xy}/\tau_0, \quad \tau_{yy} = \hat{\tau}_{yy}/\tau_0,\\
&T = \hat{T}/T_0, \quad c_p = \hat{c}_p/c_{p_0}, \quad \rho = \hat{\rho}/\rho_0, \quad q_x = \hat{q}_x/q_0,\\
&q_y = \hat{q}_y/q_0, \quad k = \hat{k}/k_0
\end{aligned} \tag{2.16}
$$

We note that p_0 and τ_0 can not be independent of each other, hence we must choose $p_0 = \tau_0$. We can either choose

$$p_0 = \tau_0 = \rho_0 u_0^2, \qquad \text{characteristic kinetic energy} \tag{2.17}$$

$$\text{or} \qquad p_0 = \tau_0 = \frac{\eta_0 u_0}{L_0}, \qquad \text{characteristic viscous stress} \tag{2.18}$$

We generally consider the larger of the above two.

Using equations (2.16) and (2.10) - (2.15) with hat (ˆ) on all quantities, we substitute from (2.16) into (2.10) - (2.15) to derive the following.

Continuity:

$$\rho\left(\frac{\partial u}{\partial x} + \frac{\partial v}{\partial y}\right) = 0 \tag{2.19}$$

Momentum Equations:

$$\rho\left(u\frac{\partial u}{\partial x}+v\frac{\partial u}{\partial y}\right)+\left(\frac{p_0}{\rho_0 u_0^2}\right)\frac{\partial p}{\partial x}-\left(\frac{\tau_0}{\rho_0 u_0^2}\right)\left(\frac{\partial \tau_{xx}}{\partial x}+\frac{\partial \tau_{xy}}{\partial y}\right)=0$$
$$\rho\left(u\frac{\partial v}{\partial x}+v\frac{\partial v}{\partial y}\right)+\left(\frac{p_0}{\rho_0 u_0^2}\right)\frac{\partial p}{\partial y}-\left(\frac{\tau_0}{\rho_0 u_0^2}\right)\left(\frac{\partial \tau_{xy}}{\partial x}+\frac{\partial \tau_{yy}}{\partial y}\right)=0 \tag{2.20}$$

Energy Equation:

$$\frac{c_{p_0}\rho_0 u_0 T_0}{L_0}c_p\rho\left(u\frac{\partial T}{\partial x}+v\frac{\partial T}{\partial y}\right)+\frac{q_0}{L_0}\left(\frac{\partial q_x}{\partial x}+\frac{\partial q_y}{\partial y}\right)-$$
$$\frac{\tau_0 u_0}{L_0}\left(\tau_{xx}\frac{\partial u}{\partial x}+\tau_{yy}\frac{\partial v}{\partial y}+\tau_{xy}\left(\frac{\partial u}{\partial y}+\frac{\partial v}{\partial x}\right)\right)=0 \tag{2.21}$$

or

$$\frac{1}{\frac{u_0^2}{c_{p_0}T_0}}c_p\rho\left(u\frac{\partial T}{\partial x}+v\frac{\partial T}{\partial y}\right)+\frac{q_0}{\rho_0 u_0^3}\left(\frac{\partial q_x}{\partial x}+\frac{\partial q_y}{\partial y}\right)-$$
$$\frac{\tau_0}{\rho_0 u_0^2}\left(\tau_{xx}\frac{\partial u}{\partial x}+\tau_{yy}\frac{\partial v}{\partial y}+\tau_{xy}\left(\frac{\partial u}{\partial y}+\frac{\partial v}{\partial x}\right)\right)=0 \tag{2.22}$$

We leave equation (2.22) in this form for the time being.

2.4.1 Constitutive Equations for $[\tau]$:

Newtonian fluids:

$$\tau_{ij}=\left(\frac{\eta_0 u_0}{L_0\tau_0}\right)2\eta D_{ij} \tag{2.23}$$

Power-law fluids:

We begin with

$$\hat{\eta}=\hat{\eta}^0\left(\hat{I}_2\right)^{\frac{n-1}{2}} \tag{2.24}$$

or
$$\hat{\eta}=\left(\eta_0\left(\frac{u_0}{l_0}\right)^{n-1}\right)\eta^0\left(I_2\right)^{\frac{n-1}{2}} \tag{2.25}$$

$$\text{Let} \qquad \eta = \eta^0 \left(I_2\right)^{\frac{n-1}{2}} \tag{2.26}$$

$$\text{Then} \qquad \hat{\eta} = \eta_0 \left(\frac{u_0}{l_0}\right)^{n-1} \eta \tag{2.27}$$

where η is dimensionless viscosity.

Consider

$$\hat{\tau}_{ij} = 2\hat{\eta}\hat{D}_{ij} \tag{2.28}$$

Non-dimensionalizing (2.28) and substituting for $\hat{\eta}$ from (2.27) into (2.28), we get

$$\tau_{ij} = 2\frac{1}{\tau_0}\left(\eta_0 \left(\frac{u_0}{L_0}\right)^{n-1}\right)\eta\frac{u_0}{L_0}D_{ij} \tag{2.29}$$

$$\text{or} \qquad \tau_{ij} = 2\eta\left(\frac{\eta_0 u_0^n}{L_0^n \tau_0}\right)D_{ij} \tag{2.30}$$

If $\tau_0 = \rho_0 u_0^2$ then

$$\tau_{ij} = 2\eta\left(\frac{\eta_0}{\rho_0 L_0^n u_0^{2-n}}\right)D_{ij} \tag{2.31}$$

$$\text{or} \qquad \tau_{ij} = 2\eta\left(\frac{1}{Re_n}\right)D_{ij} \tag{2.32}$$

$$\text{where} \qquad Re_n = \frac{\rho_0 L_0^n u_0^{2-n}}{\eta_0}; \qquad \text{is Reynolds number for power-law fluid} \tag{2.33}$$

In summary, we have the following for power-law fluid.

$$\tau_{ij} = \frac{2\eta}{Re_n}D_{ij}$$

$$\eta = \eta^0 \left(I_2\right)^{\frac{n-1}{2}}$$

where η^0 is zero shear rate dimensionless viscosity.

Carreau Model:

Consider

$$\hat{\eta} = \hat{\eta}^0 + \left(\hat{\eta}^0 - \hat{\eta}^\infty\right)\left(1 + \lambda^2 \hat{I}_2\right)^{\frac{m-1}{2}} \tag{2.34}$$

$$\text{or} \qquad \hat{\eta} = \eta_0 \left(\eta^0 + \left(\eta^0 - \eta^\infty\right)\left(1 + \left(\frac{\lambda u_0}{L_0}\right)^2 I_2\right)^{\frac{m-1}{2}}\right) \tag{2.35}$$

Let

$$\frac{\lambda u_0}{L_0} = Cu; \qquad \text{Carreau number} \tag{2.36}$$

Substituting from (2.36) into (2.35)

$$\hat{\eta} = \eta_0 \left(\eta^0 + \left(\eta^0 - \eta^\infty\right)\left(1 + Cu^2 I_2\right)^{\frac{m-1}{2}}\right) = \eta_0 \eta \tag{2.37}$$

$$\text{where} \qquad \eta = \eta^0 + \left(\eta^0 - \eta^\infty\right)\left(1 + Cu^2 I_2\right)^{\frac{m-1}{2}} \tag{2.38}$$

with η, η^0 and η^∞ all being dimensionless viscosities.

Hence, for τ_{ij} we have

$$\tau_{ij} = 2\eta \left(\frac{\eta_0 u_0}{L_0 \tau_0}\right) D_{ij} \tag{2.39}$$

If $\tau_0 = \rho_0 u_0^2$ then

$$\tau_{ij} = 2\eta \left(\frac{\eta_0}{L_0 \rho_0 u_0}\right) D_{ij} \tag{2.40}$$

$$\text{or} \qquad \tau_{ij} = \frac{2\eta}{Re} D_{ij} \tag{2.41}$$

$$\text{where} \qquad Re = \frac{L_0 \rho_0 u_0}{\eta_0}; \qquad \text{Reynolds number} \tag{2.42}$$

Constitutive equation for $\{q\}$*:*

Consider

$$\{\hat{q}\} = -\hat{k} \begin{Bmatrix} \frac{\partial \hat{T}}{\partial \hat{x}} \\ \\ \frac{\partial \hat{T}}{\partial \hat{y}} \end{Bmatrix} \tag{2.43}$$

$$\text{or} \qquad \{q\} = -\frac{k_0 T_0}{L_0 q_0} k \begin{Bmatrix} \frac{\partial T}{\partial x} \\ \\ \frac{\partial T}{\partial y} \end{Bmatrix} \tag{2.44}$$

If we let

$$q_0 = \frac{k_0 T_0}{L_0} \tag{2.45}$$

then

$$\{q\} = -k \begin{Bmatrix} \frac{\partial T}{\partial x} \\ \\ \frac{\partial T}{\partial y} \end{Bmatrix} \tag{2.46}$$

is the dimensionless form of the constitutive equation for heat flux.

Now we go back to the energy equation (2.22) and use (2.45) for q_0.

$$\frac{1}{E_c} c_p \rho \left(u \frac{\partial T}{\partial x} + v \frac{\partial T}{\partial y} \right) + \frac{k_0 T_0}{L_0 \rho_0 u_0^3} \left(\frac{\partial q_x}{\partial x} + \frac{\partial q_y}{\partial y} \right) - \frac{\tau_0}{\rho_0 u_0^2} \left(\tau_{xx} \frac{\partial u}{\partial x} + \tau_{yy} \frac{\partial v}{\partial y} + \tau_{xy} \left(\frac{\partial u}{\partial y} + \frac{\partial v}{\partial x} \right) \right) = 0 \tag{2.47}$$

If we use Reynolds number, Brinkman number and Eckret number

$$Re = \frac{\rho_0 u_0 L_0}{\eta_0}, \qquad Br = \frac{\eta_0 u_0^2}{k_0 T_0}, \qquad E_c = \frac{u_0^2}{C_{p_0} T_0} \tag{2.48}$$

$$\text{then,} \qquad ReBr = \frac{L_0 \rho_0 u_0^3}{k_0 T_0} \tag{2.49}$$

Hence, (2.47) can be written as

$$\frac{1}{E_c} c_p \rho \left(u \frac{\partial T}{\partial x} + v \frac{\partial T}{\partial y} \right) + \frac{1}{ReBr} \left(\frac{\partial q_x}{\partial x} + \frac{\partial q_y}{\partial y} \right) - \frac{\tau_0}{\rho_0 u_0^2} \left(\tau_{xx} \frac{\partial u}{\partial x} + \tau_{yy} \frac{\partial v}{\partial y} + \tau_{xy} \left(\frac{\partial u}{\partial y} + \frac{\partial v}{\partial x} \right) \right) = 0 \tag{2.50}$$

This is the final dimensionless form of the energy equation.

The final dimensionless mathematical model consists of equations (2.19), (2.20) and (2.50) for the continuity equation, momentum equations and energy equation, and the constitutive equations for τ_{ij} and $\{q\}$ are already defined in previous sections.

2.5 Remarks

1. Consider the mathematical model for non-isothermal flow of Newtonian fluid in dependent variables u, v, p, τ_{xx}, τ_{yy}, τ_{xy}, T, q_x and q_y. In this mathematical model it is possible to solve for u, v, p, τ_{xx}, τ_{yy} and τ_{xy} using continuity equation, momenta equations and the constitutive equation for τ_{ij}. With u, v, p, τ_{xx}, τ_{yy} and τ_{xy} known, the energy equation and the heat flux equations can be used to solve for the temperature field T and the heat fluxes. This suggests that the energy equation and heat flux equations are decoupled from the rest of the mathematical model, or in other words the temperature field T, q_x and q_y are decoupled from u, v, p, τ_{xx}, τ_{yy} and τ_{xy}. On the other hand, appearance of the velocity field and stress tensor in the energy equation suggests coupling, or weak coupling, between the energy equation and heat fluxes and the rest of the mathematical model. Thus, it should be possible to solve for u, v, p, τ_{xx}, τ_{yy}, τ_{xy}, T, q_x and q_y using combined mathematical model. However, the deformation field obtained from the combined model must exhibit that u, v, p, τ_{xx}, τ_{yy} and τ_{xy} and not influenced by the thermal field, i.e. T, q_x and q_x.

2. Based on remark (1), it is straight forward to conclude that the deformation field u, v, p, τ_{xx}, τ_{yy} and τ_{xy} obtained using the mathematical model for the isothermal flows of Newtonian fluids, as well as, the one from the mathematical model for non-isothermal flows of Newtonian fluids should be identical.

3. In the case of generalized Newtonian fluids the viscosity is a function of the second invariant of the strain rate tensor, i.e. the viscosity is a function of the velocity gradients but independent of temperature (in the present work), hence remarks (1) and (2)

also hold for generalized Newtonian fluids.

4. In the present work we only consider shear thinning generalized Newtonian fluids in which the viscosity decreases with increasing scalar shear rates, i.e. increasing values of the second invariant of the strain rate tensor. Thus, for the same values of the strain rate tensor, shear thinning generalized Newtonian fluids produce lower or weaker stress fields compared to Newtonian fluids ($n = 1$ or $m = 1$).

5. In the present work we only consider the thermal field due to dissipation, i.e. we only consider conversion of mechanical energy into heat for an insulated system. Remarks (1)-(3) also hold for systems containing externally applied heat flux (heating or cooling) in addition to viscous dissipation.

Chapter 3

hpk Least Squares Finite Element Processes

3.1 Introductions

The mathematical models describing steady isothermal and non-isothermal 2D flows of Newtonian and generalized Newtonian fluids over a circular cylinder are a system of non-linear PDEs, i.e. non-linear boundary value problems. It has been shown by Surana et. al and co-workers [25, 31, 32, 34, 35] that hpk finite element processes based on the residual functional (least squares finite element method or process, LSP) are ideally suited for such BVPs containing non-linear differential operators. Authors have shown that when the system of non-linear algebraic equations resulting from the LSP are solved using Newton's linear method, in which the second variation of the residual is neglected in the second variation of the residual functional, the LSP yields a variationally consistent integral form that ensures unconditionally stable computational processes. The coefficient matrices in

the algebraic systems are always symmetric and positive definite. In the present work we use this approach for obtaining numerical solutions of the BVPs resulting from the mathematical models. A brief summary of the LSP and the solution procedure is presented in section 3.2. Sections 3.3 and 3.4 contain details of the local approximations, residuals and their variation for isothermal and non-isothermal flows.

3.2 Least Squares Finite Element Process Based on Residual Functional

Let the domain of definition $\bar{\Omega}$ of the BVP be discretized using nine node p-version 2D finite elements. Let $\bar{\Omega}^T = \underset{e}{\cup}\bar{\Omega}^e$ be the discretization of $\bar{\Omega}$ in which $\bar{\Omega}^e$ is the typical finite element 'e' such that $\bar{\Omega}^e = \Omega^e \cup \Gamma^e$ with Γ^e being the closed boundary of Ω^e.

Let ${}^i\phi \ ; \ i = 1, 2, ..., n$ be the dependent variables and ${}^i\phi_h^e \ ; \ i = 1, 2, ..., n$ be the local approximations of ${}^i\phi \ ; \ i = 1, 2, ..., n$ over $\bar{\Omega}^e$ such that ${}^i\phi_h = \underset{e}{\cup}{}^i\phi_h^e \ ; \ i = 1, 2, ..., n$ are the global approximations of ${}^i\phi \ ; \ i = 1, 2, ..., n$ over $\bar{\Omega}^T$ Let the local approximations ${}^i\phi_h^e \ ; \ i = 1, 2, ..., n$ be defined by

$$ {}^i\phi_h^e = \sum_{j=1}^{\underline{n}} {}^iN_j {}^i\delta_j^e = \left[{}^iN\right] \left\{{}^i\delta^e\right\} \ ; \ i = 1, 2, ..., n \tag{3.1} $$

In which ${}^iN_j$ are local approximation functions for a variable ${}^i\phi$, and $\{{}^i\delta^e\}$ are the nodal degrees of freedom (dofs). When ${}^i\phi_h^e \ ; \ i = 1, 2, ..., n$ are substituted in the PDEs, we obtain residuals $E_j^e \ ; \ j = 1, 2, ..., n$ over $\bar{\Omega}^e$ for an element 'e' of $\bar{\Omega}^T$. Let $\{\delta\} = \underset{e}{\cup}\{\delta^e\}$ and $\{\delta^e\} = \underset{i}{\cup}\{{}^i\delta^e\}$ be the dofs for $\bar{\Omega}^T$ and for an element 'e', respectively.

Let I and I^e be the residual functionals over $\bar{\Omega}^T$ and $\bar{\Omega}^e$, then we define the following conditions.

1. Existence of I (by construction):

$$I = \sum_e \sum_{j=1}^{n} \left(E_j^e, E_j^e\right)_{\bar{\Omega}^e} = \sum_e I^e \tag{3.2}$$

2. Necessary condition: If I is differentiable in its arguments (i.e.$\{\delta\}$) then $\delta I = 0$ is a necessary condition for an extremum of I.

$$\delta I = \sum_e \delta I^e = \sum_e \left(\sum_{j=1}^{n} 2\left(E_j^e, \delta E_j^e\right) \right) = 2 \sum_e \{g^e\} = 2\{g\} = 0 \tag{3.3}$$

$$\text{or} \qquad \{g\} = 0 \tag{3.4}$$

3. Sufficient condition or extremum principle [33]:

$$\delta^2 I \cong 2 \sum_e \left(\sum_{j=1}^{n} \left(\delta E_j^e, \delta E_j^e\right) \right) > 0 \qquad \forall\, \delta E_j^e \tag{3.5}$$

Thus a $\{\delta\}$ obtained from equation (3.4) minimizes I in (3.2).

Following Surana et. al and co-workers [31–33,35], we find a $\{\delta\}$ that satisfies $\{g\} = 0$ in (3.2) iteratively using Newton's linear method with line search. Let $\{\delta\}_0$ be an assumed solution, then

$$\{\Delta\delta\} = -\frac{1}{2}\left[\delta^2 I\right]^{-1}_{\{\delta\}_0} \{g\left(\{\delta\}_0\right)\} \tag{3.6}$$

$$\text{and} \qquad \{\delta\} = \{\delta\}_0 + \alpha\{\Delta\delta\}\ ; \qquad 0 < \alpha < 2 \tag{3.7}$$

$$\text{such that} \qquad I\left(\{\delta\}\right) \leq I\left(\{\delta\}_0\right) \tag{3.8}$$

If $\|g_i\|_{max} \leq \Delta$, a preset tolerance for zero, the we have a solution $\{\delta\}$ that satisfies $\{g\} = \{0\}$, otherwise we set $\{\delta\}_0 = \{\delta\}$ and repeat (3.2) - (3.8).

Thus, in order to use this procedure for a BVP we need: (i) local approximations for the dependent variables, (ii) residual equations resulting from the PDEs in the mathematical

model, (iii) variations of the residual equations and (iv) assumed or starting solution for $\{\delta\}_0$. We present details for the isothermal and non-isothermal cases in the following sections.

3.3 Least Squares Finite Element Process for 2D Non-Isothermal Case

3.3.1 Mathematical Model (Dimensionless Form):

Using $p_0 = \tau_0 = \rho_0 u_0^2$, we have the following

$$
\begin{aligned}
&\rho\left(\frac{\partial u}{\partial x}+\frac{\partial v}{\partial y}\right)=0\\
&\rho\left(u\frac{\partial u}{\partial x}+v\frac{\partial u}{\partial y}\right)+\frac{\partial p}{\partial x}-\left(\frac{\partial \tau_{xx}}{\partial x}+\frac{\partial \tau_{xy}}{\partial y}\right)=0\\
&\rho\left(u\frac{\partial v}{\partial x}+v\frac{\partial v}{\partial y}\right)+\frac{\partial p}{\partial y}-\left(\frac{\partial \tau_{xy}}{\partial x}+\frac{\partial \tau_{yy}}{\partial y}\right)=0\\
&\frac{c_p\rho}{E_c}\left(u\frac{\partial T}{\partial x}+v\frac{\partial T}{\partial y}\right)+\frac{1}{ReBr}\left(u\frac{\partial q_x}{\partial x}+v\frac{\partial q_y}{\partial y}\right)-\\
&\qquad\qquad \tau_{xx}\frac{\partial u}{\partial x}-\tau_{yy}\frac{\partial v}{\partial y}-\tau_{xy}\left(\frac{\partial u}{\partial y}+\frac{\partial v}{\partial x}\right)=0\\
&\tau_{xx}=\frac{2\eta}{R}\frac{\partial u}{\partial x},\quad \tau_{yy}=\frac{2\eta}{R}\frac{\partial v}{\partial y},\quad \tau_{xy}=\frac{\eta}{R}\left(\frac{\partial u}{\partial y}+\frac{\partial v}{\partial x}\right)\\
&q_x=-k\frac{\partial T}{\partial x},\quad q_y=-k\frac{\partial T}{\partial y}
\end{aligned}
\tag{3.9}
$$

in which $R = Re$ for Newtonian and Carreau fluids and $R = Re_n$ for power-law fluids. For Newtonian fluids we consider η to be constant.

For power-law fluids

$$\eta = \eta^0 \left(I_2\right)^{\frac{n-1}{2}} \tag{3.10}$$

For Carreau model fluids

$$\eta = \eta^0 + \left(\eta^0 - \eta^\infty\right)\left(1 + C_u^2 I_2\right)^{\frac{m-1}{2}} \tag{3.11}$$

$$\text{where} \qquad I_2 = \left(\frac{\partial u}{\partial x}\right)\left(\frac{\partial v}{\partial y}\right) - \frac{1}{4}\left(\frac{\partial u}{\partial y} + \frac{\partial v}{\partial x}\right)^2 \tag{3.12}$$

3.3.2 Local Approximations and Residual Equations:

Let the approximations for the dependent variables u, v, p, τ_{xx}, τ_{yy}, τ_{xy}, T, q_x and q_y over an element 'e' with domain $\bar{\Omega}^e$ be defined as

$$\begin{aligned}
&u_h^e = [N^u]\{u^e\}, \quad v_h^e = [N^v]\{v^e\}, \\
&p_h^e = [N^p]\{p^e\}, \quad (\tau_{xx})_h^e = [N^{\tau_{xx}}]\{\tau_{xx}^e\}, \\
&(\tau_{yy})_h^e = [N^{\tau_{yy}}]\left\{\tau_{yy}^e\right\}, \quad (\tau_{xy})_h^e = [N^{\tau_{xy}}]\left\{\tau_{xy}^e\right\}, \\
&T_h^e = \left[N^T\right]\{T^e\}, \quad (q_x)_h^e = [N^{q_x}]\{q_x^e\}, \\
&(q_y)_h^e = [N^{q_y}]\left\{q_y^e\right\}
\end{aligned} \tag{3.13}$$

in which $\{u^e\}$, $\{v^e\}$, $\{p^e\}$, $\{\tau_{xx}^e\}$, $\left\{\tau_{yy}^e\right\}$, $\left\{\tau_{xy}^e\right\}$, $\{T^e\}$, $\{q_x^e\}$ and $\left\{q_y^e\right\}$ are degrees of freedom for approximations u_h^e, v_h^e, p_h^e, $(\tau_{xx})_h^e$, $(\tau_{yy})_h^e$, $(\tau_{xy})_h^e$, T_h^e, $(q_x)_h^e$ and $(q_y)_h^e$. $[N^u]$, $[N^v]$,... are the corresponding local approximation functions. Equation (3.13) permits unequal degree and unequal order local approximations of the dependent variables over $\bar{\Omega}^e$. When (3.13) is substituted in (3.9), we obtain residual equations E_j^e ; $j = 1, 2, ..., 9 \quad \forall x, y \in \bar{\Omega}^e$.

$$\begin{aligned}
E_1^e &= \rho\left(\frac{\partial u_h^e}{\partial x} + \frac{\partial v_h^e}{\partial y}\right) \\
E_2^e &= \rho\left(u_h^e\frac{\partial u_h^e}{\partial x} + v_h^e\frac{\partial u_h^e}{\partial y}\right) + \frac{\partial p_h^e}{\partial x} - \left(\frac{\partial\left(\tau_{xx}\right)_h^e}{\partial x} + \frac{\partial\left(\tau_{xy}\right)_h^e}{\partial y}\right) \\
E_3^e &= \rho\left(u_h^e\frac{\partial v_h^e}{\partial x} + v_h^e\frac{\partial v_h^e}{\partial y}\right) + \frac{\partial p_h^e}{\partial y} - \left(\frac{\partial\left(\tau_{xy}\right)_h^e}{\partial x} + \frac{\partial\left(\tau_{yy}\right)_h^e}{\partial y}\right)
\end{aligned}$$

$$E_4^e = \frac{c_p \rho}{E_c}\left(u_h^e \frac{\partial T_h^e}{\partial x} + v_h^e \frac{\partial T_h^e}{\partial y}\right) + \frac{1}{ReBr}\left(\frac{\partial \left(q_x\right)_h^e}{\partial x} + \frac{\partial \left(q_y\right)_h^e}{\partial y}\right) - \left(\left(\tau_{xx}\right)_h^e \frac{\partial u_h^e}{\partial x} + \left(\tau_{yy}\right)_h^e \frac{\partial v_h^e}{\partial y} + \left(\tau_{xy}\right)_h^e \left(\frac{\partial u_h^e}{\partial y} + \frac{\partial v_h^e}{\partial x}\right)\right) \tag{3.14}$$

$$E_5^e = \left(\tau_{xx}\right)_h^e - \frac{2\eta}{R}\frac{\partial u_h^e}{\partial x}$$

$$E_6^e = \left(\tau_{yy}\right)_h^e - \frac{2\eta}{R}\frac{\partial v_h^e}{\partial y}$$

$$E_7^e = \left(\tau_{xy}\right)_h^e - \frac{\eta}{R}\left(\frac{\partial u_h^e}{\partial y} + \frac{\partial v_h^e}{\partial x}\right)$$

$$E_8^e = \left(q_x\right)_h^e - k\frac{\partial T_h^e}{\partial x}$$

$$E_9^e = \left(q_y\right)_h^e - k\frac{\partial T_h^e}{\partial y}$$

Variations of $E_i^e \ ; \ i = 1, 2, ..., 9$ can be obtained using

$$\delta E_i^e = \left\{\frac{\partial E_i^e}{\{\delta^e\}}\right\} \ ; \ i = 1, 2, ..., 9 \tag{3.15}$$

where

$$\{\delta^e\}^T = \left[\left[u^e\right], \left[v^e\right], \left[p^e\right], \left[\tau_{xx}^e\right], \left[\tau_{yy}^e\right], \left[\tau_{xy}^e\right], \left[T^e\right], \left[q_x^e\right], \left[q_y^e\right]\right] \tag{3.16}$$

Once we have $E_i^e, \delta E_i^e \ ; \ i = 1, 2, ..., 9$, the LSP follows the steps given in Section 3.2.

3.4 Least Squares Finite Element Process for 2D Isothermal Case

3.4.1 Mathematical Model (Dimensionless Form):

Using $p_0 = \tau_0 = \rho_0 u_0^2$, we have the following.

$$
\begin{aligned}
&\rho\left(\frac{\partial u}{\partial x}+\frac{\partial v}{\partial y}\right)=0\\
&\rho\left(u\frac{\partial u}{\partial x}+v\frac{\partial u}{\partial y}\right)+\frac{\partial p}{\partial x}-\left(\frac{\partial \tau_{xx}}{\partial x}+\frac{\partial \tau_{xy}}{\partial y}\right)=0\\
&\rho\left(u\frac{\partial v}{\partial x}+v\frac{\partial v}{\partial y}\right)+\frac{\partial p}{\partial y}-\left(\frac{\partial \tau_{xy}}{\partial x}+\frac{\partial \tau_{yy}}{\partial y}\right)=0\\
&\tau_{xx}=\frac{2\eta}{R}\frac{\partial u}{\partial x}\\
&\tau_{yy}=\frac{2\eta}{R}\frac{\partial v}{\partial y}\\
&\tau_{xy}=\frac{\eta}{R}\left(\frac{\partial u}{\partial y}+\frac{\partial v}{\partial x}\right)
\end{aligned}
\tag{3.17}
$$

3.4.2 Local Approximations and Residual Equations:

The local approximations for u, v, p, τ_{xx}, τ_{yy} and τ_{xy} follow equation (3.13). Upon substituting local approximations u_h^e, v_h^e, p_h^e, $(\tau_{xx})_h^e$, $(\tau_{yy})_h^e$ and $(\tau_{xy})_h^e$ from (3.13) into (3.17) we obtain residual equations $E_j^e\ ;\ j=1,2,...,6$ for $\bar{\Omega}^e$.

$$
\begin{aligned}
E_1^e&=\rho\left(\frac{\partial u_h^e}{\partial x}+\frac{\partial v_h^e}{\partial y}\right)\\
E_2^e&=\rho\left(u_h^e\frac{\partial u_h^e}{\partial x}+v_h^e\frac{\partial u_h^e}{\partial y}\right)+\frac{\partial p_h^e}{\partial x}-\left(\frac{\partial\left(\tau_{xx}\right)_h^e}{\partial x}+\frac{\partial\left(\tau_{xy}\right)_h^e}{\partial y}\right)\\
E_3^e&=\rho\left(u_h^e\frac{\partial v_h^e}{\partial x}+v_h^e\frac{\partial v_h^e}{\partial y}\right)+\frac{\partial p_h^e}{\partial y}-\left(\frac{\partial\left(\tau_{xy}\right)_h^e}{\partial x}+\frac{\partial\left(\tau_{yy}\right)_h^e}{\partial y}\right)\\
E_4^e&=(\tau_{xx})_h^e-\frac{2\eta}{R}\frac{\partial u_h^e}{\partial x}\\
E_5^e&=(\tau_{yy})_h^e-\frac{2\eta}{R}\frac{\partial v_h^e}{\partial x}\\
E_6^e&=(\tau_{xy})_h^e-\frac{\eta}{R}\left(\frac{\partial u_h^e}{\partial y}+\frac{\partial v_h^e}{\partial x}\right)
\end{aligned}
\tag{3.18}
$$

variations of E_i^e ; $i = 1, 2, ..., 6$ can be obtained using

$$\delta E_i^e = \left\{ \frac{\partial E_i^e}{\{\delta^e\}} \right\} \ ; \ i = 1, 2, ..., 6 \tag{3.19}$$

where

$$\{\delta^e\}^T = \left[[u^e], [v^e], [p^e], [\tau_{xx}^e], \left[\tau_{yy}^e\right], \left[\tau_{xy}^e\right] \right] \tag{3.20}$$

3.5 Transport properties

For Newtonian fluid we assume η and k to be constant and $R = Re$.

For power-law model

$$\eta = \eta^0 \left(I_2\right)^{\frac{n-1}{2}} \tag{3.21}$$

$$\text{where} \qquad I_2 = \left(\frac{\partial u_h^e}{\partial x}\right)\left(\frac{\partial v_h^e}{\partial y}\right) - \frac{1}{4}\left(\frac{\partial u_h^e}{\partial y} + \frac{\partial v_h^e}{\partial x}\right)^2 \tag{3.22}$$

$$\text{and} \qquad R = Re_n \tag{3.23}$$

For Carreau model

$$\eta = \eta^0 + \left(\eta^0 - \eta^\infty\right)\left(1 + Cu^2 I_2\right)^{\frac{m-1}{2}} \tag{3.24}$$

I_2 is the same as in equation (3.22) and $R = Re$.

3.6 Approximation Spaces

We choose $H^{p,k}\left(\bar{\Omega}^e\right)$ spaces for local approximations with $k = 1$, $p \geq 2k - 1$. In LSP equal order, equal degree local approximations yield convergent finite element processes, hence we use this in the present work. When $k = 1$, i.e. local approximations of class $C^0\left(\bar{\Omega}^e\right)$, the integrals in the least squares process are in Lebesgue sense. For $k \geq 2$, all integrals in the least squares finite element process are Riemann.

Chapter 4

Numerical Studies

4.1 Introduction

In this chapter we present numerical studies for isothermal and non-isothermal flows of Newtonian, power-law and Carreau fluids for flow over a circular cylinder at Reynolds numbers of 20, 40, 60, 100, and 200 using mathematical models described in Chapter 2 and the hpk finite element computational framework presented in Chapter 3. We consider local approximations of class $C^0\left(\bar{\Omega}^e\right)$ for all dependent variables with equal p-levels. The size of the physical domain, discretization and the p-levels are chosen such that: (i) the boundaries of the domain do not influence the flow features around the cylinder, (ii) the residual functional I in all numerical studies is of the order of $O\left(10^{-6}\right)$ or lower, (iii) the Newton's linear method with line search is considered converged when $\|g_i\|_{max} \leq O\left(10^{-6}\right)$. Even though the local approximations of class $C^0\left(\bar{\Omega}_x\right)$ produce inter-element discontinuities of the deviations of the dependent variables normal to the boundaries, the residual I values of the order of $O\left(10^{-6}\right)$ or lower ensure that these are not significant in

the numerical results presented in this chapter.

4.2 Transport Properties

In all numerical studies presented in this chapter we use the following transport properties of Newtonian, power-law and Carreau fluids.

4.2.1 Newtonian Fluid

We assume $\hat{\eta}$ to be constant. We consider Newtonian behavior of the polymeric fluid called Tylose MH 4000 with 1% concentration with the following transport properties

$$\hat{\rho} = 1001 \text{ kg/m}^2, \quad \hat{\eta} = 0.180 \text{ kg/(m-s)}, \quad \hat{k} = 0.268 \text{ W/m/K}, \quad \hat{c_p} = 2.367 \text{ KJ/kg/K}$$

4.2.2 Power-Law Fluid

For shear thinning Tylose MH 4000 with 1% concentration we have the following transport properties based on Machac et. al [39].

$$\hat{\rho} = 1001 \text{ kg/m}^2, \quad \hat{\eta}^0 = 0.332 \text{ kg/(m-s)}, \quad n = 0.738$$

$$\hat{k} = 0.268 \text{ W/m/K}, \quad \hat{c_p} = 2.367 \text{ KJ/kg/K}$$

4.2.3 Carreau Fluid (Isothermal)

Also based on Machac et. al [39], Tylose MH 4000 with 1% concentration can be described using Carreau model with the following transport properties

$$\hat{\rho} = 1001 \text{kg/m}^2, \quad \hat{\eta}^0 = 0.180 \text{ kg/(m-s)}, \quad \hat{\eta}^\infty = 0 \text{ kg/(m-s)}$$

$$\lambda = 0.048, \quad m = 0.729, \quad \hat{k} = 0.268 \text{ W/m/K}, \quad \hat{c_p} = 2.367 \text{ KJ/kg/K}$$

In all studies we choose $D_0 = 1.5$ cm and $L_0 = 0.03$ m, hence $D = 0.5$ (dimensionless cylinder diameter.

4.3 Domain Size, Discretization and p-levels

Figure 4.1(a) shows a schematic of the domain in the physical space. Figure 4.1(b) shows the schematic in the dimensionless space. Due to the symmetry conditions, we only need to consider the lower half (or the upper half) of the total domain. Figures 4.1(c) and 4.1(d) show the computational domain in the dimensionless space including the isothermal boundary conditions. At the inlet we assume constant velocity, $u = 1$. Boundaries at $y = 0$ and $y = H$ are planes of symmetry. Velocity u on the boundary located at $y = H$ is the same as the inlet velocity, i.e. $u = 1$. All external boundaries are assumed insulated so that there is no heat flow in or out of the domain. The computational domain is divided into different zones shown in figure 4.2. The sizes of the sub-domains (shown in yellow) are kept fixed (dimensions of domain are shown in figures 4.1(a) and 4.1(b)). Length L_1 and height H are varied to arrive at their values such that the boundaries do not influence the flow around and in the neighborhood of the cylinder. For this purpose we consider Newtonian fluid with constant properties. The discretization details for various regions of the computational domain are considered in the following. These studies are conducted for all values of Reynolds numbers to ensure adequate choices of length L_1 and height H, even though the determination of adequate L_1 and H for the lowest Reynolds number would suffice for higher values of Reynolds numbers as well. Numerical studies for this case are presented for $Re = 200$. Similar behavior and conclusions hold for lower Reynolds

numbers.

In these studies we choose $L_1 = 2.5,\ 5.0,\ 10.0$ and $H = 2.5,\ 5.0,\ 10.0,\ 20.0$. For a fixed value of L_1, H is varied to 2.5, 5.0, 10.0 and 20.0, yielding a series of solutions that are compared to decide the best choices of L_1 and H for which boundaries do not influence the flow around and in the neighborhood of the cylinder. We choose isothermal Newtonian fluid with the following values of the reference quantities.

$\rho_0 = \hat{\rho} = 1001$ kg/m^2, $\quad \eta_0 = \hat{\eta} = 0.180$ kg/(m-s), $\quad c_{p_0} = \hat{c_p} = 2.367$ KJ/kg/K,

$k_0 = \hat{k} = 0.268$ W/m/K, $\quad L_0 = 0.03$ m, $\quad T_0 = 293.15$ K

$u_0 =$ 0.11988 m/s, 0.23976 m/s, 0.35964 m/s, 0.5994 m/s and 1.1988 m/s

These give $\rho = 1$, $\eta = 1$, $C_p = 1$, $k = 1$ and $Re =$ 20, 40, 60, 100 and 200. We consider $Re =$ 200 in the following studies. In the first study, we choose $L_1 = 2.5$ and consider H values of 2.5, 5.0, 10.0 and 20.0. The discretization used is shown in figure 4.3. p-level of 5 is chosen based on the p-convergence studies for the discretization in figure 4.3. The studies are repeated for $L_1 = 5.0$ and $L_1 = 10.0$ using $H =$ 2.5, 5.0, 10.0 and 20.0. The behavior of the pressure p is perhaps the best measure of the quality of the solution and hence is presented in this section to compare results obtained from various contributions of L_1 and H. Details of the discretizations used for various sub-domains of the computational domain for different choices of L_1 and H are given in Appendix A in various figures listed below.

Figure A.1: $L_1 = 2.5,\ H = 5.0$; Figure A.2: $L_1 = 2.5,\ H = 10.0$

Figure A.3: $L_1 = 2.5,\ H = 20.0$; Figure A.9: $L_1 = 5.0,\ H = 2.5$

Figure A.10: $L_1 = 5.0,\ H = 5.0$; Figure A.11: $L_1 = 5.0,\ H = 10.0$

Figure A.12: $L_1 = 5.0,\ H = 20.0$; Figure A.18: $L_1 = 10.0,\ H = 2.5$

Figure A.19: $L_1 = 10.0,\ H = 5.0$; Figure A.20: $L_1 = 10.0,\ H = 10.0$

Figure A.21: $L_1 = 10.0,\ H = 20.0$

Figures 4.4 - 4.6 show plots of p versus y at $x = 0$ for $L_1 = 2.5$, 5.0 and 10.0. Each plot shows results for $H = 2.5$, 5.0, 10.0 and 20.0. We note for $L_1 = 10$ and $H = 10$ the results are almost the same as for $L_1 = 10$ and $H = 20$. Thus, we can conclude that for $L_1 = 10$ and $H = 10$ we have sufficient inlet length and height to ensure that the boundaries of the domain do not influence the flow around and in the neighborhood of the cylinder. The graphs of $u\,(x)$, $u\,(y)$, $v\,(y)$, $\tau_{xy}\,(y)$ and $p\,(x)$ for various combinations of L_1 and H are also presented for isothermal flow of Newtonian fluid in Appendix A.

For $L_1 = 2.5$:

Figure A.4: u versus y at $x = 0$; Figure A.5: v versus y at $x = 0$

Figure A.6: τ_{xy} versus y at $x = 0$; Figure A.7: u versus x at $y = 0$

Figure A.8: p versus x at $y = 0$

For $L_1 = 5.0$:

Figure A.13: u versus y at $x = 0$; Figure A.14: v versus y at $x = 0$

Figure A.15: τ_{xy} versus y at $x = 0$; Figure A.16: u versus x at $y = 0$

Figure A.17: p versus x at $y = 0$

For $L_1 = 10.0$:

Figure A.22: u versus y at $x = 0$; Figure A.23: v versus y at $x = 0$

Figure A.24: τ_{xy} versus y at $x = 0$; Figure A.25: u versus x at $y = 0$

Figure A.26: p versus x at $y = 0$

These also confirm that $L_1 = 10$ and $H = 10$ are good choices for $Re = 200$. Numerical studies conducted for other Reynolds numbers confirm these values of L_1 and H to be adequate.

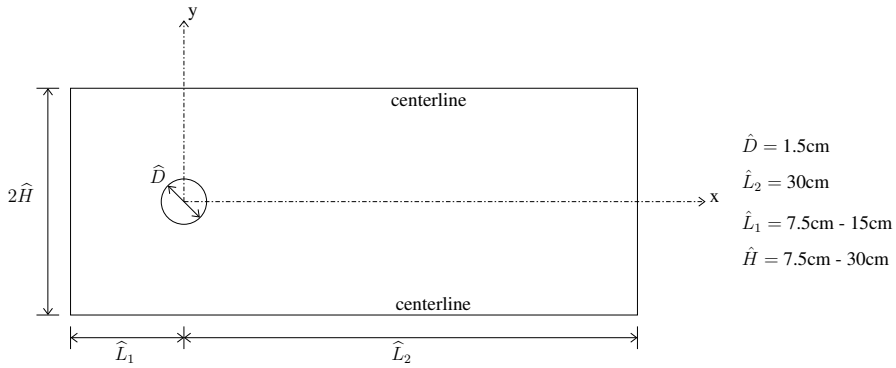

(a) Schematic of Physical Domain

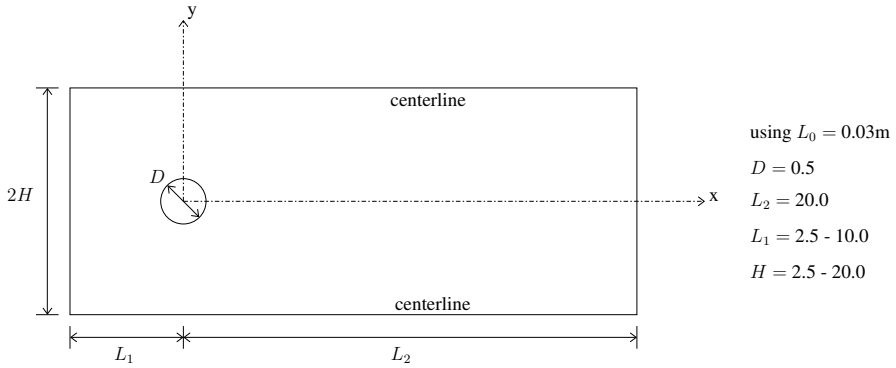

(b) Schematic of Dimensionless Domain

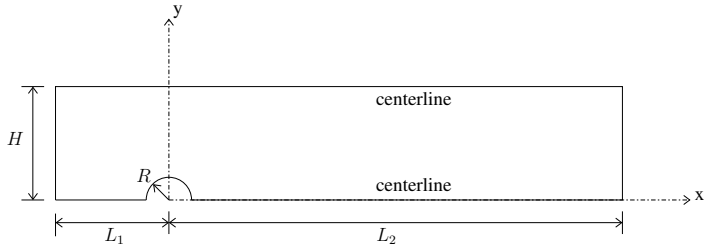

(c) Schematic of Computational Domain

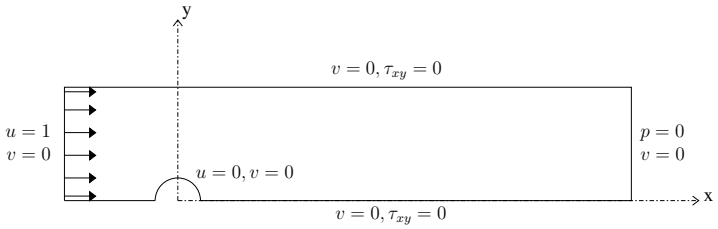

(d) Schematic of Isothermal Boundary Conditions

Figure 4.1: Schematics

Figure 4.2: Subdivisions of Computational Domain into Zones

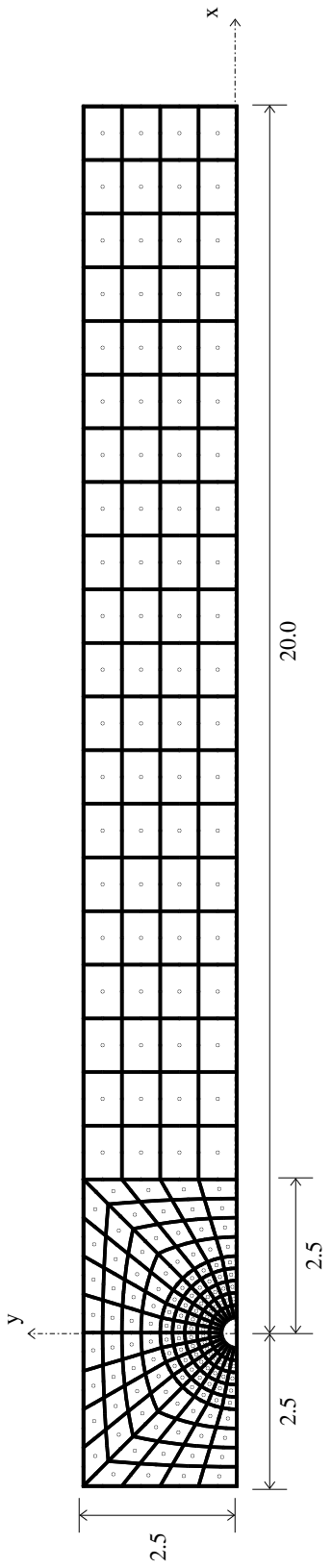

Figure 4.3: A 224 Element Discretization for L_1 = 2.5 and H = 2.5

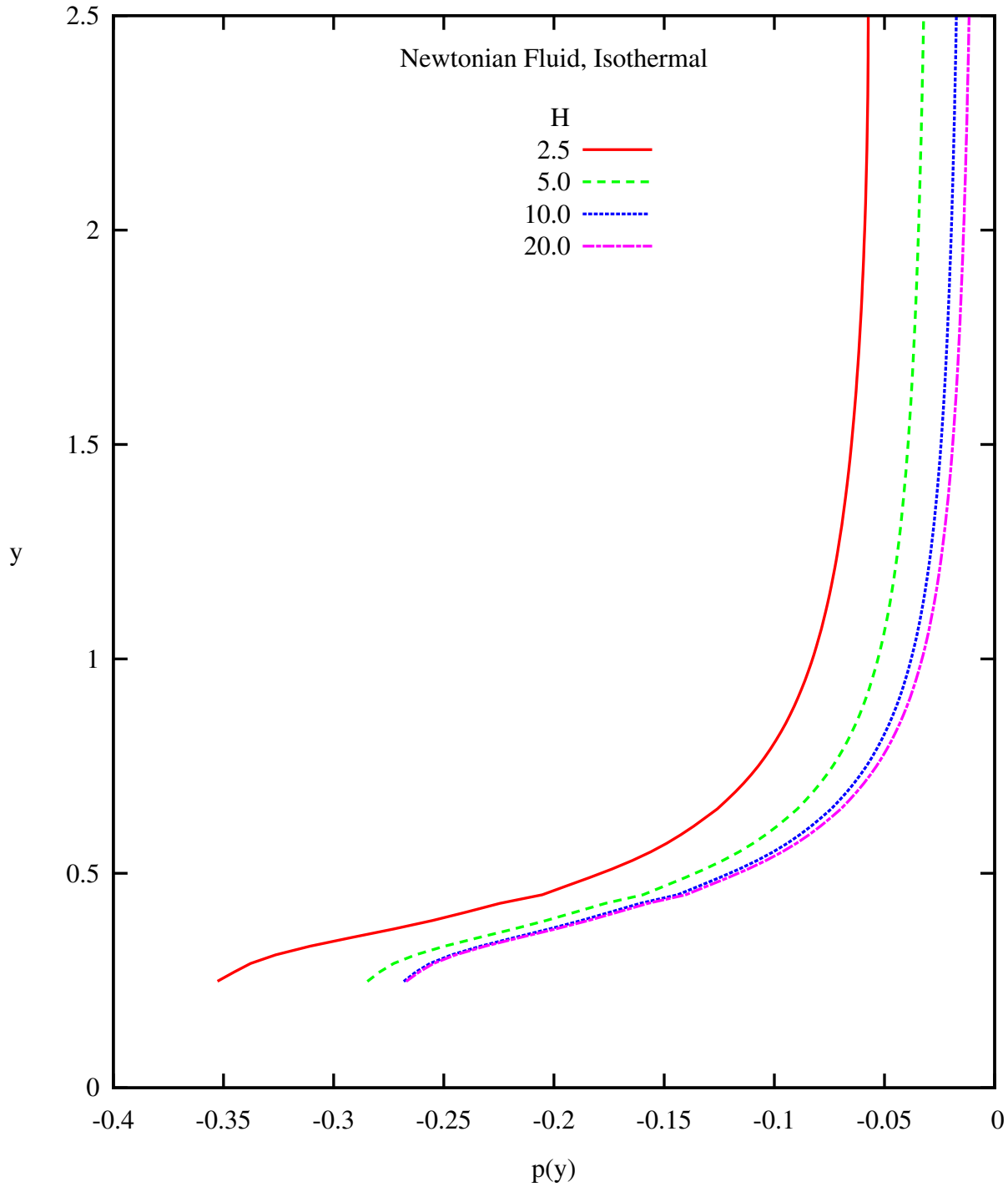

Figure 4.4: Pressure p versus y at $x = 0$ (Newtonian Fluid, Isothermal): L_1 = 2.5, Re = 200

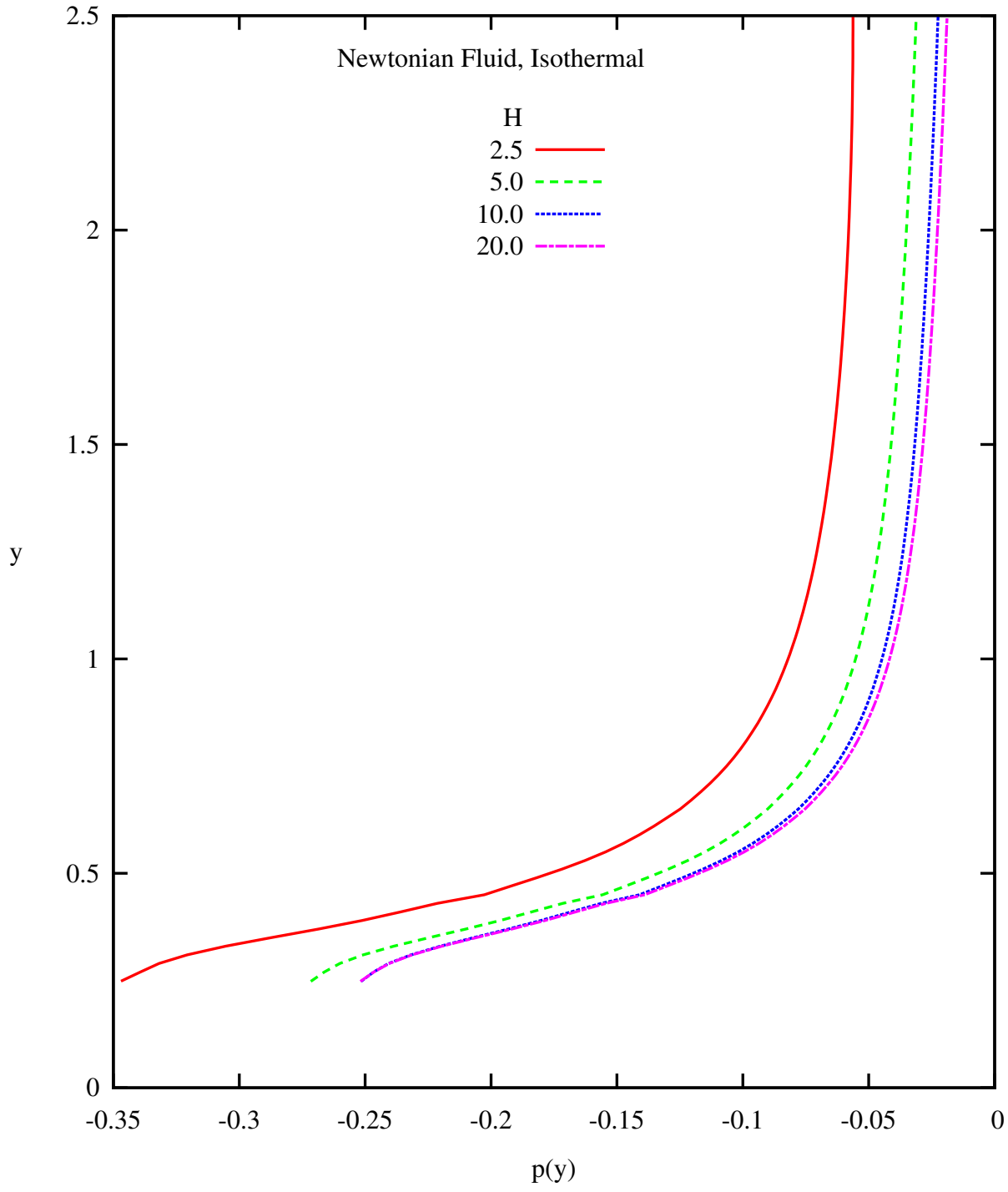

Figure 4.5: Pressure p versus y at $x = 0$ (Newtonian Fluid, Isothermal): L_1 = 5.0, Re = 200

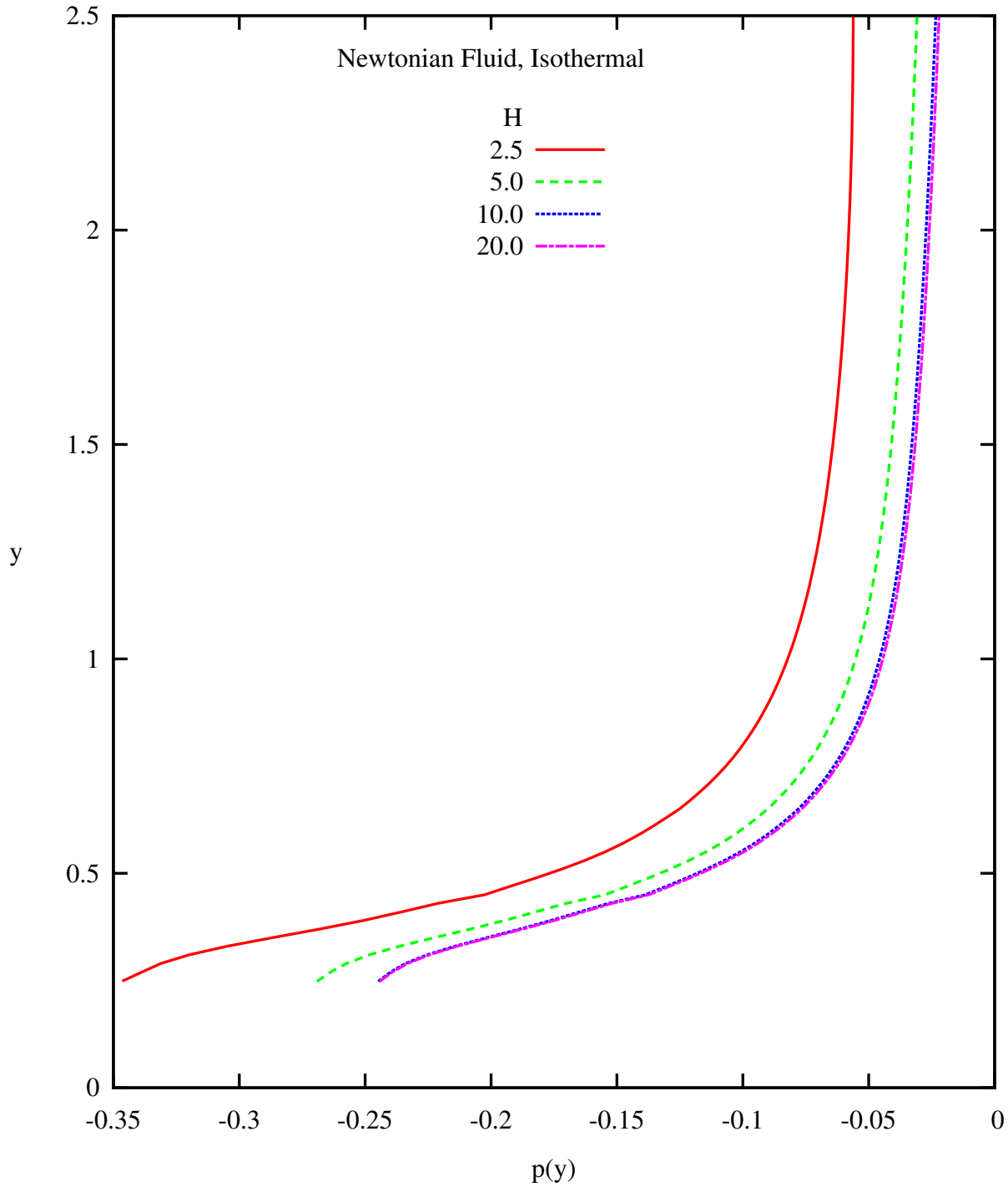

Figure 4.6: Pressure p versus y at $x = 0$ (Newtonian Fluid, Isothermal): L_1 = 10.0, Re = 200

4.4 Isothermal flows

In this section we present numerical studies for isothermal flow of Newtonian, power-law and Carreau fluids using $L_1 = 10.0$, $L_2 = 20.0$, $L_3 = L_4 = H_1 = 2.5$, $H = 10.0$ and $D = 0.5$. The discretization around the cylinder is further refined (figures 4.7 and 4.8) to ensure accuracy of the computed results. The reference velocity u_0 is varied ($u_0 = 0.11988$ m/s, 0.23976 m/s, 0.35964 m/s, 0.5994 m/s and 1.1988 m/s) to obtain desired Reynolds numbers of 20, 40, 60, 100 and 200 for Newtonian and Carreau fluids. Re_n for power-law fluid will obviously be different. Table 4.1 provides details of u_0, Re and Re_n.

	Newtonian $n = 1$	Power-Law $n = 0.738$	Carreau $n = 0.729$
u_0	Re	Re_n	Re
0.11988	20	15.6	20
0.23976	40	37.4	40
0.35964	60	62.4	60
0.5994	100	118.8	100
1.1988	200	285.0	200

Table 4.1: Reynolds numbers for Newtonian, Power-Law and Carreau Fluids Corresponding to u_0

We present the numerical results for all three fluids in the following sections, as well as, the discussion of the results.

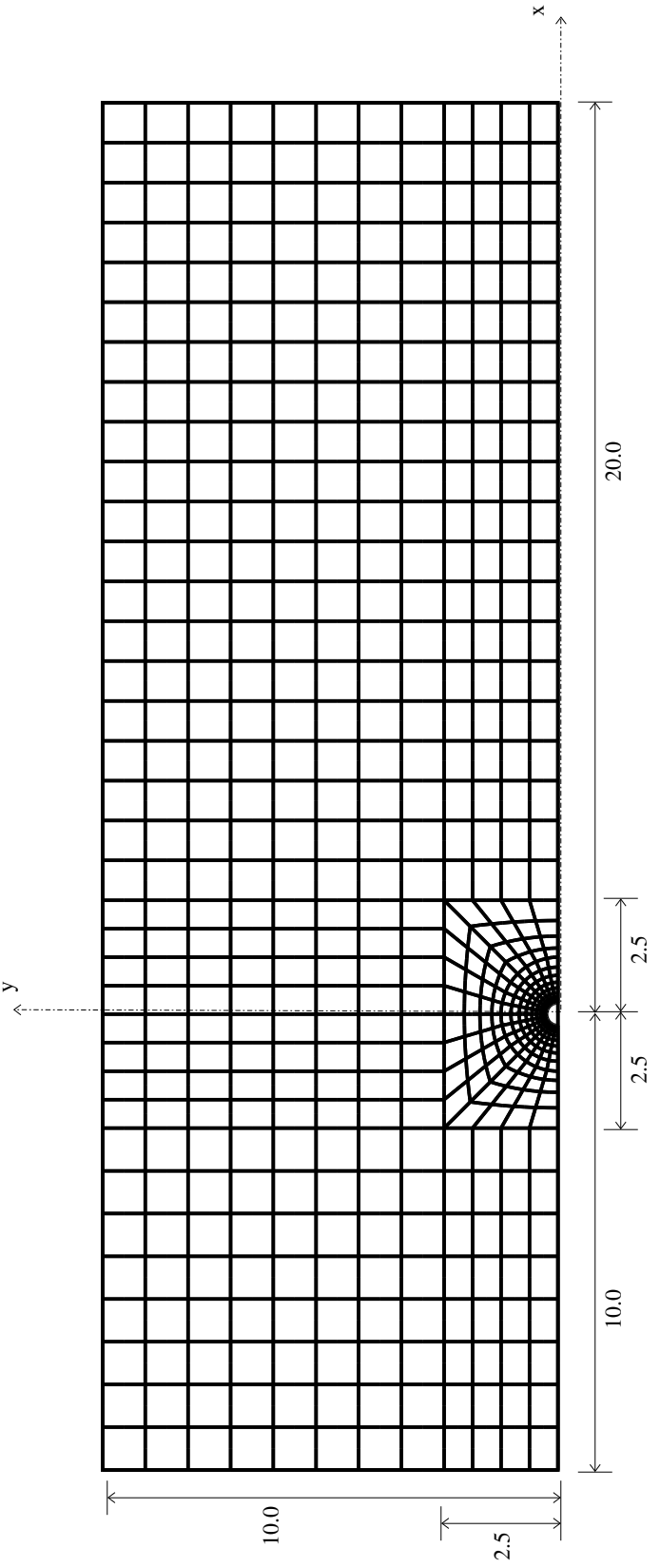

Figure 4.7: A 592 Element Discretization Used for Both Isothermal and Non-isothermal Flows with L_1 = 10.0 and H = 10.0

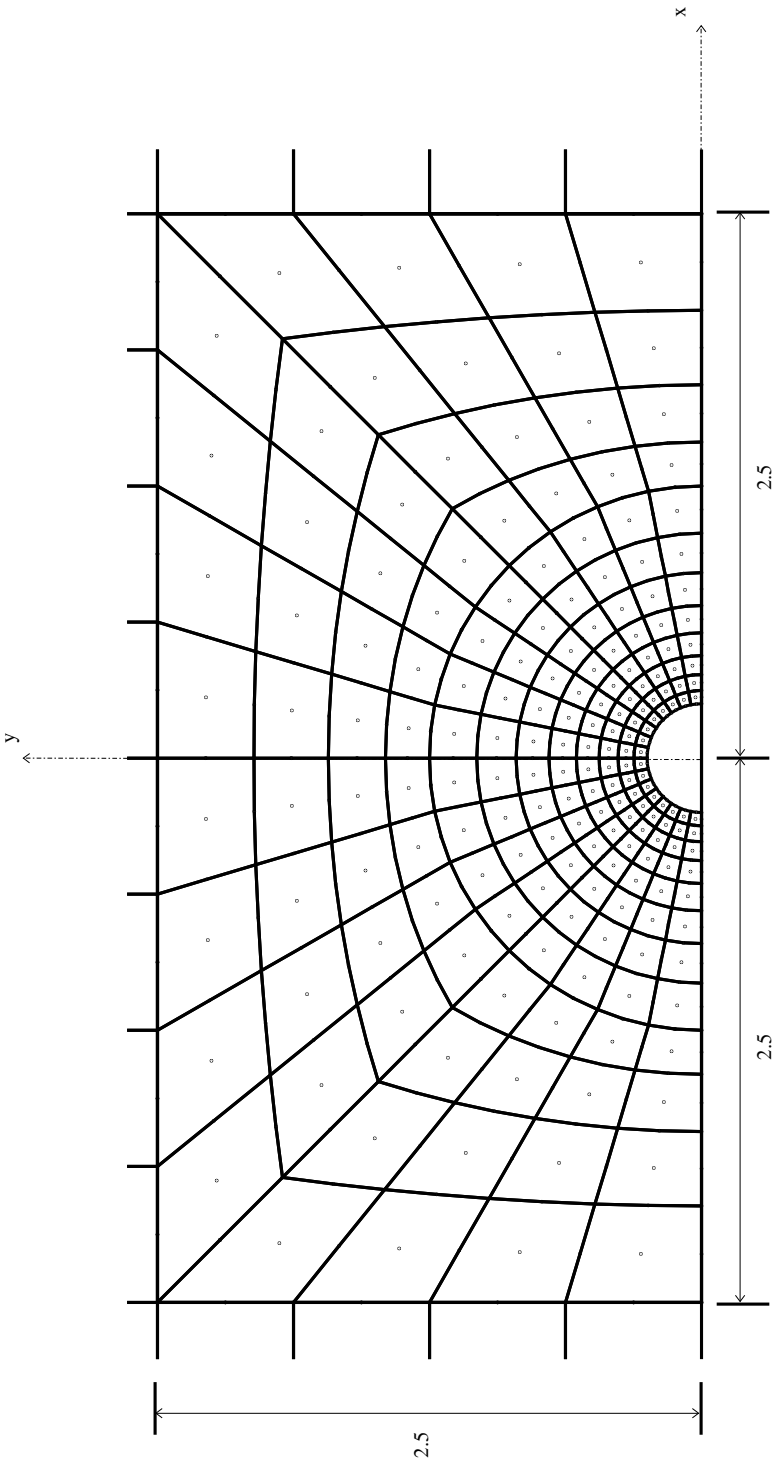

Figure 4.8: Element Discretization in the Vicinity of the Cylinder for Both Isothermal and Non-isothermal Flows with L_1 = 10.0 and H = 10.0

4.4.1 Newtonian Fluid (Isothermal Flows)

We use the following values of the reference quantities for Newtonian fluid.

$\rho_0 = \hat{\rho} = 1001$ kg/m^2, $\eta_0 = \hat{\eta} = 0.180$ kg/(m-s), $c_{p_0} = \hat{c_p} = 2.367$ KJ/kg/K,

$k_0 = \hat{k} = 0.268$ W/m/K, $L_0 = 0.03$ m, $T_0 = 293.15$ K

$u_0 =$ 0.11988 m/s, 0.23976 m/s, 0.35964 m/s, 0.5994 m/s and 1.1988 m/s

The corresponding Reynolds numbers are $Re =$ 20, 40, 60, 100 and 200. Plots of u, v, p, τ_{xy} versus y at $x = 0$ and u, p versus x at $y = 0$ are shown in figures 4.9 - 4.14 for Re = 20, 40, 60, 100 and 200. Contour (or carpet) plots of velocity u and streamlines for Re = 20, 40, 60, 100 and 200 are shown in figures 4.15 - 4.17. Similar plots for pressure p for Re = 20, 40, 60, 100 and 200 are shown in figures 4.18 - 4.20 and those of τ_{xy} in figure 4.21 - 4.23.

4.4.2 Power-Law Fluid (Isothermal Flows)

In the case of power-law fluid, we use the following values of the reference quantities.

$\rho_0 = \hat{\rho} = 1001$ kg/m^2, $\eta^0 = \hat{\eta} = 0.332$ kg/(m-s), $c_{p_0} = \hat{c_p} = 2.367$ KJ/kg/K,

$k_0 = \hat{k} = 0.268$ W/m/K, $L_0 = 0.03$ m, $T_0 = 293.15$ K, $n = 0.738$

$u_0 =$ 0.11988 m/s, 0.23976 m/s, 0.35964 m/s, 0.5994 m/s and 1.1988 m/s

The corresponding Reynolds numbers are $Re_n =$ 15.6, 37.4, 62.4, 118.8 and 285.0. The discretizations shown in figures 4.7 and 4.8 are also used in these numerical studies with p-level of 5. Plots of u, v, p, τ_{xy} versus y at $x = 0$ and u, p versus x at $y = 0$ are shown in figures 4.24 - 4.29 for Re_n = 15.6, 37.4, 62.4, 118.8 and 285.0 that correspond to the same

u_0 as used for Newtonian fluids for Re = 20, 40, 60, 100 and 200. Carpet and contour plots are omitted as their behavior is similar to Newtonian fluid.

4.4.3 Carreau Fluid (Isothermal Flows)

In the case of Carreau fluid, we use the following values of the reference quantities.

$\rho_0 = \hat{\rho} = 1001$ kg/m^2, $\quad \eta^0 = \hat{\eta} = 0.180$ kg/(m-s), $\quad c_{p_0} = \hat{c_p} = 2.367$ KJ/kg/K,

$k_0 = \hat{k} = 0.268$ W/m/K, $\quad L_0 = 0.03$ m, $\quad T_0 = 293.15$ K,

$m = 0.729$, $\quad \lambda = 0.048$, $\quad \eta^\infty = 0$ kg/(m-s),

$u_0 =$ 0.11988 m/s, 0.23976 m/s, 0.35964 m/s, 0.5994 m/s and 1.1988 m/s

The corresponding Reynolds numbers are $Re = 20$, 40, 60, 100 and 200. The discretizations shown in figures 4.7 and 4.8 are also used in these numerical studies with p-level of 5. Plots of u, v, p, τ_{xy} versus y at $x = 0$ and u, p versus x at $y = 0$ are shown in figures 4.30 - 4.35 for Re = 20, 40, 60, 100 and 200. Carpet plots are not presented as their appearance is similar to Newtonian fluids.

4.4.4 Discussion and Comparison of Results (Isothermal Flows)

If flow rate $\hat{Q}$ and the dimensionless flow rate Q at the inlet are given by

$$Q = \frac{\hat{Q}}{u_0 L_0} = \frac{\hat{Q}}{Q_0} = \int_{-H}^{H} u dx = \text{constant} \tag{4.1}$$

and since u = 1 at the inlet for all Reynolds numbers, the dimensionless flow rate is constant in all numerical studies throughout the domain, clearly implying that flow rate Q (more complex than (4.1) as we move closer to cylinder) is constant at any cross-section.

Thus, in figure 4.9 for Newtonian fluid , $u\,(y)$ versus y at $x = 0$, we clearly observe the increase in peak velocity with progressively increasing Reynolds numbers, however Q remains constant for all Reynolds numbers. Similarly, peak values of v also increase with progressively increasing Reynolds numbers. p and τ_{xy} adjust accordingly. We also notice rise in peak value of velocity u in figure 4.13 ($u\,(x)$ versus x at $y = 0$).

In the cases of power-law and Carreau fluids (shear thinning), the viscosity decreases with increasing shear rate. At low shear rate, the viscosity is not affected much by I_2, hence we expect similar behavior as Newtonian case for increasing, but still low, Reynolds numbers (figures 4.24 and 4.30). At $Re_n = 285.0$ and $Re = 200$, we observe decrease in the peak velocity compared to $Re_n = 118.8$ and $Re = 100$. Velocity v continues to increase at these Reynolds numbers but not as significantly as in Newtonian case (figures 4.25 and 4.31). Figures 4.36 - 4.41 show plots of u, v, p, τ_{xy} versus y at $x = 0$ and u, p versus x at $y = 0$ for Re = 20 (15.6, P.L.) and Re = 200 (285.0, P.L.) for Newtonian, power-law and Carreau model. These figures demonstrate that the difference between power-law and Carreau model fluids is localized around the cylinder for high Reynolds number but is not for low Reynolds number. All repeated results are free of oscillations and satisfy constant flow rate condition. In all cases $I \leq O\,(10^{-6})$ and $\|g_i\|_{max} \leq O\,(10^{-6})$ are obtained, confirming good accuracy of the results.

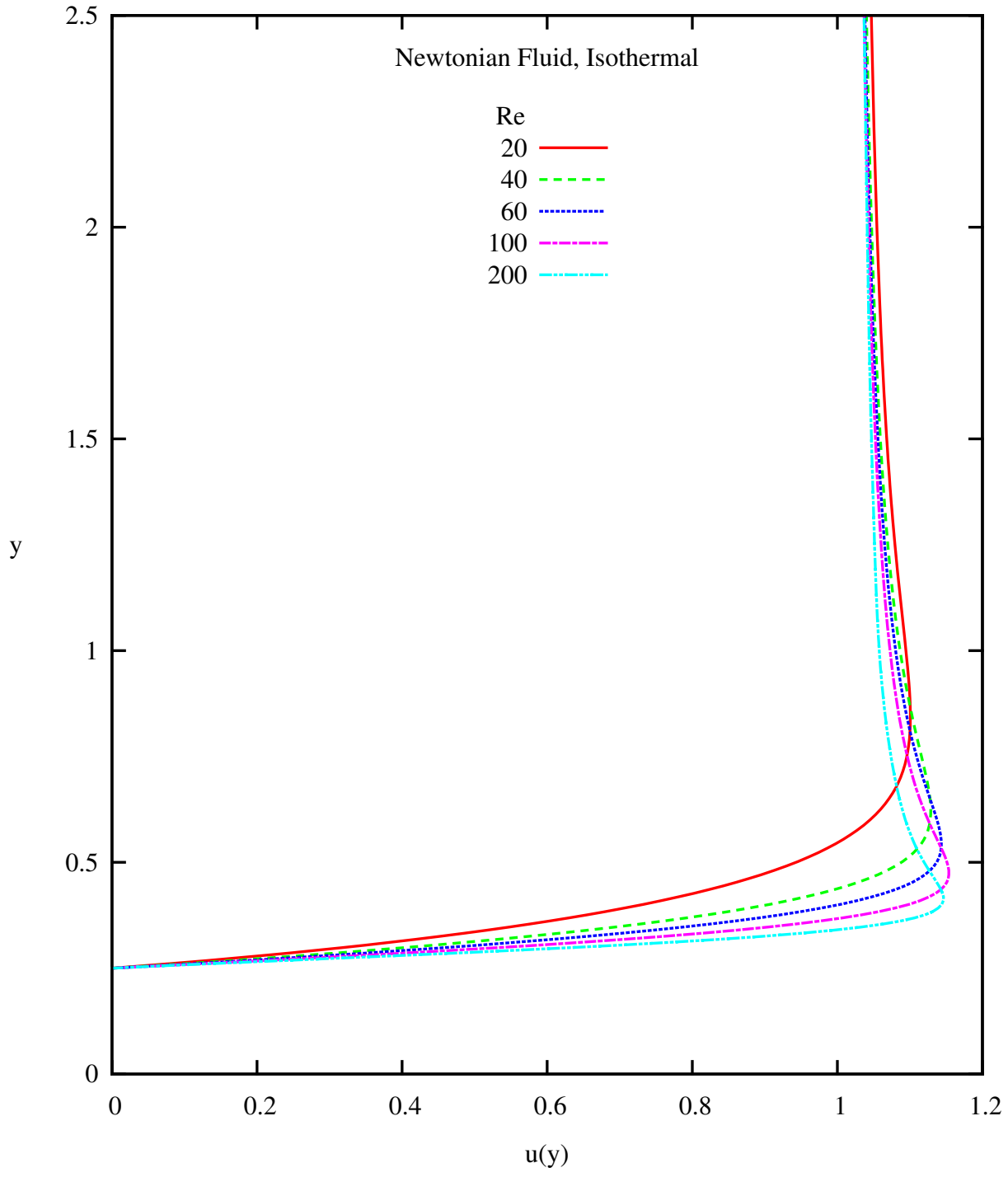

Figure 4.9: Velocity u versus y at $x = 0$ (Newtonian, Isothermal)

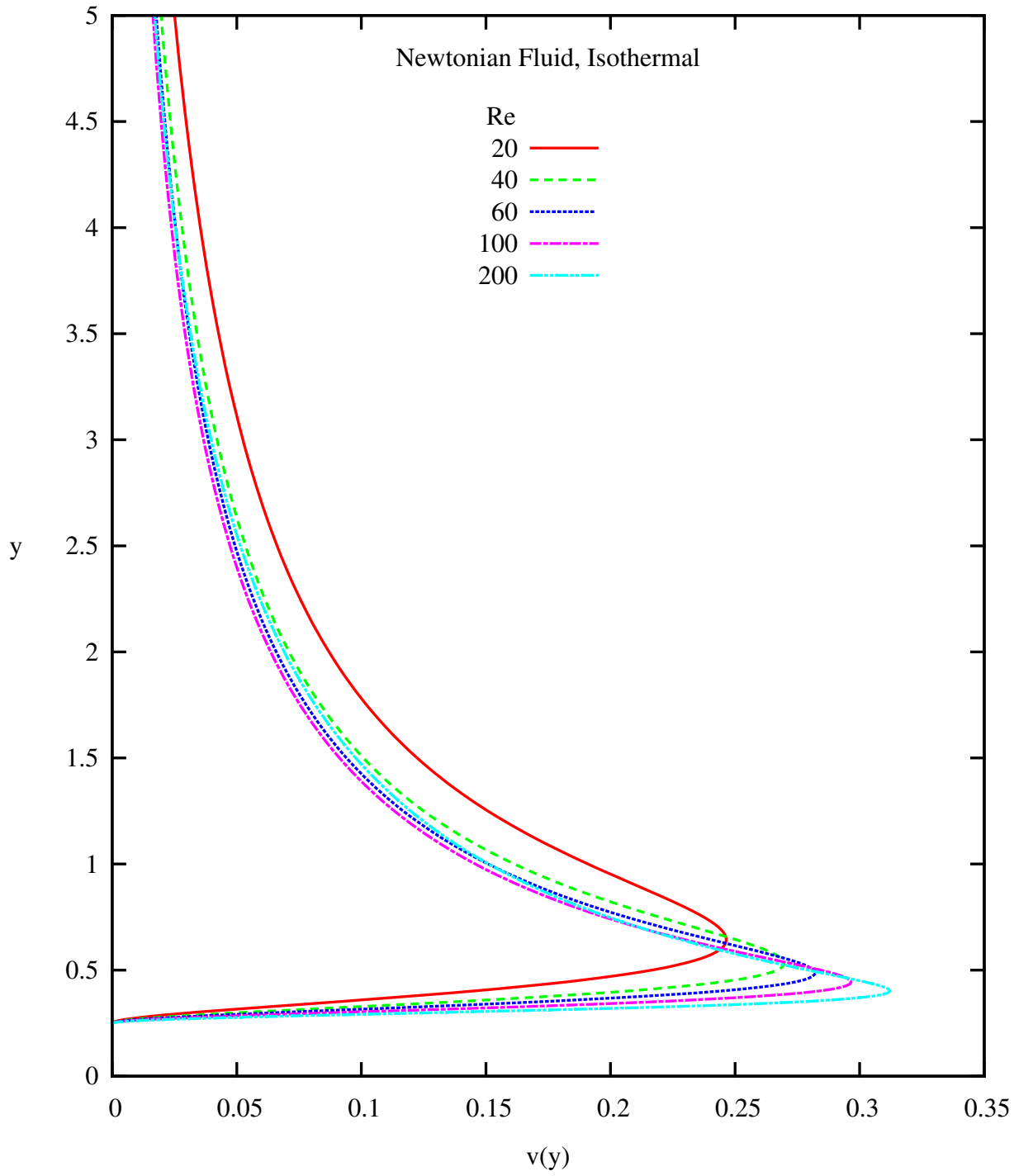

Figure 4.10: Velocity v versus y at $x = 0$ (Newtonian, Isothermal)

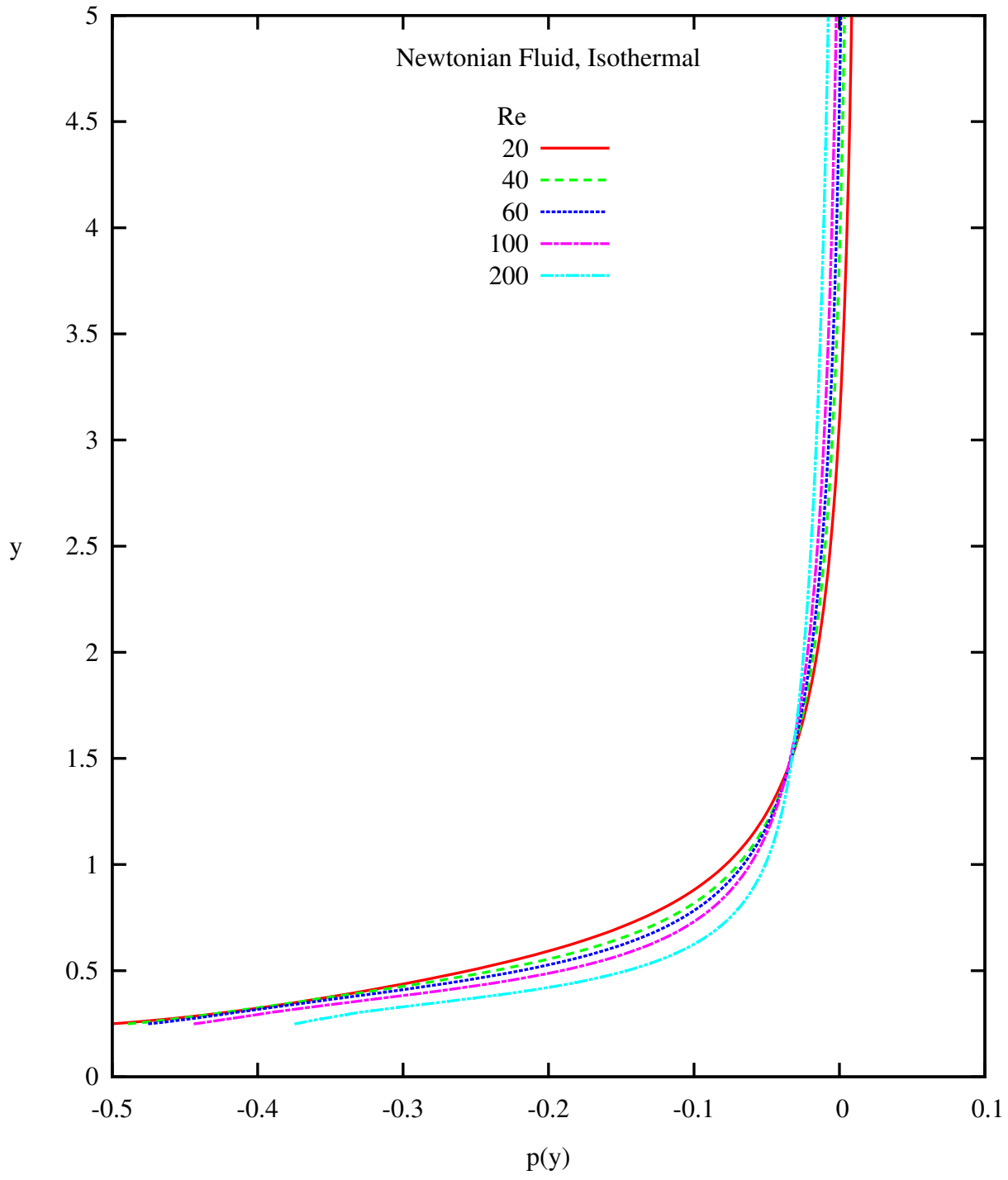

Figure 4.11: Pressure p versus y at $x = 0$ (Newtonian, Isothermal)

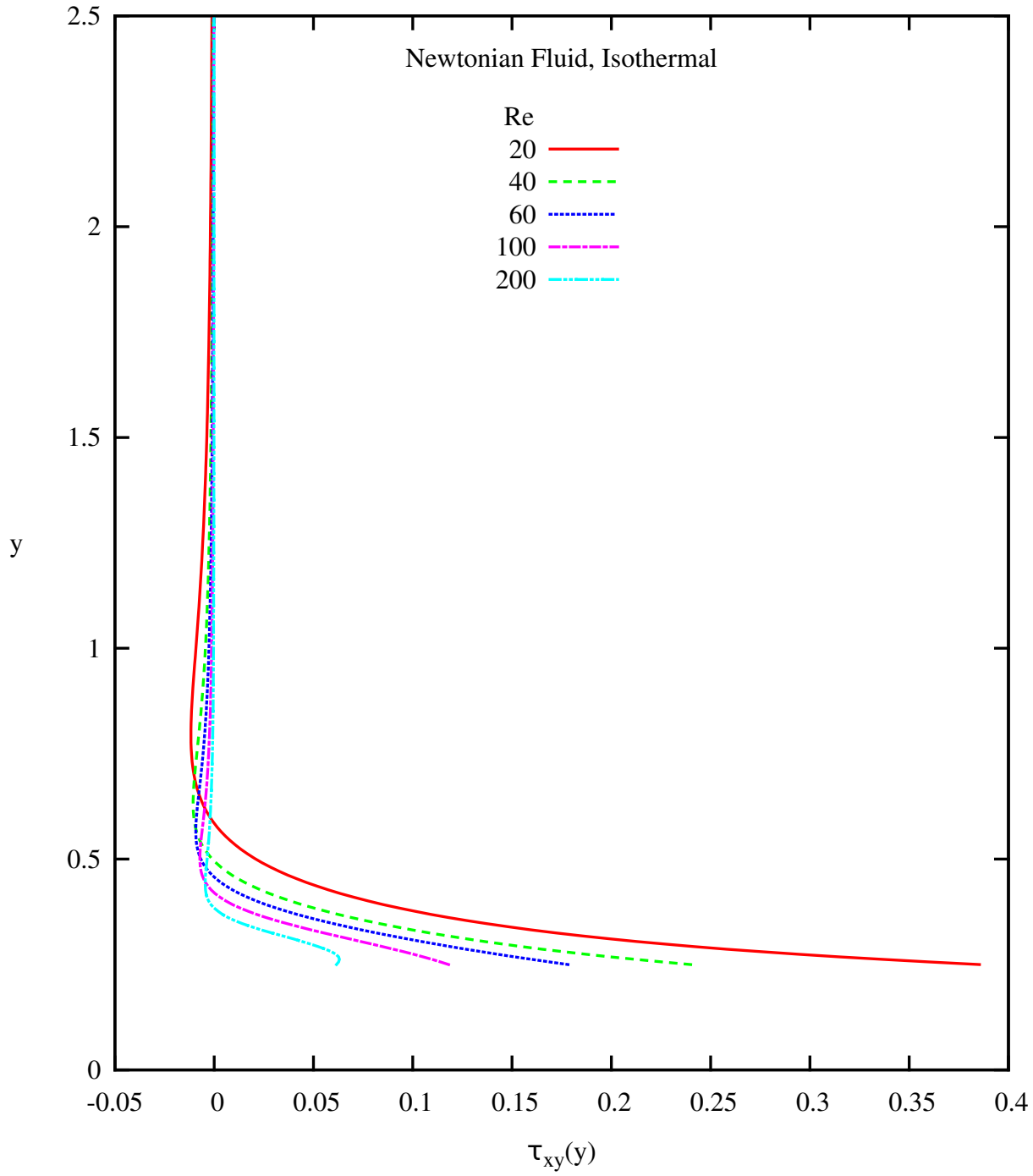

Figure 4.12: Shear Stress τ_{xy} versus y at $x = 0$ (Newtonian, Isothermal)

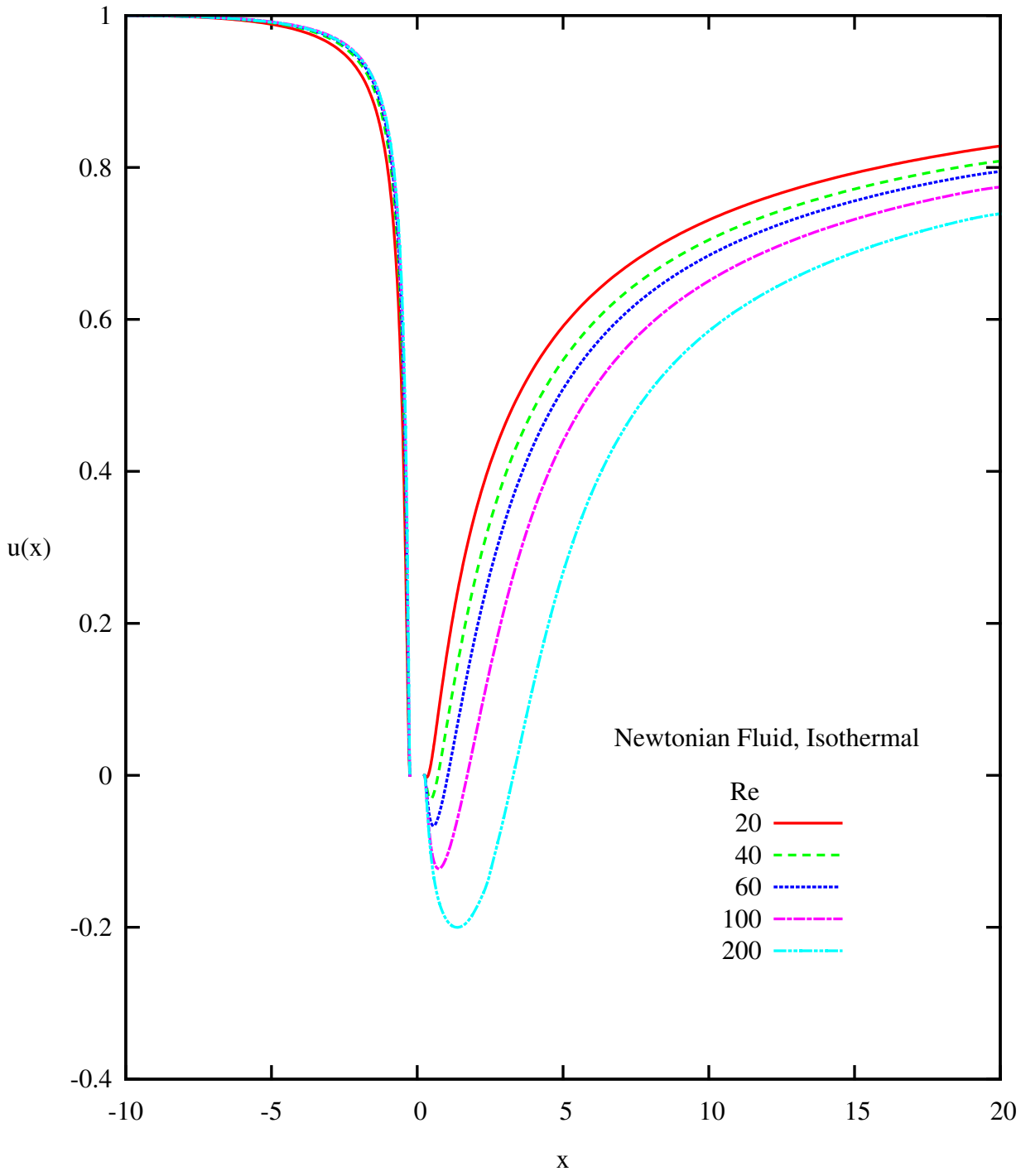

Figure 4.13: Velocity v versus x at $y = 0$ (Newtonian, Isothermal)

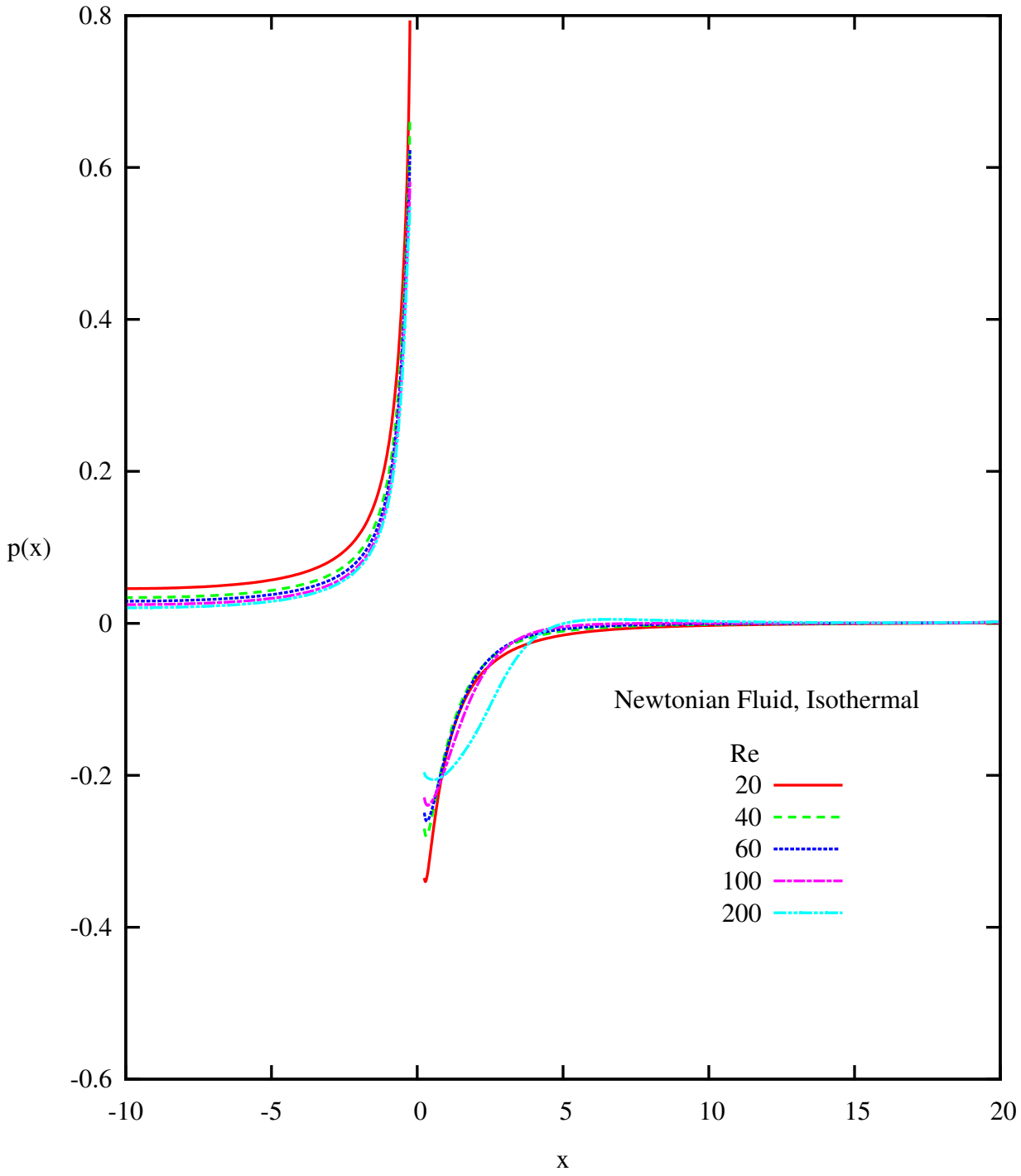

Figure 4.14: Pressure p versus x at $y = 0$ (Newtonian, Isothermal)

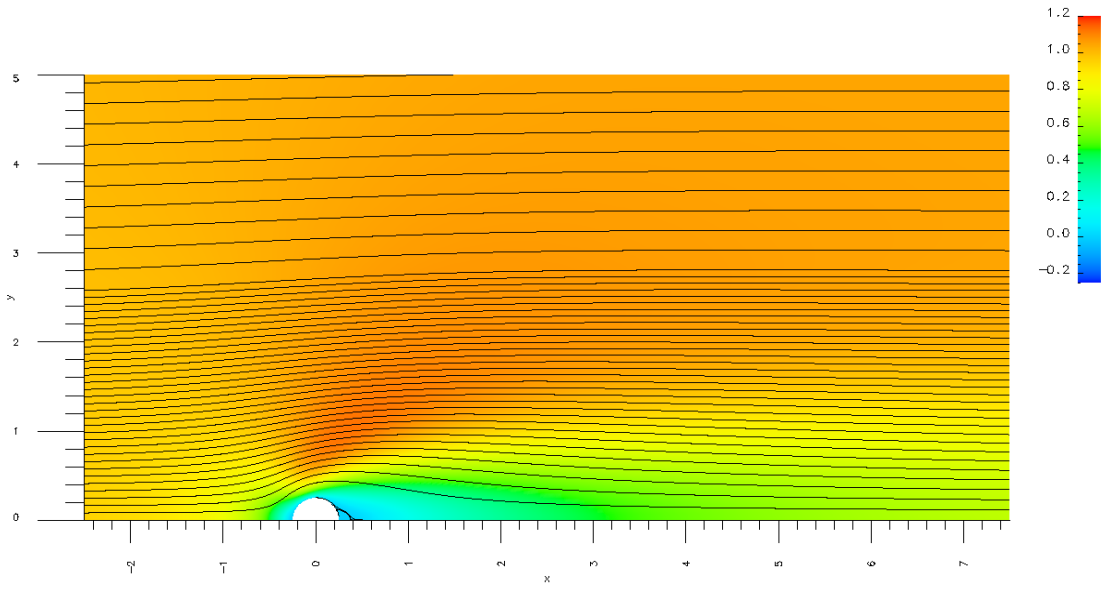

(a) Re = 20

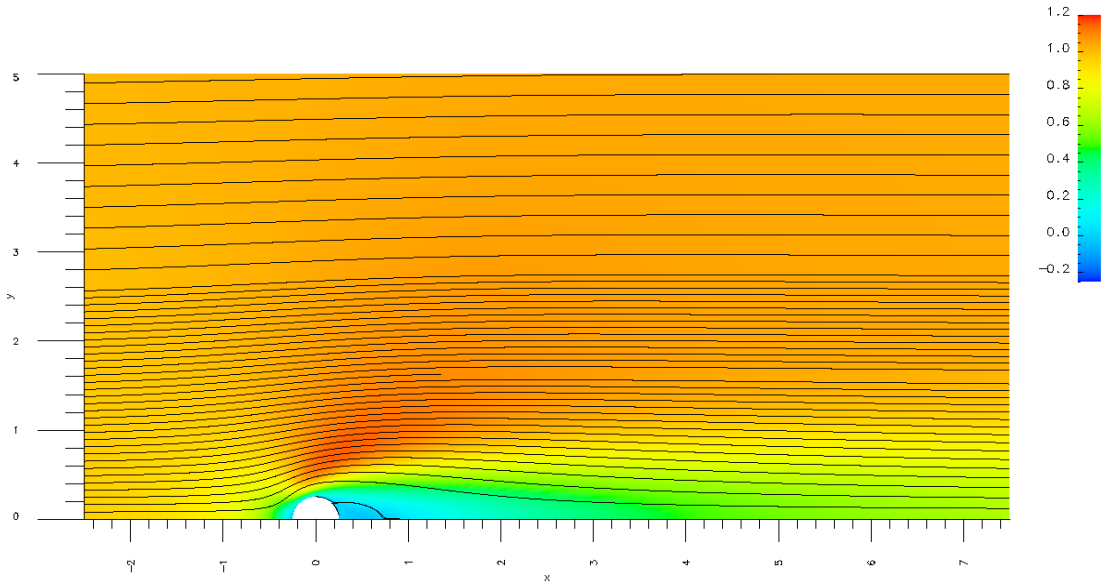

(b) Re = 40

Figure 4.15: Carpet and Streamline Plot of u at Re = 20 and 40 (Newtonian, Isothermal)

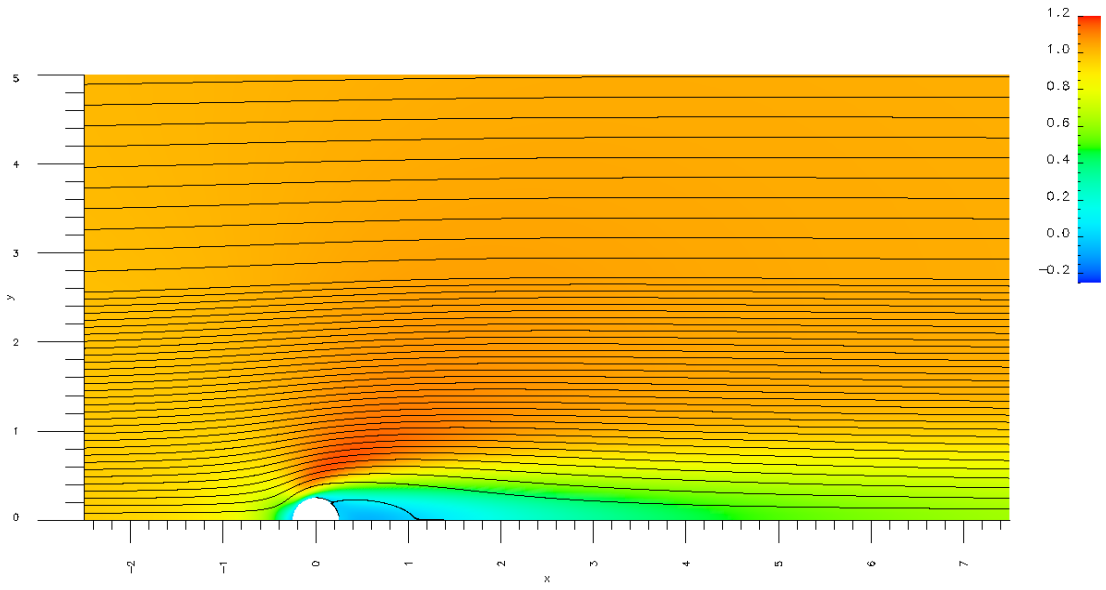

(a) Re = 60

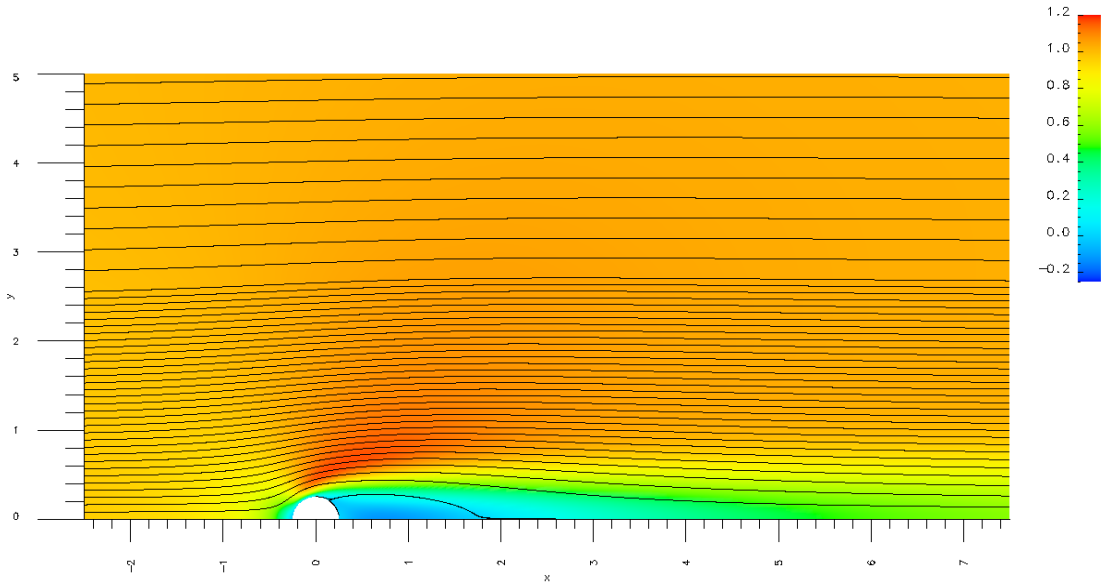

(b) Re = 100

Figure 4.16: Carpet and Streamline Plot of u at Re = 60 and 100 (Newtonian, Isothermal)

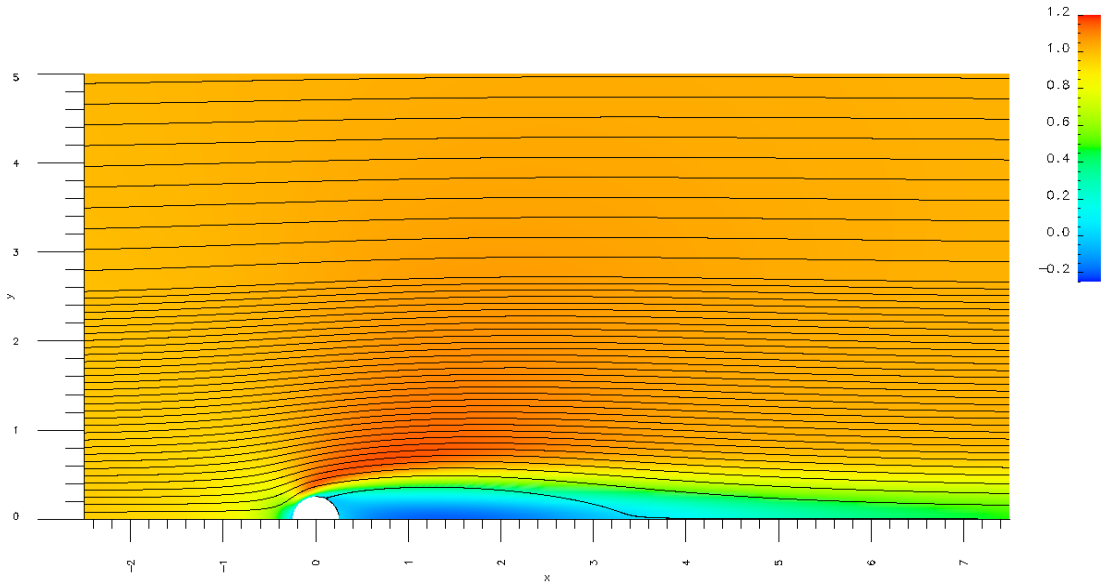

Figure 4.17: Carpet and Streamline Plot of u at Re = 200 (Newtonian, Isothermal)

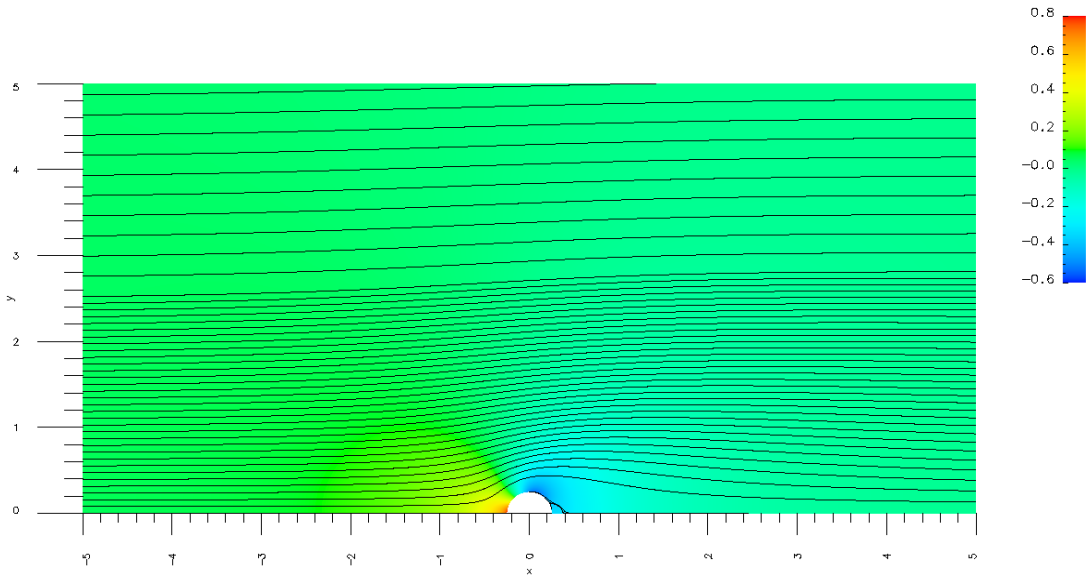

(a) Re = 20

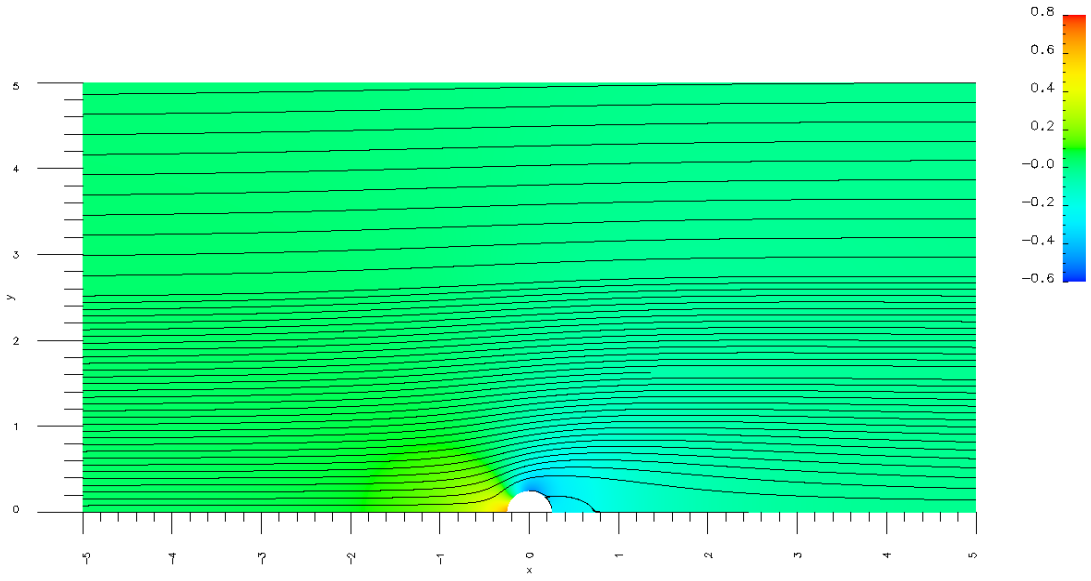

(b) Re = 40

Figure 4.18: Carpet and Streamline Plot of p at Re = 20 and 40 (Newtonian, Isothermal)

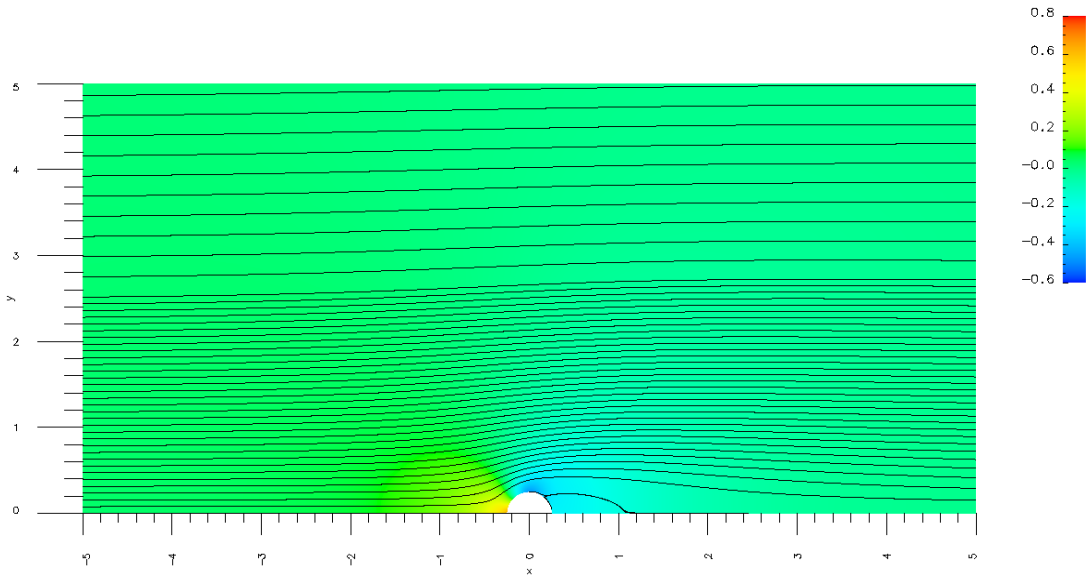

(a) Re = 60

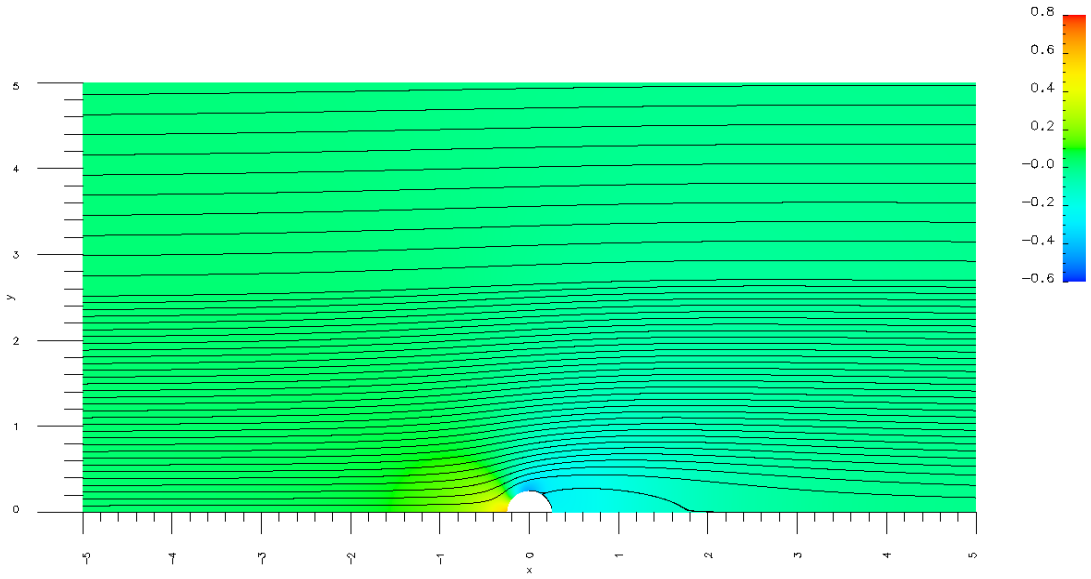

(b) Re = 100

Figure 4.19: Carpet and Streamline Plot of p at Re = 60 and 100 (Newtonian, Isothermal)

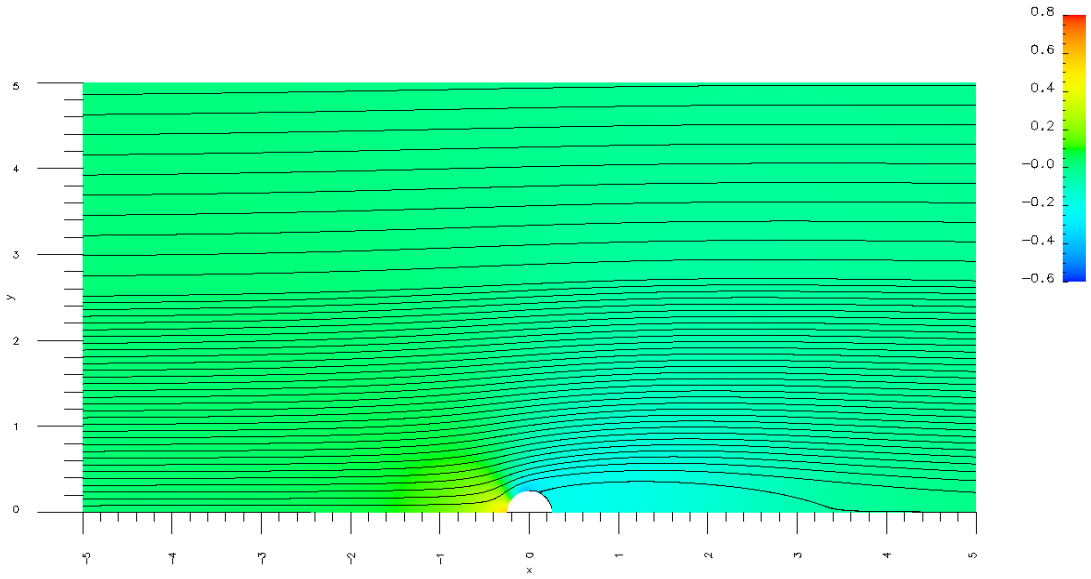

Figure 4.20: Carpet and Streamline Plot of p at Re = 200 (Newtonian, Isothermal)

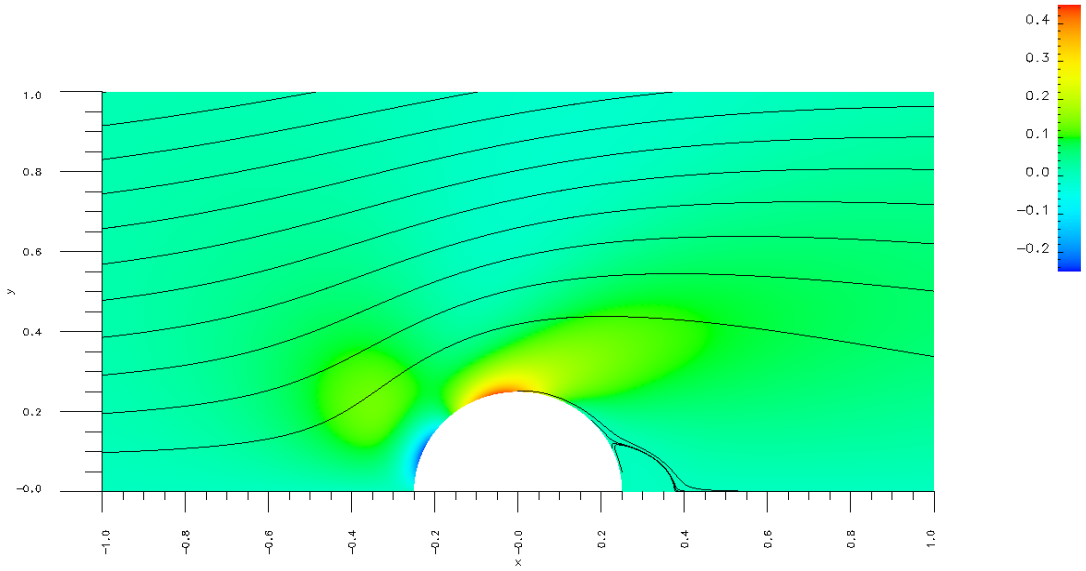

(a) Re = 20

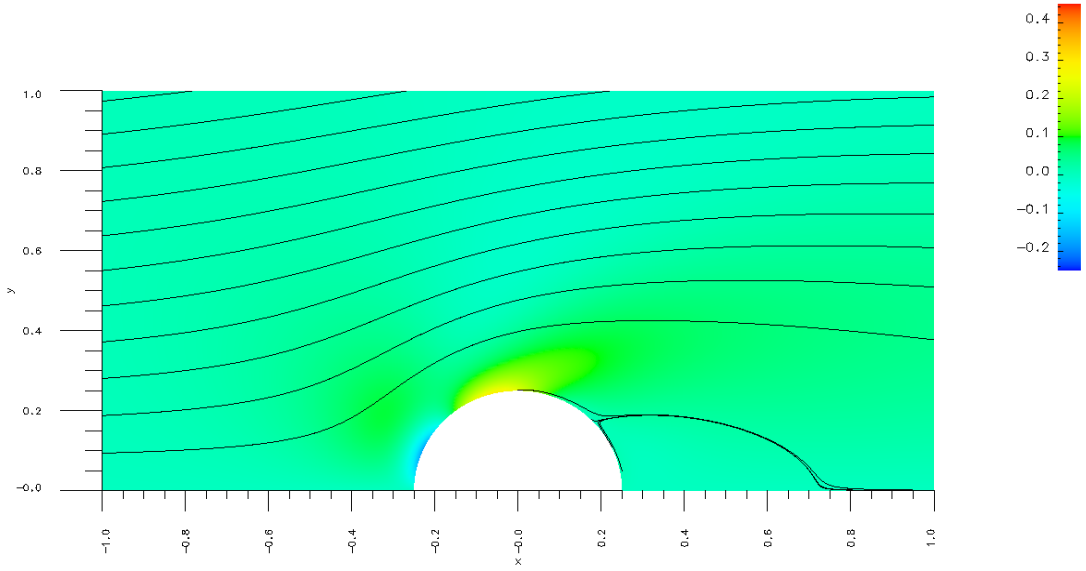

(b) Re = 40

Figure 4.21: Carpet and Streamline Plot of τ_{xy} at Re = 20 and 40 (Newtonian, Isothermal)

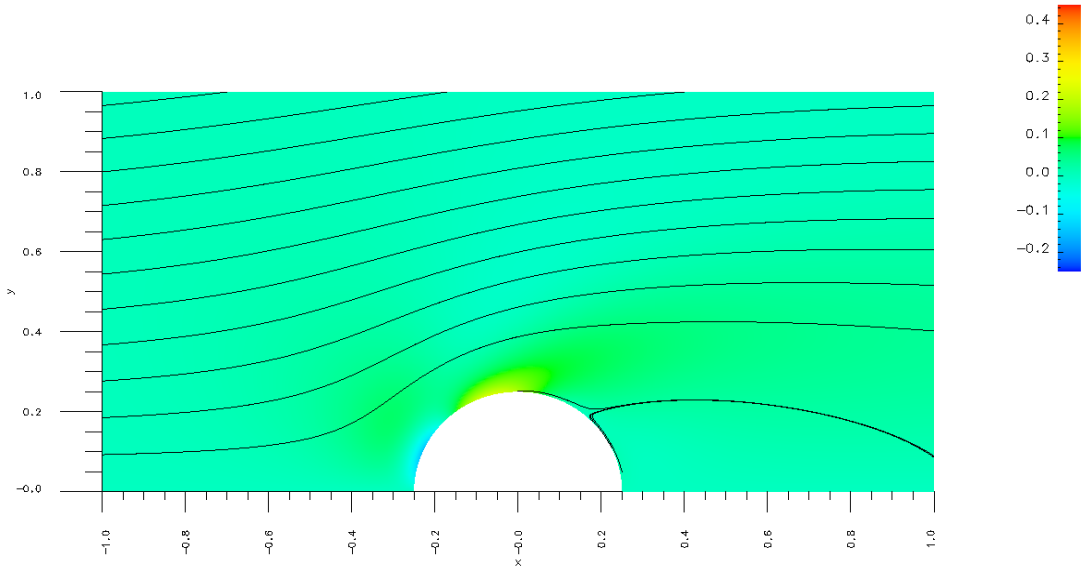

(a) Re = 60

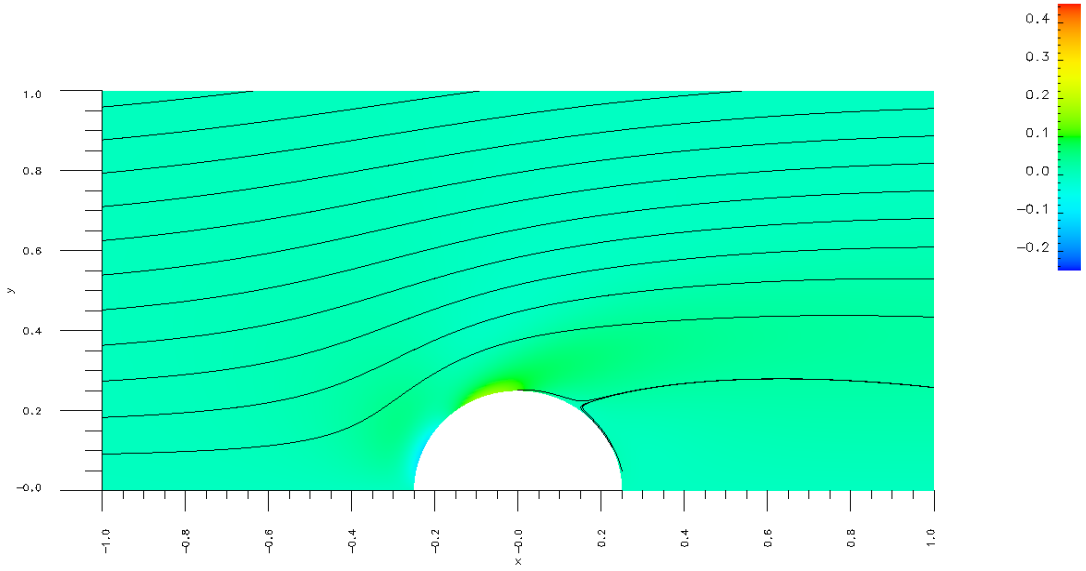

(b) Re = 100

Figure 4.22: Carpet and Streamline Plot of τ_{xy} at Re = 60 and 100 (Newtonian, Isothermal)

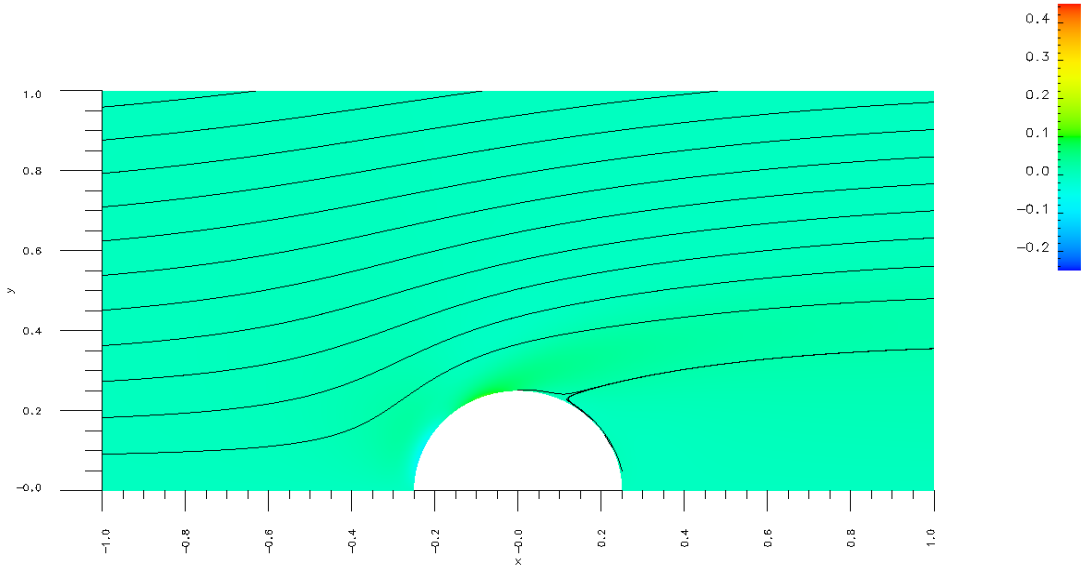

Figure 4.23: Carpet and Streamline Plot of τ_{xy} at Re = 200 (Newtonian, Isothermal)

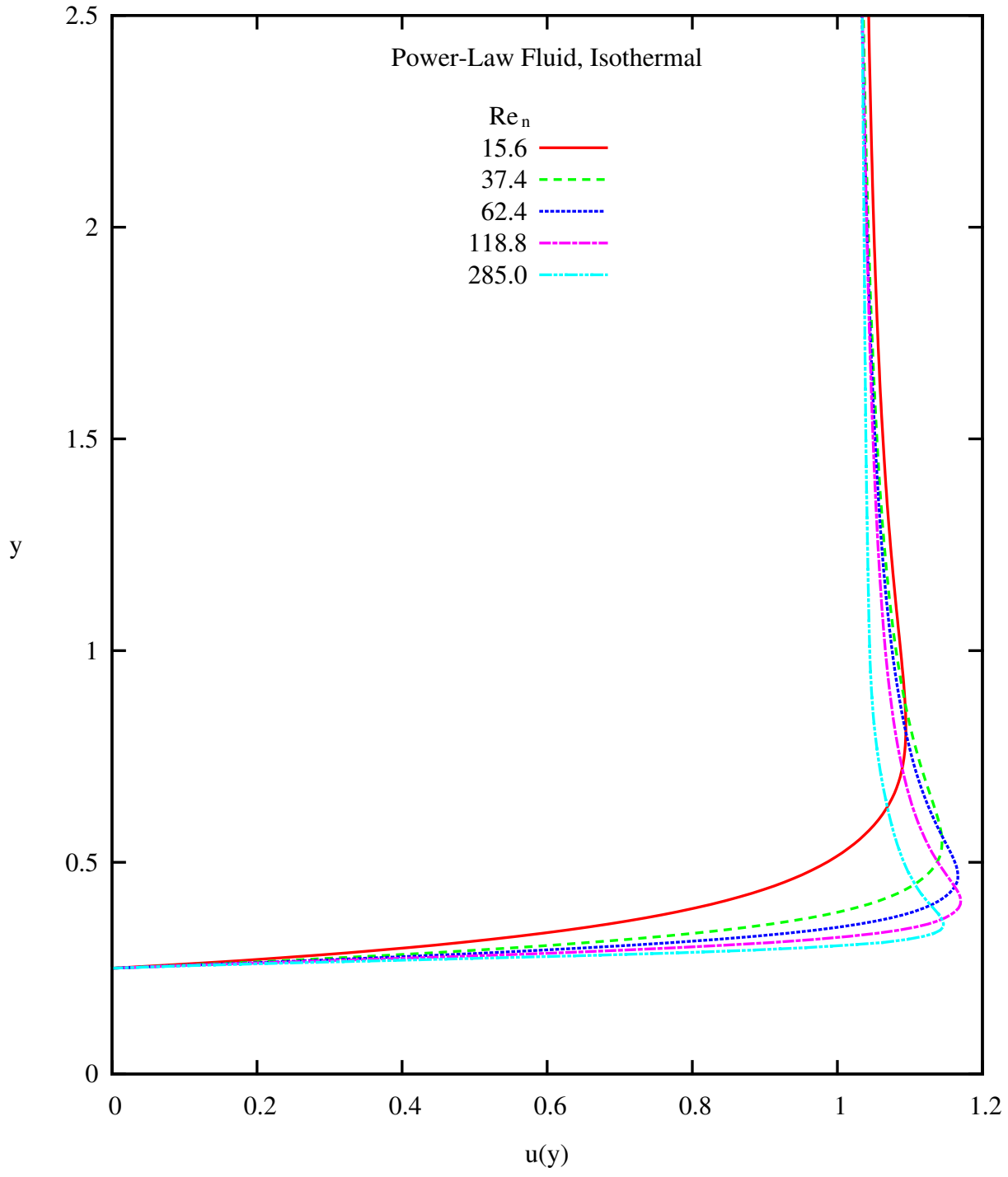

Figure 4.24: Velocity u versus y at $x = 0$ (Power-Law, Isothermal)

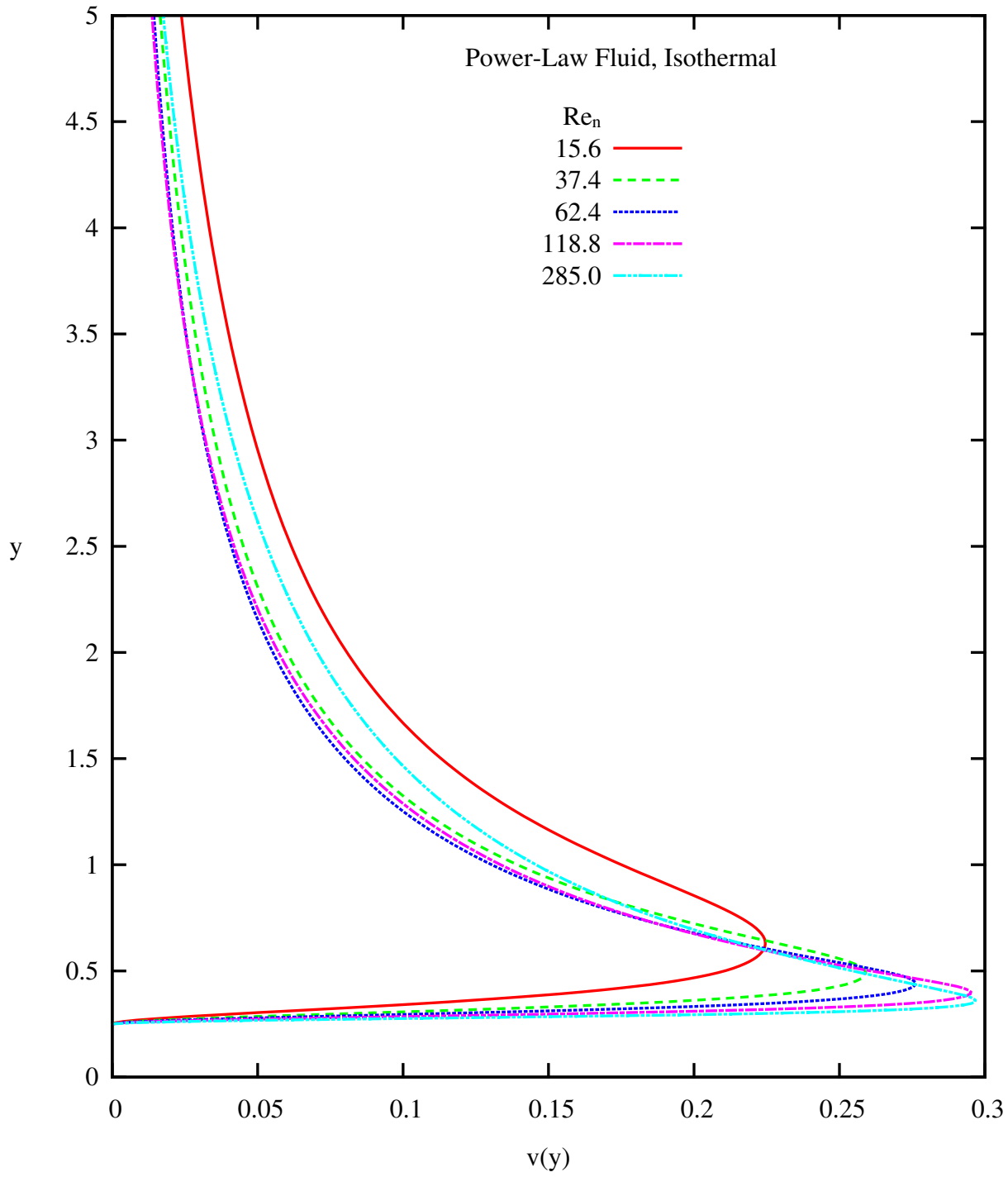

Figure 4.25: Velocity v versus y at $x = 0$ (Power-Law, Isothermal)

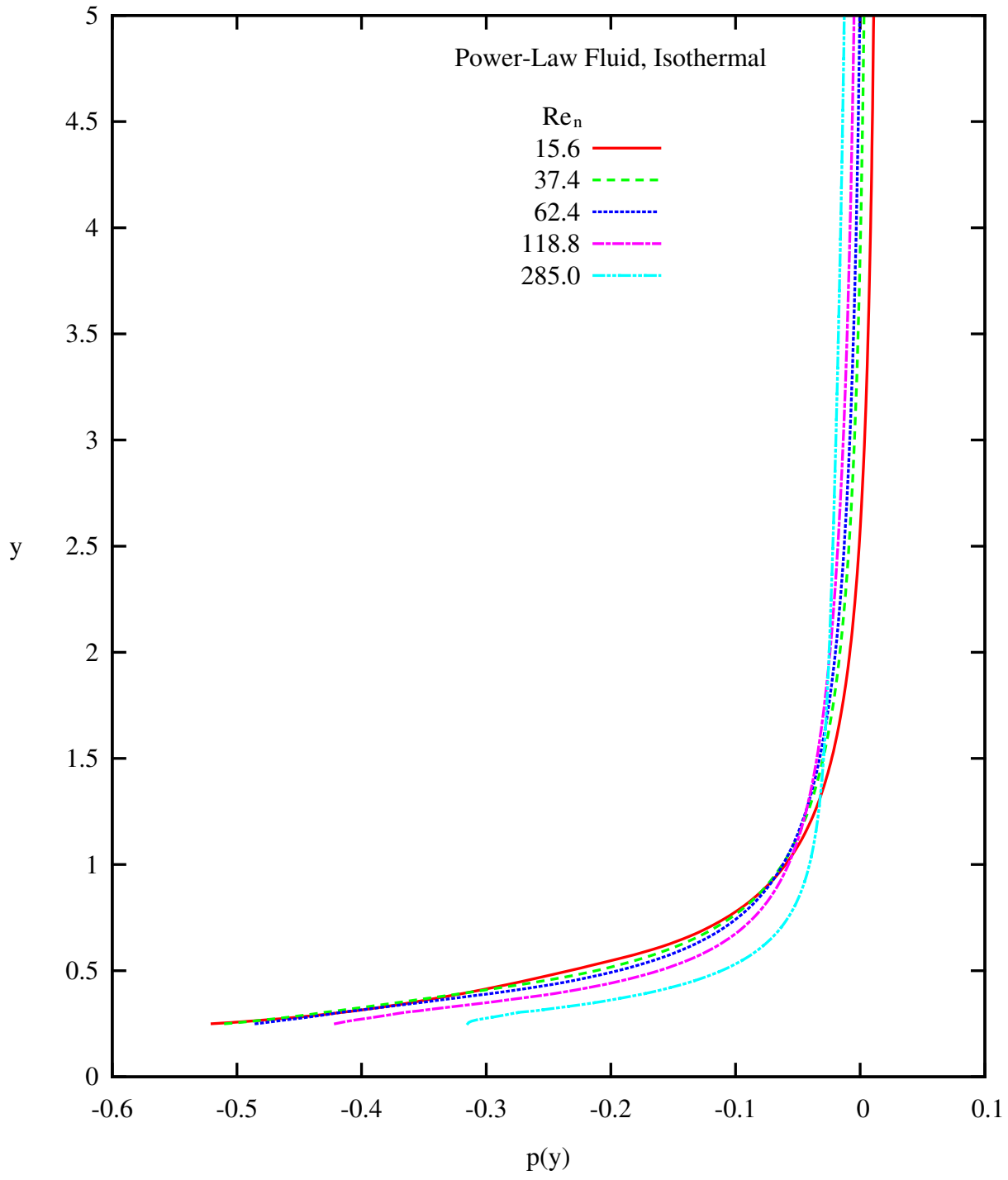

Figure 4.26: Pressure p versus y at $x = 0$ (Power-Law, Isothermal)

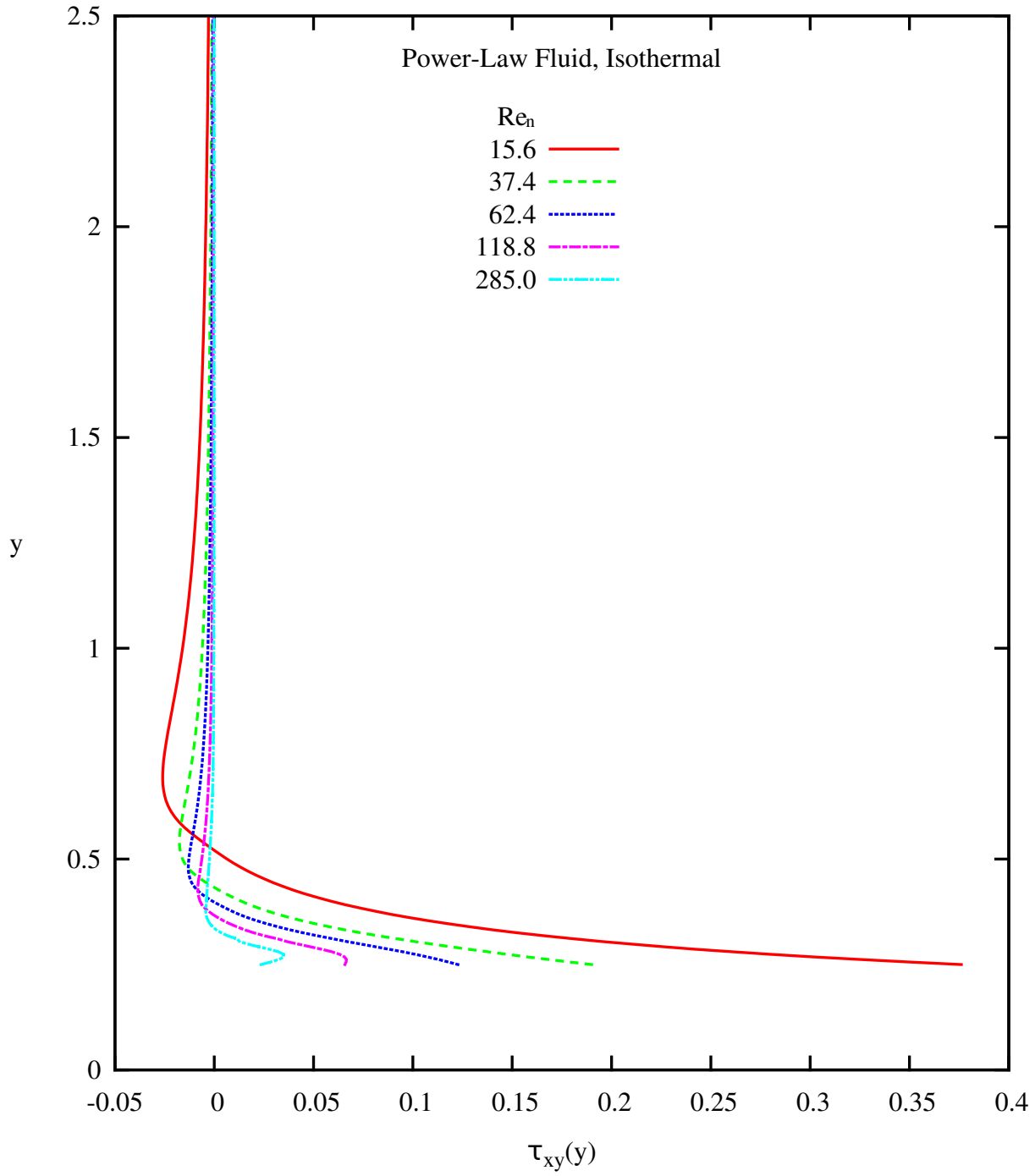

Figure 4.27: Shear Stress τ_{xy} versus y at $x = 0$ (Power-Law, Isothermal)

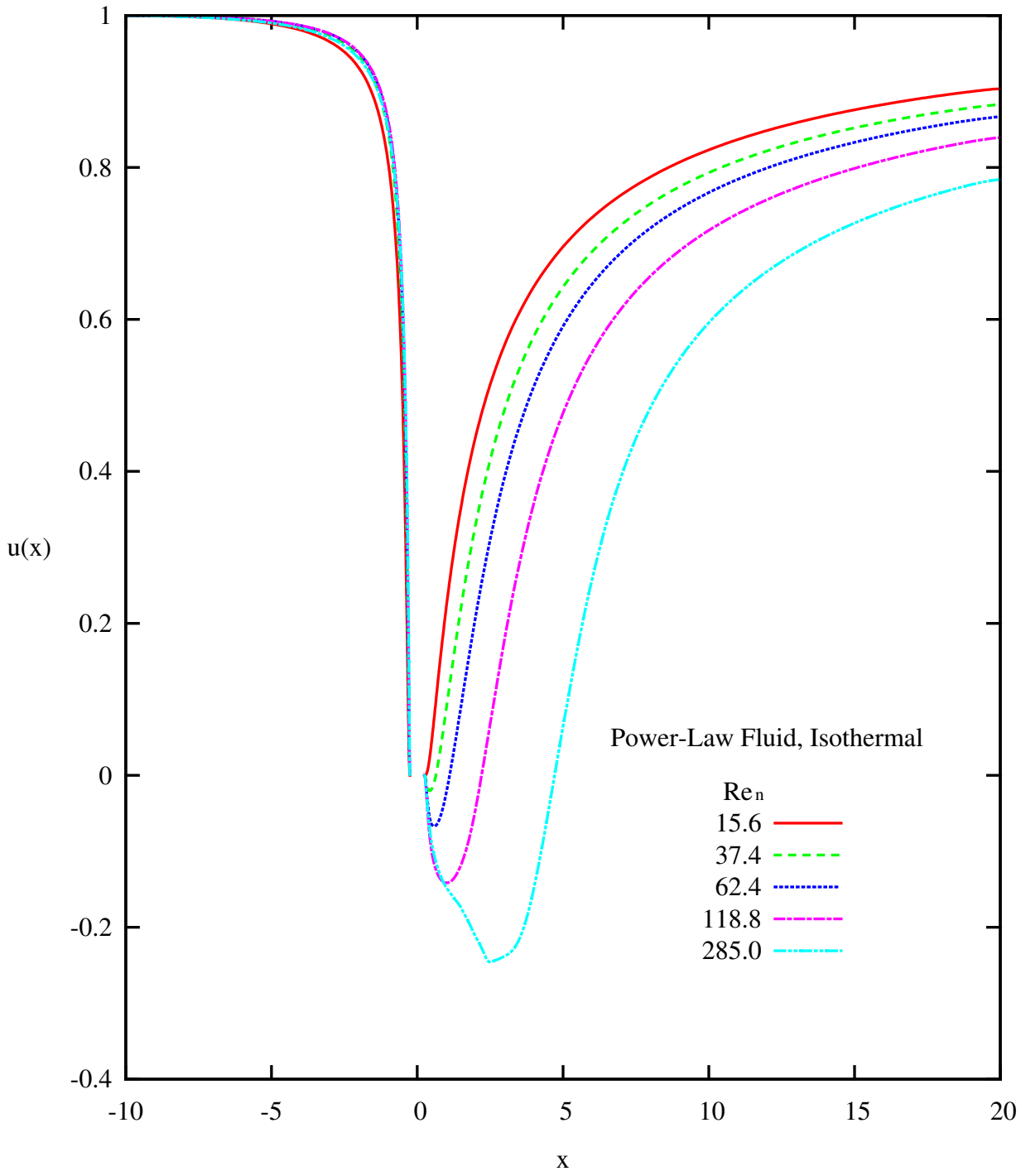

Figure 4.28: Velocity u versus x at $y = 0$ (Power-Law, Isothermal)

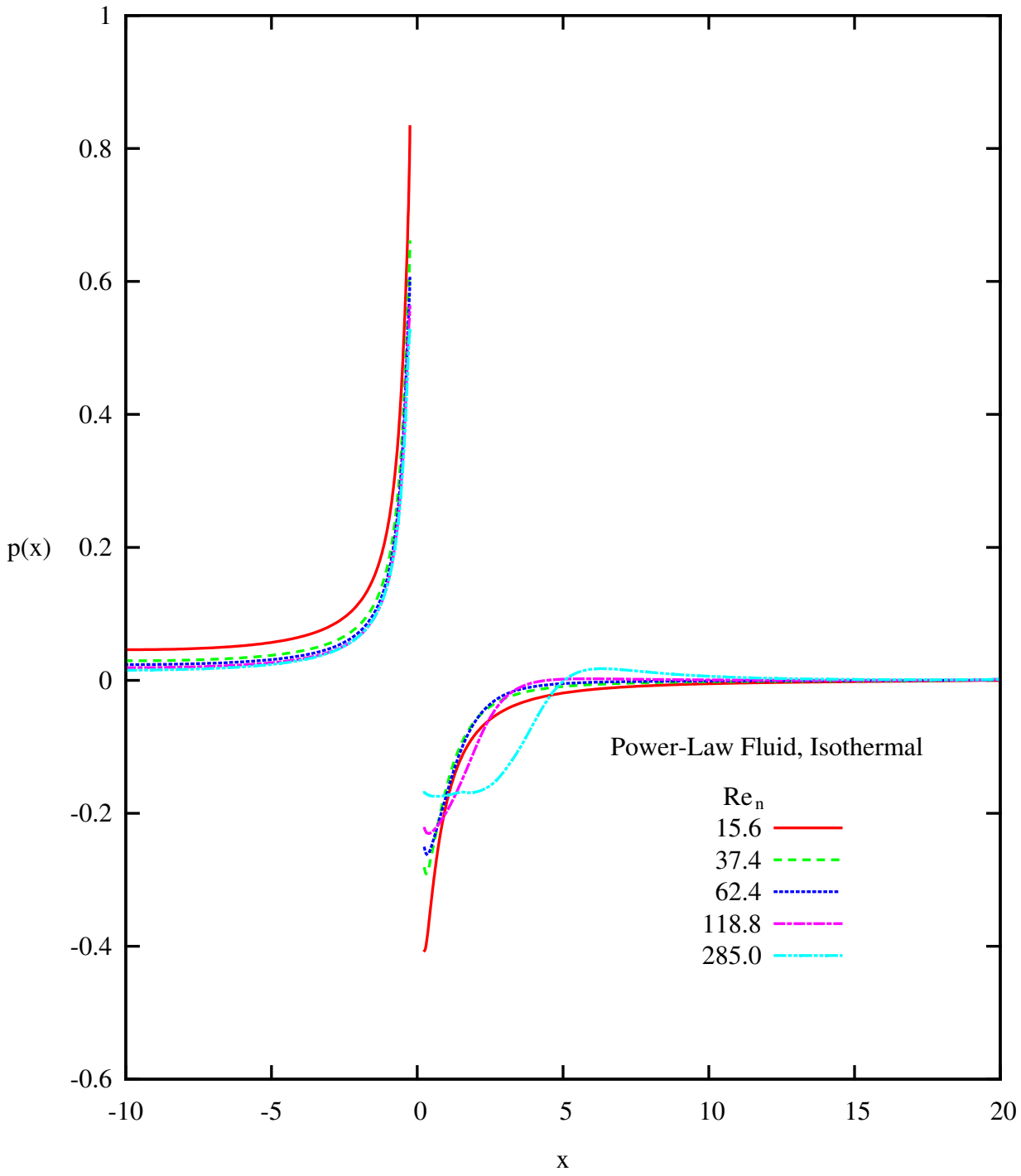

Figure 4.29: Pressure p versus x at $y = 0$ (Power-Law, Isothermal)

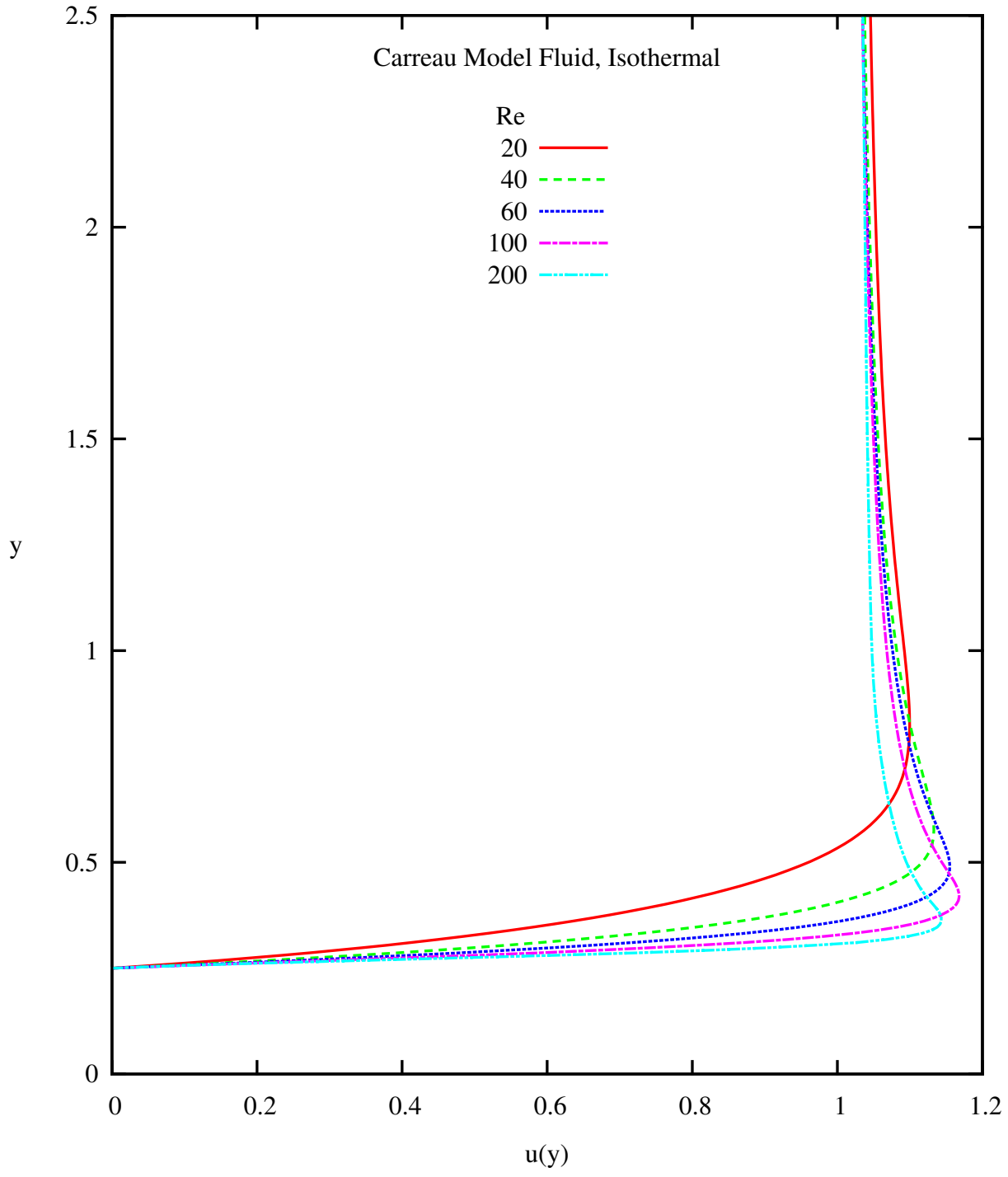

Figure 4.30: Velocity u versus y at $x = 0$ (Carreau Model, Isothermal)

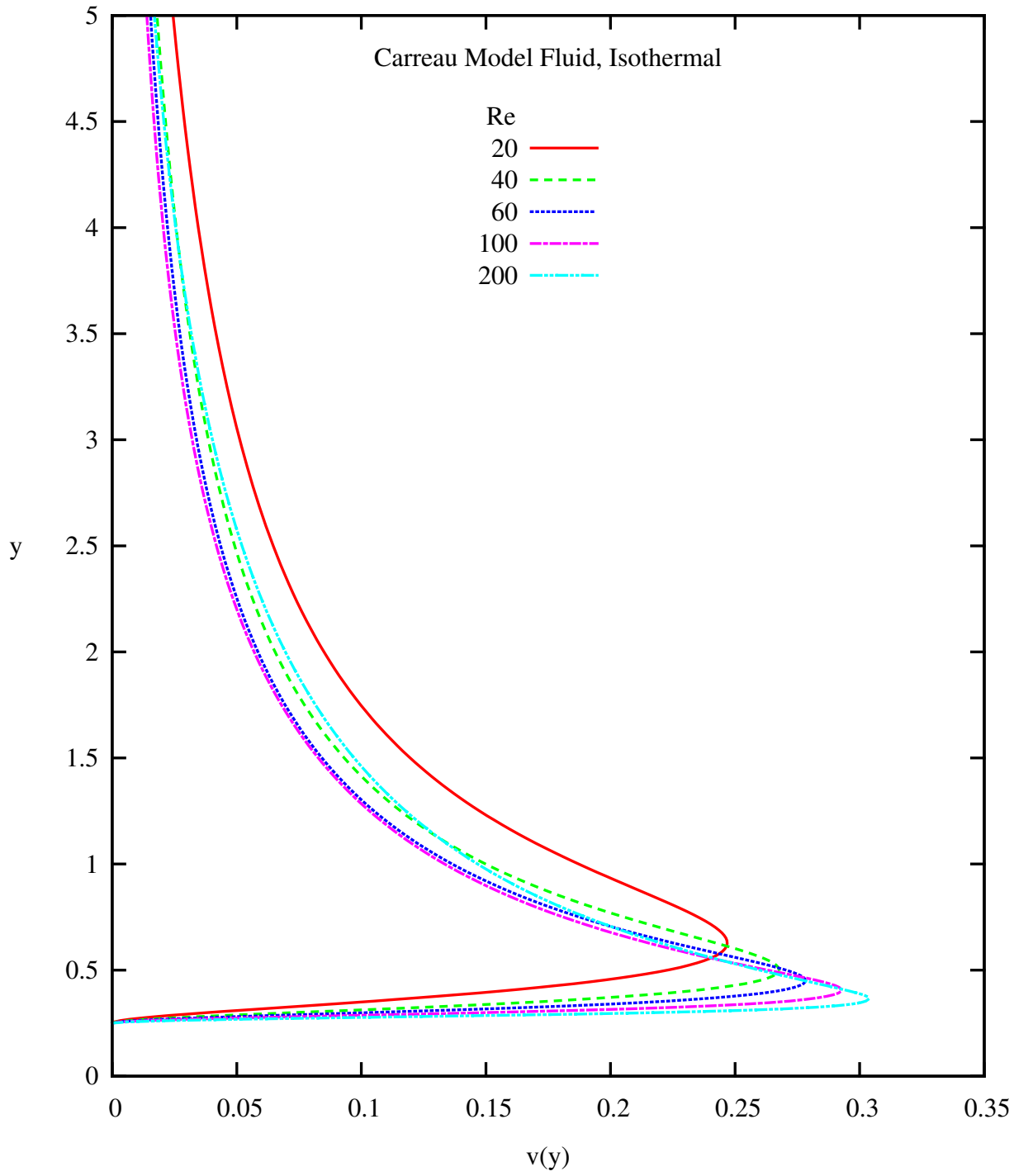

Figure 4.31: Velocity v versus y at $x = 0$ (Carreau Model, Isothermal)

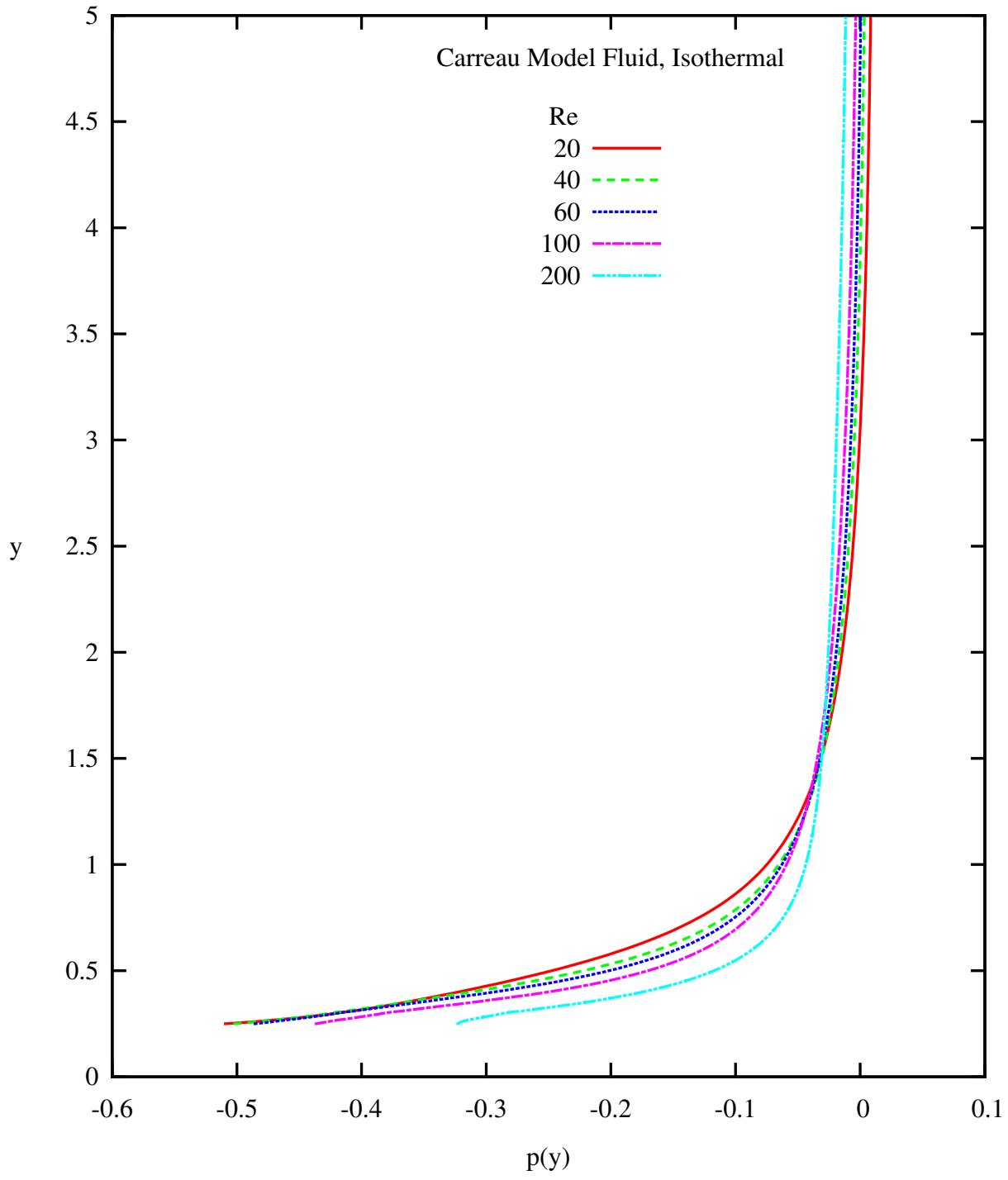

Figure 4.32: Pressure p versus y at $x = 0$ (Carreau Model, Isothermal)

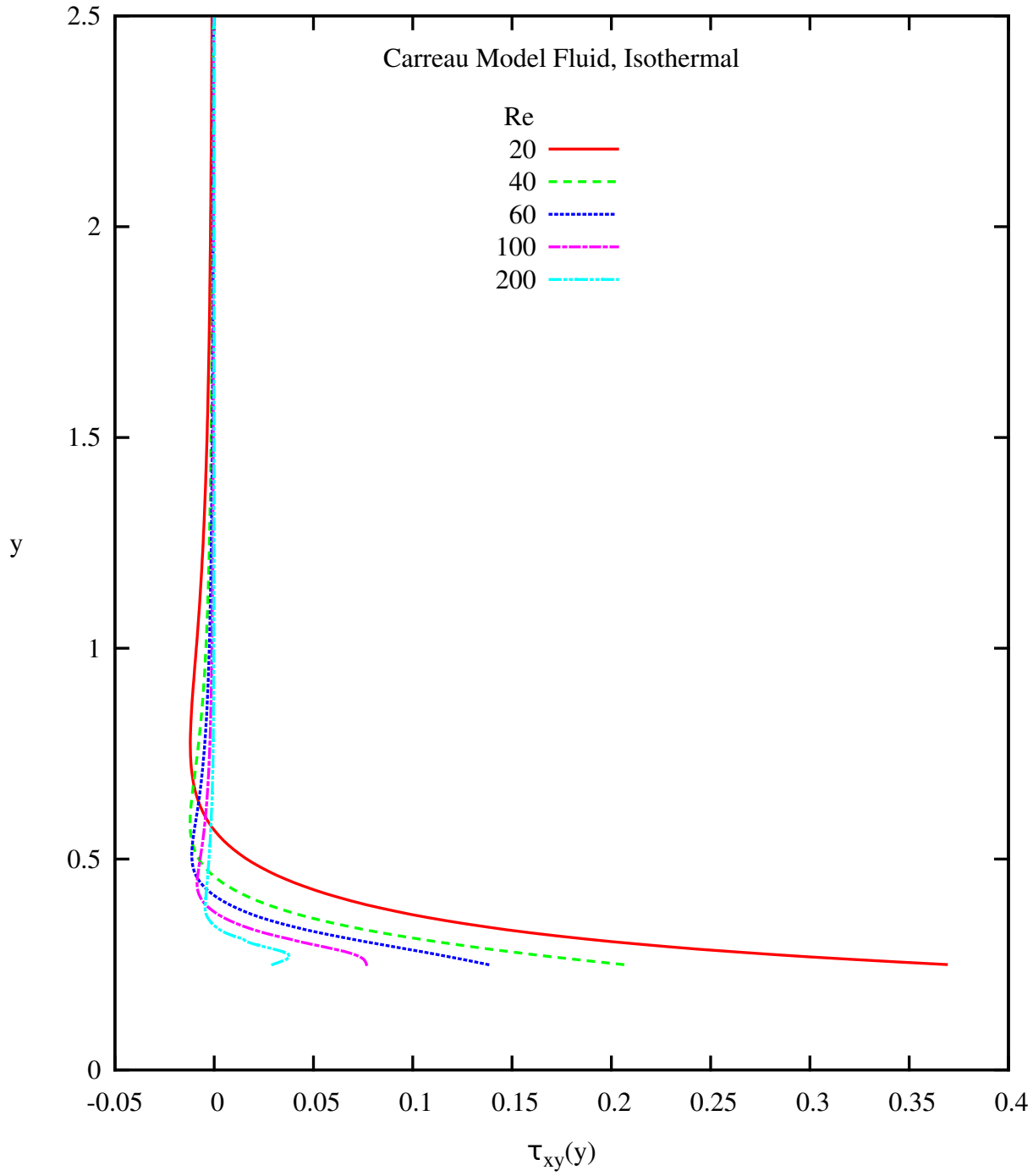

Figure 4.33: Shear Stress τ_{xy} versus y at $x = 0$ (Carreau Model, Isothermal)

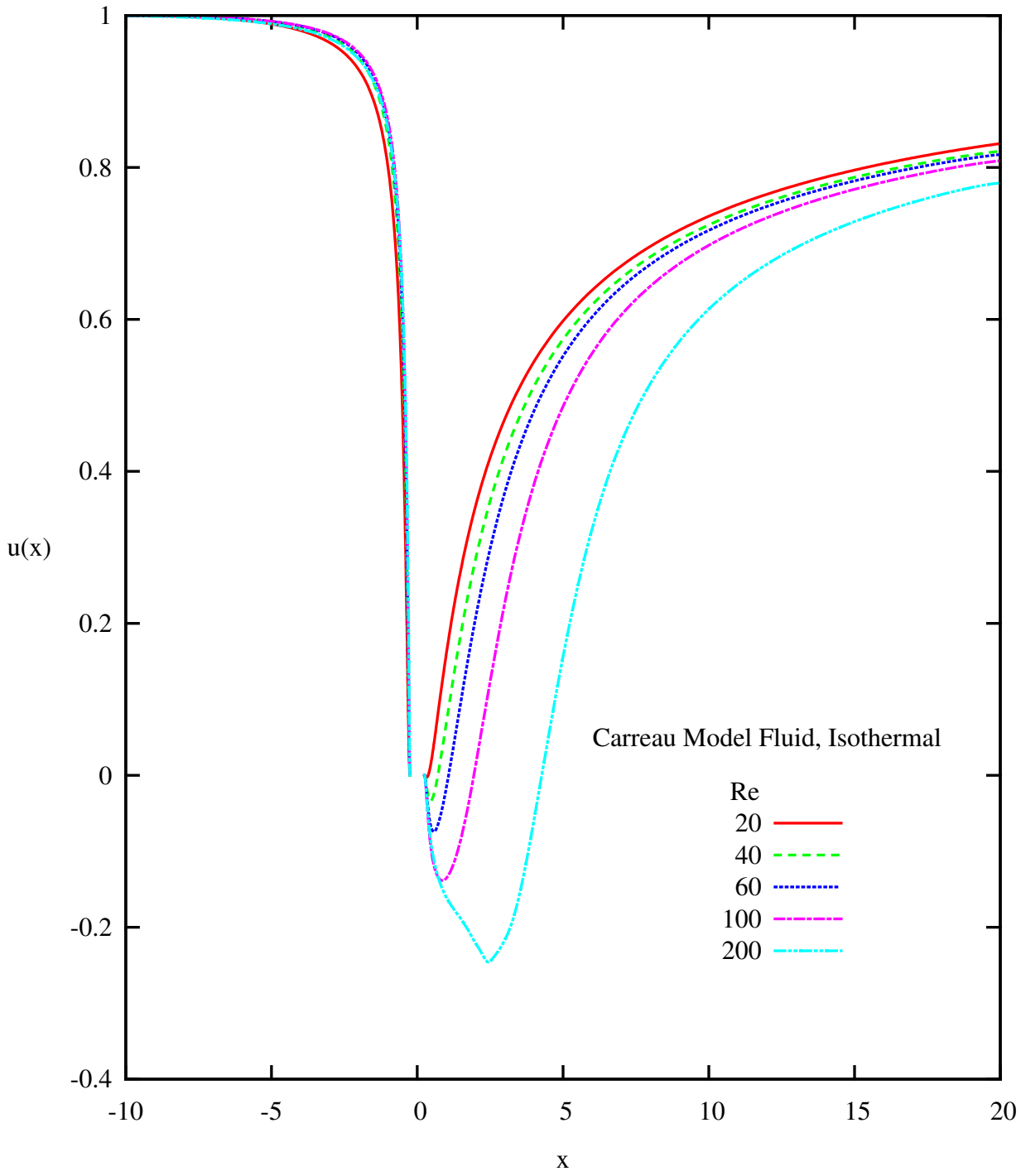

Figure 4.34: Velocity u versus x at $y = 0$ (Carreau Model, Isothermal)

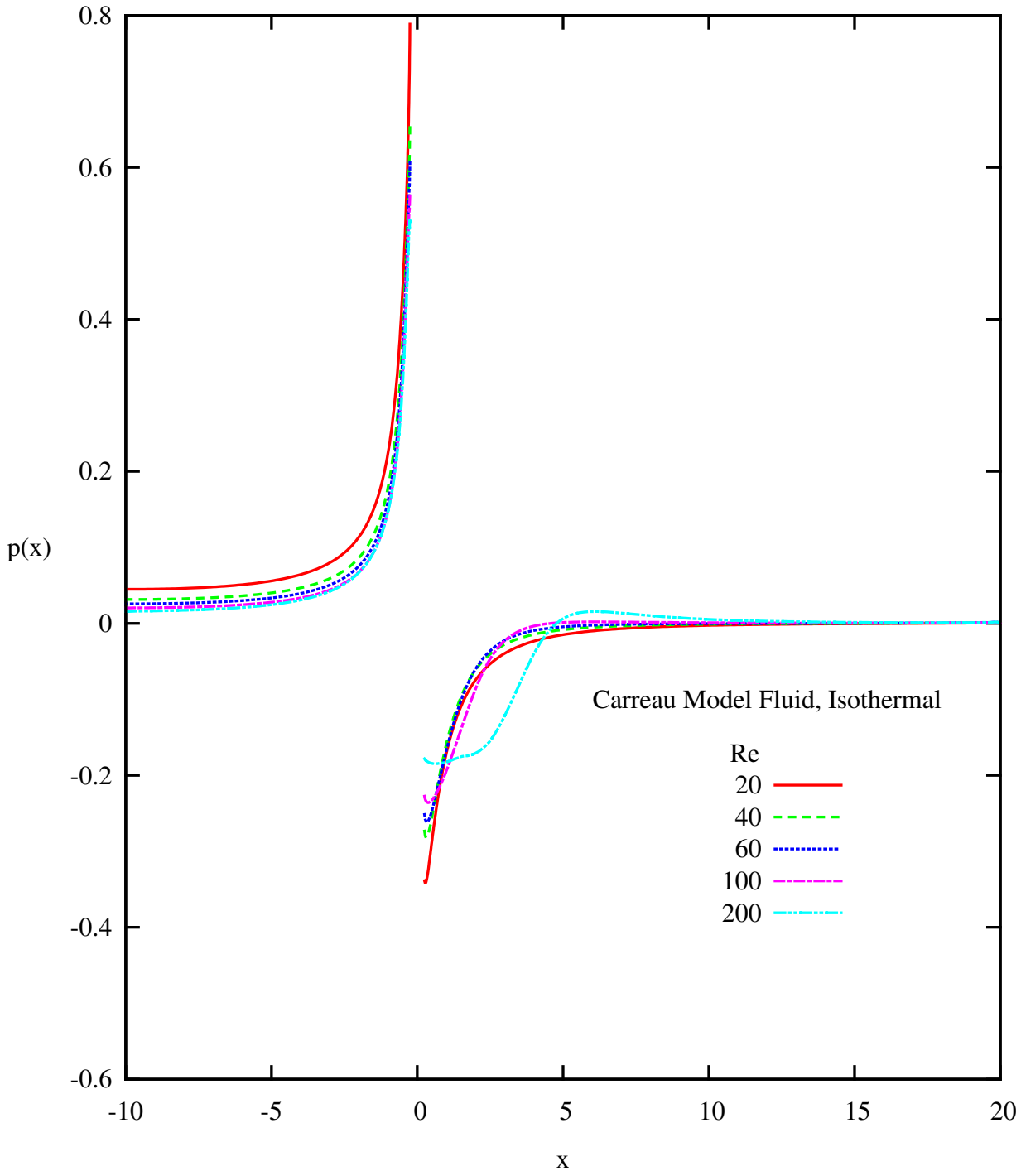

Figure 4.35: Pressure p versus x at $y = 0$ (Carreau Model, Isothermal)

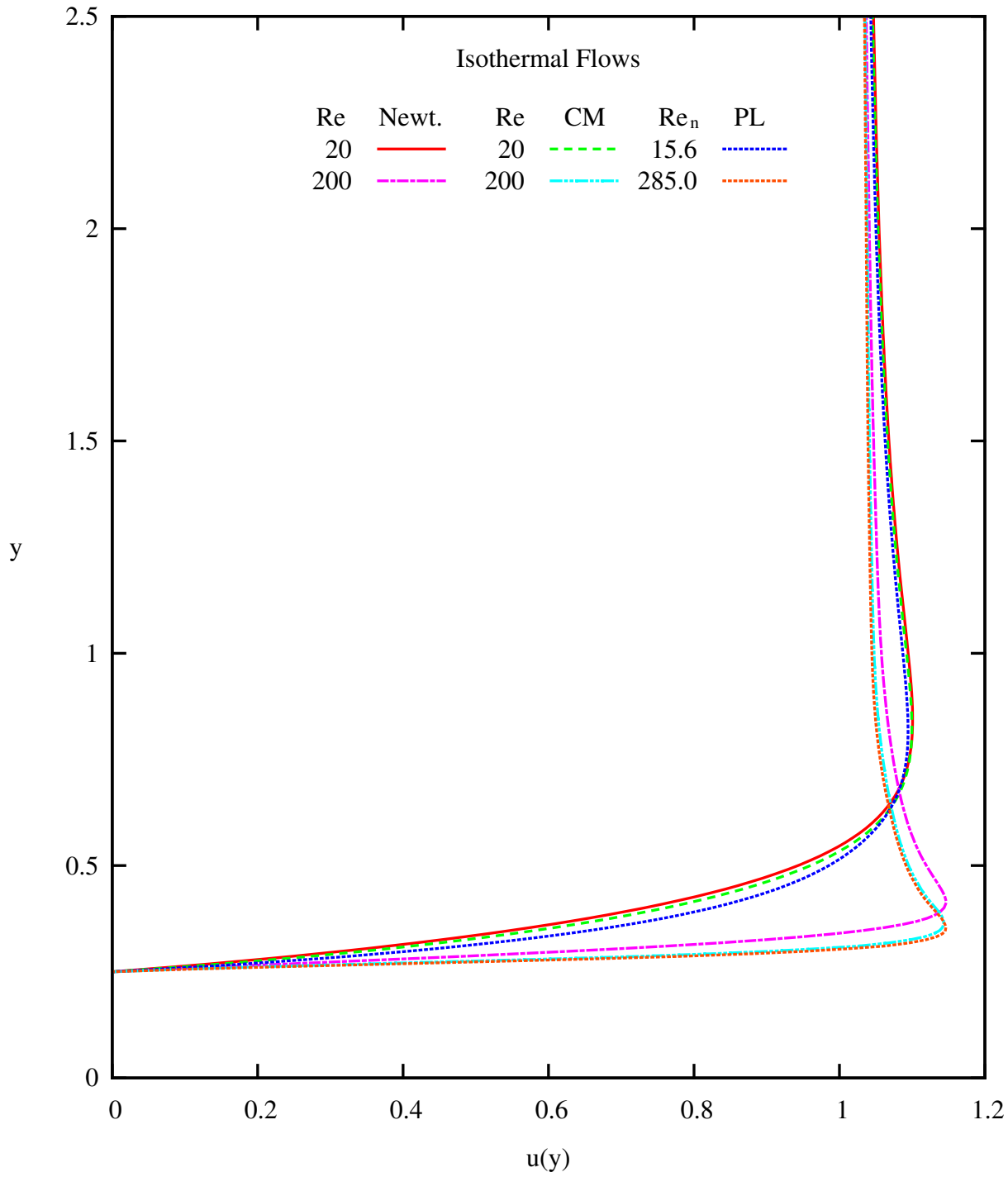

Figure 4.36: Velocity u versus y at $x = 0$: Comparison of Solutions for Newtonian, Power-Law and Carreau Fluids (Isothermal)

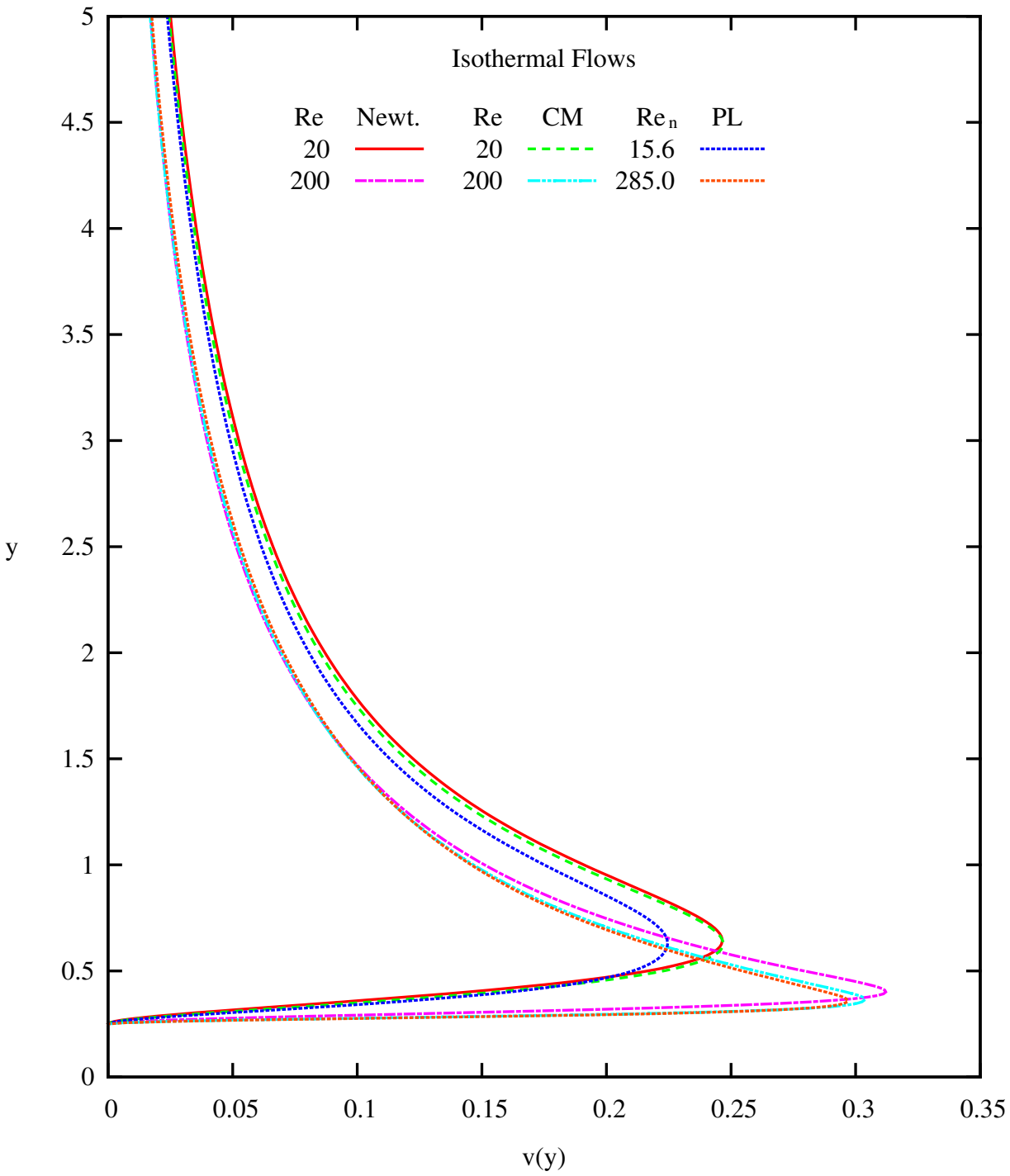

Figure 4.37: Velocity v versus y at $x = 0$: Comparison of Solutions for Newtonian, Power-Law and Carreau Fluids (Isothermal)

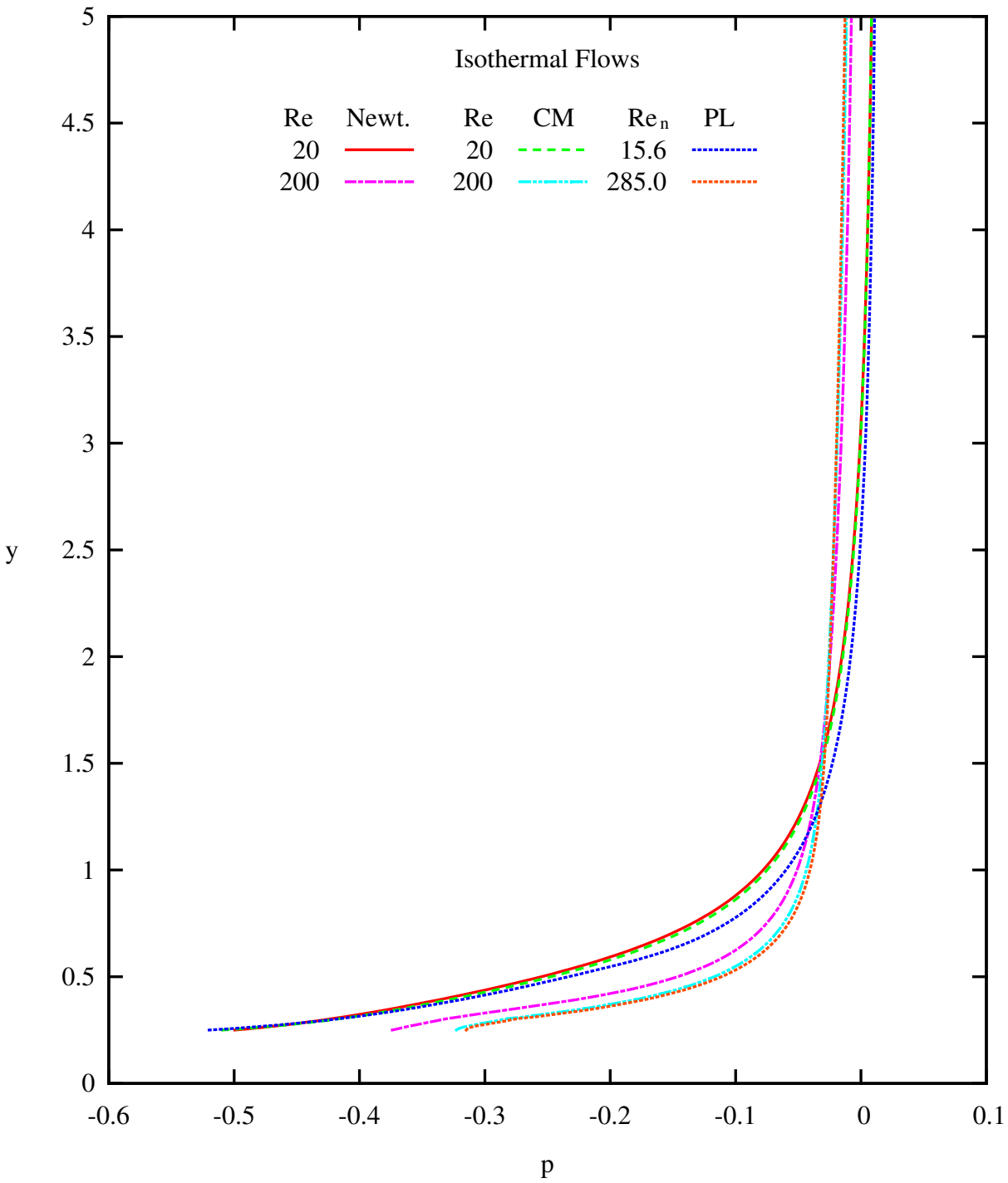

Figure 4.38: Pressure p versus y at $x = 0$: Comparison of Solutions for Newtonian, Power-Law and Carreau Fluids (Isothermal)

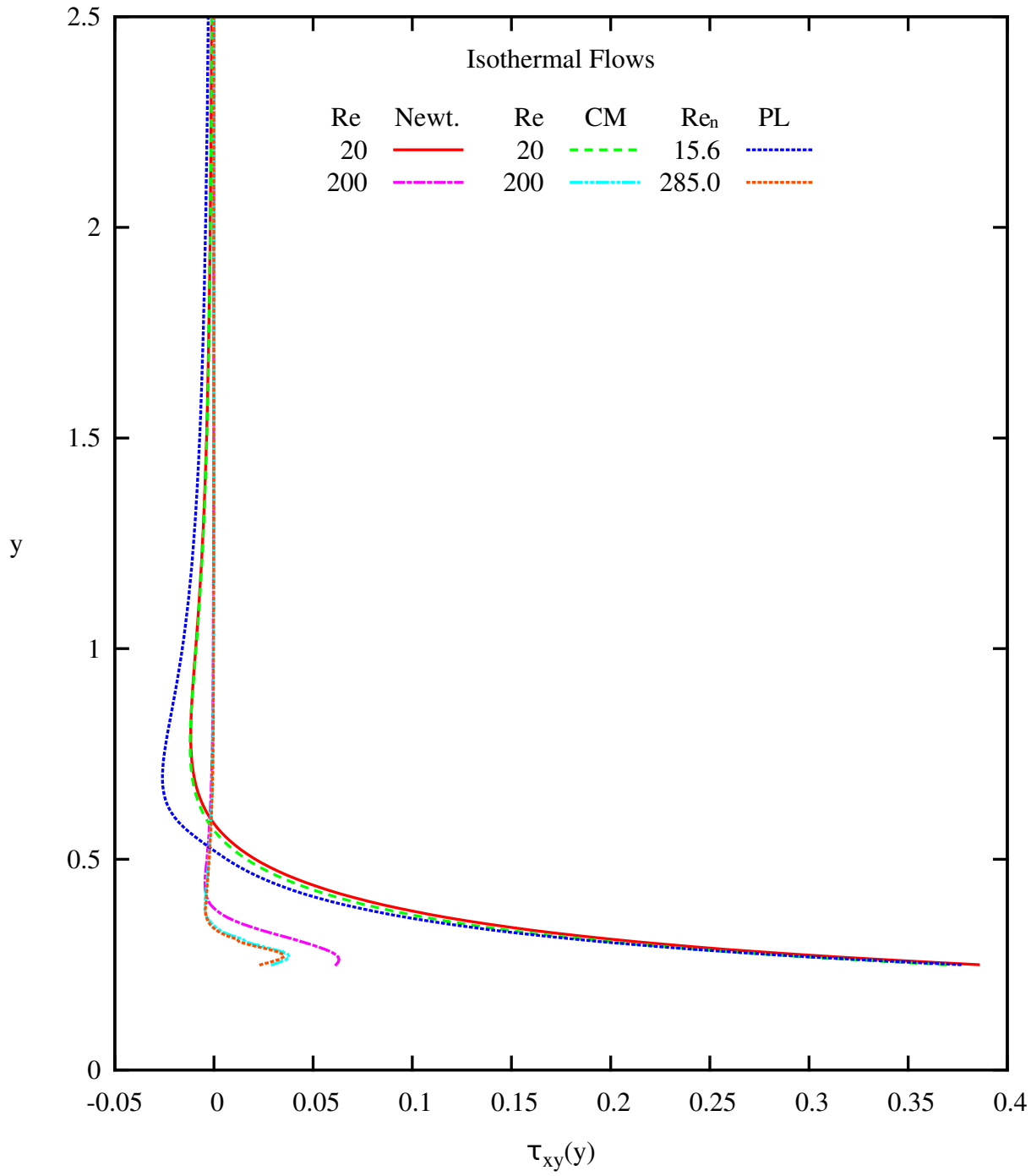

Figure 4.39: Shear Stressτ_{xy} versus y at $x = 0$: Comparison of Solutions for Newtonian, Power-Law and Carreau Fluids (Isothermal)

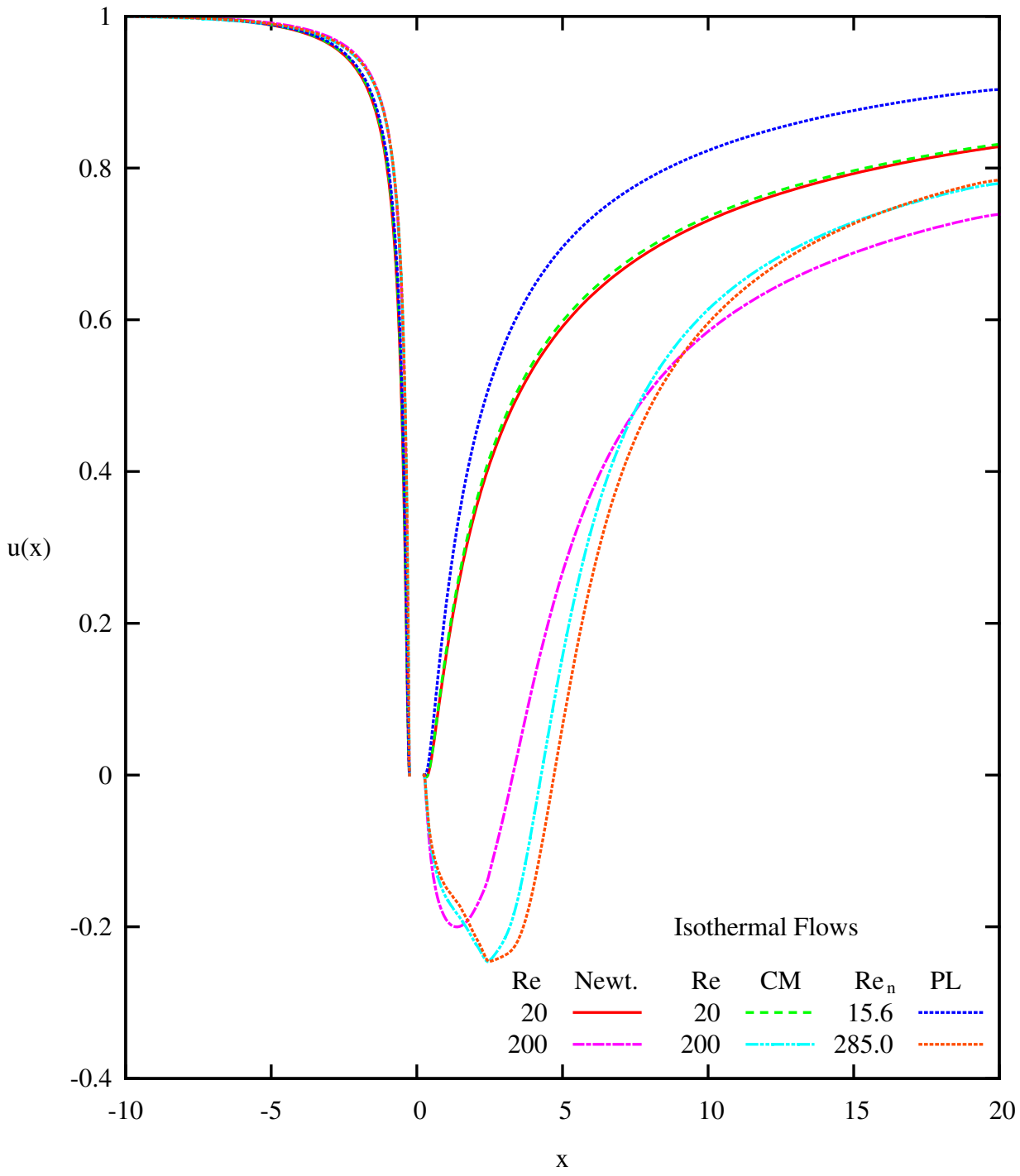

Figure 4.40: Velocity v versus x at $y = 0$: Comparison of Solutions for Newtonian, Power-Law and Carreau Fluids (Isothermal)

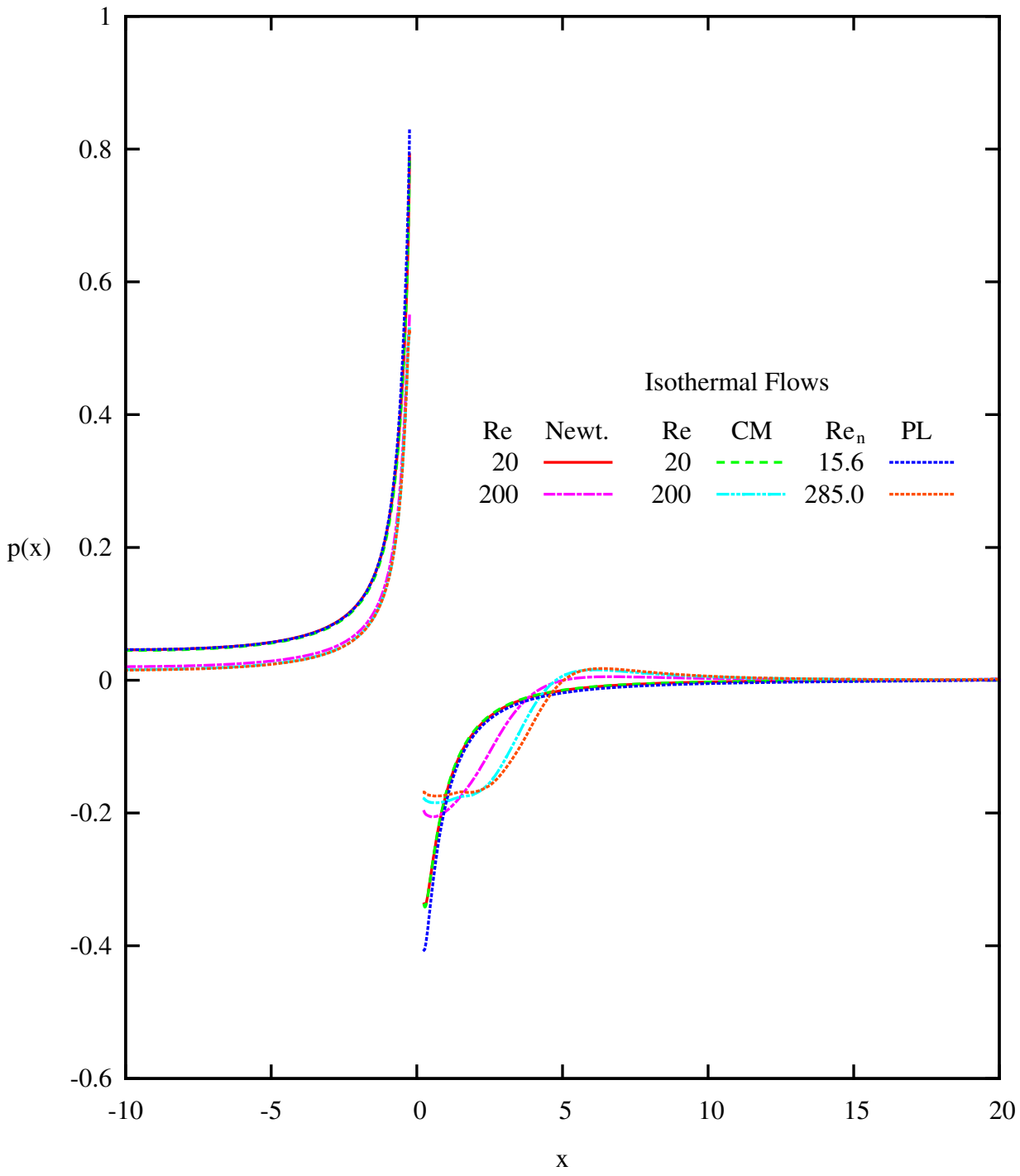

Figure 4.41: Pressure p versus x at $y = 0$: Comparison of Solutions for Newtonian, Power-Law and Carreau Fluids (Isothermal)

4.5 Non-Isothermal Flows

In this section we present numerical studies for non-isothermal flows of Newtonian, power-law and Carreau fluids using the same domain size used in the case of isothermal studies presented in section 4.4. The discretizations shown in figures 4.7 and 4.8 are also used in these numerical studies.

The reference velocity u_0 and the corresponding Reynolds numbers for Newtonian, power-law and Carreau fluids remain the same as shown in table 4.1. The temperature and the heat flux boundary conditions are shown in figure 4.42. The system is insulated, hence the heat generation is only due to viscous dissipation. The results are presented in the following sections. All computations are performed using the combined mathematical model.

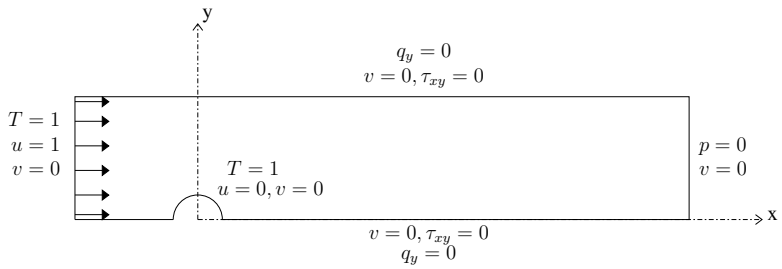

Figure 4.42: Schematic of Non-Isothermal Boundary Conditions

4.5.1 Newtonian Fluid (Non-Isothermal Flows)

As discussed in section 2.5, when the transport properties are constant, the energy equation and heat flux equations are only weakly coupled (or decoupled) with the rest of the mathematical model, hence we expect u, v, p, τ_{xx}, τ_{yy}, and τ_{xy} to be the same for isothermal and non-isothermal flows. Figure 4.43 shows a plot of u versus y at $x = 0$ for $Re = 200$

and a comparison with the results obtained from the isothermal flow study. Both velocity profiles agree quite well. Plots of v, p, τ_{xy} versus y at $x = 0$ and u, p versus x at $y = 0$ for non-isothermal flows and comparisons with isothermal results are shown in Appendix B in figures B.1 - B.5. We observe excellent agreement between the two.

Graphs of temperature T versus y at $x = 0$ and T versus x at $y = 0$ for Re = 20, 40, 60, 100 and 200 are shown in 4.44 - 4.46. Pronounced increase in heat generation at the leading boundary of the cylinder and hence progressively increasing temperature field is quite obvious with increasing Reynolds numbers. The carpet plots of temperature and streamlines are shown in figures 4.47 - 4.49 for Re = 20, 40, 60, 100 and 200. As seen in x, y plots in figures 4.44 - 4.46, for low Reynolds numbers the viscous dissipation is weak but beyond Re = 100, we observe significant temperature rise at the leading boundary of the cylinder ($x = -0.25$, $y = 0.0$ and $x = 0.0$, $y = 0.25$) which, due to conduction, causes significant temperature rise in the recirculation zone behind the cylinder. Results for u, v, p, τ_{xx}, τ_{yy}, and τ_{xy} for Re = 20, 40, 60 and 100 are not shown as they are identical to those for isothermal case.

4.5.2 Power-Law Fluid (Non-Isothermal Flows)

For this case, the viscosity is a function of the second invariant of the strain rate tensor which is a function of the velocity gradients, hence the energy equations and the heat flux equations are also decoupled (or weakly coupled) from the rest of the mathematical model. Therefore, we expect the deformation fields from isothermal and non-isothermal cases to be the same, except for temperature.

Figure 4.50 shows that velocity u versus y at $x = 0$ (Re_n = 285.0) agrees quite well

with the isothermal case. Plots of v, p, τ_{xy} versus y at $x = 0$ and u, p versus x at $y = 0$ and comparisons with isothermal case are shown in figures B.6 - B.10. Agreement of the results from isothermal and non-isothermal studies is quite good.

Plots of temperature T versus y at $x = 0$ and temperature T versus x at $y = 0$ (for all Reynolds numbers considered here) are shown in figures 4.51 - 4.53. Once again, as in the case of Newtonian fluid, progressively increasing Reynolds numbers produce progressively increasing dissipation resulting in higher temperature field at the leading boundary of the cylinder and in the recirculation zone (due to conduction). Streamline and temperature carpet plots are similar in appearance to the Newtonian case and hence are not shown.

4.5.3 Carreau Model Fluid (Non-Isothermal Flows)

In this case, as in power-law, the viscosity is a function of the second invariant of the strain rate tensor, hence we expect u, v, p, τ_{xx}, τ_{yy} and τ_{xy} to be the same as those for the isothermal case.

Figure 4.54 shows a plot of u versus y at $x = 0$ (for Re = 200) and comparison with isothermal case. Plots of v, p, τ_{xy} versus y at $x = 0$ and u, p versus x at $y = 0$ (at Re = 200) and comparisons with isothermal case are shown in figures B.11 - B.15. Good agreement between isothermal and non-isothermal results is observed.

Plots of temperature T versus y at $x = 0$ and temperature T versus x at $y = 0$ for all Reynolds numbers considered here are shown in figures 4.55 - 4.57. Once again, as in case of other fluids, we observe progressively more pronounced temperature field around the leading boundary of the cylinder and the recirculation zone with increasing Reynolds numbers. Carpet plots of temperature and streamlines are similar to Newtonian case and

hence are not shown here.

4.5.4 Discussion and Comparison of Results (Non-Isothermal Flows)

Figures 4.58 - 4.60 show plots of temperature T versus y at $x = 0$ and T versus x at $y = 0$ for Re = 20 (15.6, PL) and 200 (285.0, PL) for Newtonian, power-law and Carreau models. As expected, Newtonian fluid, which has the highest viscosity, results in the most dissipation and hence the strongest temperature field. Power-law and Carreau models used here are for shear thinning fluids, therefore lower dissipation than Newtonian case is expected and is in-fact observed from the results presented in the plots.

The power-law and Carreau models are used to describe the same fluid, thus the difference in the temperature profiles are due to the different empirical fit to the experimental data, i.e. viscosity $\eta\left(I_2\right)$ is not identically the same in the two models.

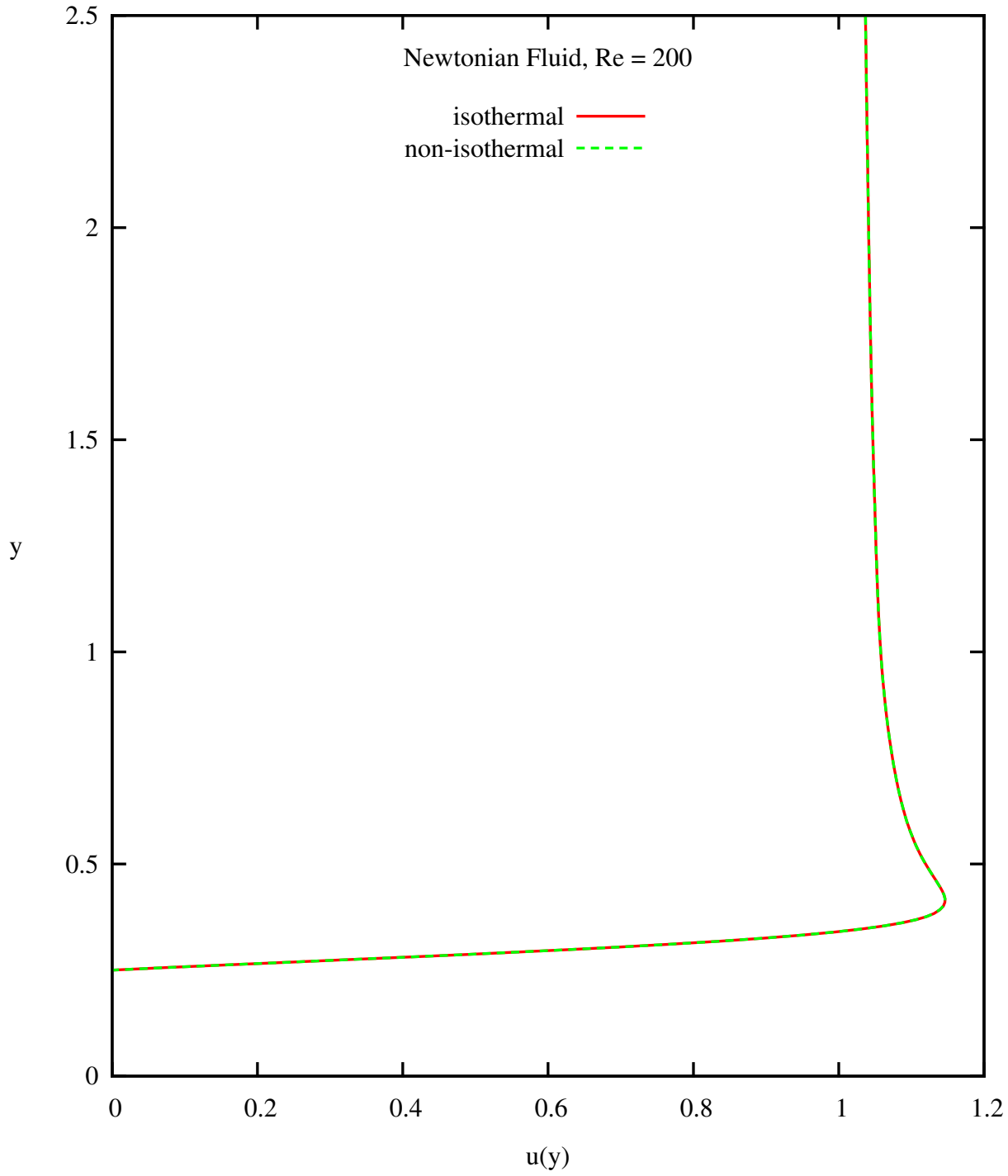

Figure 4.43: Velocity u versus y at $x = 0$: Comparison of Isothermal and Non-Isothermal Flows at Re = 200 (Newtonian)

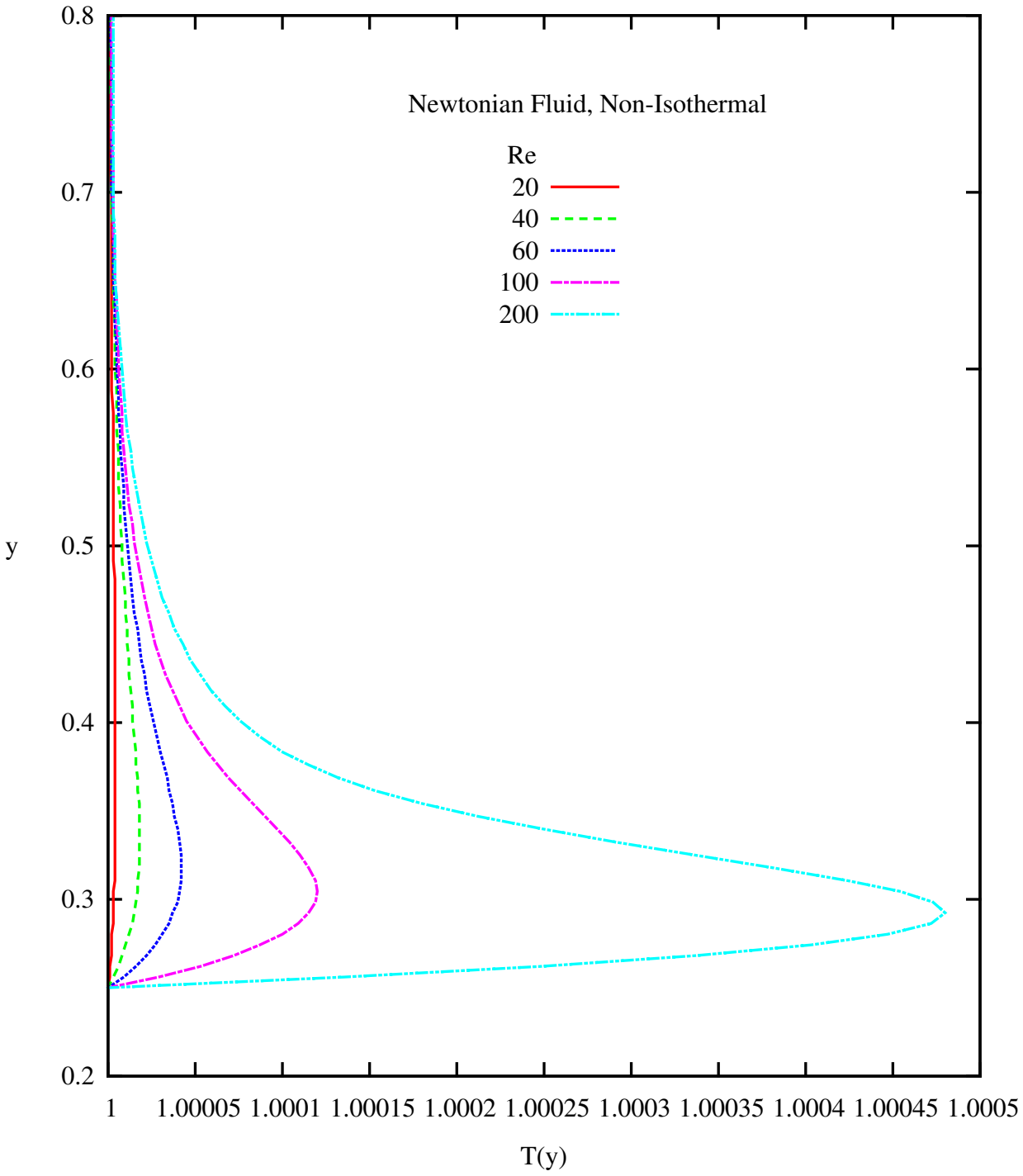

Figure 4.44: Temperature T versus y at $x = 0$ (Newtonian, Non-Isothermal)

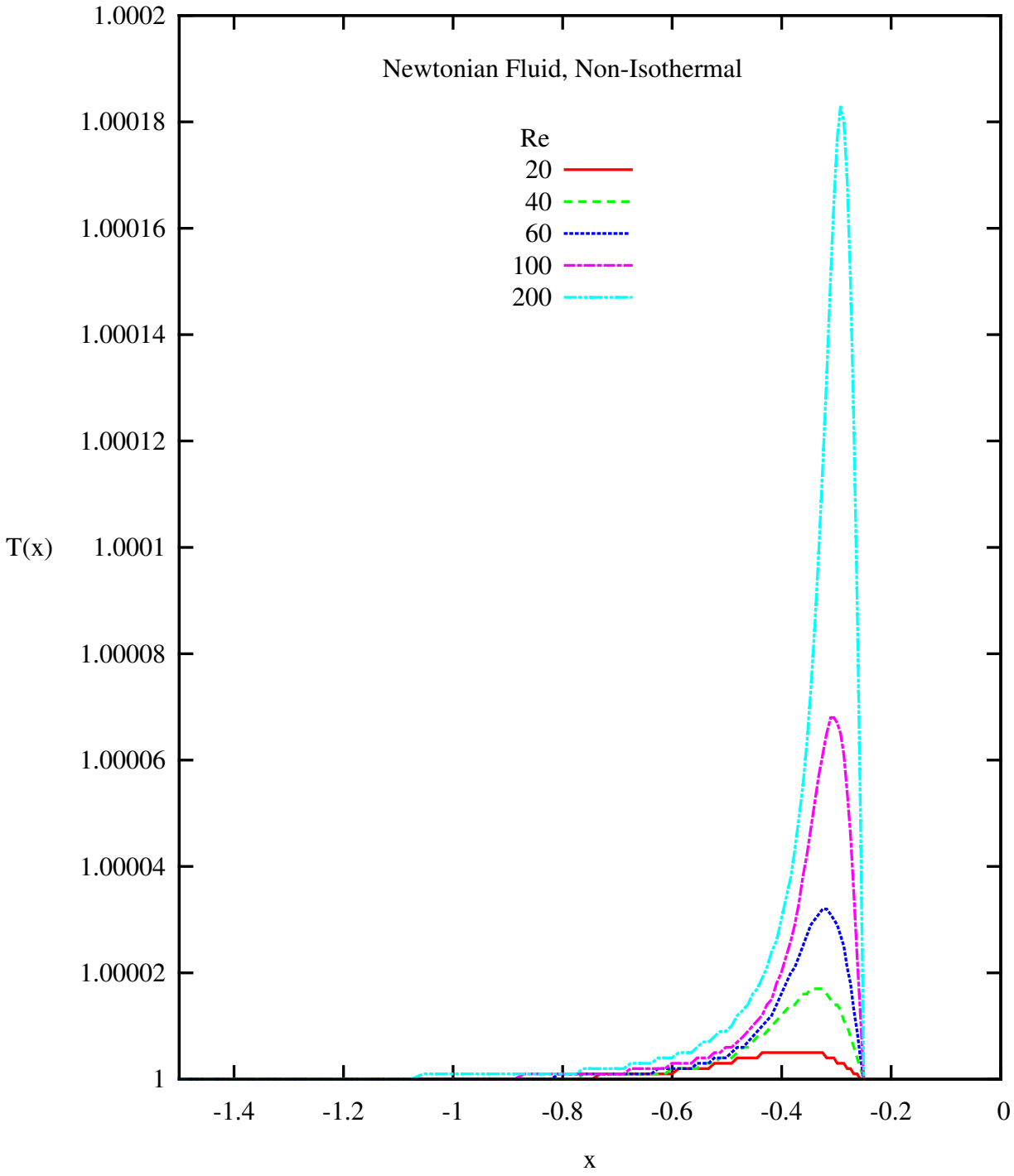

Figure 4.45: Temperature T versus x at $y = 0$, $-1.5 \leq x \leq 0$ (Newtonian, Non-Isothermal)

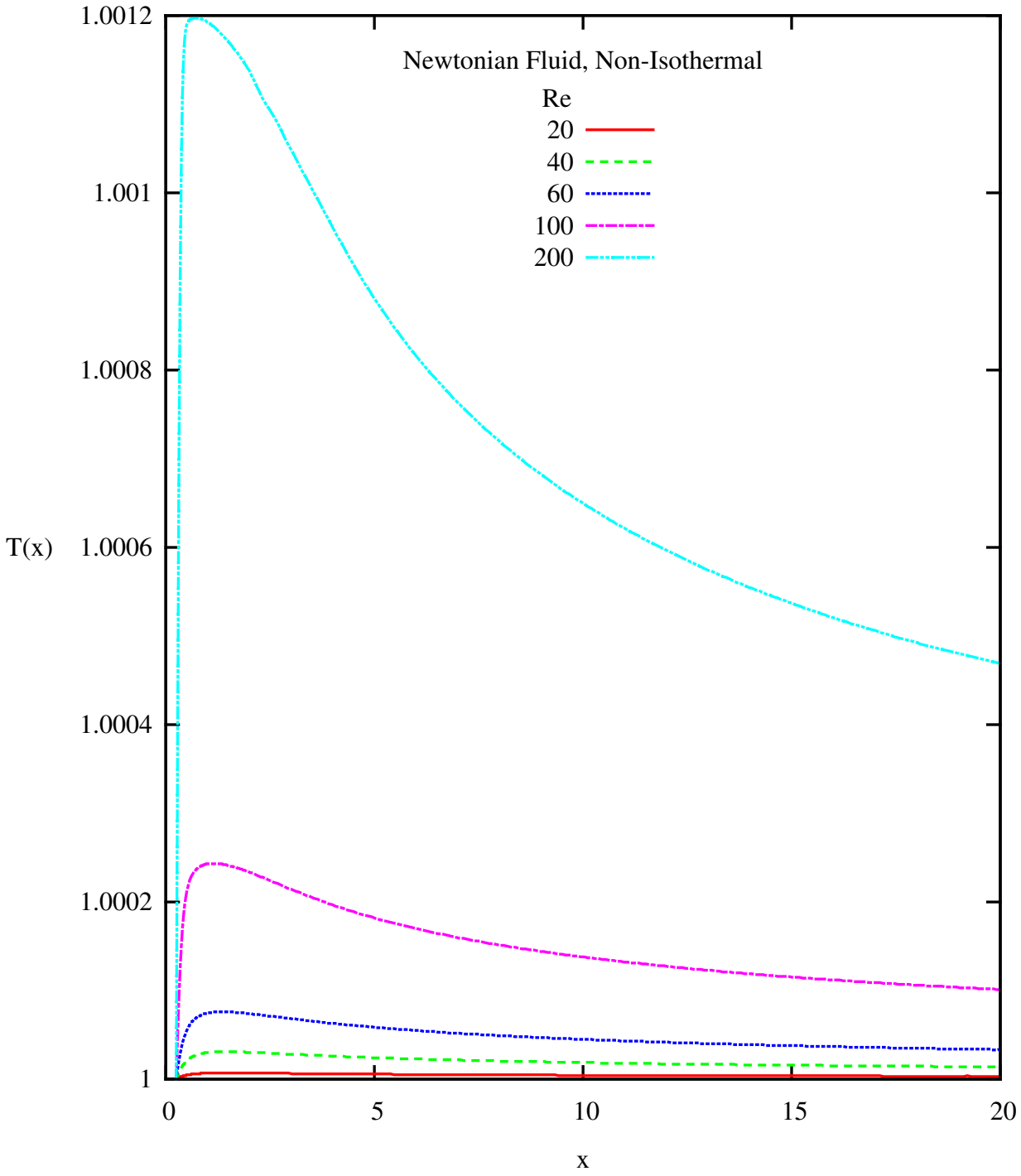

Figure 4.46: Temperature T versus x at $y = 0$, $0 \leq x \leq 20$ (Newtonian, Non-Isothermal)

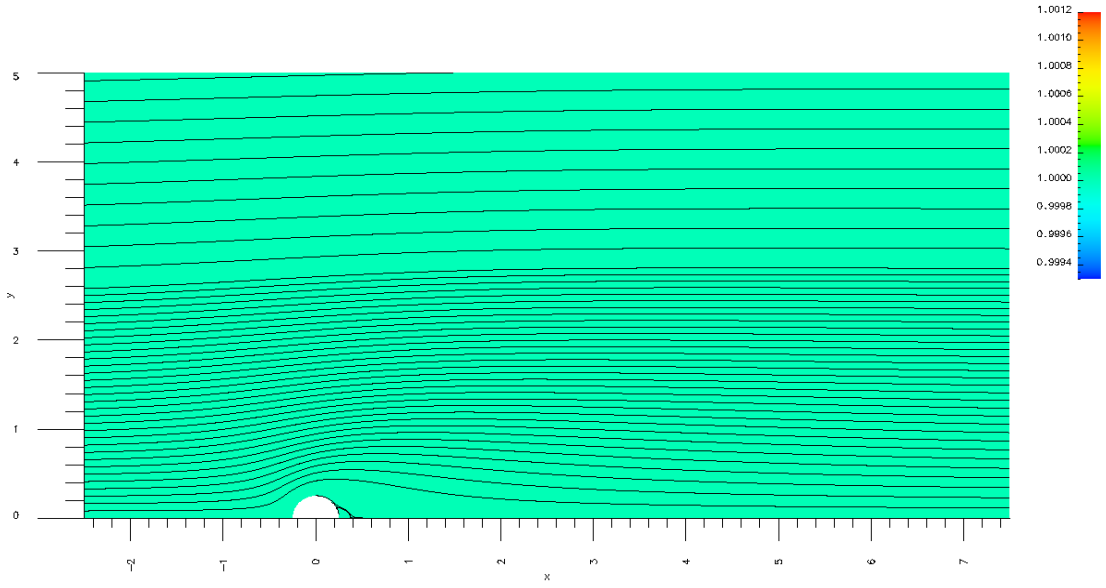

(a) Re = 20

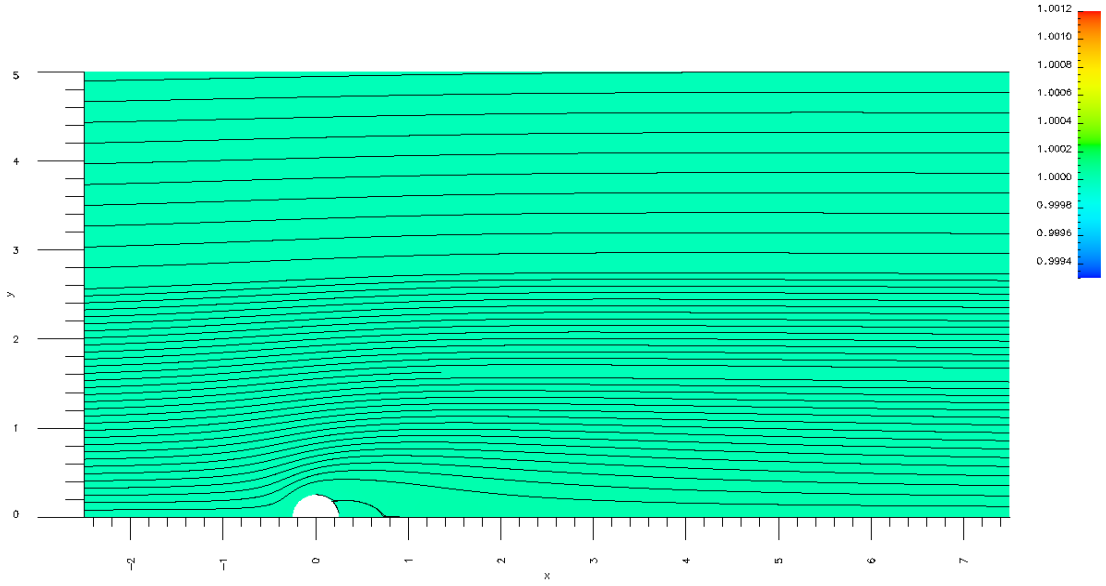

(b) Re = 40

Figure 4.47: Carpet and Streamline Plot of T at Re = 20 and 40 (Newtonian, Non-Isothermal)

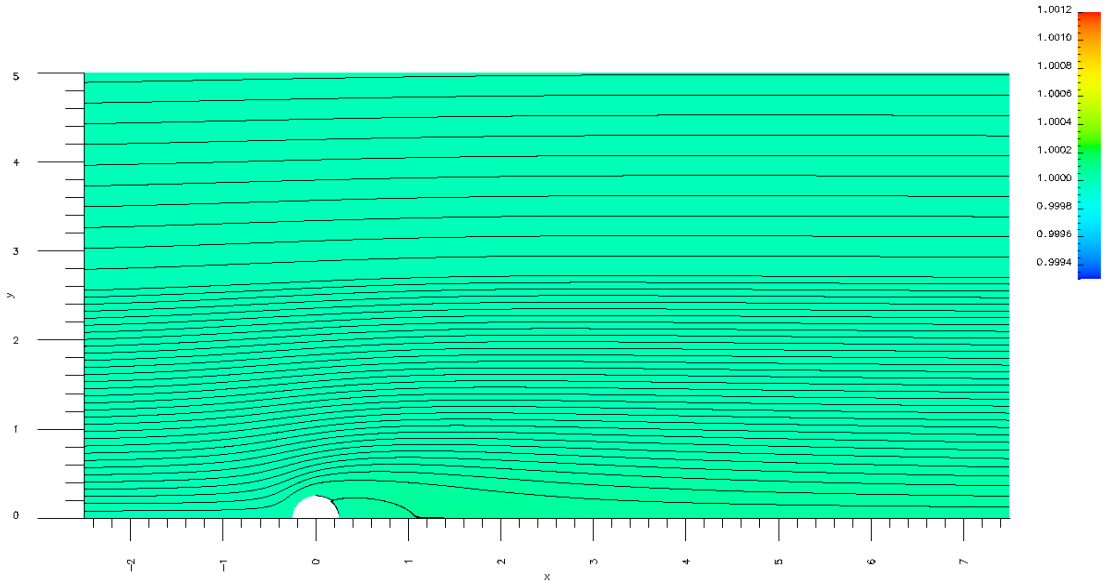

(a) Re = 60

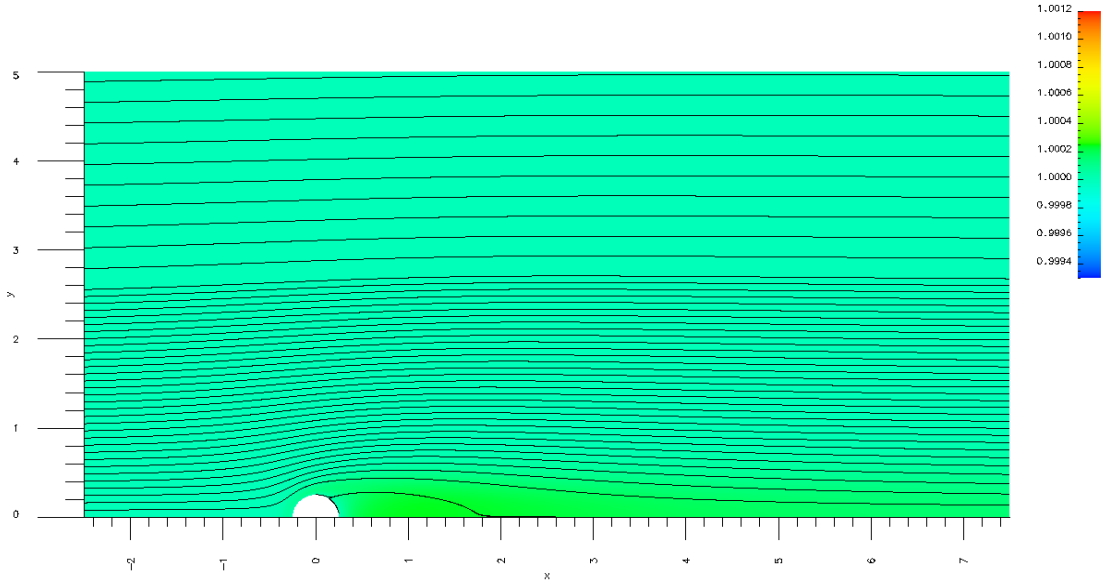

(b) Re = 100

Figure 4.48: Carpet and Streamline Plot of T at Re = 60 and 100 (Newtonian, Non-Isothermal)

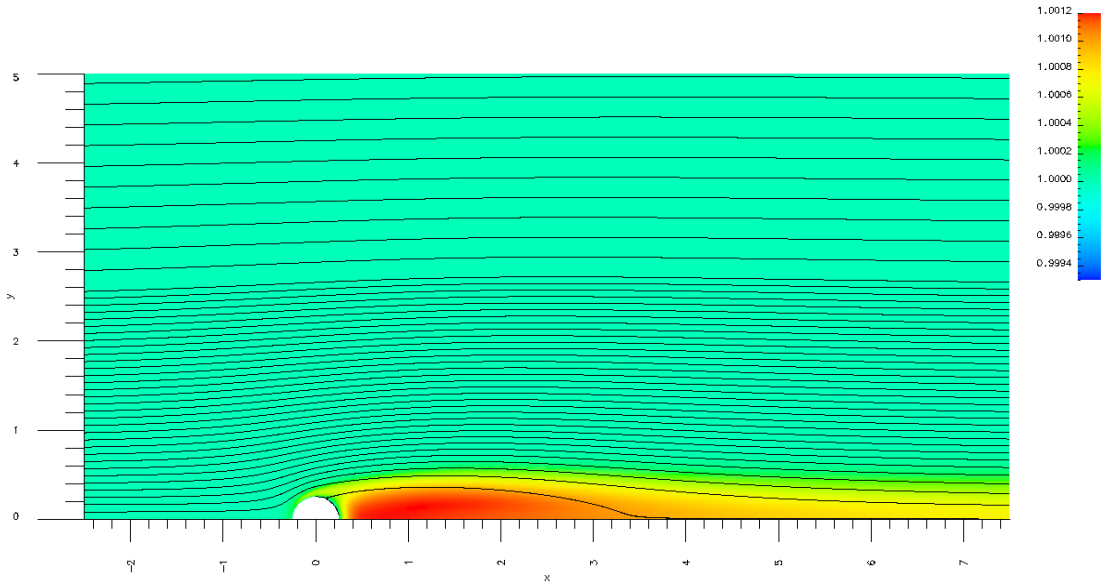

Figure 4.49: Carpet and Streamline Plot of T at Re = 200 (Newtonian, Non-Isothermal)

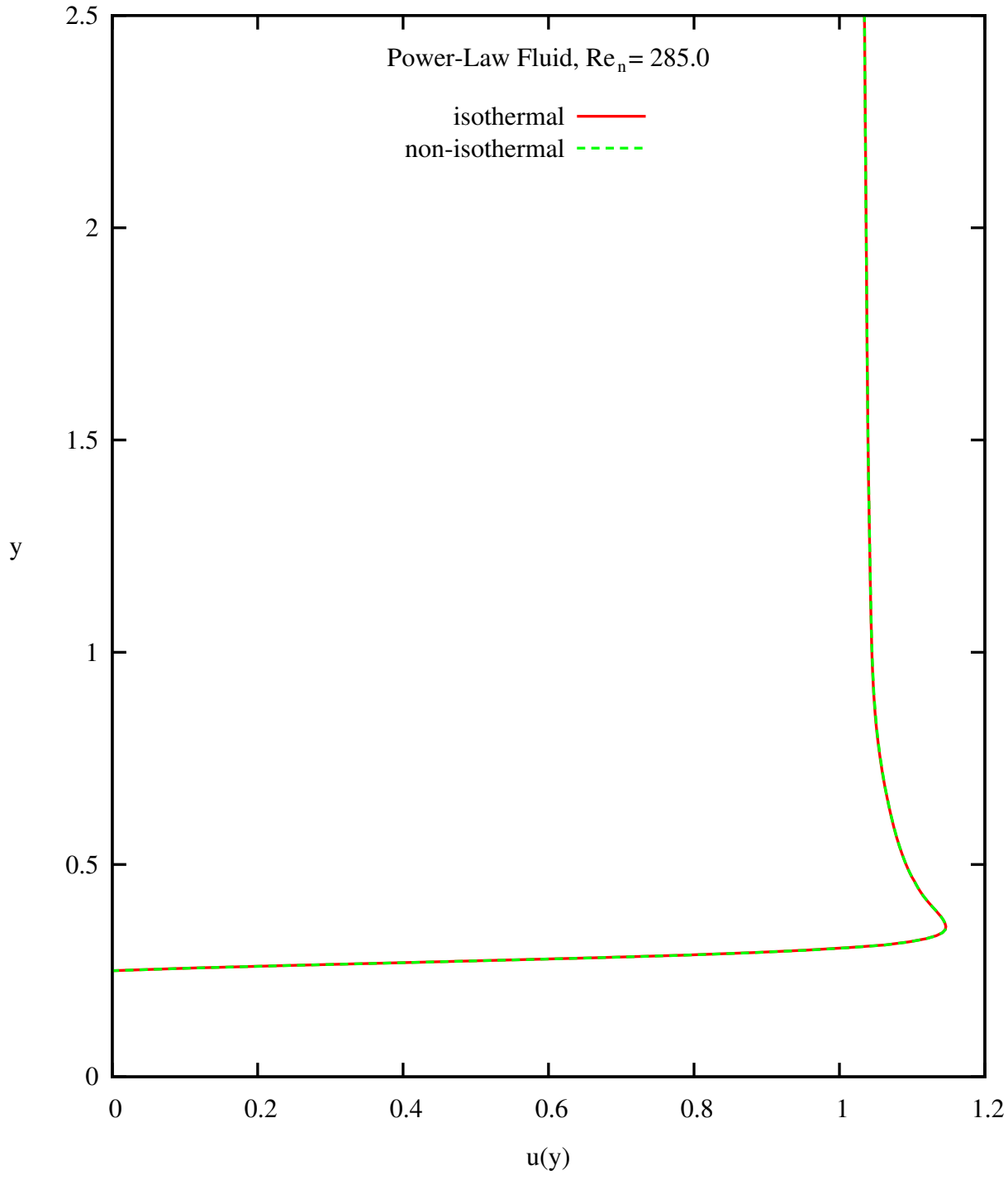

Figure 4.50: Velocity u versus y at $x = 0$: Comparison of Isothermal and Non-Isothermal Flows at Re = 285.0 (Power-Law)

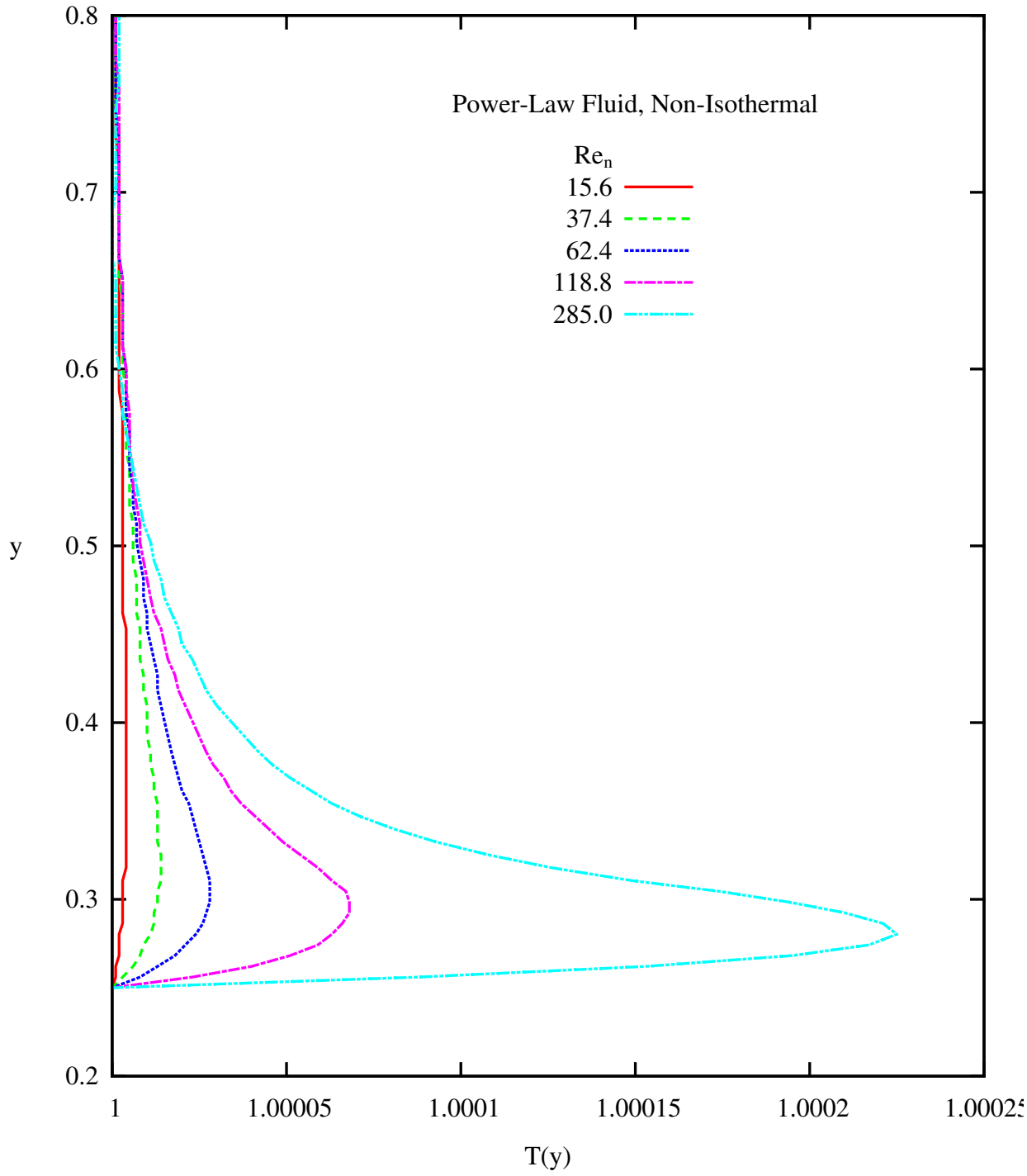

Figure 4.51: Temperature T versus y at $x = 0$ (Power-Law, Non-Isothermal)

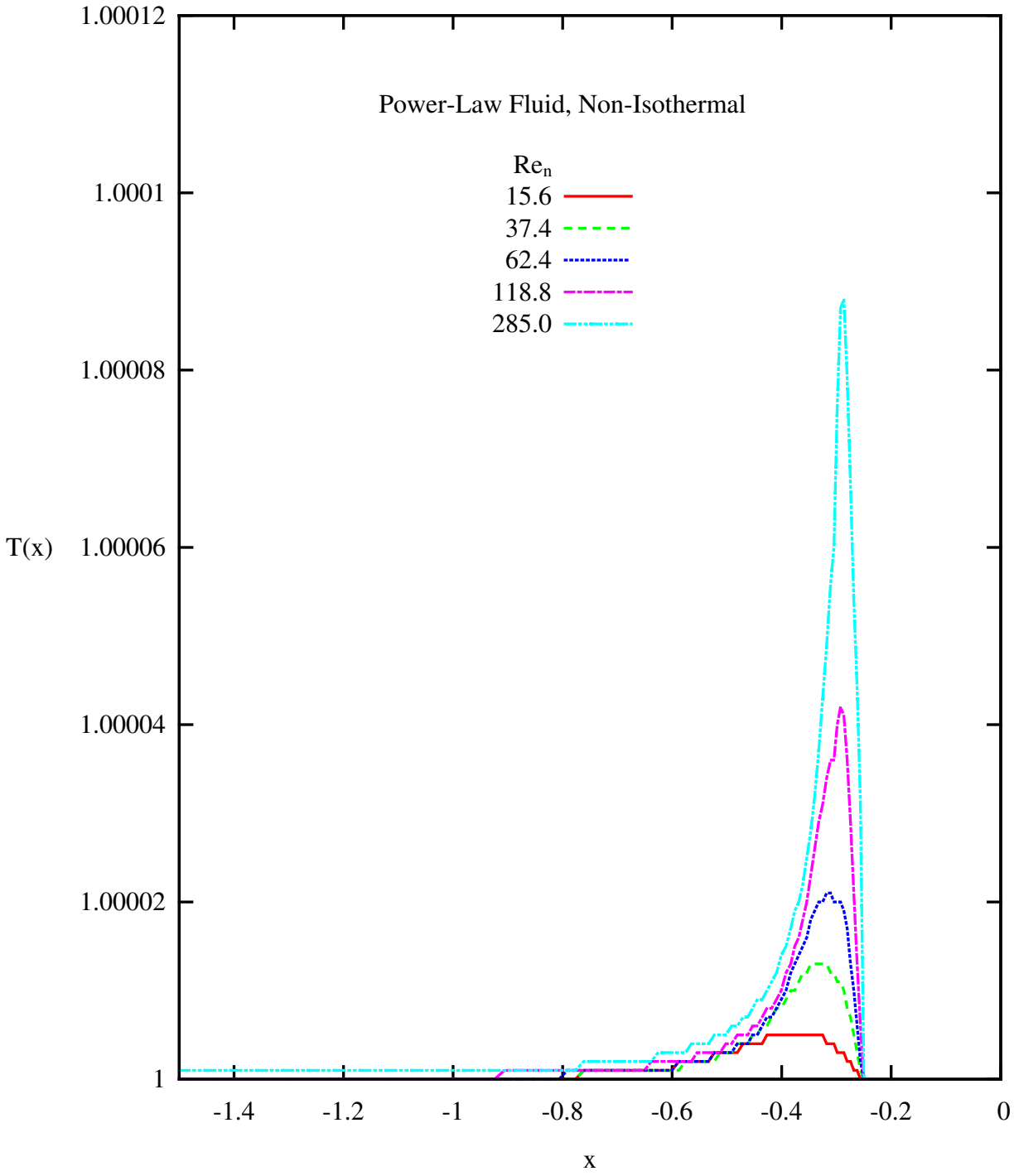

Figure 4.52: Temperature T versus x at $y = 0$, $-1.5 \leq x \leq 0$ (Power-Law, Non-Isothermal)

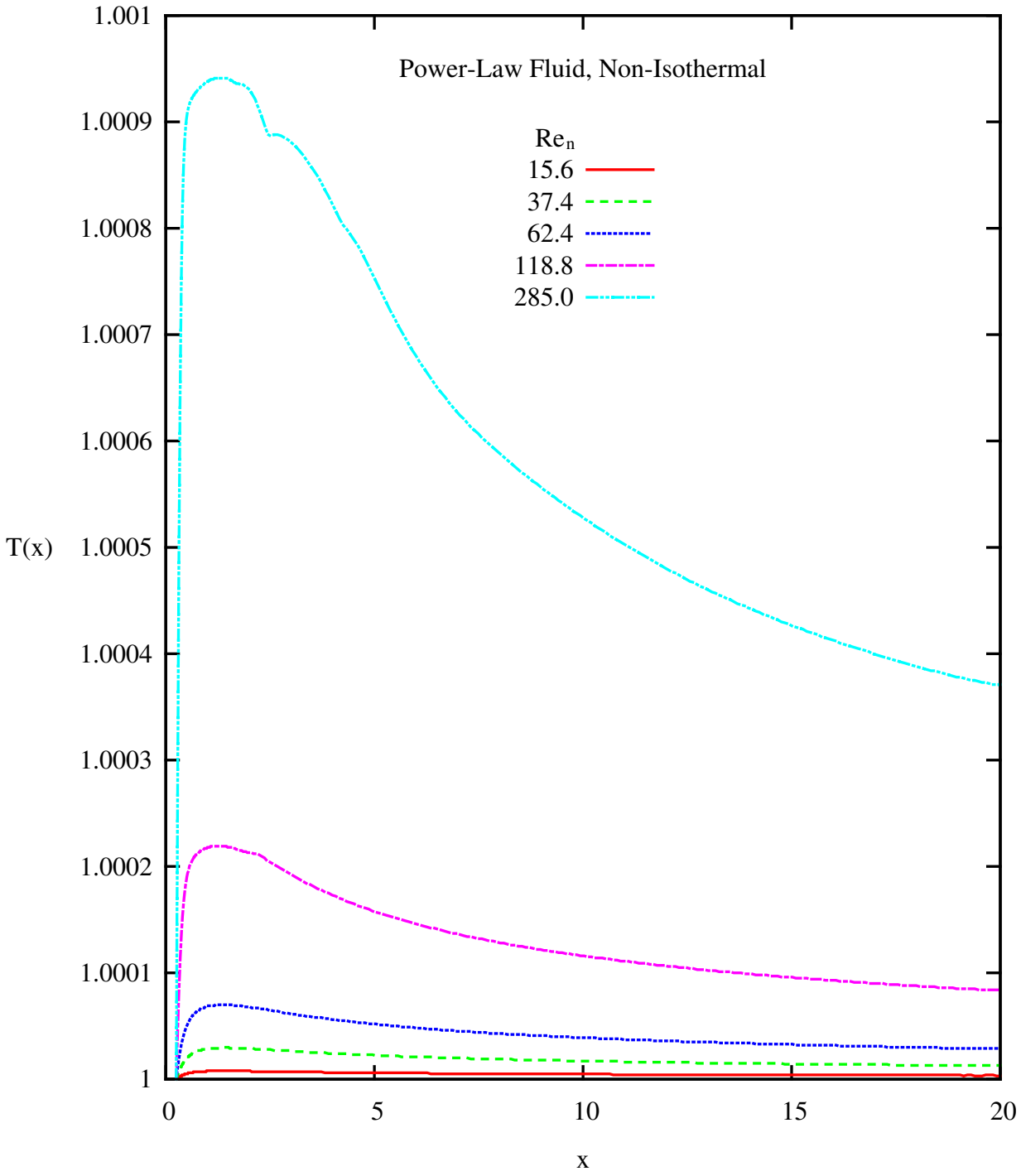

Figure 4.53: Temperature T versus x at $y = 0$, $0 \leq x \leq 20$ (Power-Law, Non-Isothermal)

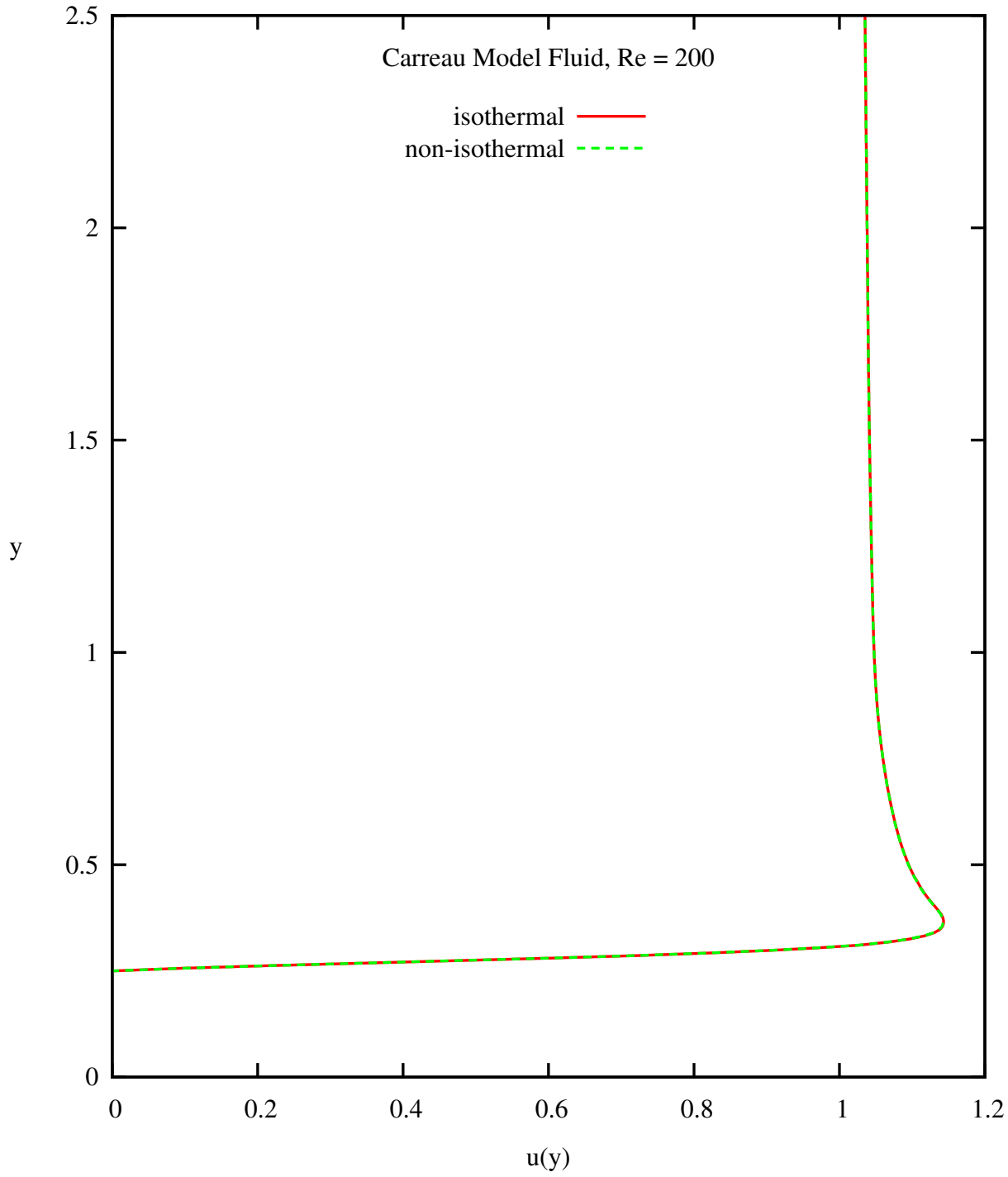

Figure 4.54: Velocity u versus y at $x = 0$: Comparison of Isothermal and Non-Isothermal Flows at Re = 200 (Carreau Model)

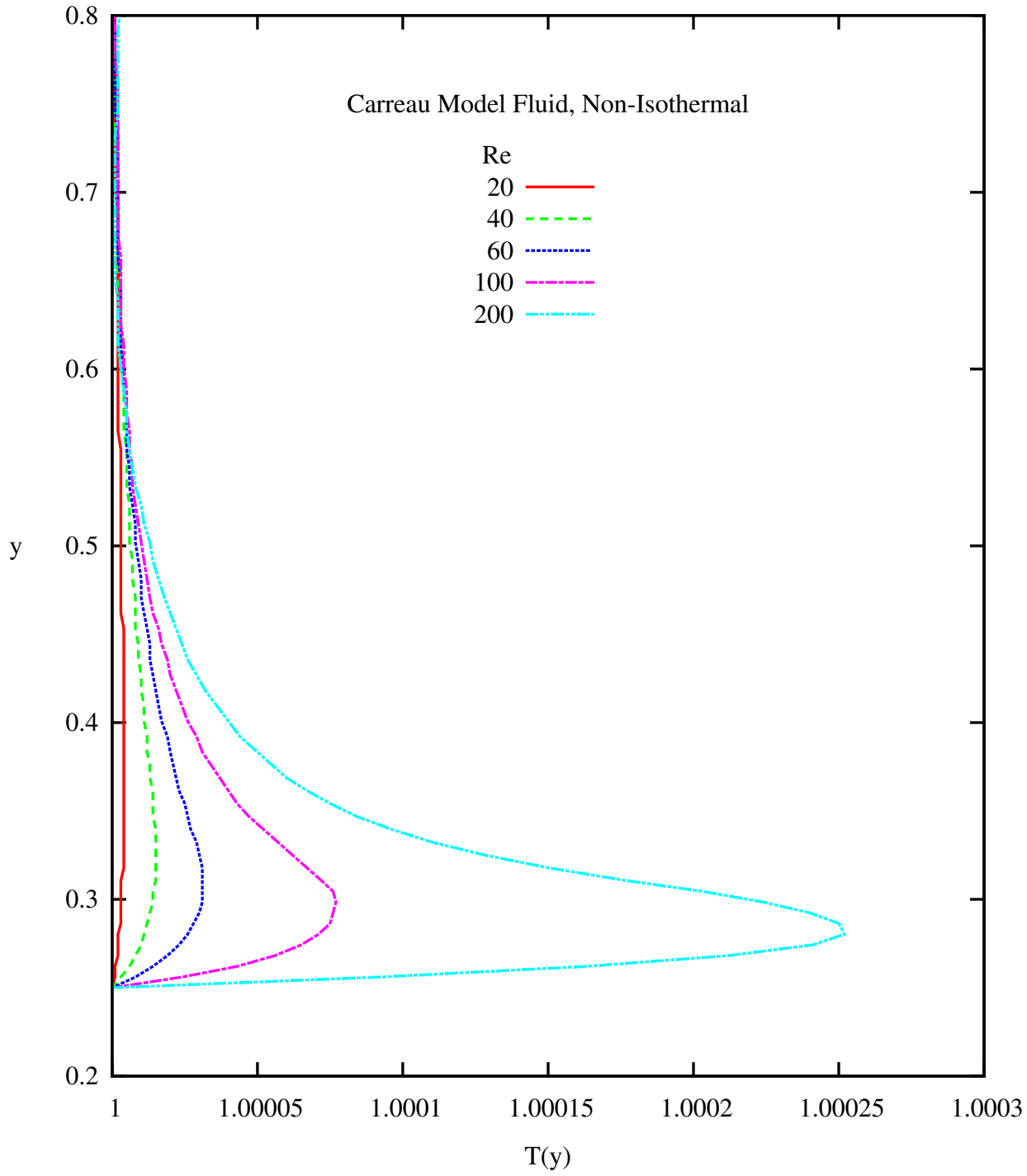

Figure 4.55: Temperature T versus y at $x = 0$ (Carreau Model, Non-Isothermal)

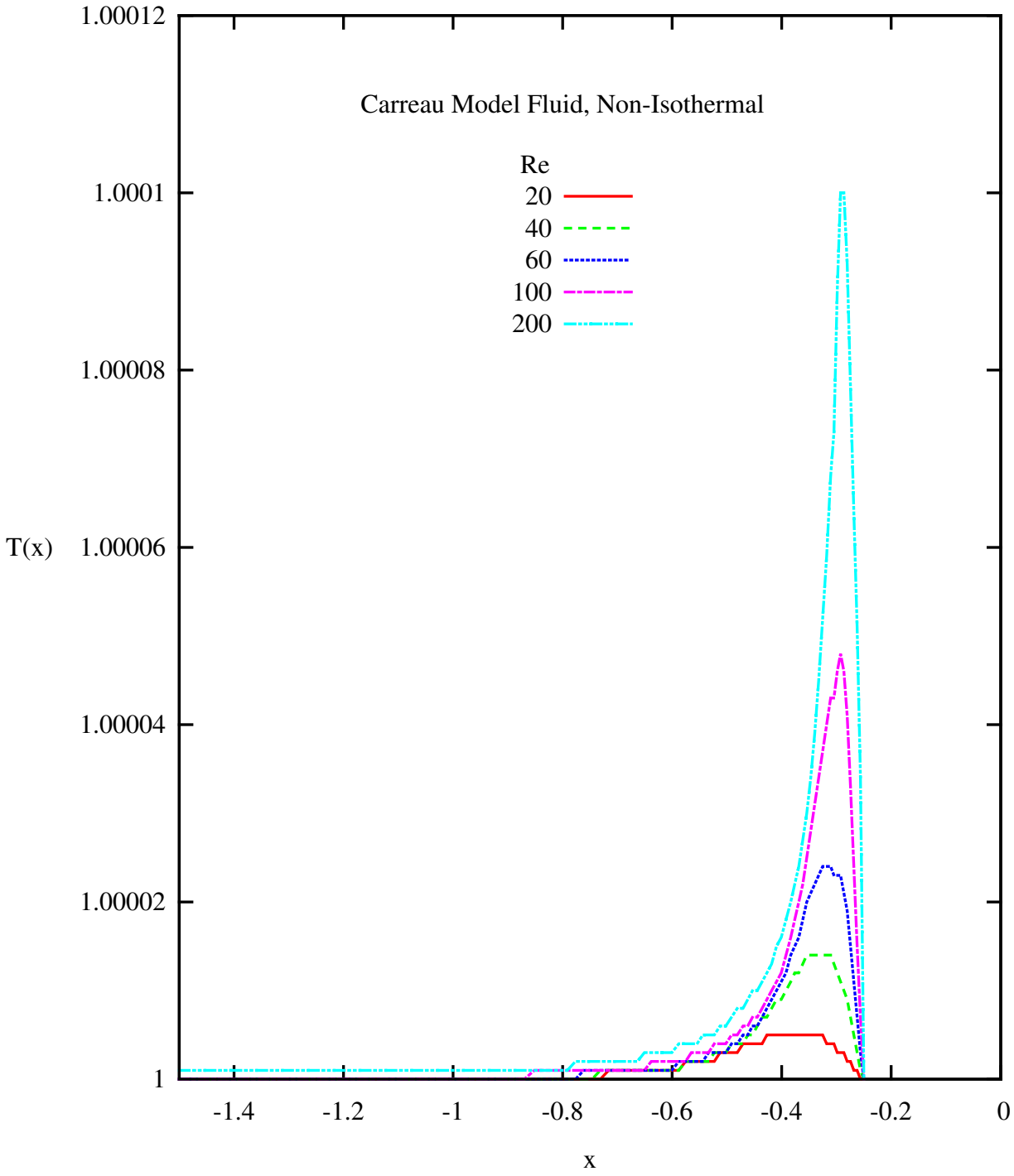

Figure 4.56: Temperature T versus x at $y = 0$, $-1.5 \leq x \leq 0$ (Carreau Model, Non-Isothermal)

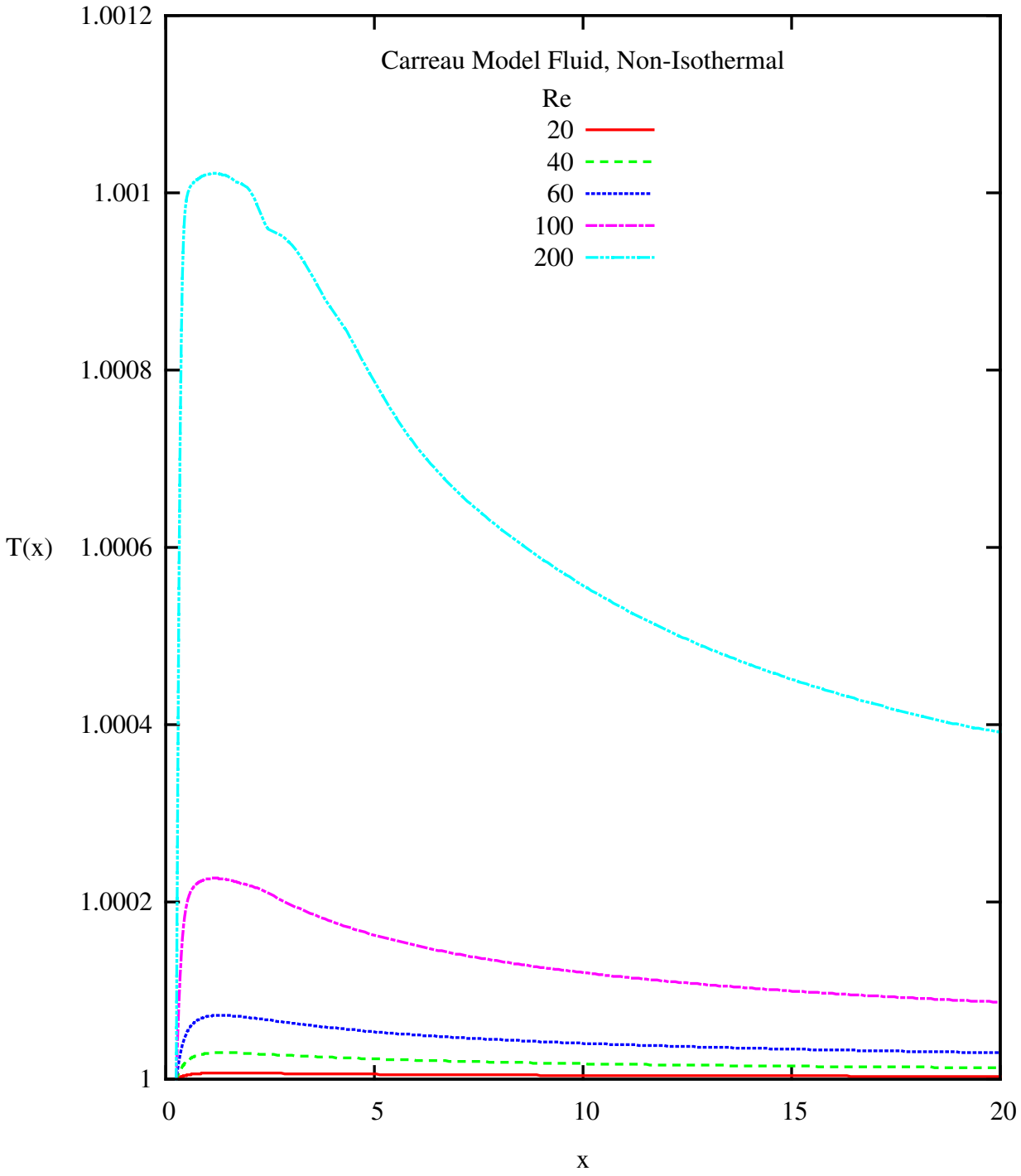

Figure 4.57: Temperature T versus x at $y = 0$, $0 \leq x \leq 20$ (Carreau Model, Non-Isothermal)

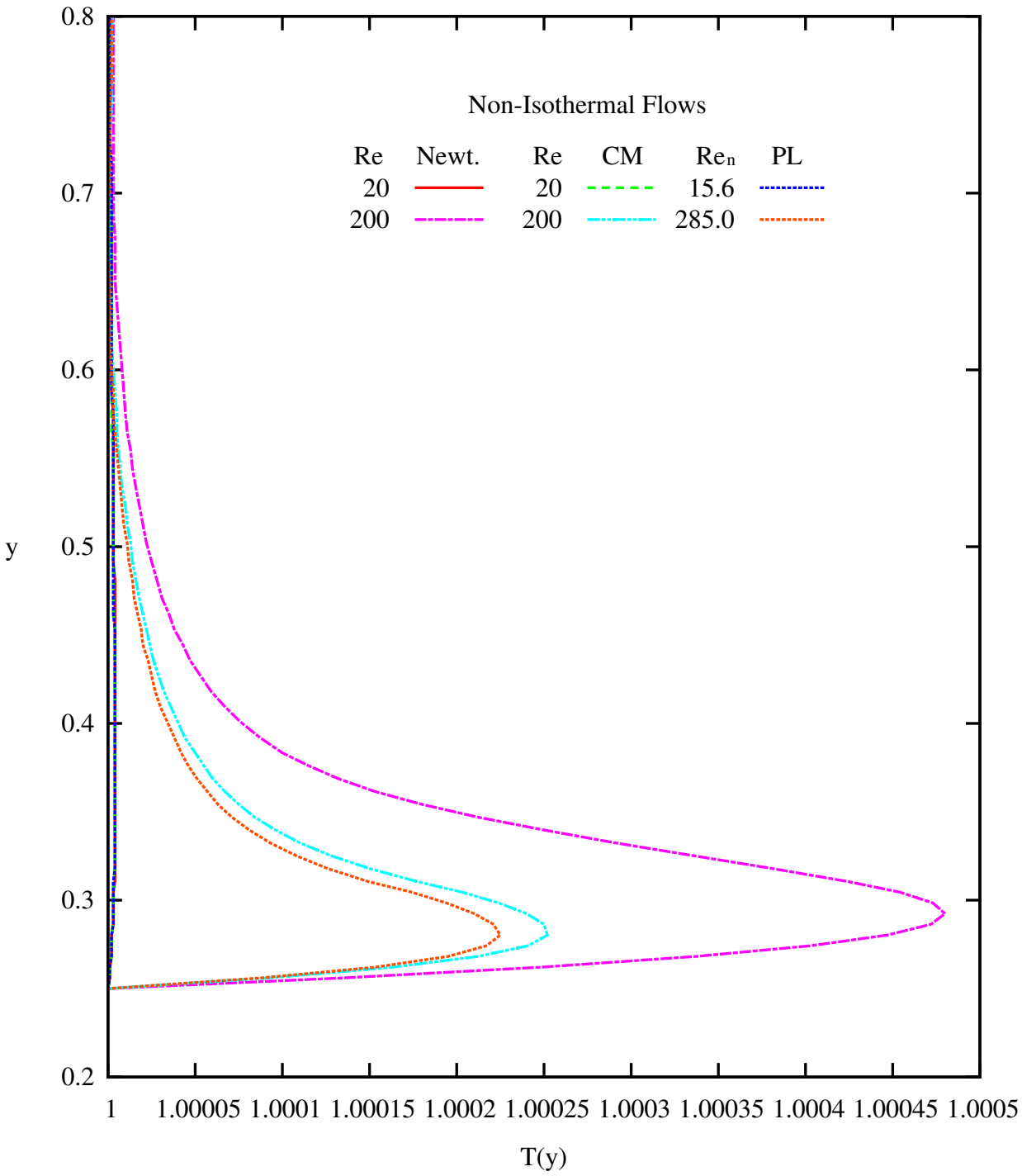

Figure 4.58: Temperature T versus y at $x = 0$: Comparison of Solutions for Newtonian, Carreau and Power-Law Fluids (Non-Isothermal)

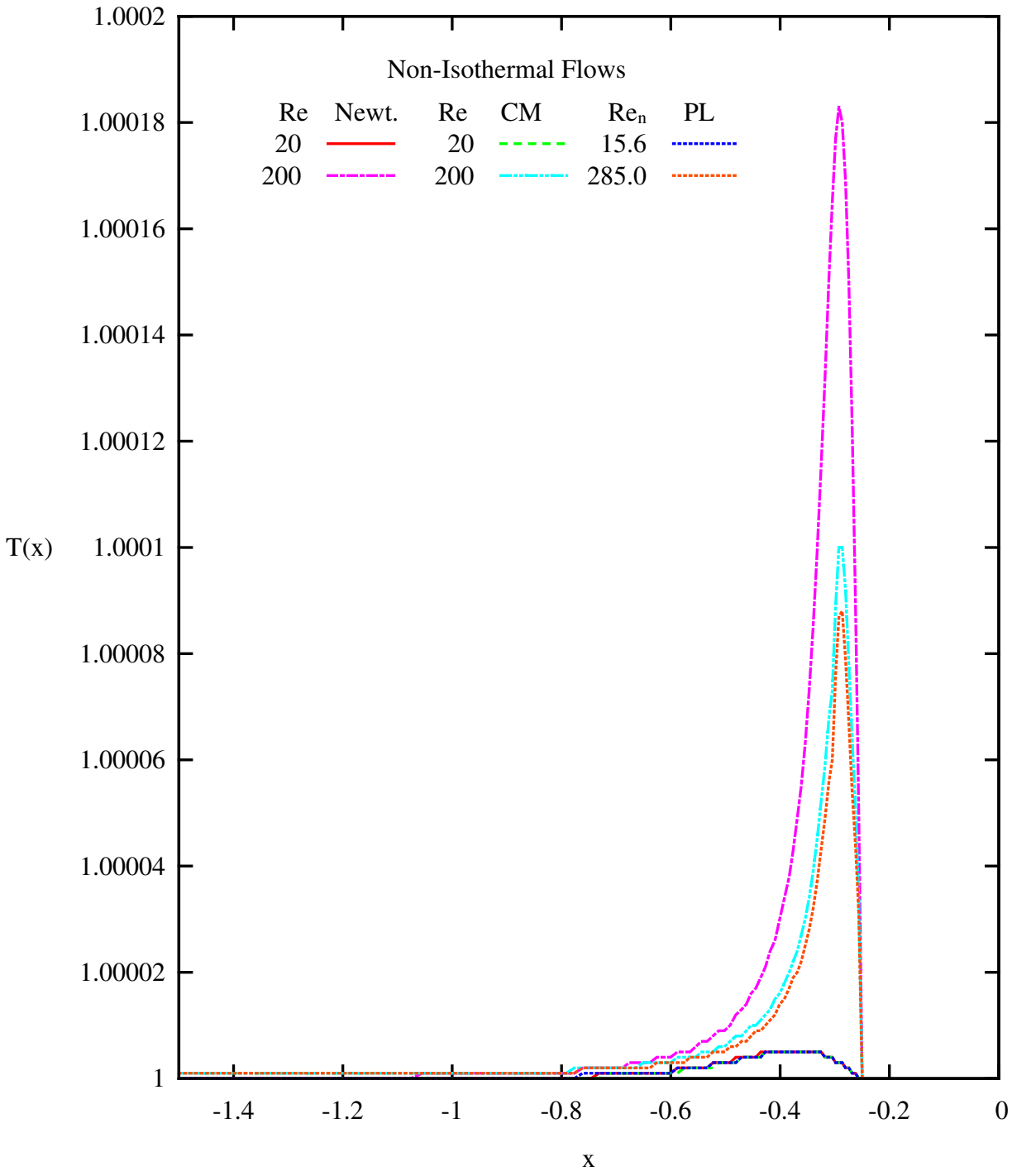

Figure 4.59: Temperature T versus x at $y = 0$, $-1.5 \leq x \leq 0$: Comparison of Solutions for Newtonian, Carreau and Power-Law Fluids (Non-Isothermal)

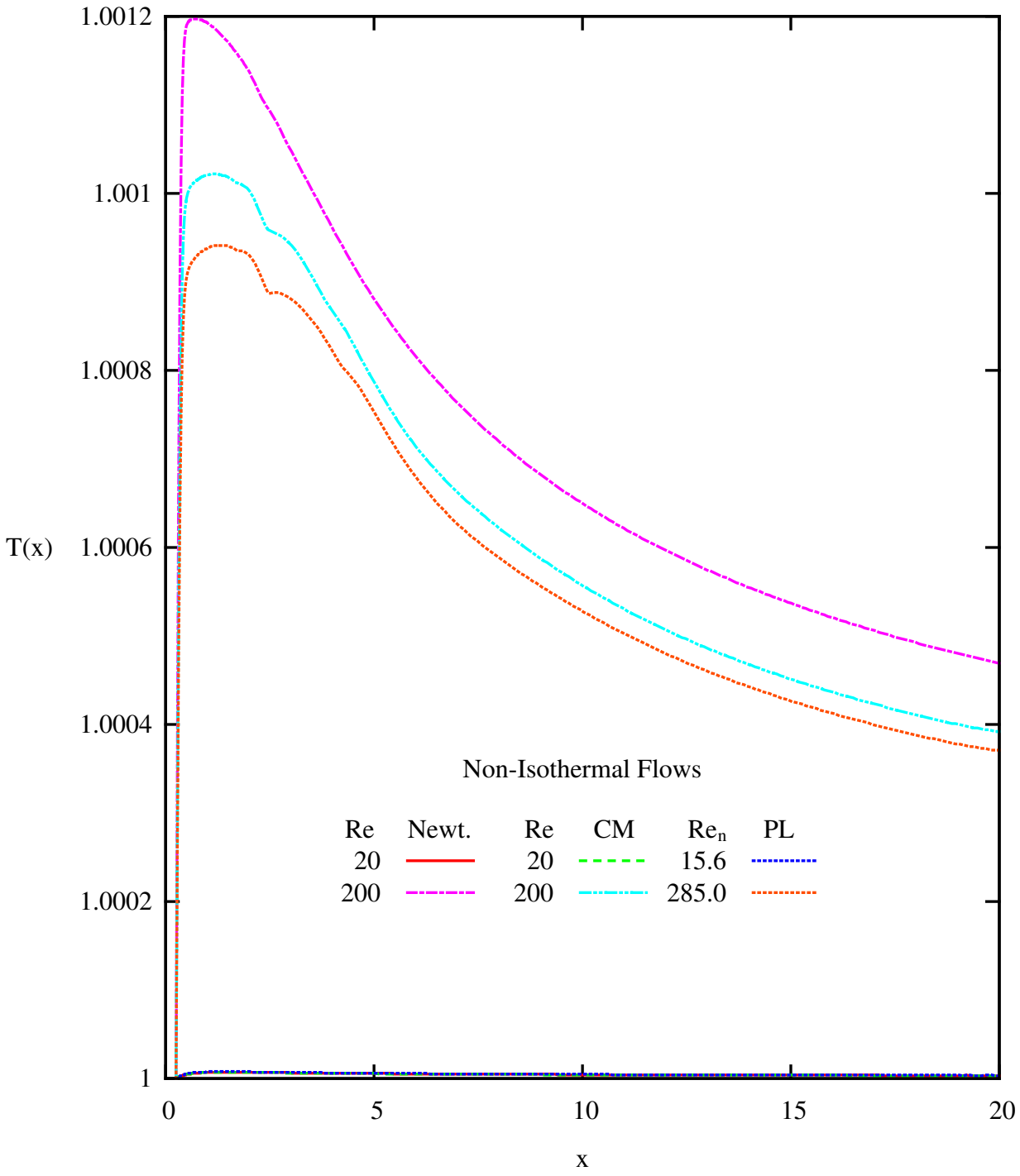

Figure 4.60: Temperature T versus x at $y = 0$, $0 \leq x \leq 20$: Comparison of Solutions for Newtonian, Carreau and Power-Law Fluids (Non-Isothermal)

Chapter 5

Summary and Conclusions

Mathematical models and their dimensionless forms are presented for isothermal and non-isothermal steady flows of incompressible, homogeneous and isotropic fluids using conservation of mass, balance of momenta and first law of thermodynamics. The constitutive equations for deviatonic Cauchy stress tensor consider Newtonian fluids with constant transport properties, and power law and Carreau fluids with shear rate dependent viscosity in which the fluid viscosity is a function of the second invariant I_2 of the strain rate tensor. Flow over a circular cylinder is considered as a model problem with the objective of presenting benchmark quality numerical solutions for progressively increasing Reynolds numbers. Numerical solutions of the non-linear partial differential equations resulting from the mathematical models (BVPs) are obtained using finite element processes based on minimization of residual functional, i.e. least squares processes. The local approximations are considered in $H^{k,p}\left(\Omega_x^e\right)$ spaces with $k = 1$, i.e. local approximations of class $C^0\left(\Omega_x^e\right)$ with equal order, equal degree local approximations for all dependent variables in the mathematical models, which are a system of first order PDEs in velocities, pressure, deviatonic

Cauchy stress tensor, temperature and heat fluxes.

Numerical studies are conducted for all Reynolds numbers considered in this work for Newtonian fluid to determine the adequate size of the computational domain such that the boundaries of the domain do not influence the flow around the cylinder and in its neighborhood. Numerical studies are performed for progressively refined discretizations and increasing p-levels for the largest Reynolds number (200 for Newtonian fluids) to achieve the residuals I for the whole discretization that are of the order $O\left(10^{-6}\right)$ or lower. $\|g_i\|_{max}$ of the order $O\left(10^{-6}\right)$ are sought in all numerical studies to ensure that Newton's linear method with line search yields accurate solution of the system of non-linear algebraic equations. These values of I and $\{g\}$ ensure that the computed numerical solutions are sufficiently accurate. Numerical studies are conducted for Reynolds numbers of 20, 40, 60, 100 and 200 for Newtonian and Carreau fluids and Reynolds numbers of 15.6, 37.4, 62.4, 118.8 and 285.0 for power-law fluid which correspond to the same flow rates as for Newtonian and Carreau fluids. Only shear thinning fluids are considered for power-law and Carreau models. In case of non-isothermal flows, the boundaries of the domain are considered insulated and, hence the thermal field is only due to viscous dissipation.

It is shown that the energy equation and the heat flux equations are decoupled (or weakly coupled) from the remaining mathematical model, thus the temperature field remains uncoupled from the velocities, pressure and deviatoric Cauchy stress tensor. This holds for Newtonian, power-law and Carreau fluids, however in the least squares processes it is possible to perform computations using the combined mathematical model as done in the present work. Since the dimensionless flow rate is constant in all numerical studies, the peak values of u and v velocities increase with progressively increasing Reynolds numbers for Newtonian fluid in which the fluid viscosity is constant. In case of power-law

and Carreau fluids (shear thinning), the viscosity decreases with increasing shear rates. At moderate shear rate, the viscosity is not affected much by I_2, hence we expect similar behavior as in the case of Newtonian fluid for increasing Reynolds numbers (but low values). At $Re = 200$ (Carreau) and $Re_n = 285.0$ (power-law) the velocity gradient and hence I_2 are significant enough to influence the velocity field (when compared to Newtonian case). For $Re_n = 285.0$ and $Re = 200$, we observe a decrease in the peak velocity compared to $Re_n = 118.8$ and $Re = 100$. Velocity v continues to increase at these Reynolds numbers but not as significantly as in Newtonian case.

In the case of non-isothermal flows (viscous dissipation only), pronounced increase in heat generation and, hence progressively increased temperature values for progressively increasing Reynolds numbers are simulated for Newtonian, power-law and Carreau fluids. I values of $O\left(10^{-6}\right)$ and $\|g_i\|_{max} \leq O\left(10^{-6}\right)$ confirm good accuracy of the results. For both isothermal and non-isothermal flows, the solutions are smooth, i.e. free of any observable spurious oscillations. Non-isothermal power-law fluid at high Reynolds number of $Re_n = 285.0$ is the only case at which these conditions are not met due to oscillations, and therefore convergence issues, in the vicinity of the cylinder. For this case, $\|g_i\|_{max} \leq O\left(10^{-4}\right)$, but I values are still of $O\left(10^{-6}\right)$ which confirms good accuracy of the solution.

In summary, benchmark quality numerical simulations are presented for flows of incompressible, homogeneous and isotropic Newtonian, power-law and Carreau fluids over a circular cylinder for isothermal as well as non-isothermal conditions for Reynolds numbers of $Re = 20$, 40, 60, 100 and 200 and $Re_n = 15.6$, 37.4, 62.4, 118.8 and 285.0.

Appendix A

Domain Size and Discretization

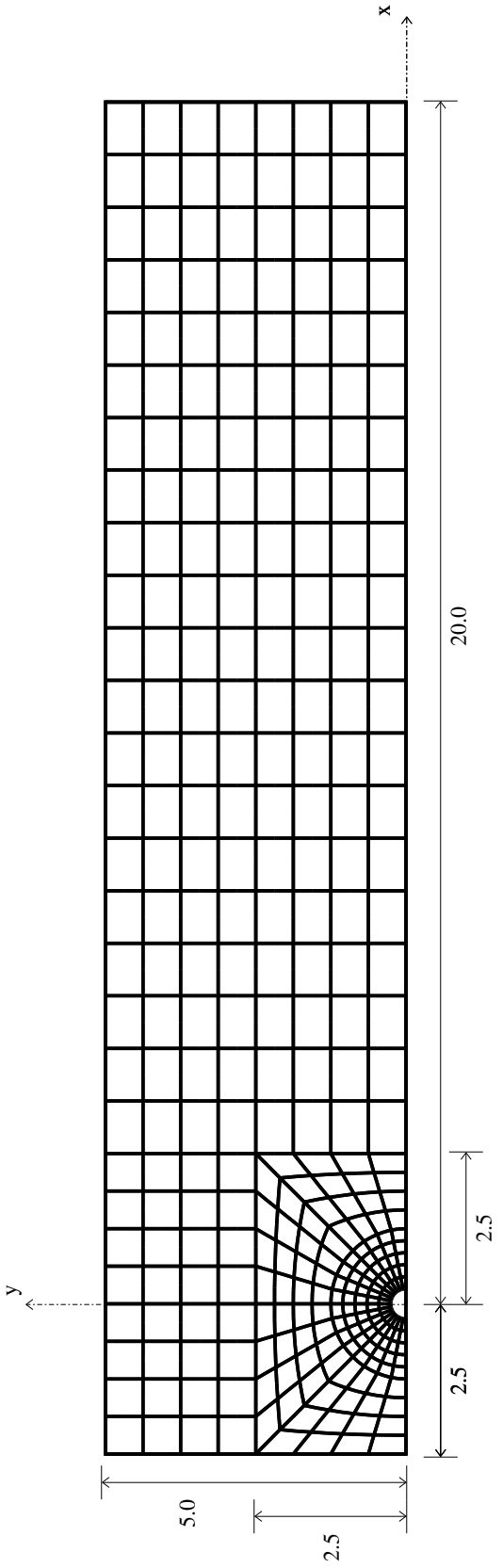

Figure A.1: A 336 Element Discretization L_1 = 2.5 and H = 5.0

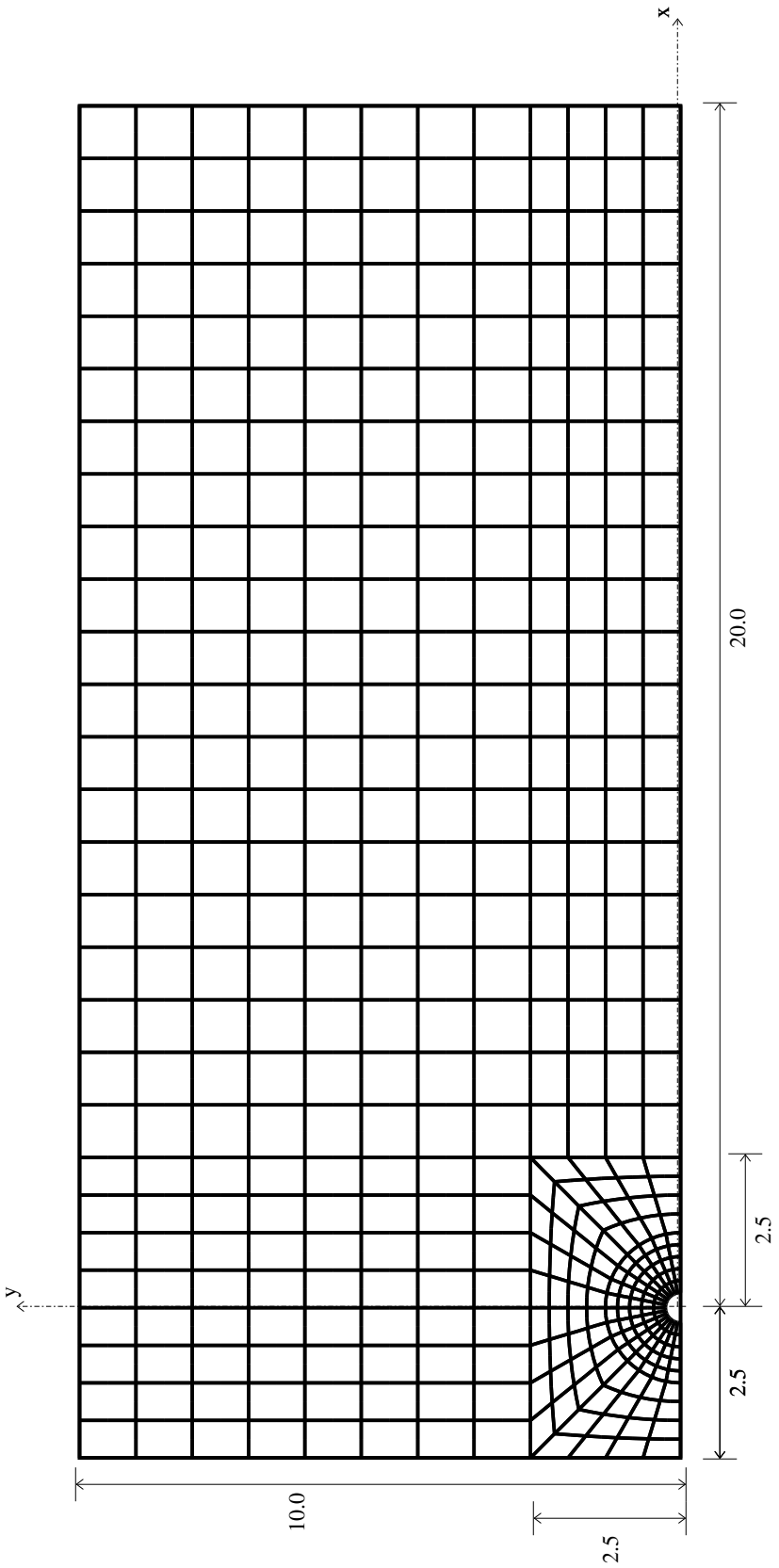

Figure A.2: A 448 Element Discretization L_1 = 2.5 and H = 10.0

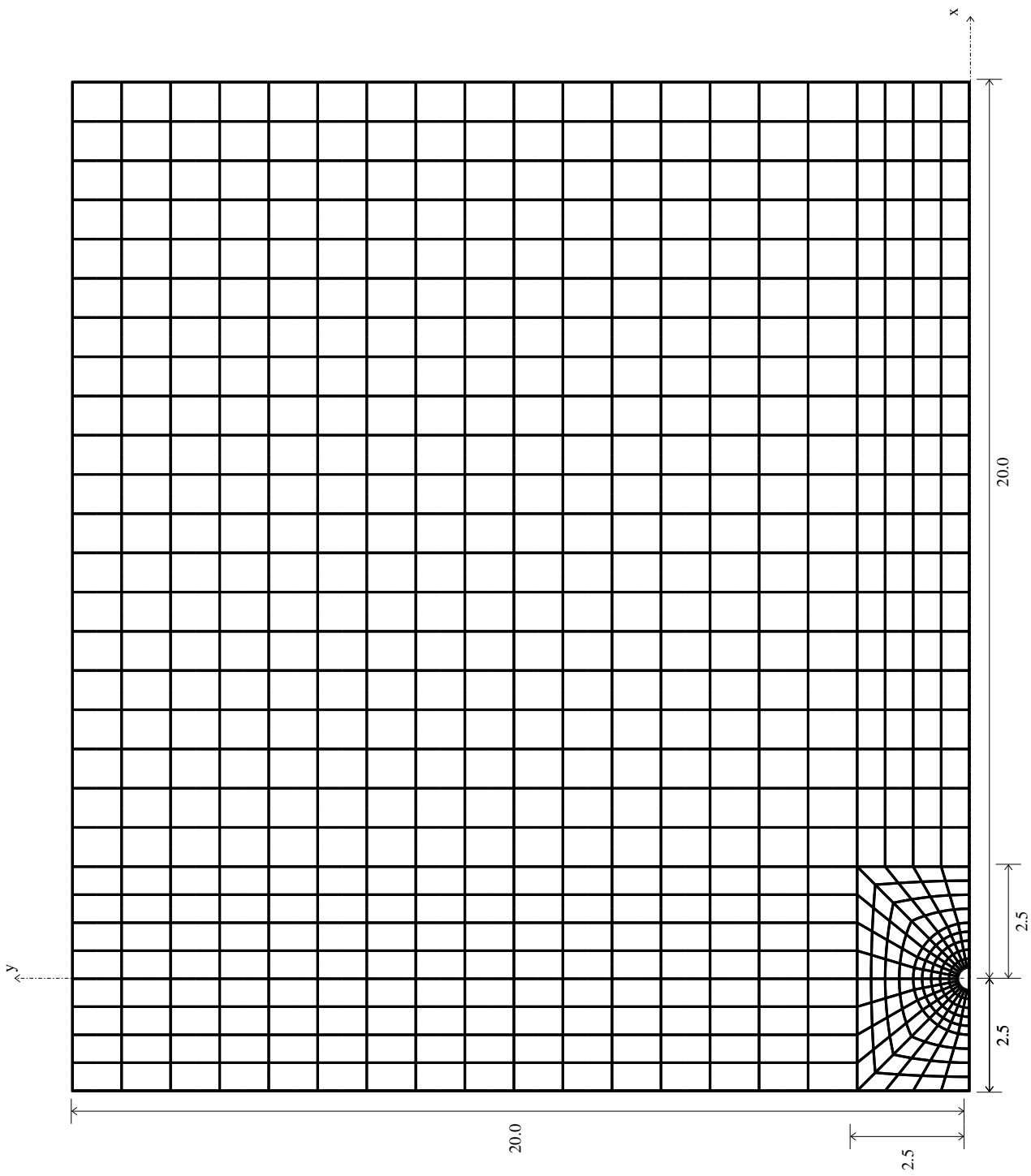

Figure A.3: A 672 Element Discretization $L_1 = 2.5$ and $H = 20.0$

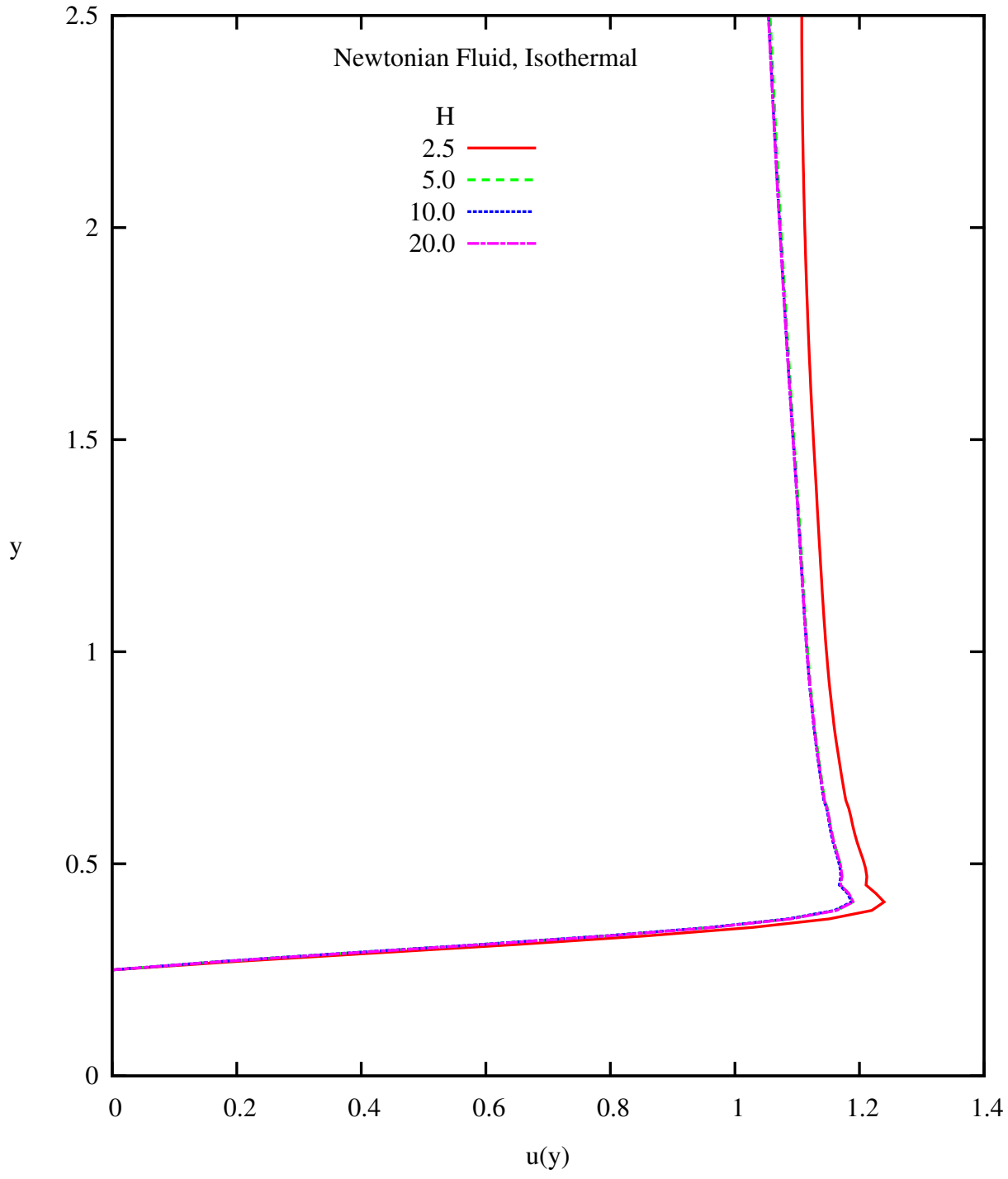

Figure A.4: Velocity u versus y at $x = 0$ (Newtonian Fluid, Isothermal): L_1 = 2.5, Re = 200

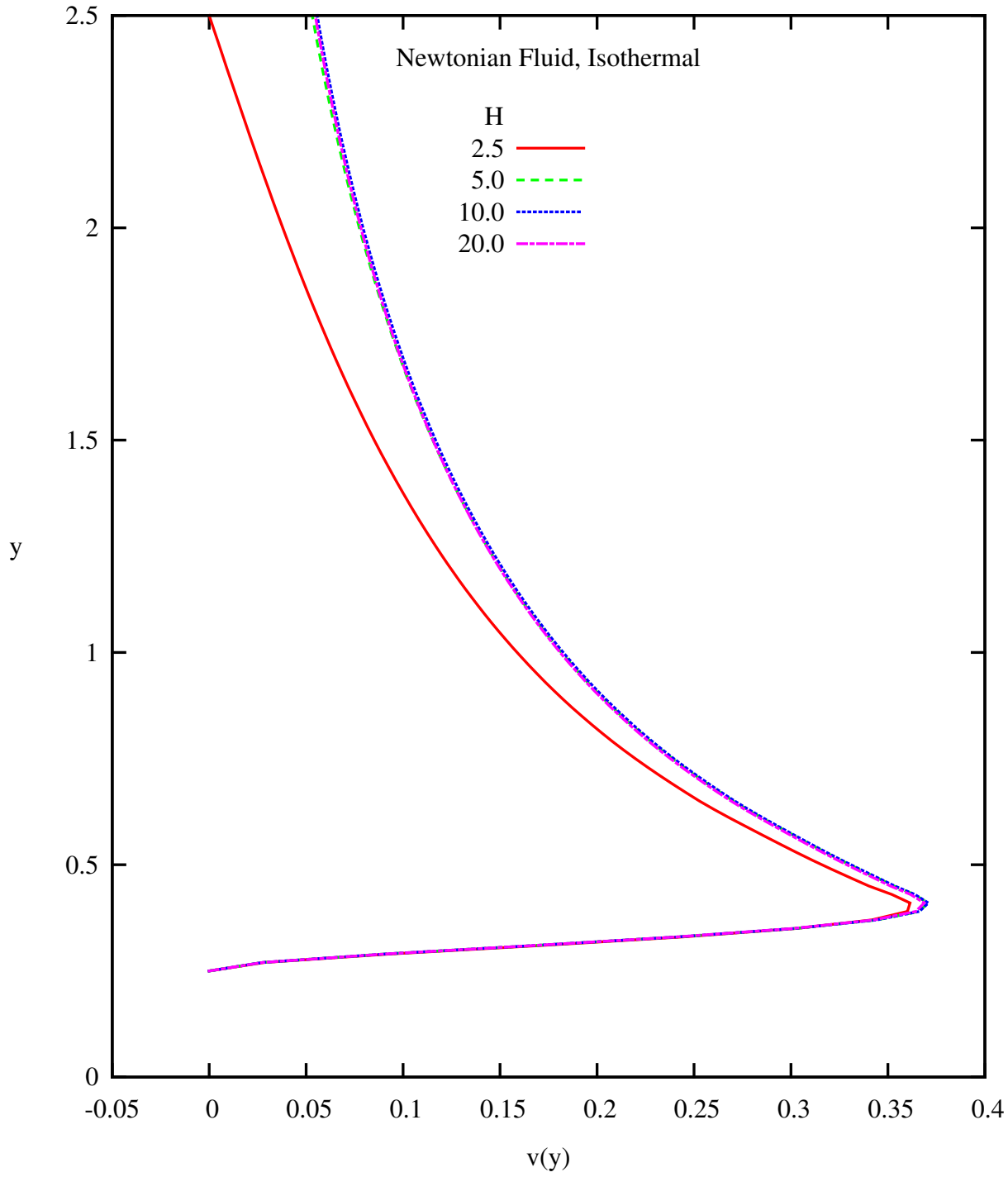

Figure A.5: Velocity v versus y at $x = 0$ (Newtonian Fluid, Isothermal): L_1 = 2.5, Re = 200

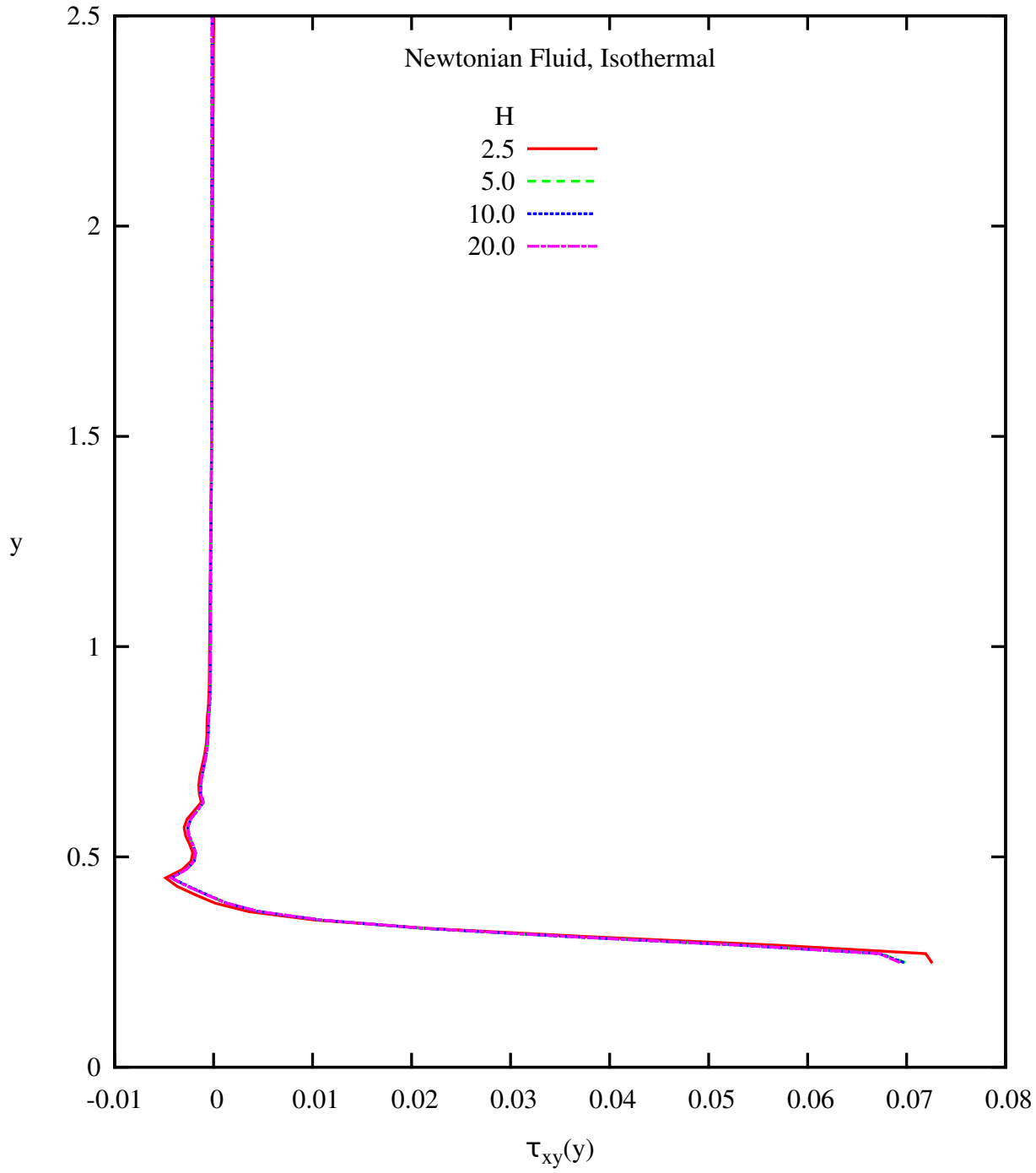

Figure A.6: Shear Stress τ_{xy} versus y at $x = 0$ (Newtonian Fluid, Isothermal): L_1 = 2.5, Re = 200

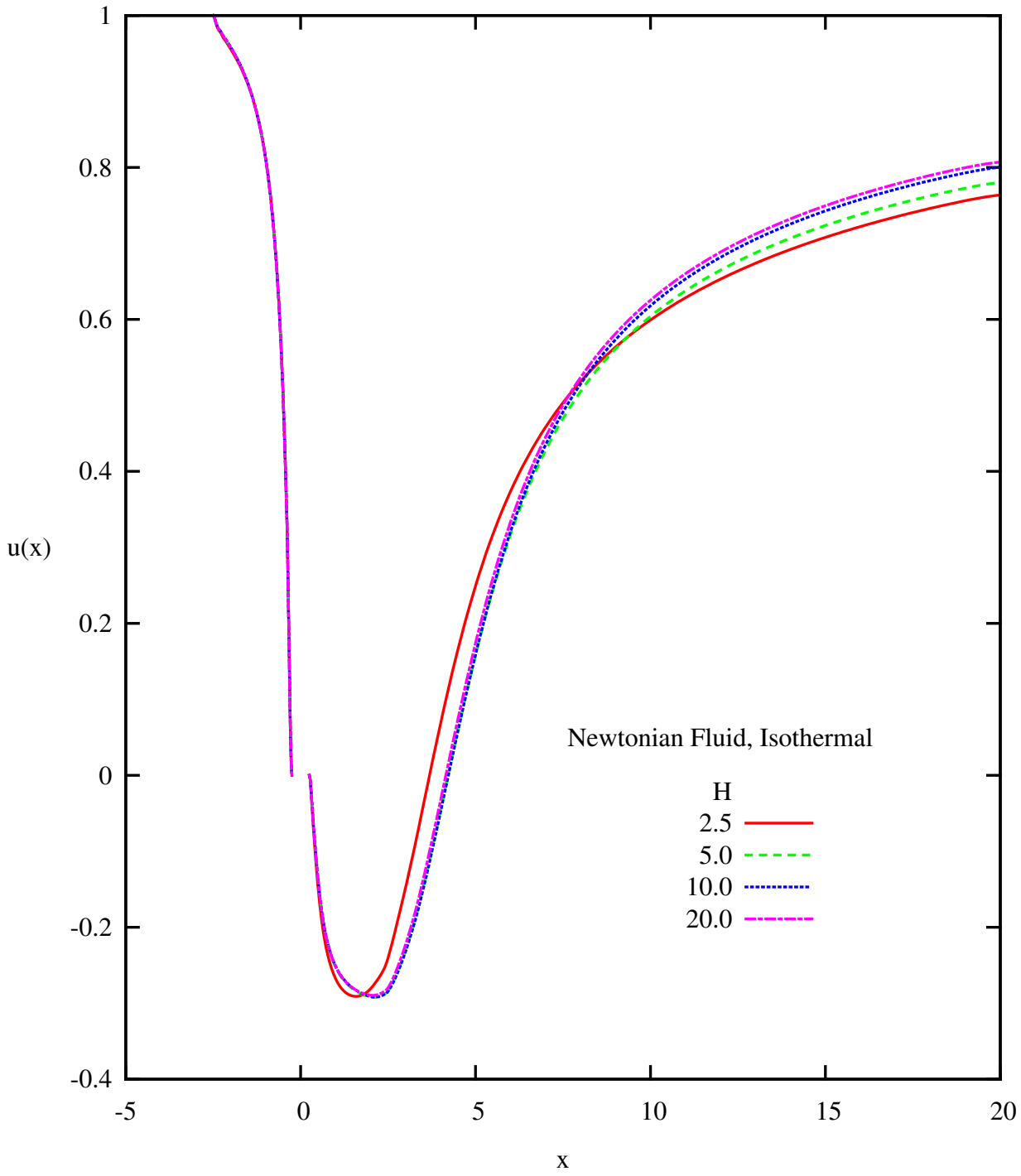

Figure A.7: Velocity u versus x at $y = 0$ (Newtonian Fluid, Isothermal): L_1 = 2.5, Re = 200

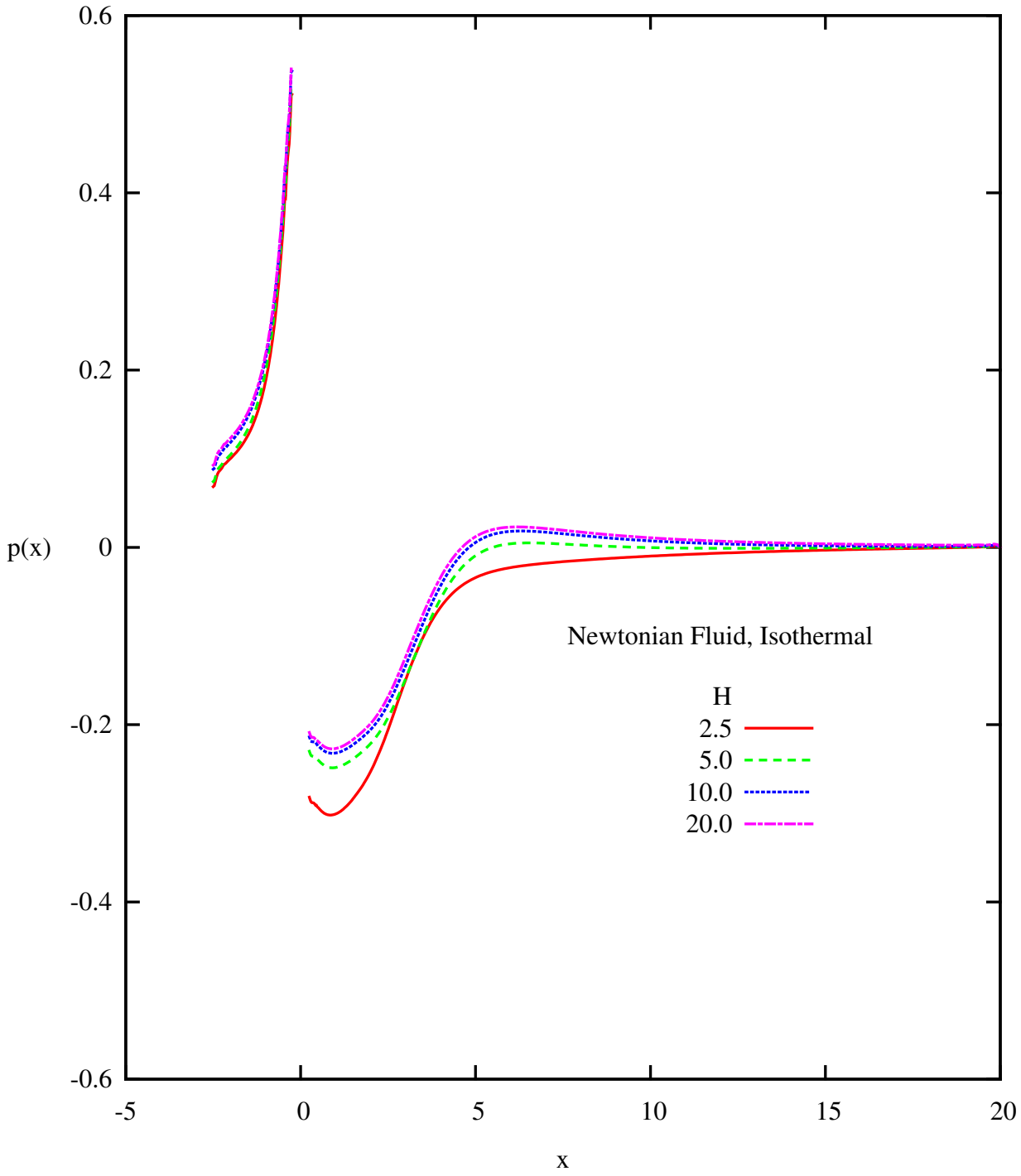

Figure A.8: Pressure p versus x at $y = 0$ (Newtonian Fluid, Isothermal): L_1 = 2.5, Re = 200

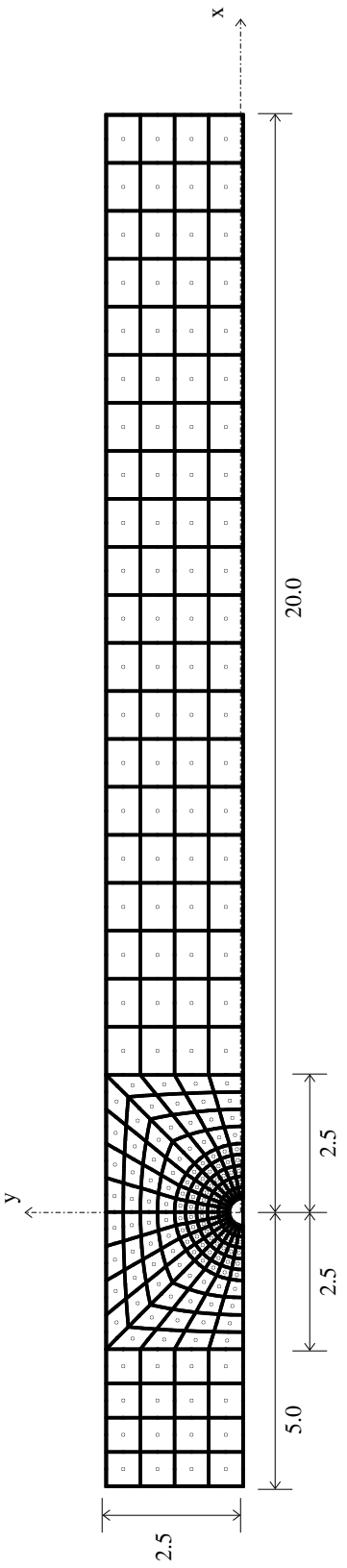

Figure A.9: A 240 Element Discretization L_1 = 5.0 and H = 2.5

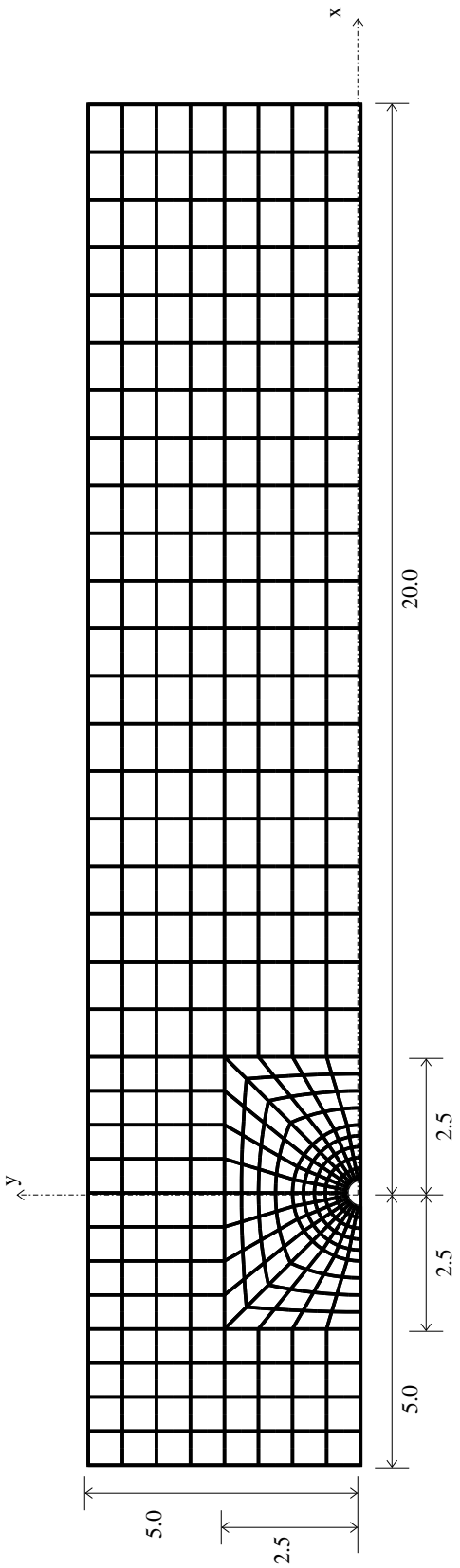

Figure A.10: A 368 Element Discretization L_1 = 5.0 and H = 5.0

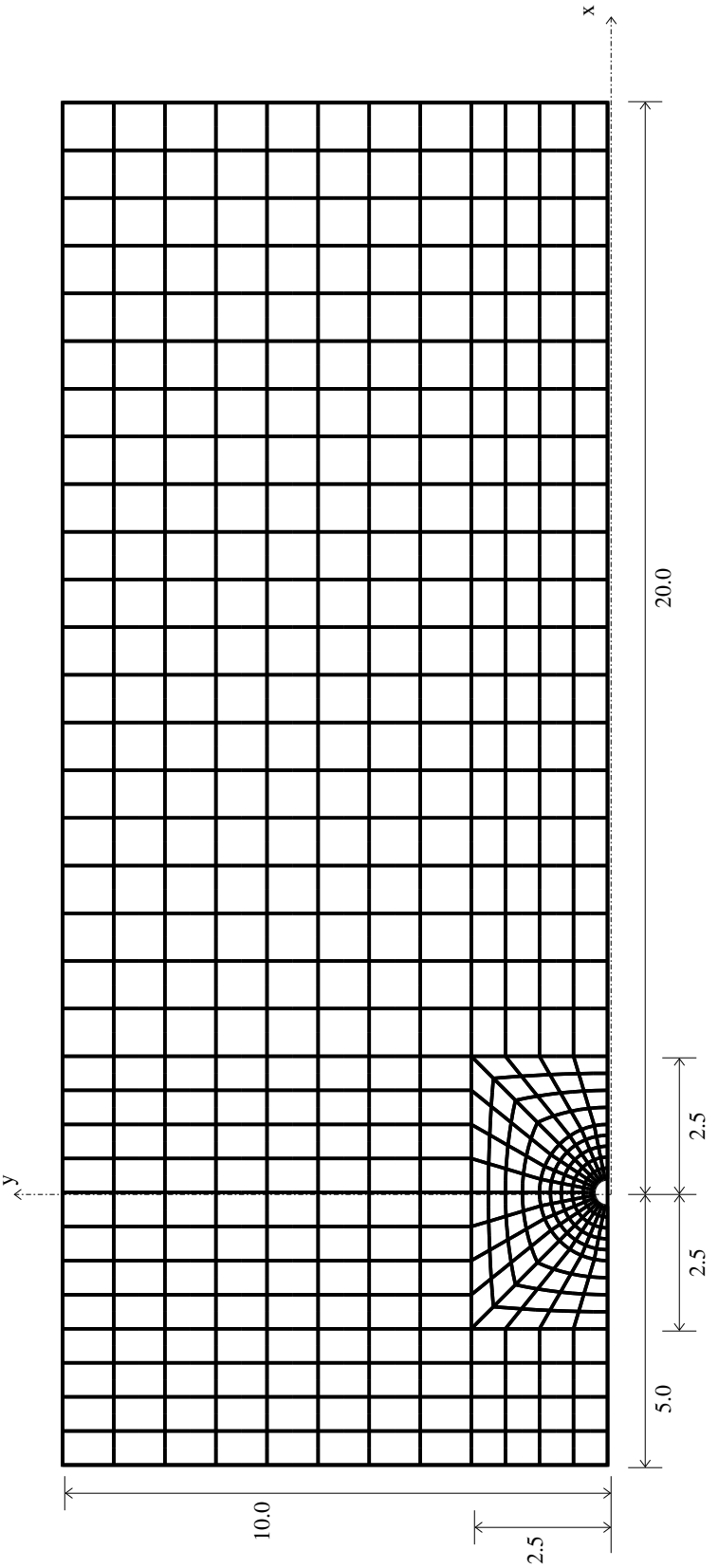

Figure A.11: A 496 Element Discretization L_1 = 5.0 and H = 10.0

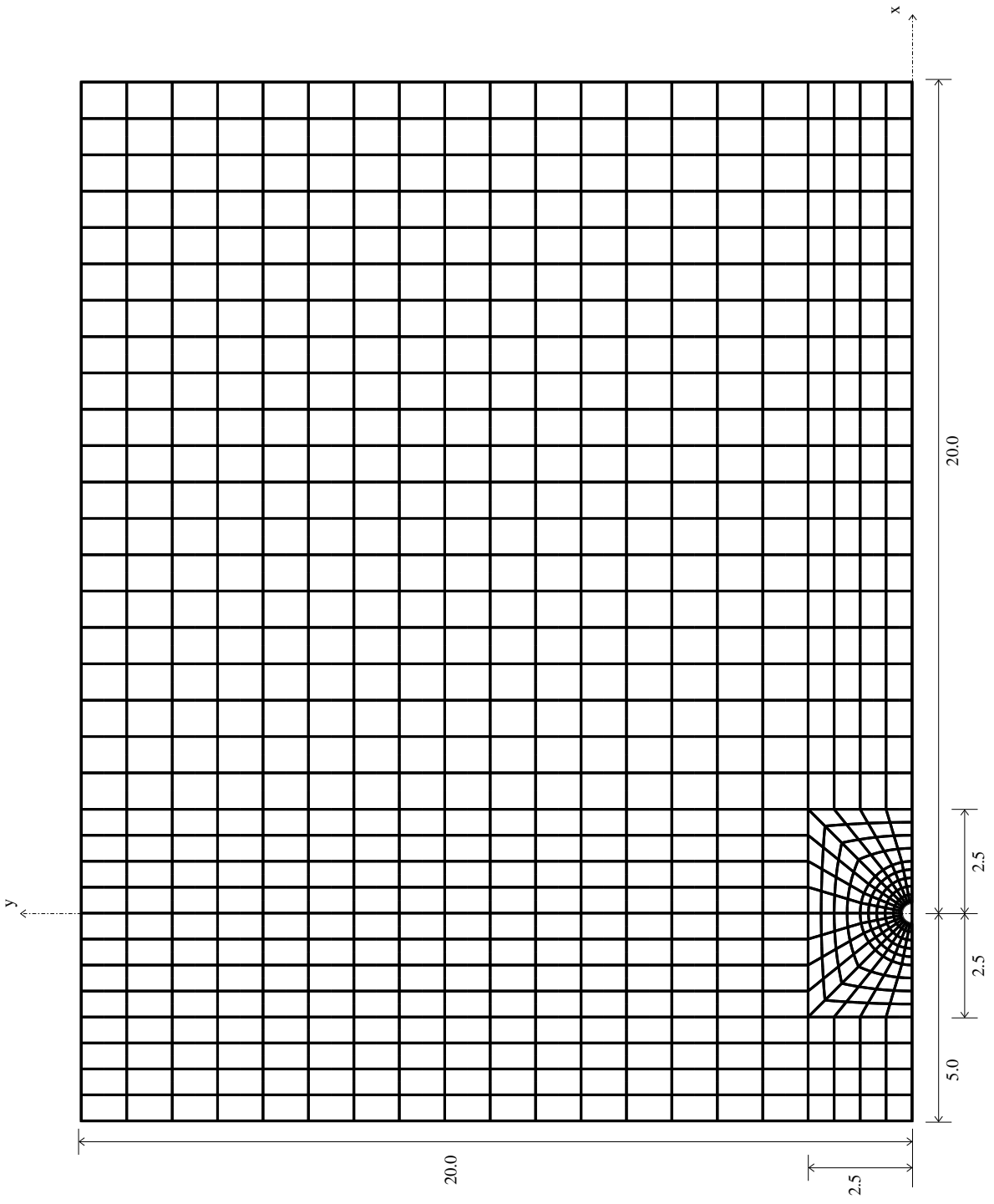

Figure A.12: A 752 Element Discretization L_1 = 5.0 and H = 20.0

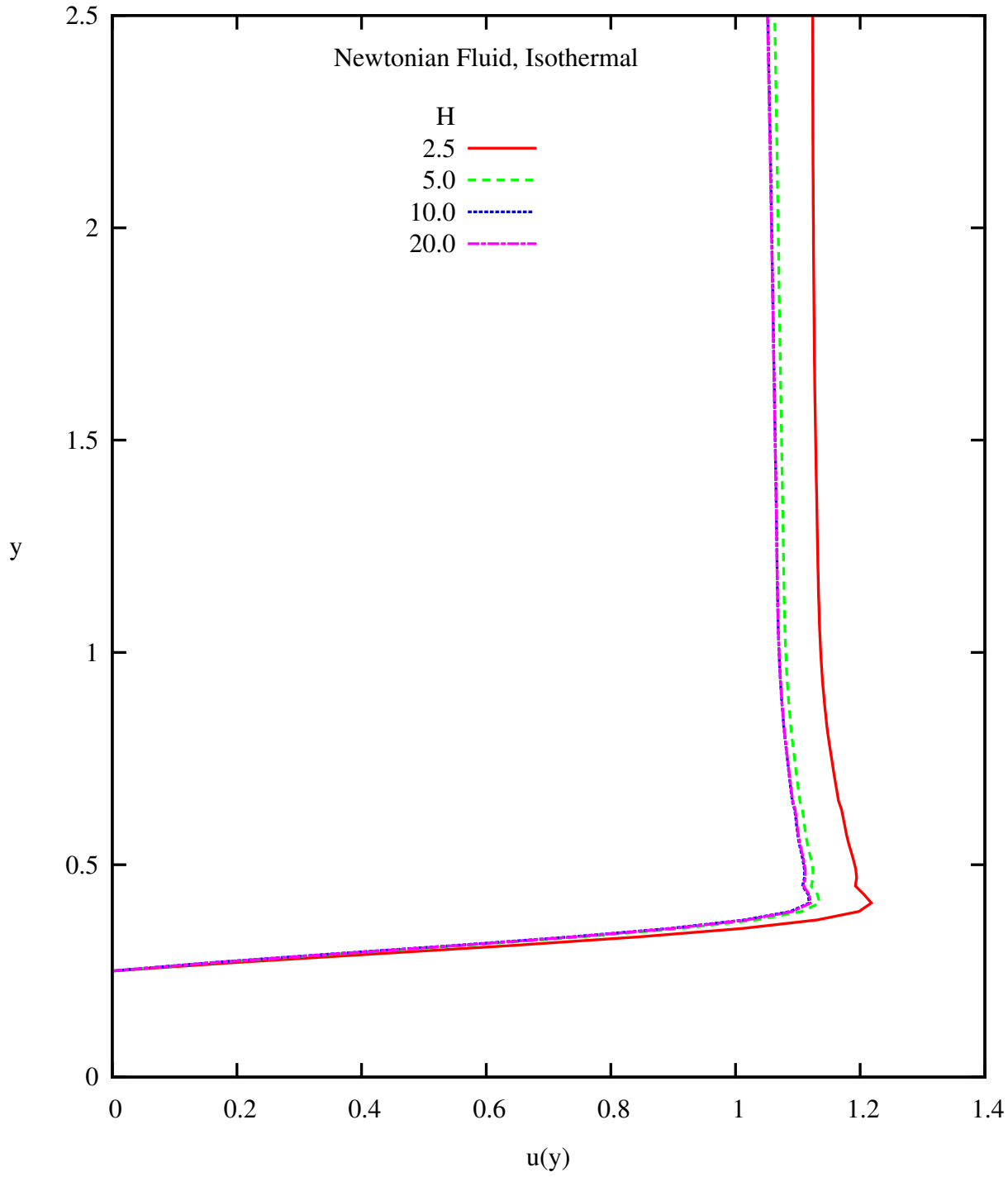

Figure A.13: Velocity u versus y at $x = 0$ (Newtonian Fluid, Isothermal): L_1 = 5.0, Re = 200

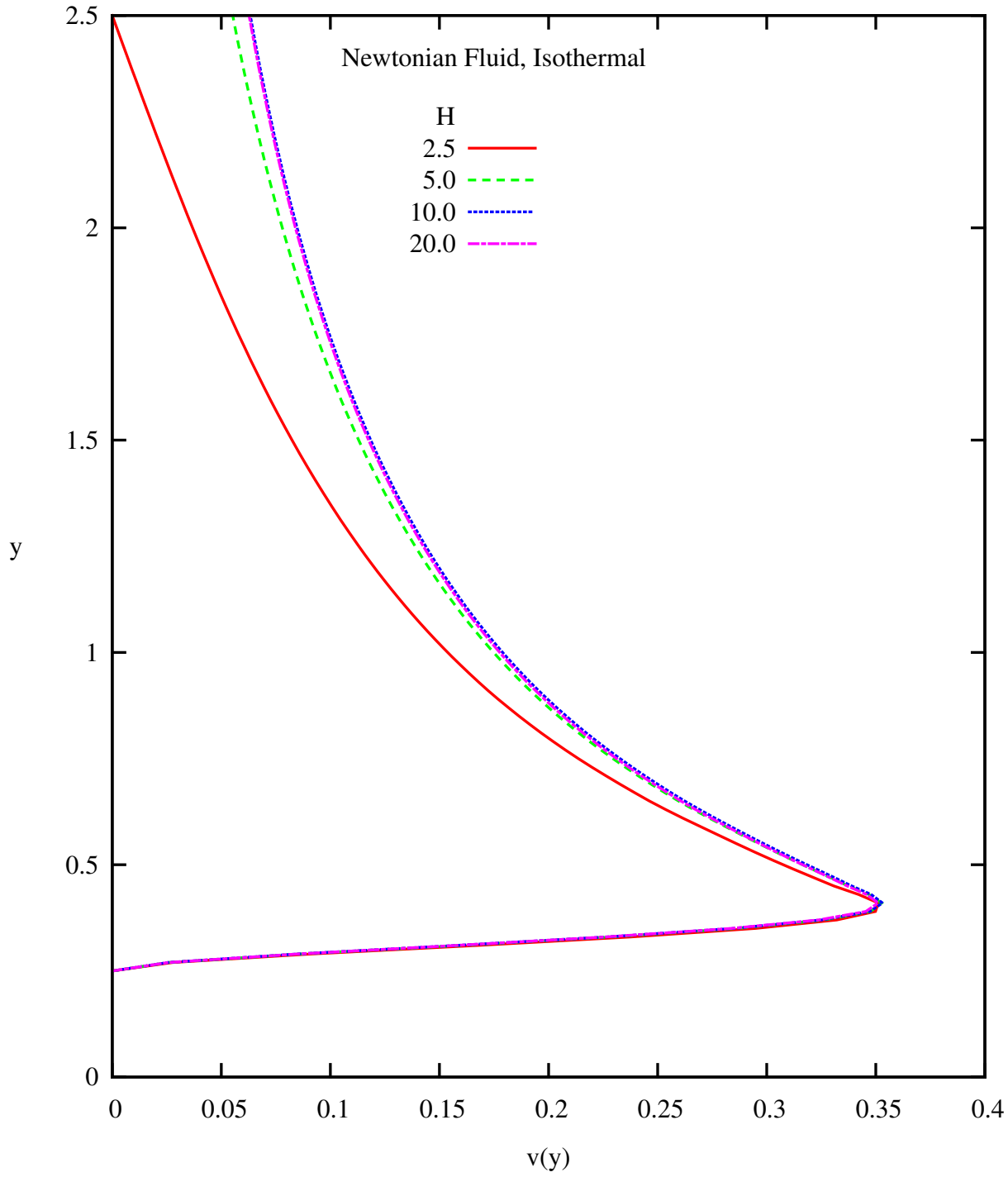

Figure A.14: Velocity v versus y at $x = 0$ (Newtonian Fluid, Isothermal): L_1 = 5.0, Re = 200

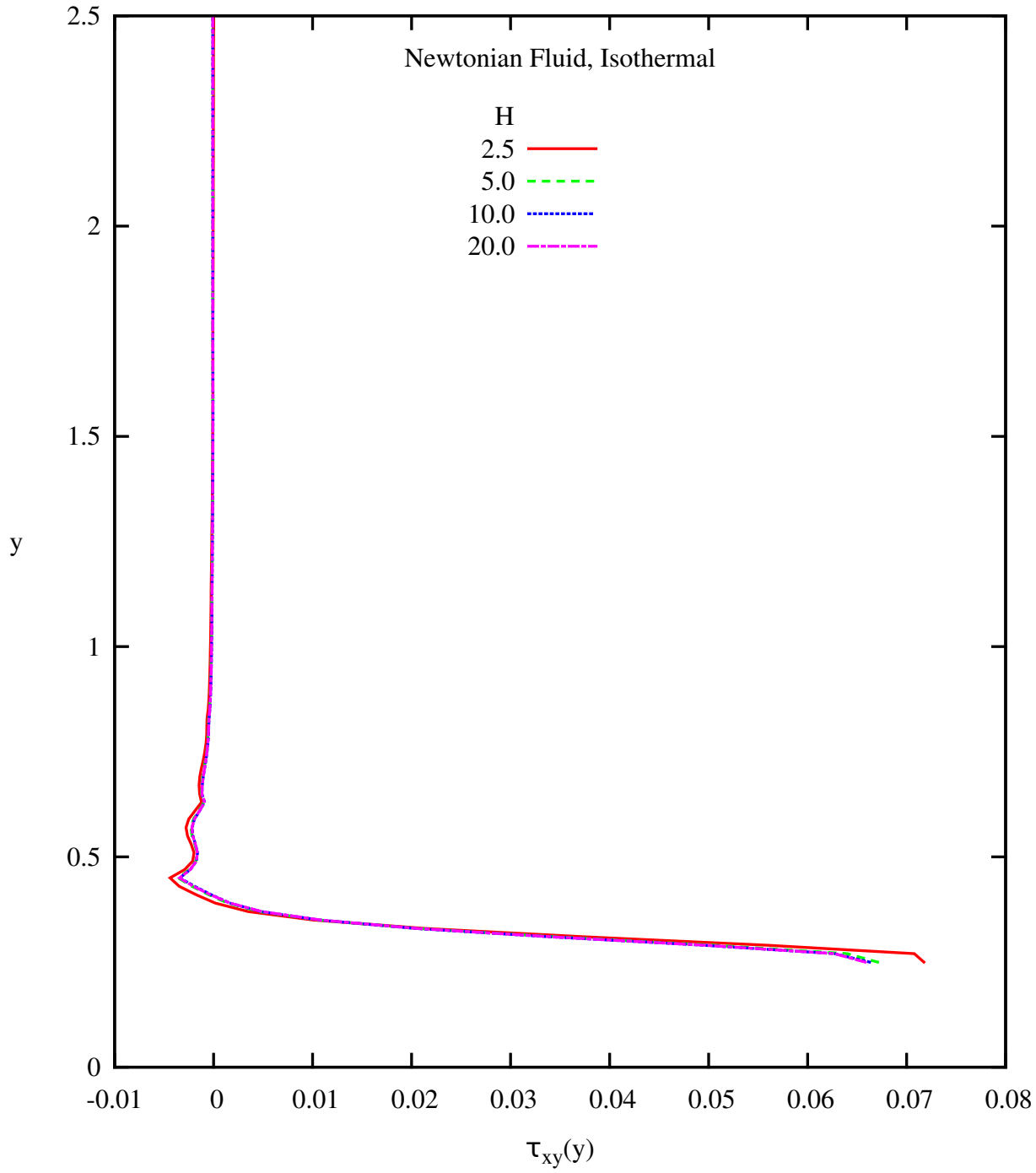

Figure A.15: Shear Stress τ_{xy} versus y at $x = 0$ (Newtonian Fluid, Isothermal):

L_1 = 5.0, Re = 200

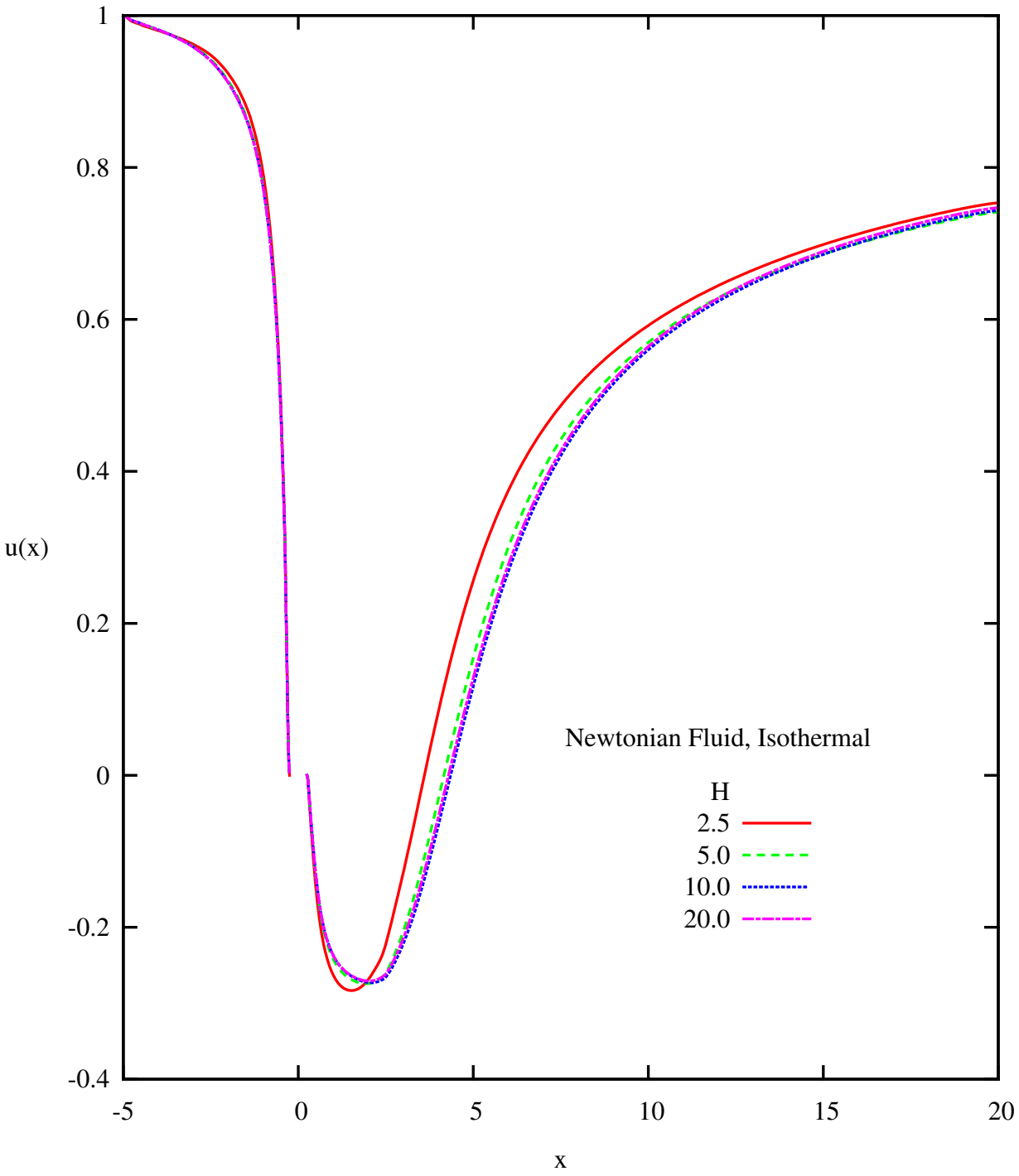

Figure A.16: Velocity u versus x at $y = 0$ (Newtonian Fluid, Isothermal): L_1 = 5.0, Re = 200

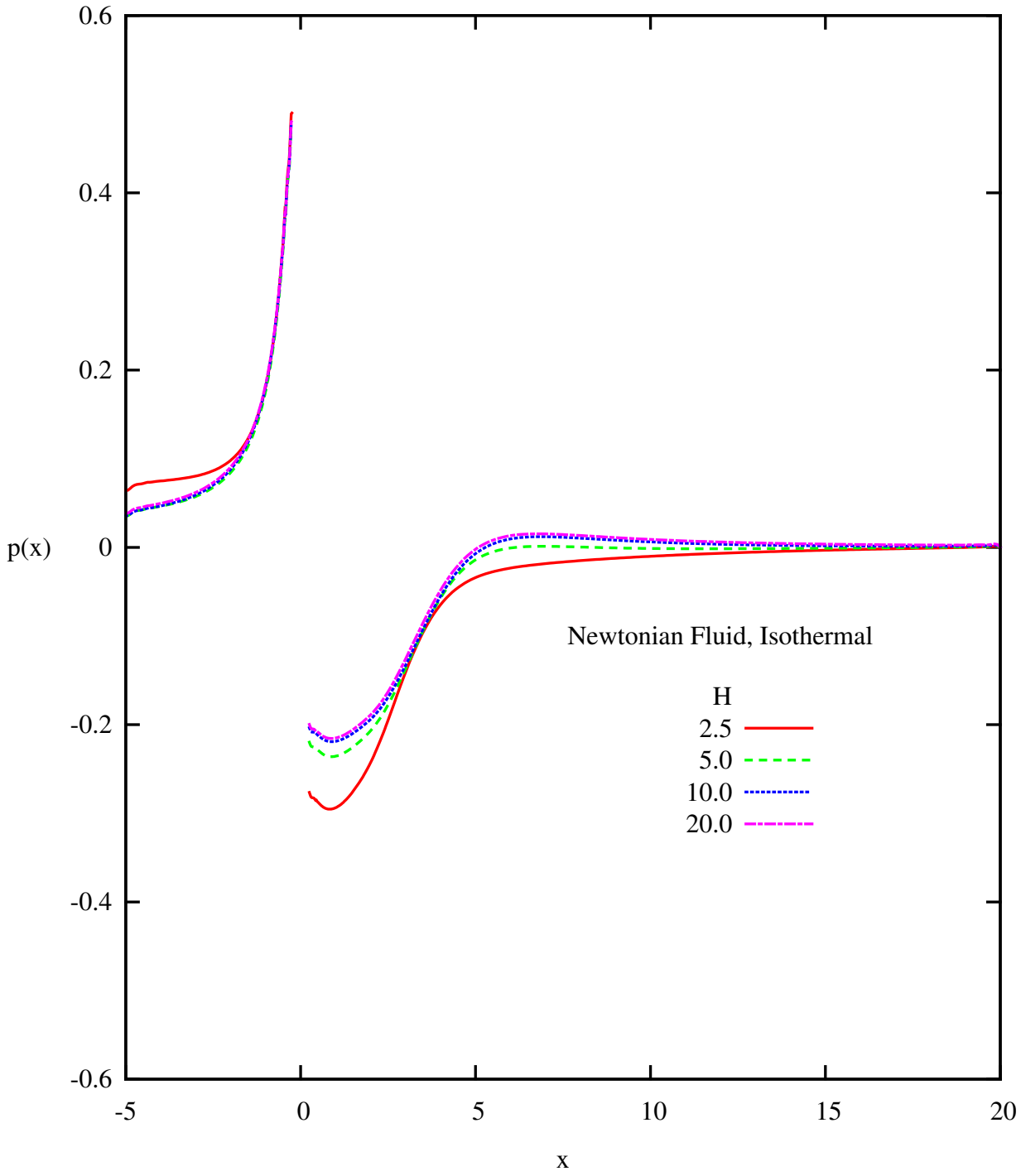

Figure A.17: Pressure p versus x at $y = 0$ (Newtonian Fluid, Isothermal): L_1 = 5.0, Re = 200

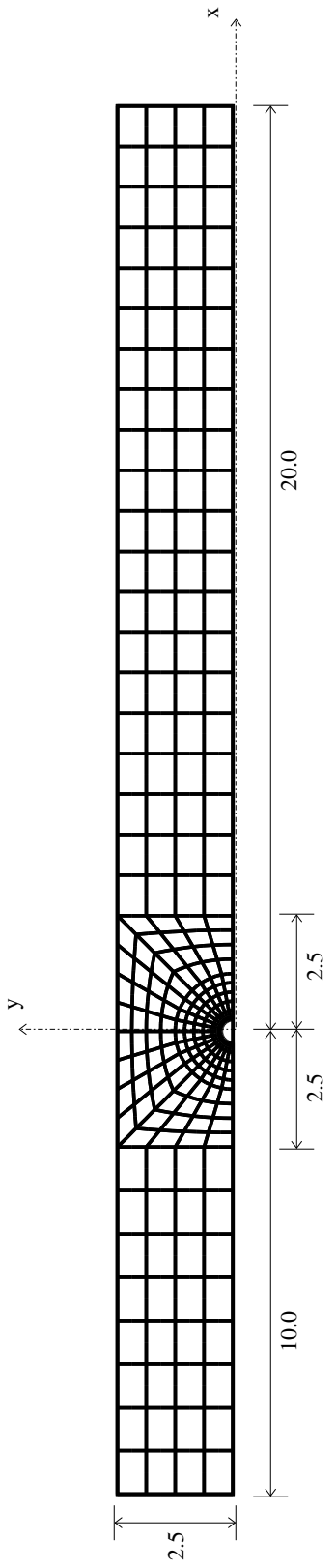

Figure A.18: A 256 Element Discretization L_1 = 10.0 and H = 2.5

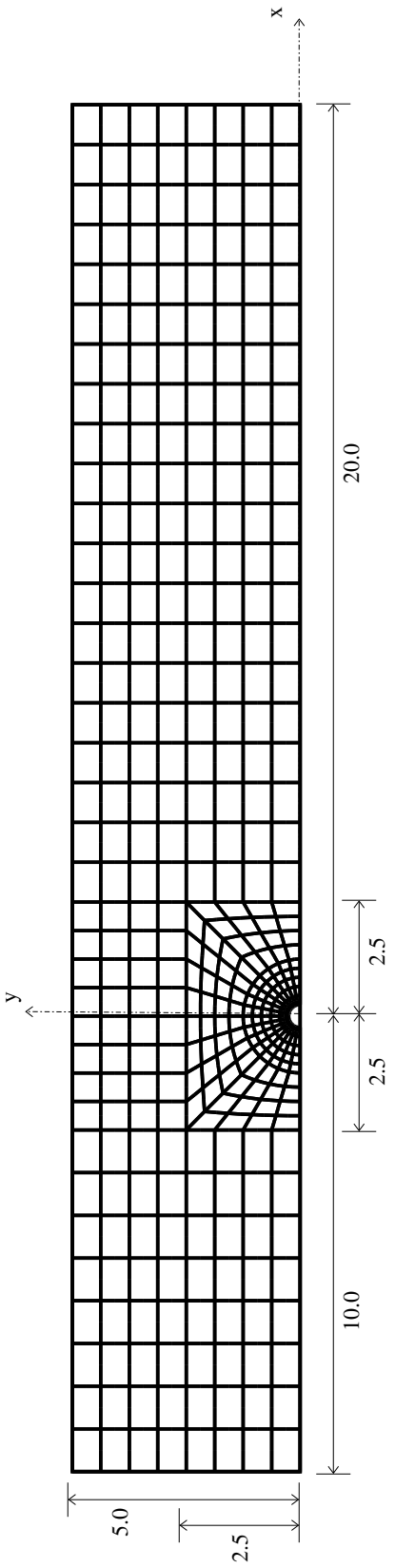

Figure A.19: A 400 Element Discretization L_1 = 10.0 and H = 5.0

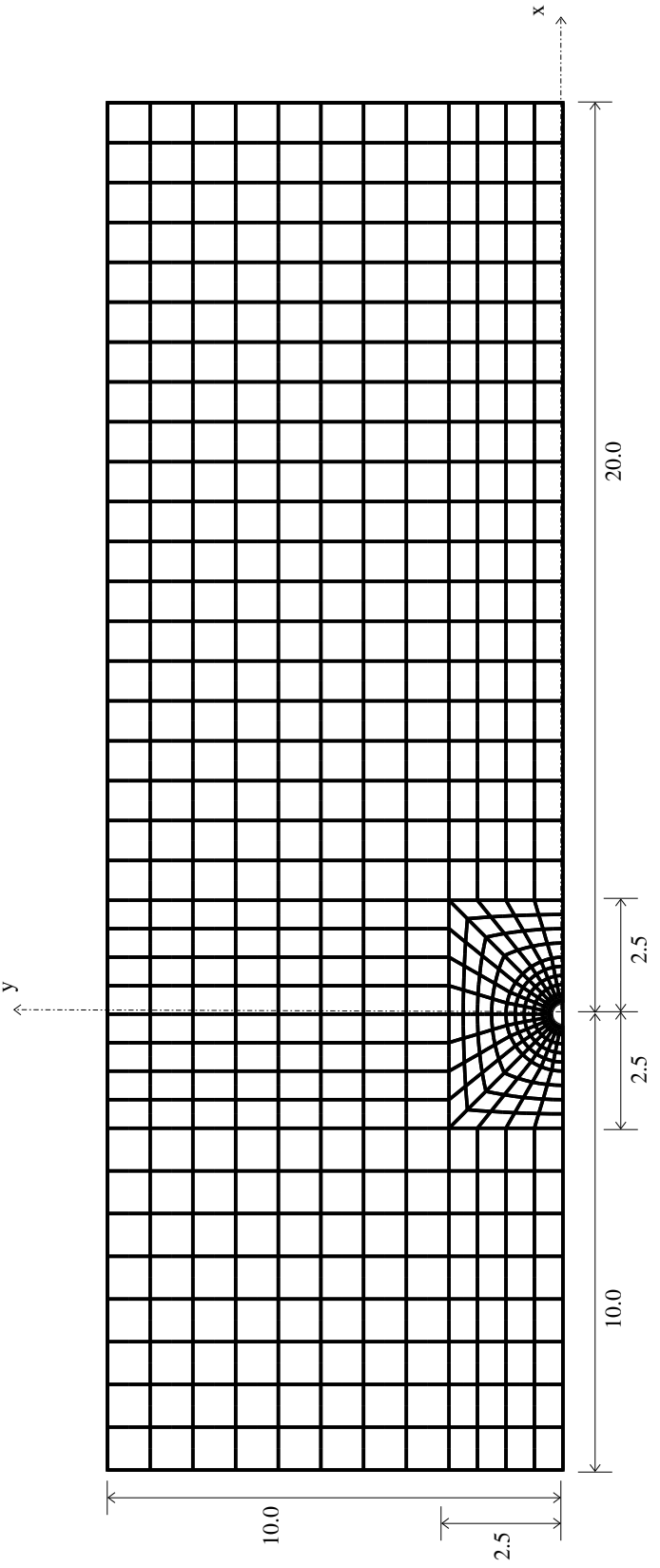

Figure A.20: A 544 Element Discretization L_1 = 10.0 and H = 10.0

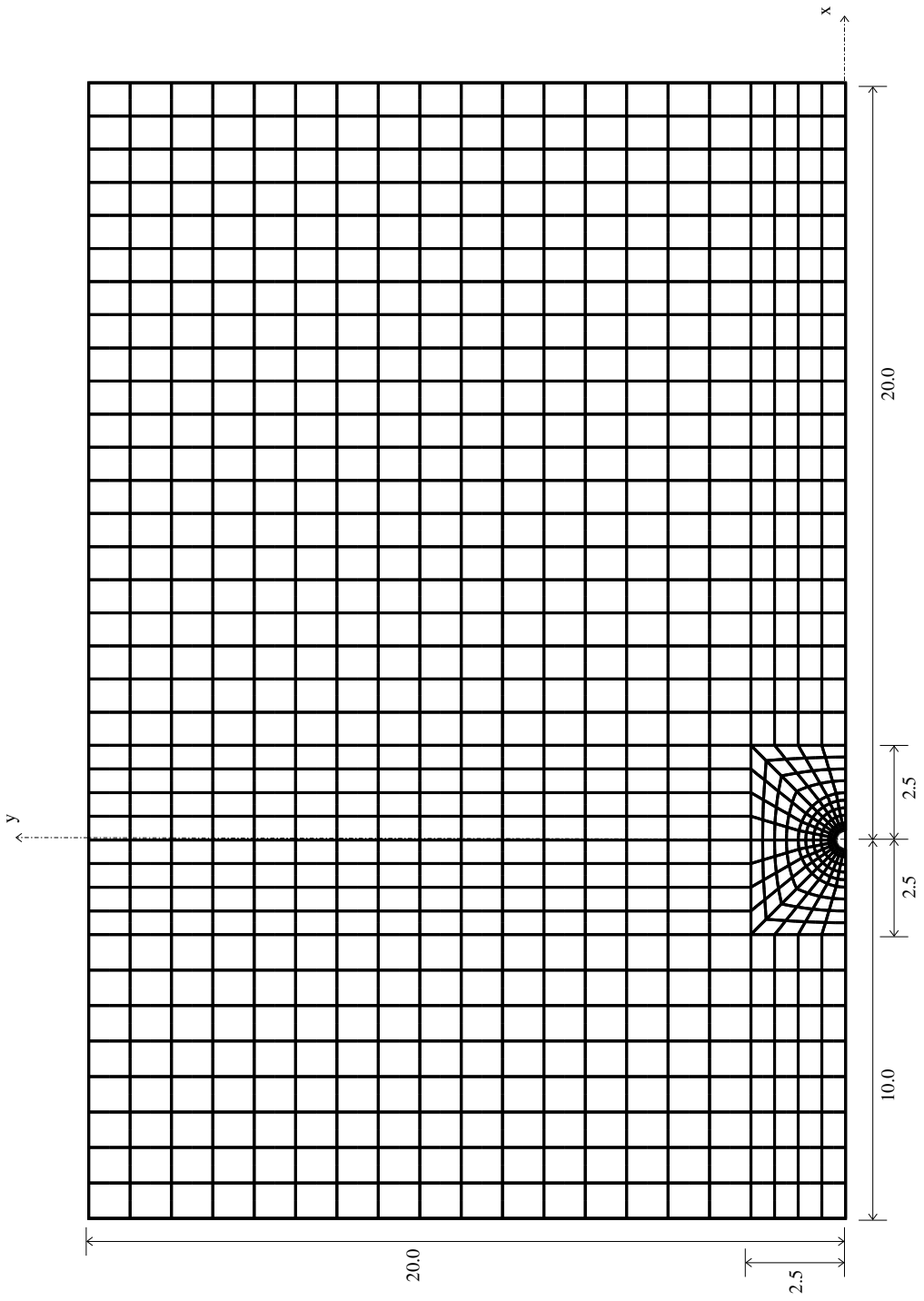

Figure A.21: A 832 Element Discretization L_1 = 10.0 and H = 20.0

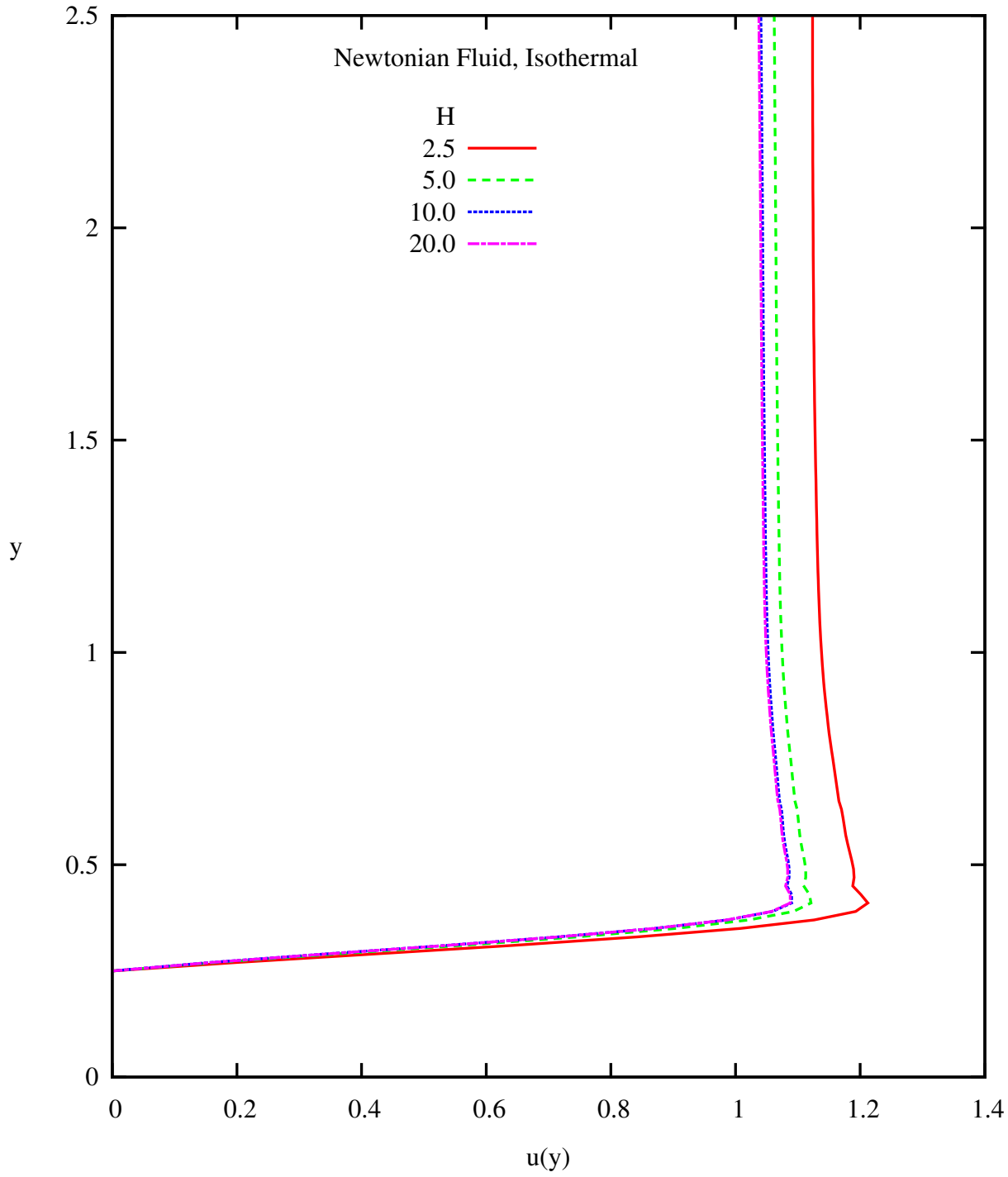

Figure A.22: Velocity u versus y at $x = 0$ (Newtonian Fluid, Isothermal): L_1 = 10.0, Re = 200

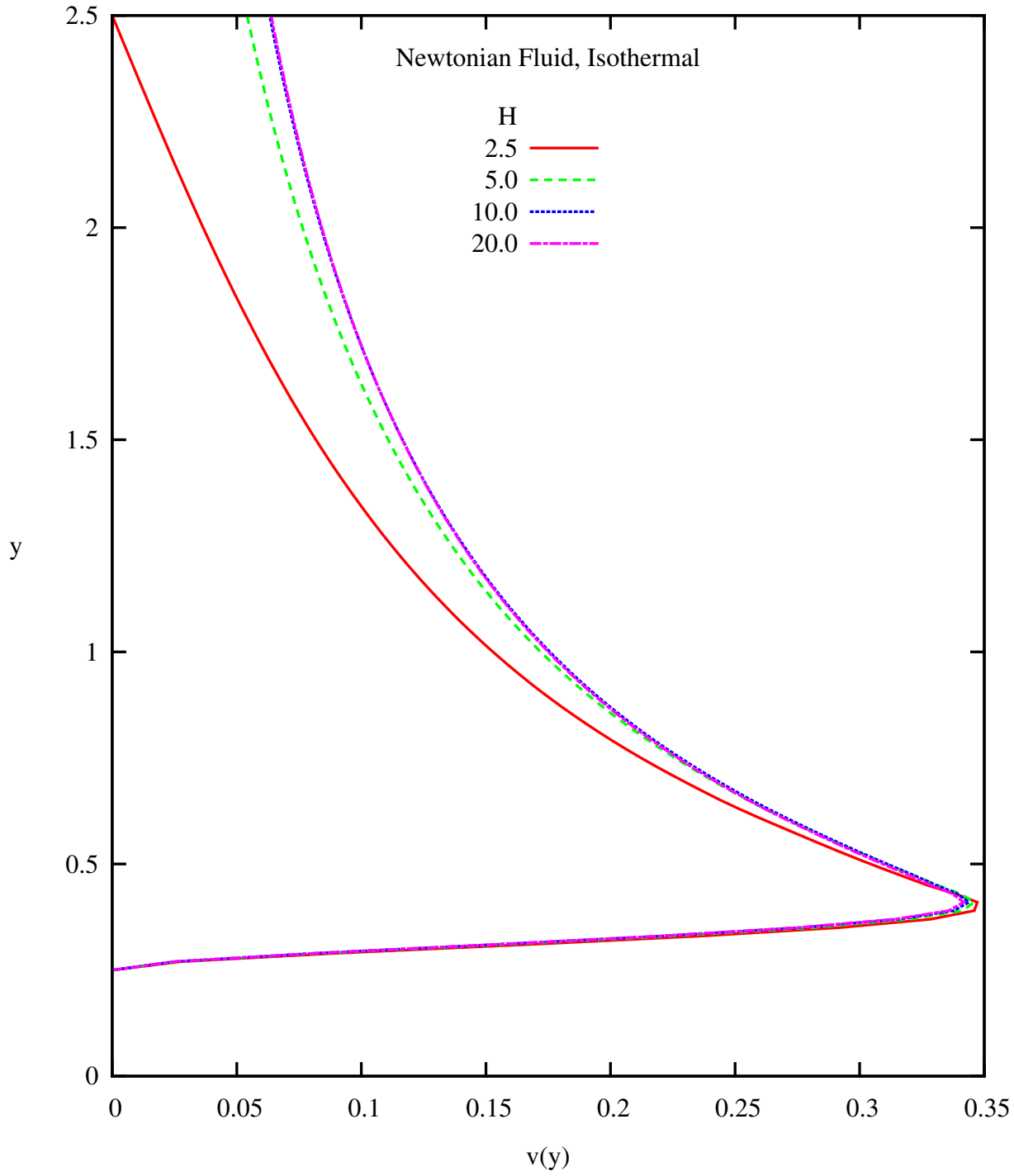

Figure A.23: Velocity v versus y at $x = 0$ (Newtonian Fluid, Isothermal): L_1 = 10.0, Re = 200

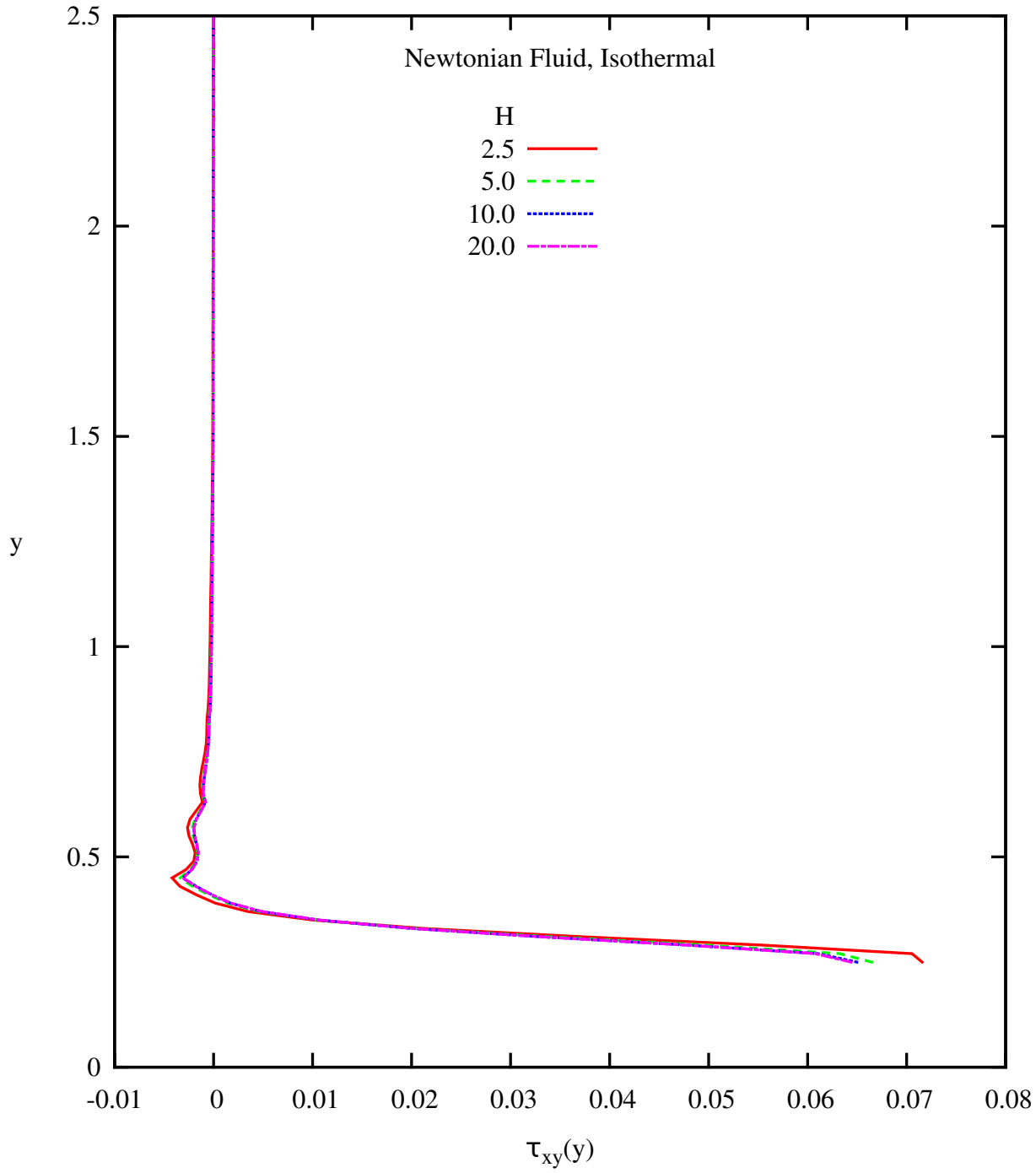

Figure A.24: Shear Stress τ_{xy} versus y at $x = 0$ (Newtonian Fluid, Isothermal):

L_1 = 10.0, Re = 200

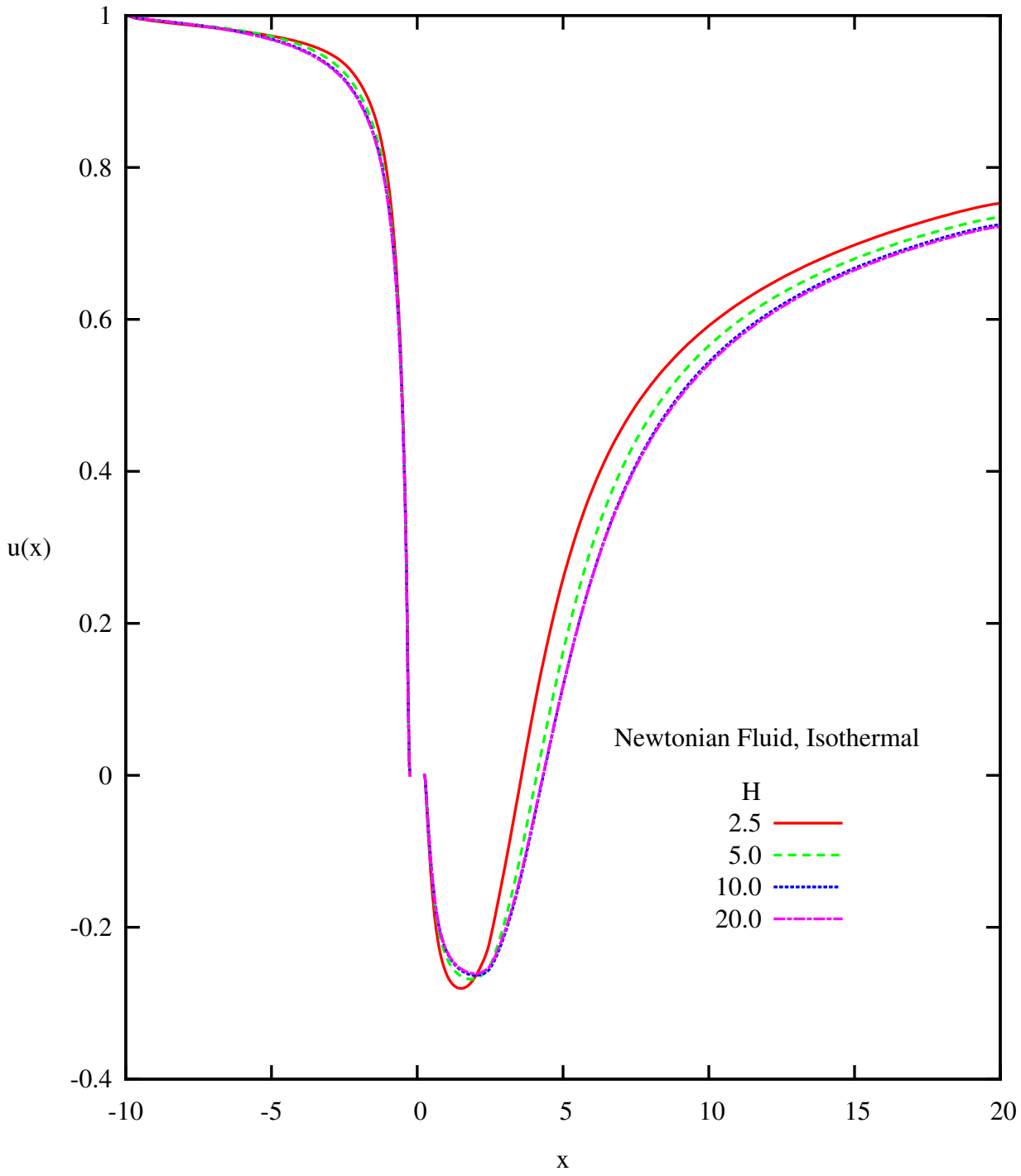

Figure A.25: Velocity u versus x at $y = 0$ (Newtonian Fluid, Isothermal): L_1 = 10.0, Re = 200

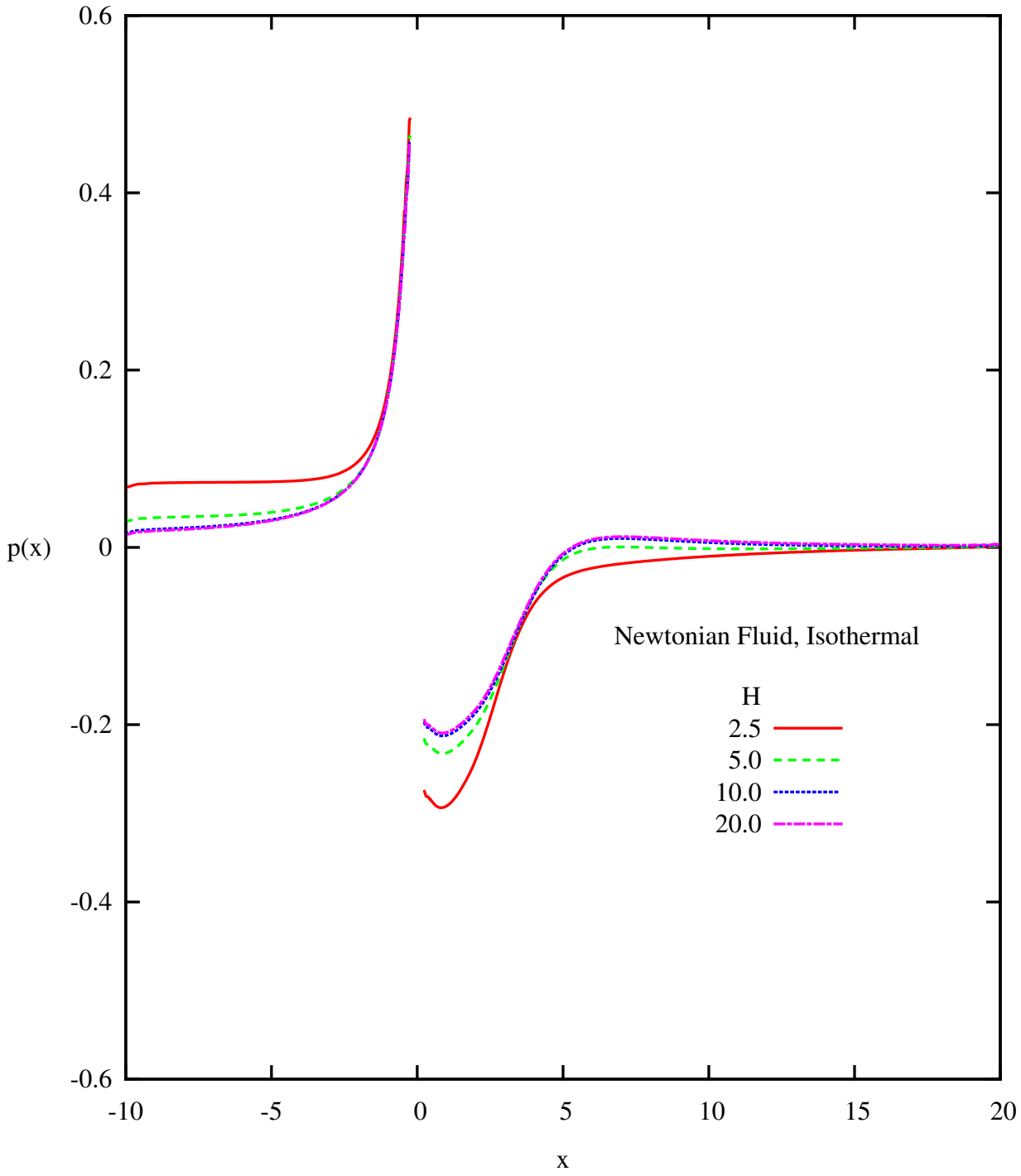

Figure A.26: Pressure p versus x at $y = 0$ (Newtonian Fluid, Isothermal): L_1 = 10.0, Re = 200

Appendix B

Non-Isothermal Flow Over a Cylinder

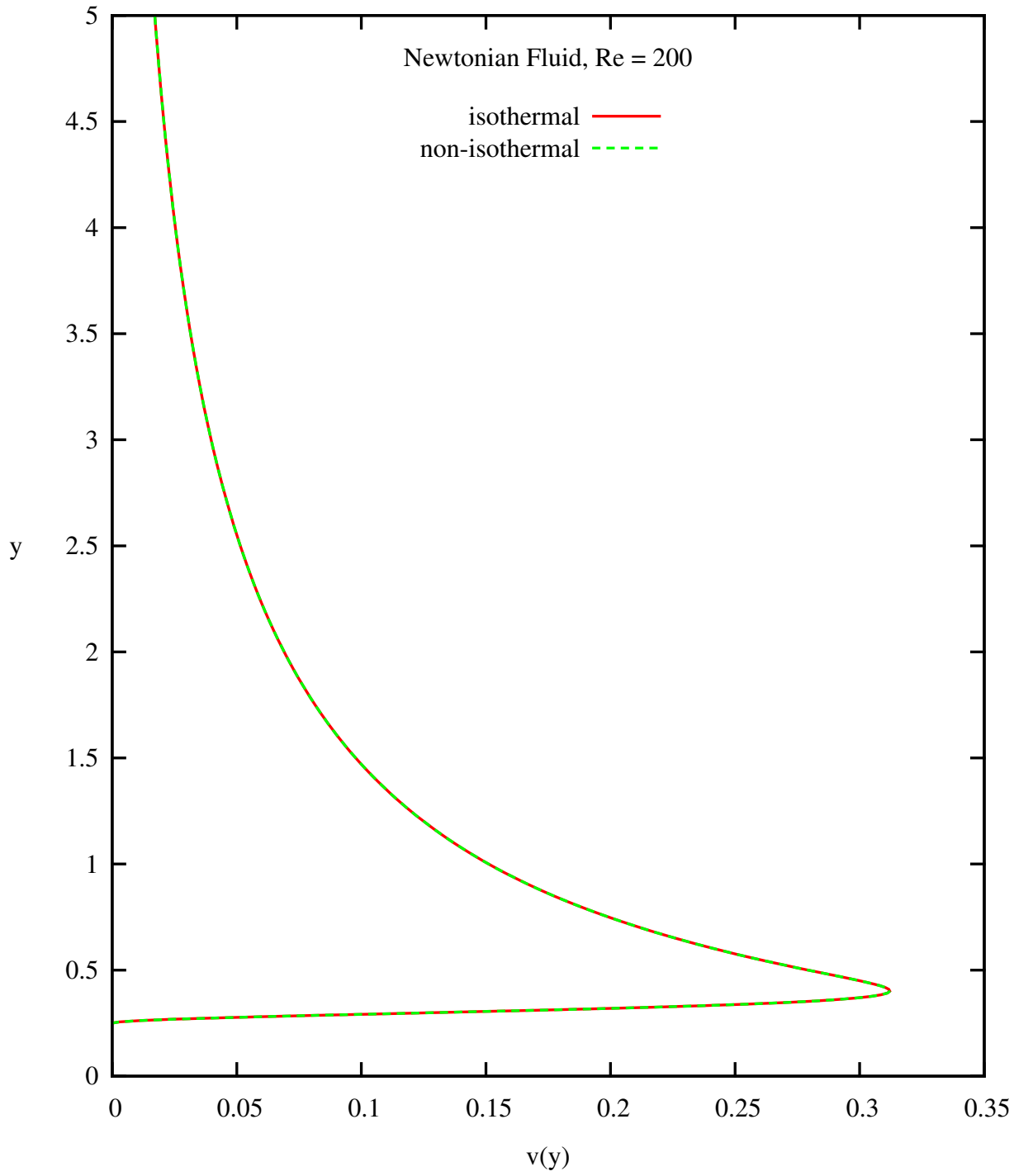

Figure B.1: Velocity v versus y at $x = 0$: Comparison of Isothermal and Non-Isothermal Flows at Re = 200 (Newtonian)

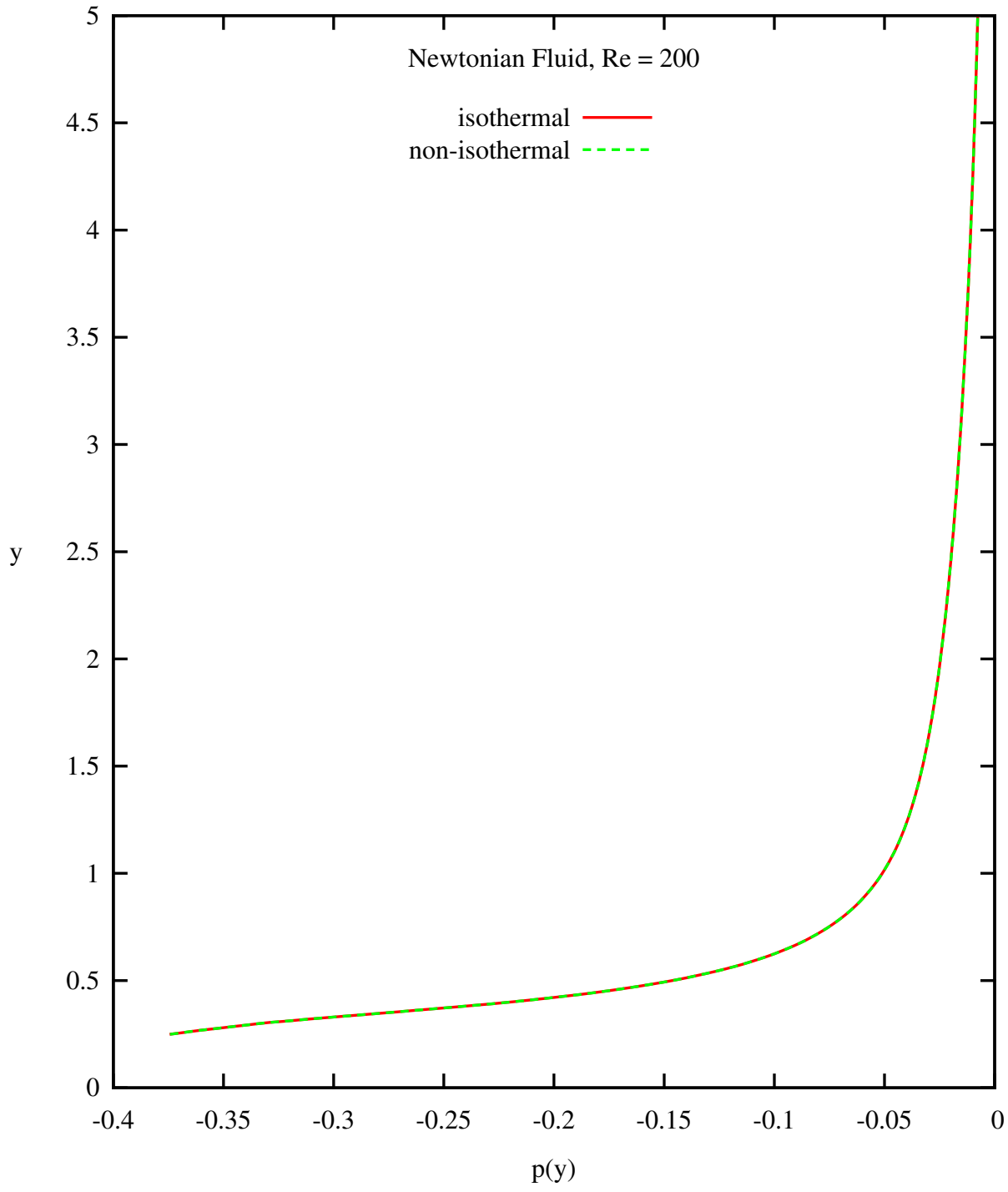

Figure B.2: Pressure p versus y at $x = 0$: Comparison of Isothermal and Non-Isothermal Flows at Re = 200 (Newtonian)

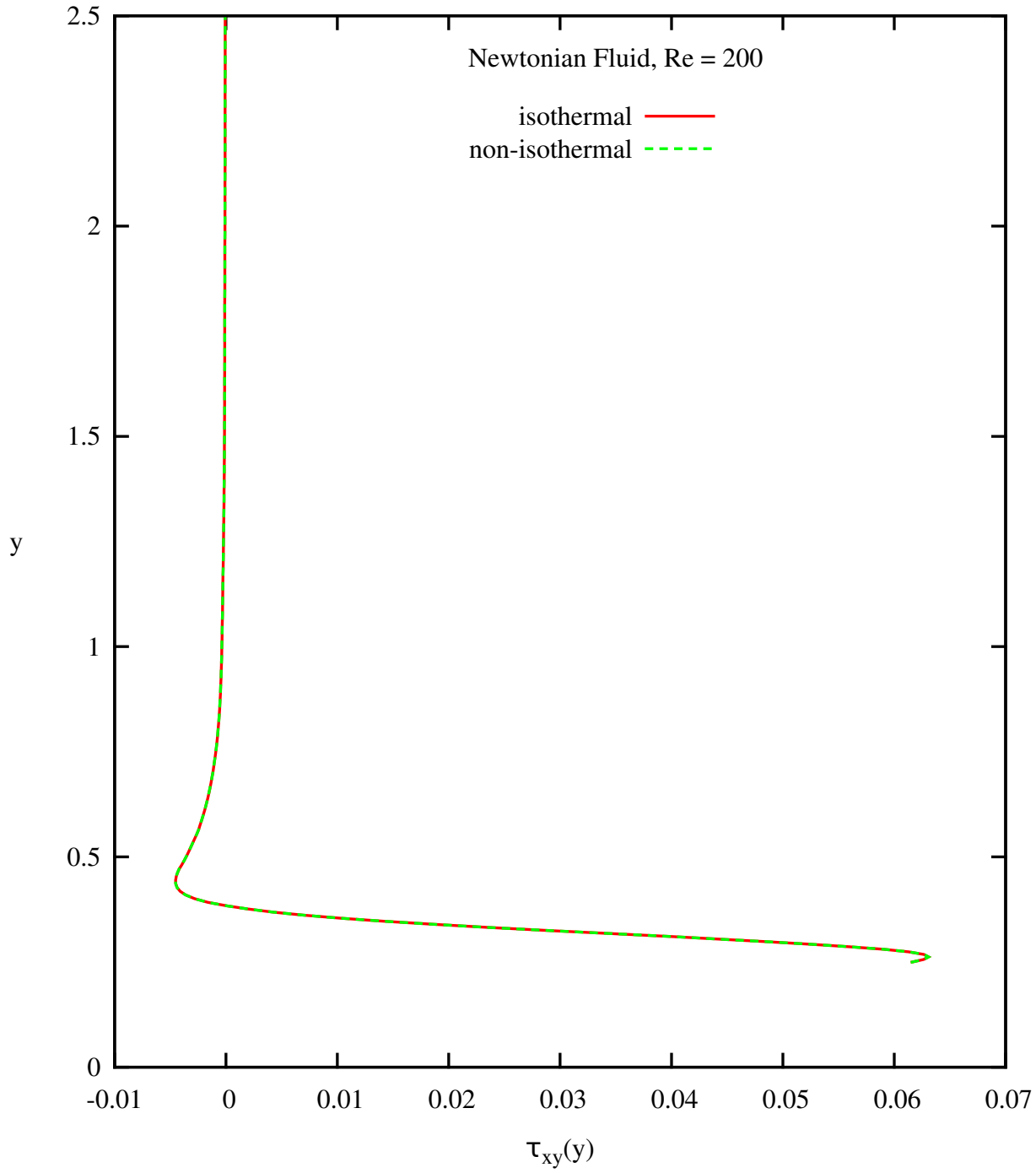

Figure B.3: Shear Stress τ_{xy} versus y at $x = 0$: Comparison of Isothermal and Non-Isothermal Flows at Re = 200 (Newtonian)

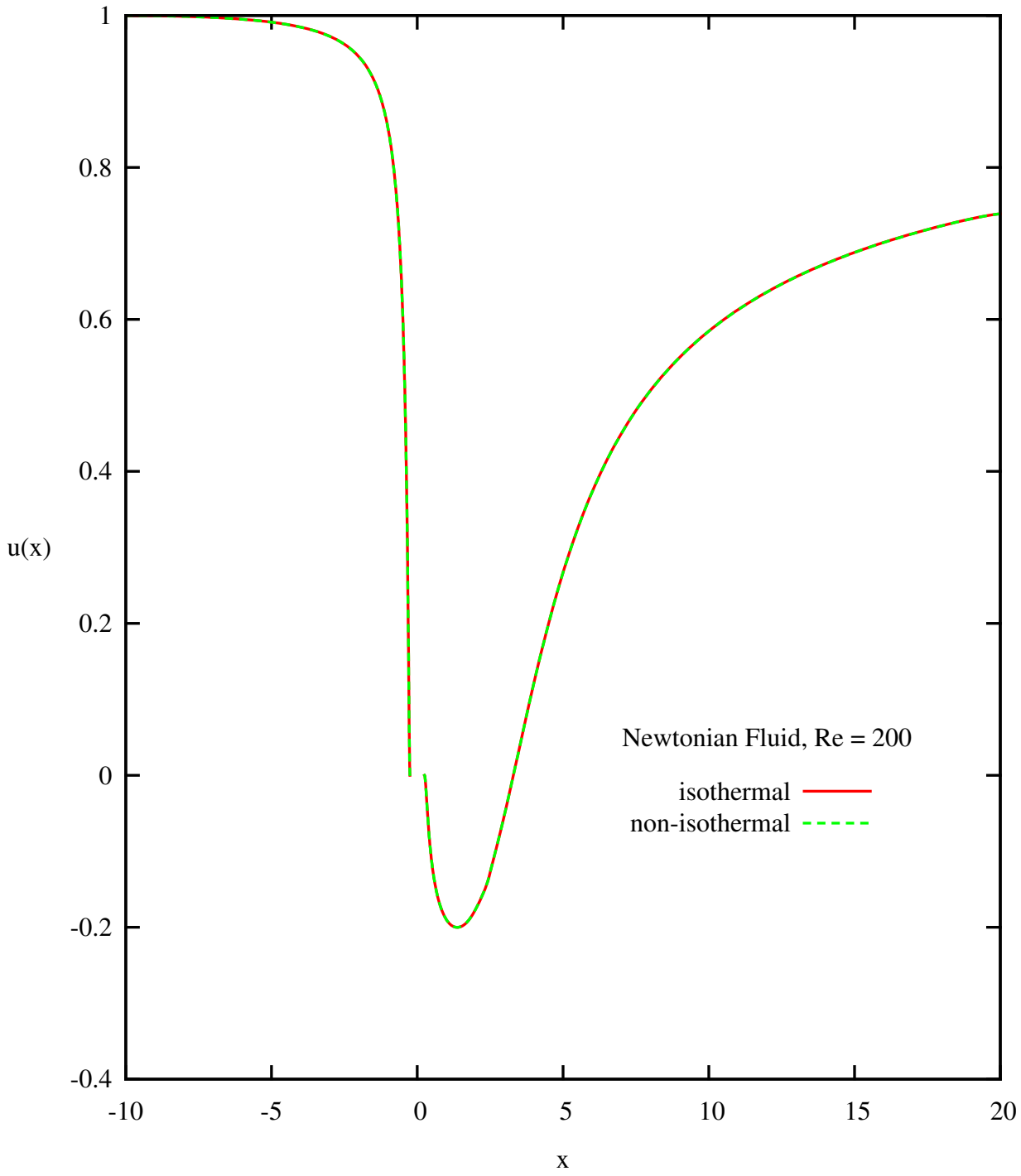

Figure B.4: Velocity u versus x at $y = 0$: Comparison of Isothermal and Non-Isothermal Flows at Re = 200 (Newtonian)

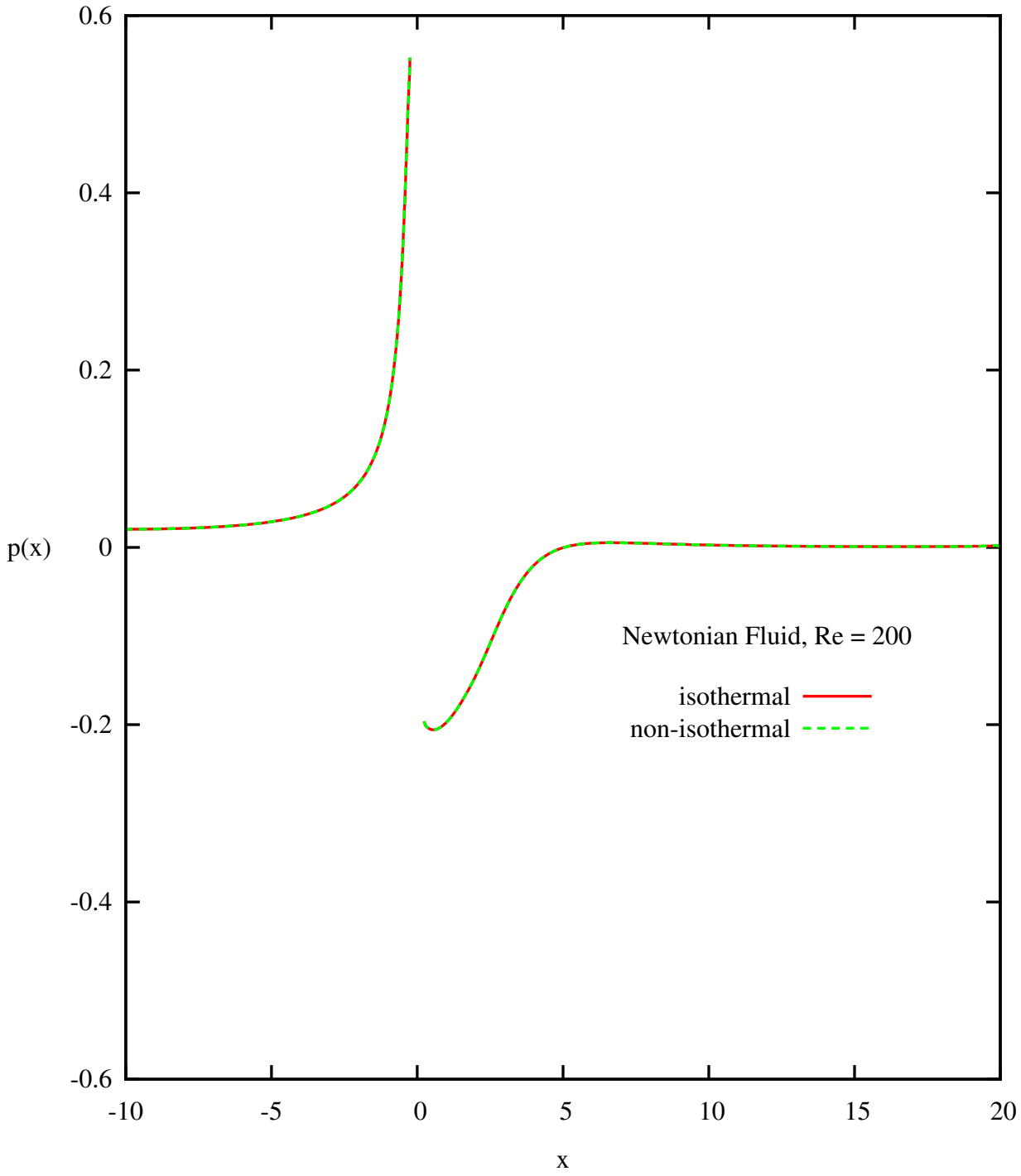

Figure B.5: Pressure p versus x at $y = 0$: Comparison of Isothermal and Non-Isothermal Flows at Re = 200 (Newtonian)

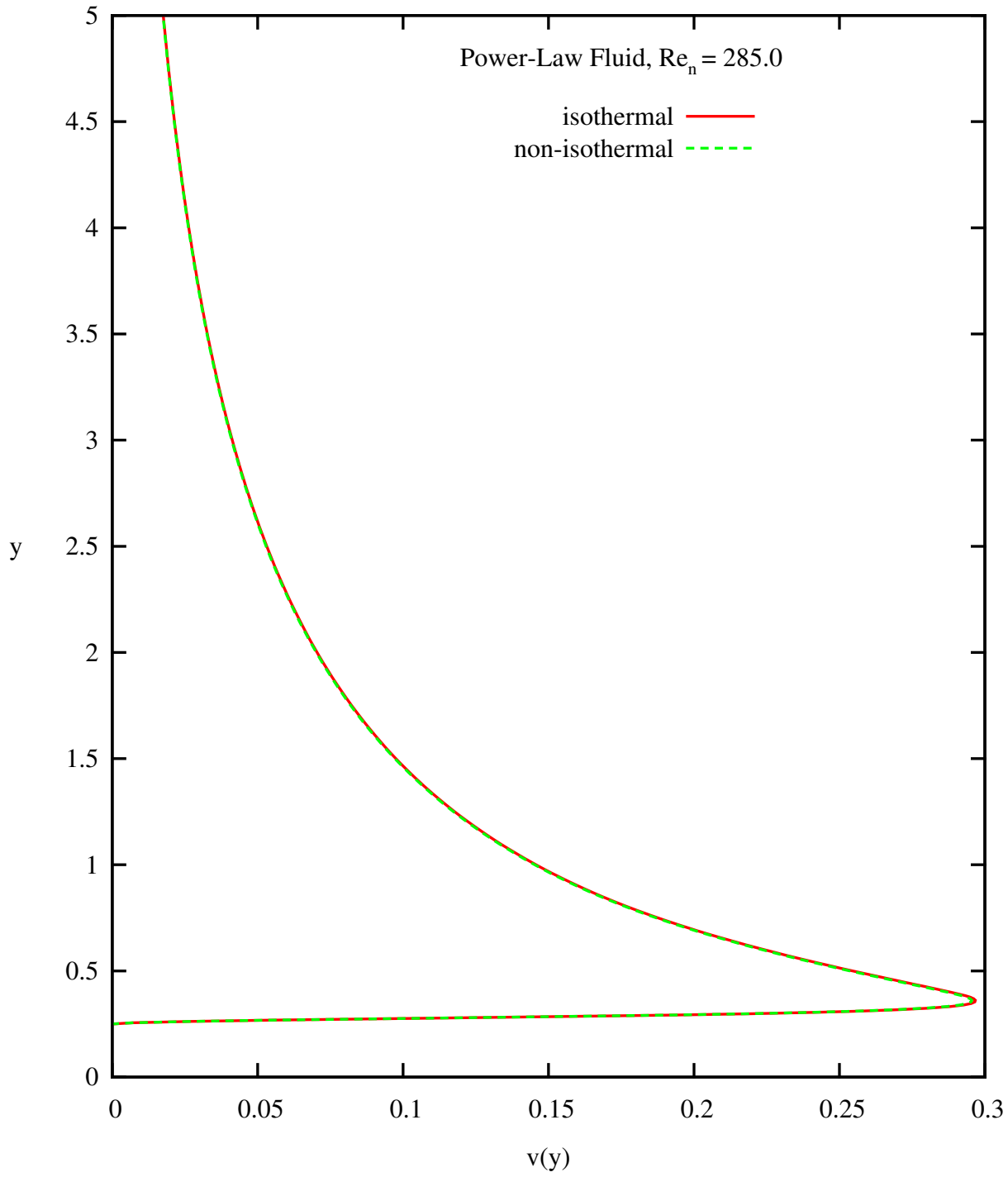

Figure B.6: Velocity v versus y at $x = 0$: Comparison of Isothermal and Non-Isothermal Flows at Re = 285.0 (Power-Law)

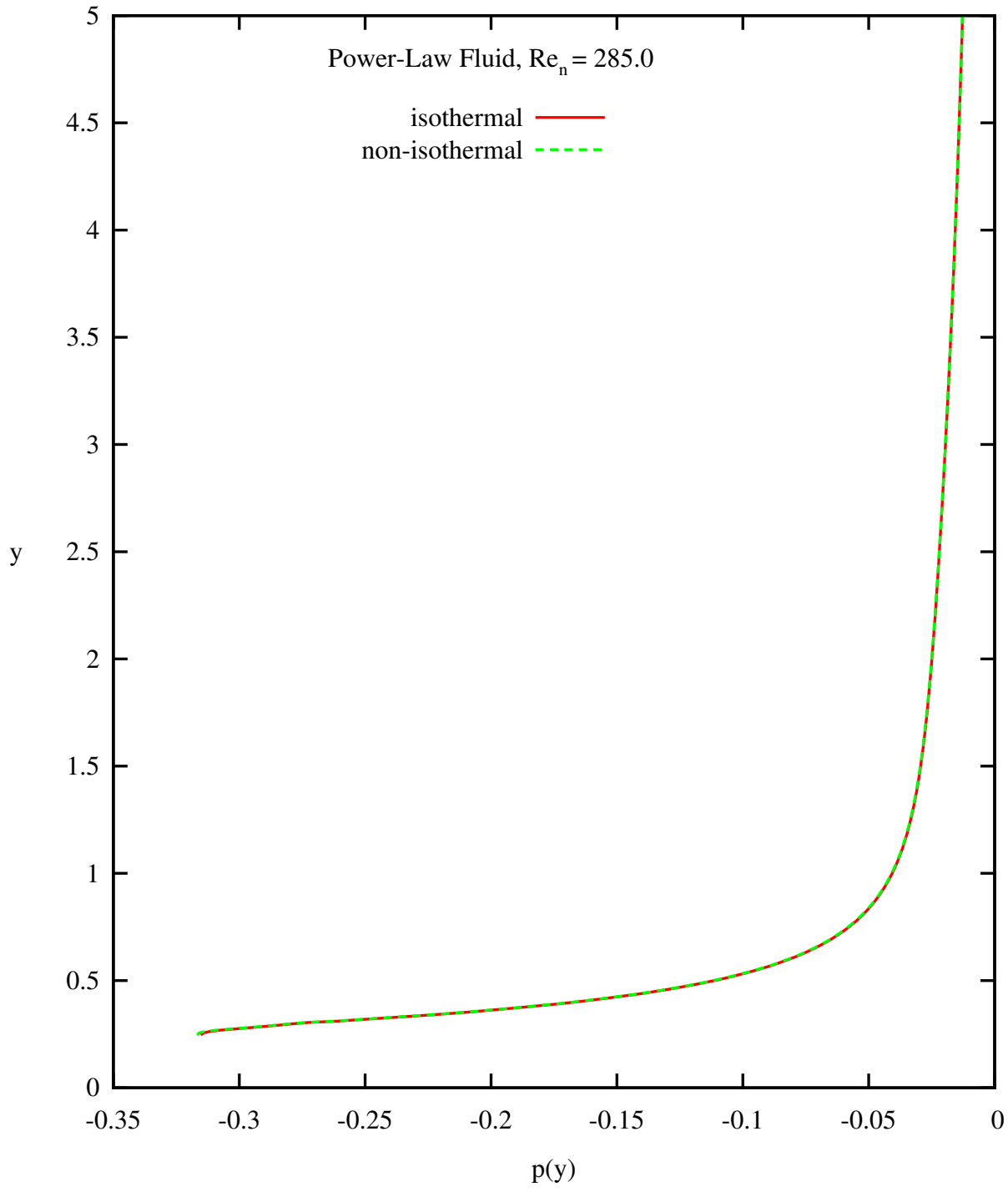

Figure B.7: Pressure p versus y at $x = 0$: Comparison of Isothermal and Non-Isothermal Flows at Re = 285.0 (Power-Law)

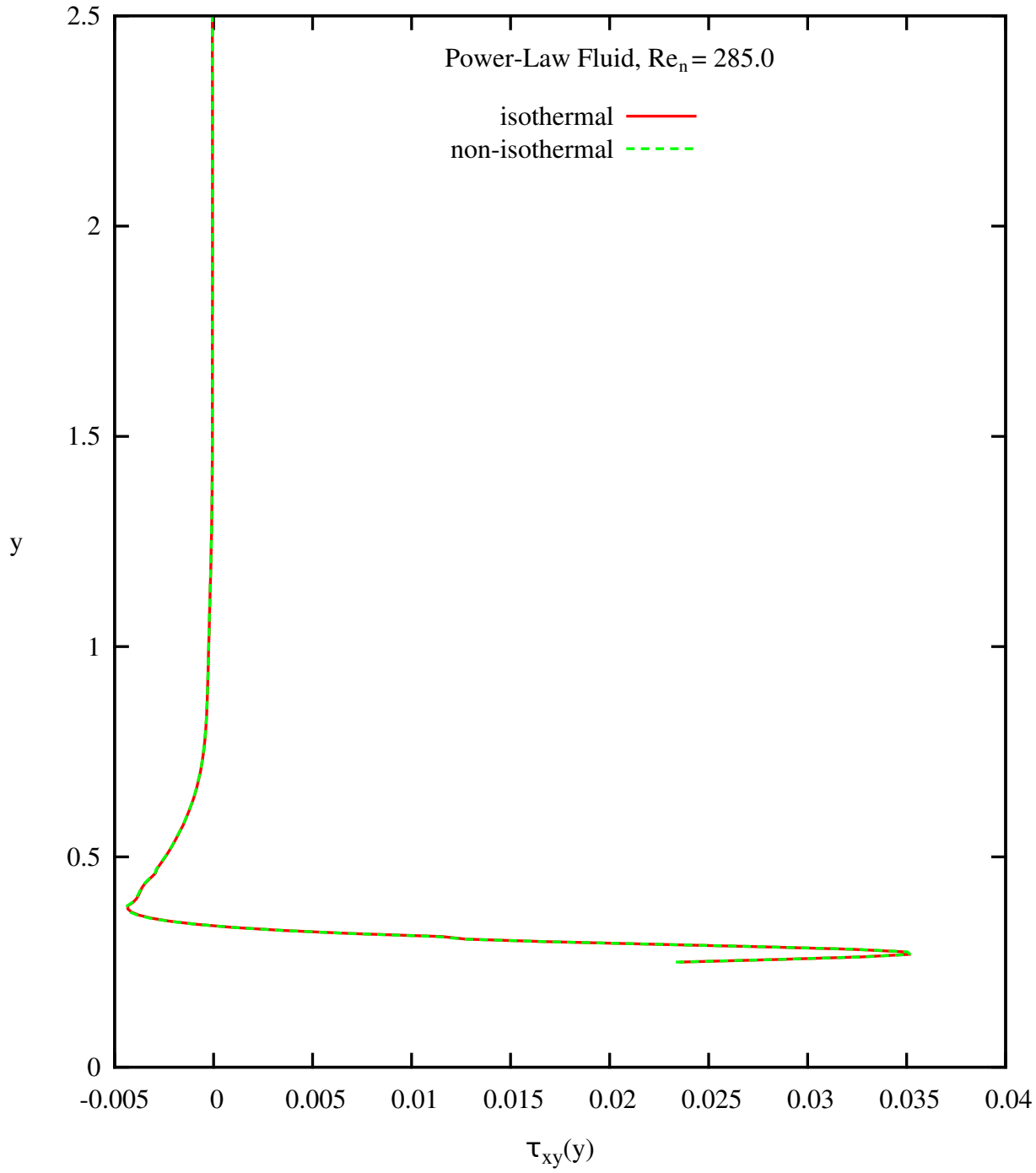

Figure B.8: Shear Stress τ_{xy} versus y at $x = 0$: Comparison of Isothermal and Non-Isothermal Flows at Re = 285.0 (Power-Law)

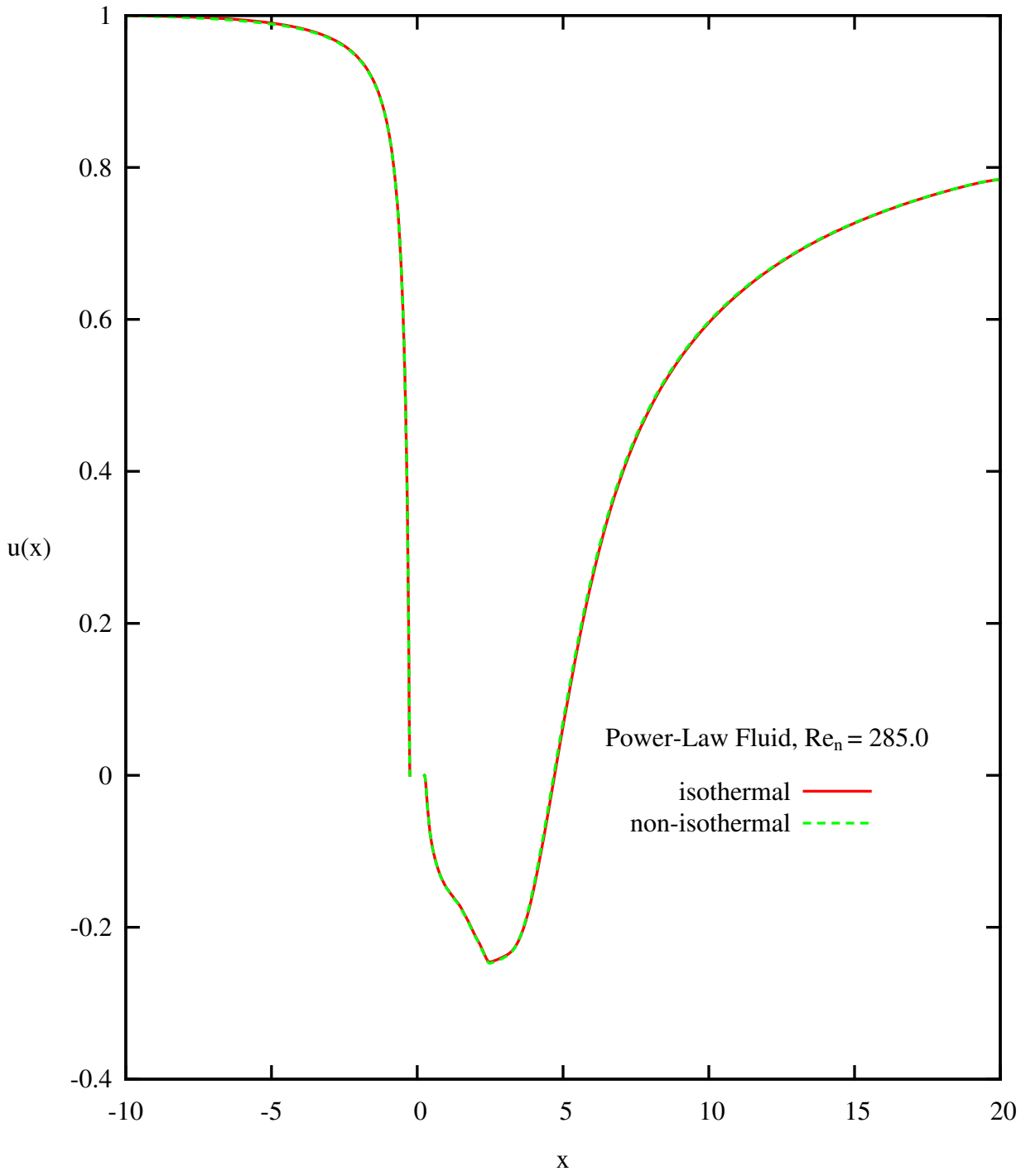

Figure B.9: Velocity v versus x at $y = 0$: Comparison of Isothermal and Non-Isothermal Flows at Re = 285.0 (Power-Law)

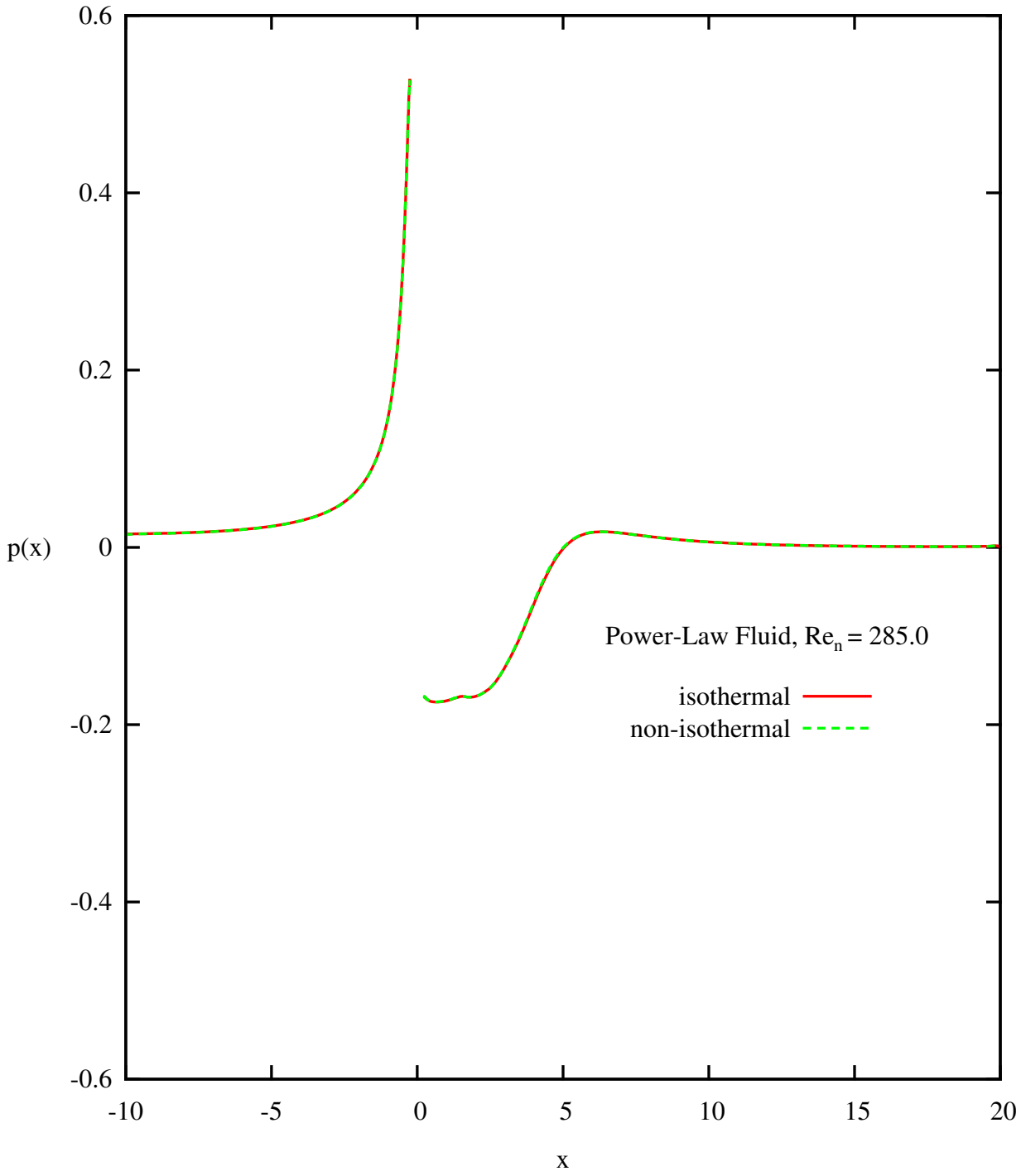

Figure B.10: Pressure p versus x at $y = 0$: Comparison of Isothermal and Non-Isothermal Flows at Re = 285.0 (Power-Law)

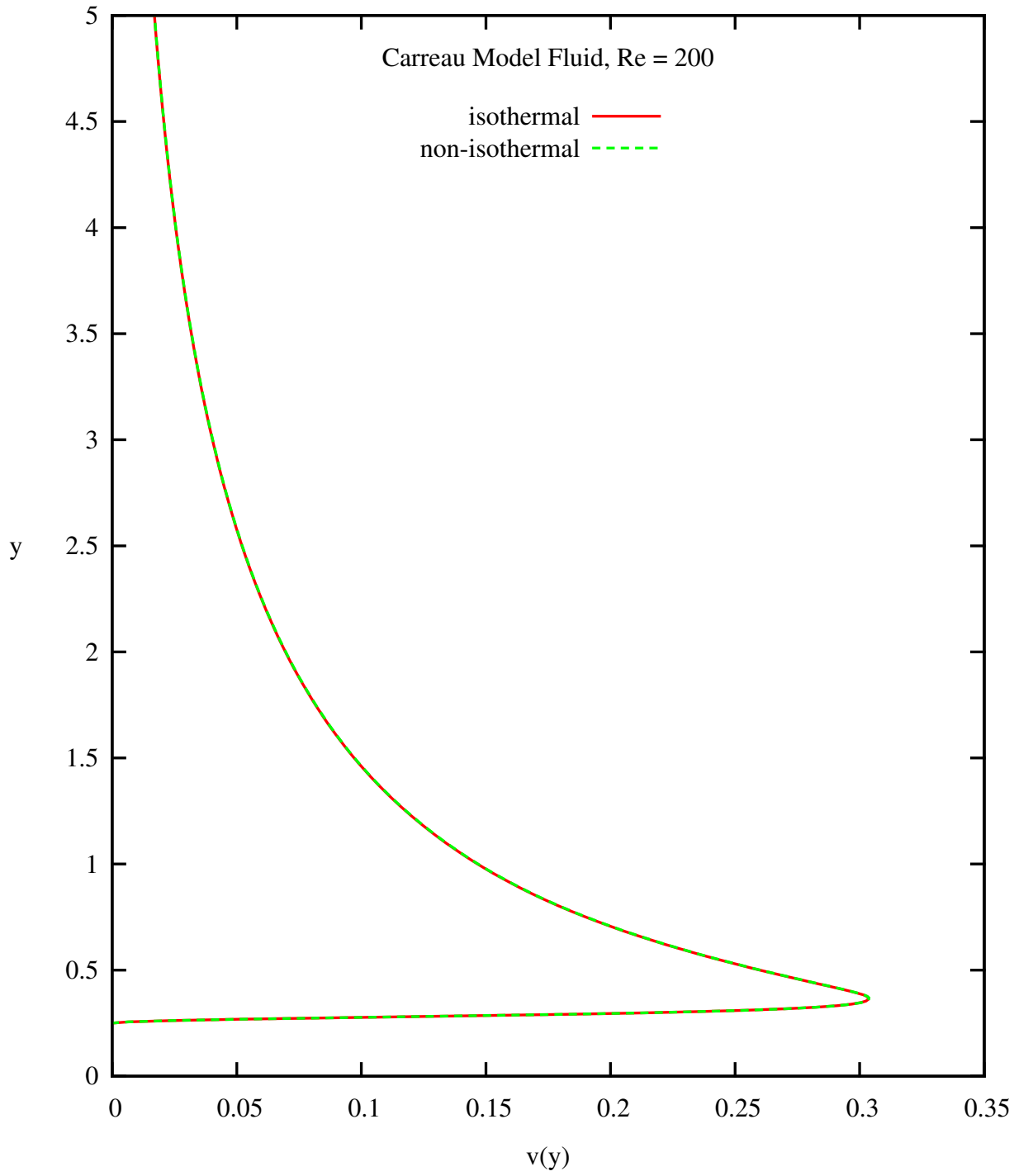

Figure B.11: Velocity v versus y at $x = 0$: Comparison of Isothermal and Non-Isothermal Flows at Re = 200 (Carreau Model)

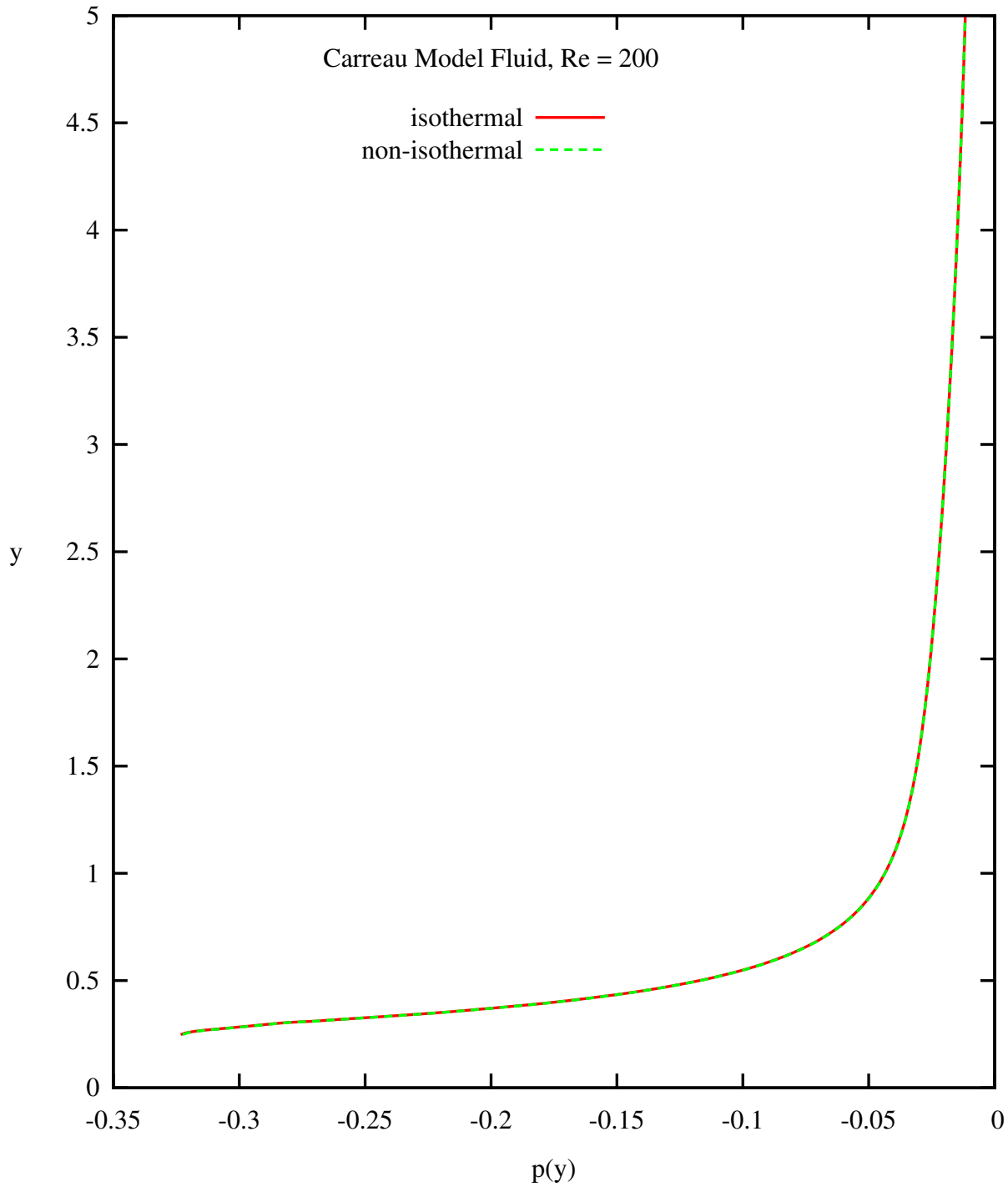

Figure B.12: Pressure p versus y at $x = 0$: Comparison of Isothermal and Non-Isothermal Flows at Re = 200 (Carreau Model)

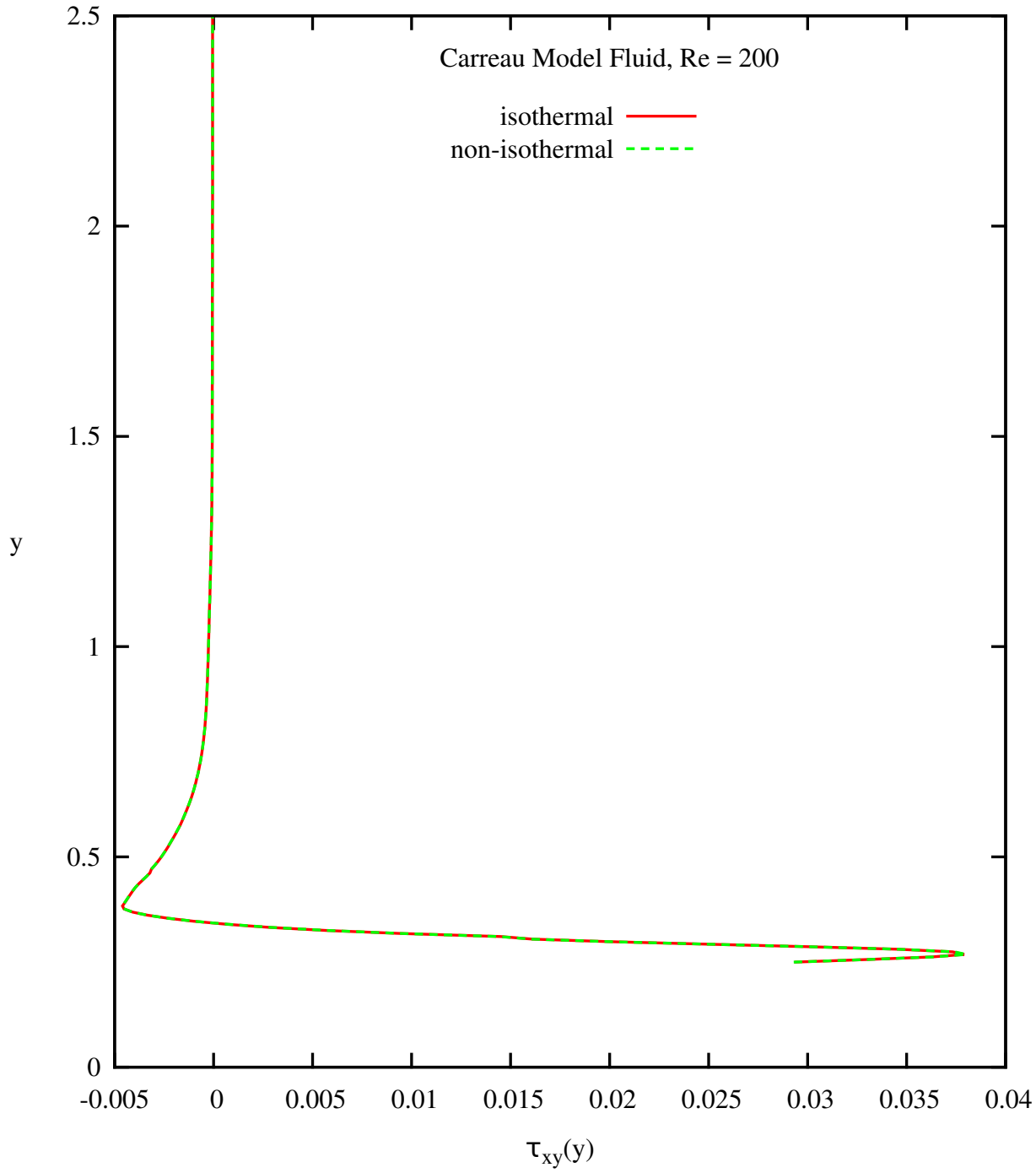

Figure B.13: Shear Stress τ_{xy} versus y at $x = 0$: Comparison of Isothermal and Non-Isothermal Flows at Re = 200 (Carreau Model)

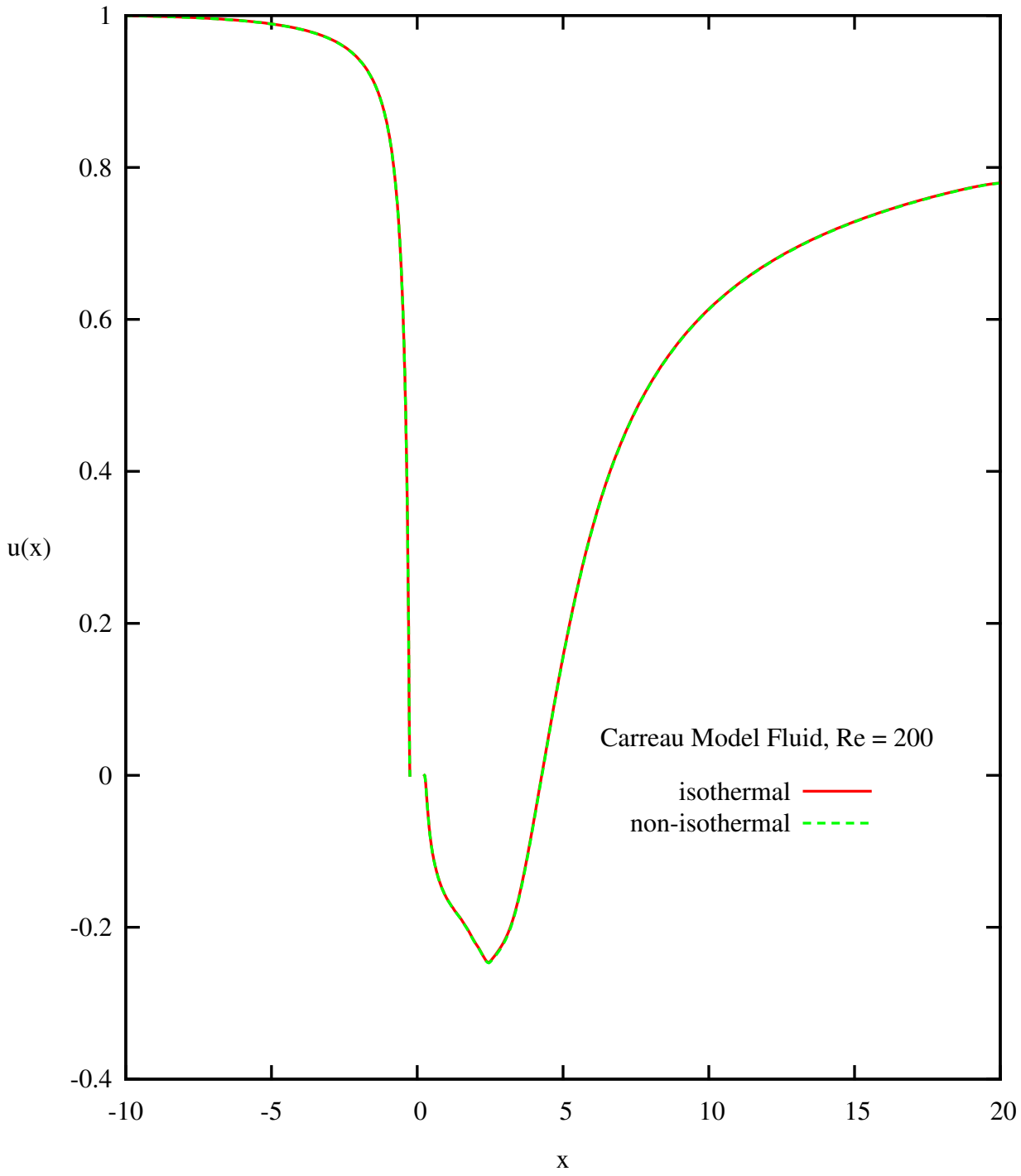

Figure B.14: Velocity v versus x at $y = 0$: Comparison of Isothermal and Non-Isothermal Flows at Re = 200 (Carreau Model)

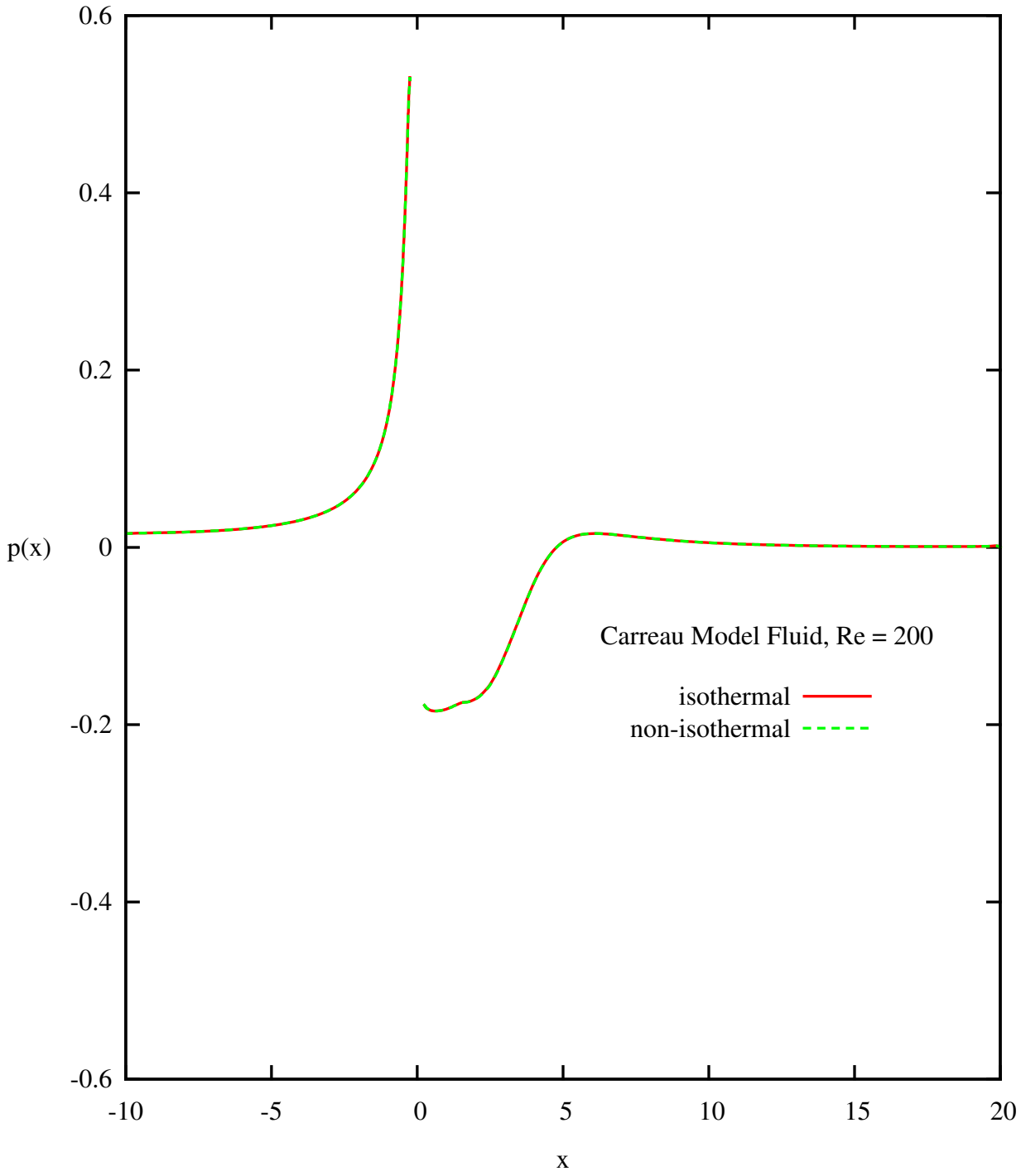

Figure B.15: Pressure p versus x at $y = 0$: Comparison of Isothermal and Non-Isothermal Flows at Re = 200 (Carreau Model)

Bibliography

[1] C.H.K. Williamson. Vortex dynamics in the cylinder wake. *Annual Review of Fluid Mechanics*, 28:477–539, 1996.

[2] M.M. Zdravkovich. *Flow Around Circular Cylinder, Volume 1: Fundamentals*. Oxford University Press, New York, USA, 1997.

[3] M.M. Zdravkovich. *Flow Around Circular Cylinder, Volume 2: Applications*. Oxford University Press, New York, USA, 2003.

[4] B.N. Rajani, A. Kandasamy, and Sekhar Majumdar. Numerical simulation of laminar flow past a circular cylinder. *Applied Mathematical Modelling*, 33(3):1228 – 1247, 2009.

[5] O. Posdziech and R. Grundmann. A systematic approach to the numerical calculation of fundamental quantities of the two-dimensional flow over a circular cylinder. *Journal of Fluids and Structures*, 23(3):479 – 499, 2007.

[6] A. E. Hamielec and J. D. Raal. Numerical studies of viscous flow around circular cylinders. *Physics of Fluids*, 12(1):11–17, 1969.

[7] Julio and Soria. An investigation of the near wake of a circular cylinder using a video-based digital cross-correlation particle image velocimetry technique. *Experimental Thermal and Fluid Science*, 12(2):221 – 233, 1996.

[8] C. Norberg. Fluctuating lift on a circular cylinder: review and new measurements. *Journal of Fluids and Structures*, 17(1):57 – 96, 2003.

[9] A. S. Grove, F. H. Shair, and E. E. Petersen. An experimental investigation of the steady separated flow past a circular cylinder. *Journal of Fluid Mechanics*, 19(01):60–80, 1964.

[10] Bengt Fornberg. A numerical study of steady viscous flow past a circular cylinder. *Journal of Fluid Mechanics*, 98(04):819–855, 1980.

[11] Bengt Fornberg. Steady viscous flow past a circular cylinder up to reynolds number 600. *Journal of Computational Physics*, 61(2):297 – 320, 1985.

[12] R.I. Tanner. Stokes paradox for power-law flow around a cylinder. *Journal of Non-Newtonian Fluid Mechanics*, 50(2-3):217 – 224, 1993.

[13] E. MaruÅąiÄĞ-Paloka. On the stokes paradox for power-law fluids. *ZAMM - Journal of Applied Mathematics and Mechanics / Zeitschrift fÃijr Angewandte Mathematik und Mechanik*, 81(1):31–36, 2001.

[14] Ram Prakash Bharti, R. P. Chhabra, and V. Eswaran. Steady flow of power law fluids across a circular cylinder. *The Canadian Journal of Chemical Engineering*, 84(4):406–421, 2006.

[15] R. P. Chhabra, A. A. Soares, and J. M. Ferreira. Steady nonâĂŞnewtonian flow past a circular cylinder: a numerical study. *Acta Mechanica*, 172:1–16, 2004. 10.1007/s00707-004-0154-6.

[16] S. D'Alessio and J. Pascal. Steady flow of a power-law fluid past a cylinder. *Acta Mechanica*, 117:87–100, 1996. 10.1007/BF01181039.

[17] M. Vijaysri, R.P. Chhabra, and V. Eswaran. Power-law fluid flow across an array of infinite circular cylinders: a numerical study. *Journal of Non-Newtonian Fluid Mechanics*, 87(2-3):263 – 282, 1999.

[18] P. Sivakumar, Ram Prakash Bharti, and R.P. Chhabra. Effect of power-law index on critical parameters for power-law flow across an unconfined circular cylinder. *Chemical Engineering Science*, 61(18):6035 – 6046, 2006.

[19] Vijaya K. Patnana, Ram P. Bharti, and Raj P. Chhabra. Two-dimensional unsteady flow of power-law fluids over a cylinder. *Chemical Engineering Science*, 64(12):2978 – 2999, 2009.

[20] P.M. Coelho and F.T. Pinho. Vortex shedding in cylinder flow of shear-thinning fluids: I. identification and demarcation of flow regimes. *Journal of Non-Newtonian Fluid Mechanics*, 110(2-3):143 – 176, 2003.

[21] P.M. Coelho and F.T. Pinho. Vortex shedding in cylinder flow of shear-thinning fluids: Ii. flow characteristics. *Journal of Non-Newtonian Fluid Mechanics*, 110(2-3):177 – 193, 2003.

[22] P.M Coelho and F.T Pinho. Vortex shedding in cylinder flow of shear-thinning fluids. iii: Pressure measurements. *Journal of Non-Newtonian Fluid Mechanics*, 121(1):55 – 68, 2004.

[23] K. S. Surana, M. K. Engelkemier, J. N. Reddy, and P. W. Tenpas. k-version least squares finite element processes for 2-d generalized newtonian fluid flows. *International Journal for Computational Methods in Engineering Science and Mechanics*, 8(4):243–261, 2007.

[24] K.S. Surana, A. Ahmadi, and J.N. Reddy. k-version of finite element method for self-adjoint operators in bvp. *International Journal of Computational Engineering Science*, 3(2):155–218, 2002.

[25] K.S. Surana, A. Ahmadi, and J.N. Reddy. k-version of finite element method for non-linear differential operators in bvp. *International Journal of Computational Engineering Science*, 5(1):133–207, 2004.

[26] W. A. Khan, J. R. Culham, and M. M. Yovanovich. Fluid flow and heat transfer in power-law fluids across circular cylinders: Analytical study. *Journal of Heat Transfer*, 128(9):870–878, 2006.

[27] Ram Bharti, R. Chhabra, and V. Eswaran. A numerical study of the steady forced convection heat transfer from an unconfined circular cylinder. *Heat and Mass Transfer*, 43:639–648, 2007. 10.1007/s00231-006-0155-1.

[28] A. A. Soares, J. M. Ferreira, and R. P. Chhabra. Flow and forced convection heat transfer in crossflow of non-newtonian fluids over a circular cylinder. *Industrial & Engineering Chemistry Research*, 44(15):5815–5827, 2005.

[29] B.K. Rao. Heat transfer to non-newtonian flows over a cylinder in cross flow. *International Journal of Heat and Fluid Flow*, 21(6):693 – 700, 2000.

[30] G.H. Wu, B.Y. Wu, S.H. Ju, and C.C. Wu. Non-isothermal flow of a polymeric fluid past a submerged circular cylinder. *International Journal of Heat and Mass Transfer*, 46(24):4733 – 4739, 2003.

[31] Brent C. Bell and Karan S. Surana. p-version least squares finite element formulation for two-dimensional, incompressible, non-newtonian isothermal and non-isothermal fluid flow. *International Journal for Numerical Methods in Fluids*, 18(2):127–162, 1994.

[32] Daniel Winterscheidt. *p-version least squares finite element method for fluid dynamics*. PhD thesis, University of Kansas, Mechanical Engineering, 1992.

[33] K.S. Surana and J.N. Reddy. *Mathematics of computations and finite element method for boundary value problems*. Book manuscript in preperation, 2012.

[34] Brent C. Bell. *p-version least squares finite element formulation for steady and unsteady fluid flow*. PhD thesis, University of Kansas, Mechanical Engineering, 1993.

[35] Srikanth Allu. *Computations of Viscous Compressible Flows in h, p, k Finite Element Framework with Variationally Consistent Integral Forms*. PhD thesis, University of Kansas, Mechanical Engineering, 2008.

[36] K.S. Surana and J.N. Reddy. *Continuum Mechanics*. Book manuscript in preparation, 2012.

[37] K. S. Surana, D. Nunez, J. N. Reddy, A. International Journal of Continuum Mechanics Romkes, and Thermodynamics. Rate constitutive theory for ordered thermofluids. *International Journal of Continuum Mechanics and Thermodynamics (under review)*, 2012.

[38] R. B. Bird and O. Hassager. *Dynamics of Polymeric Liquids*. J. Wiley, New York, 1977.

[39] I. Machac, B. Siska, and Z. Lecjaks. Inhomogeneities in fluidization of spherical particle beds with non-newtonian polymer solutions. *Chem. Papers*, 53(6):390–395, 1999.